CHEMICAL ENGINEERING SCIENCE
GENIE CHIMIQUE

VOL. 10 1959 Nos. 1/2

On the dynamics of phase growth

L. E. SCRIVEN
Chemical Engineering Department, Shell Development Company, Emeryville, California

(*Received* 15 *March* 1958)

Abstract—The equations governing spherically symmetric phase growth in an infinite medium are first formulated for the general case and are then simplified to describe growth controlled by the transport of heat and matter. All assumptions and restrictions are recounted. Exact solutions of the equations are obtained for conditions typical of bubble growth in the nucleate boiling of (a) pure materials, and (b) binary mixtures. The effect of radial convection resulting from unequal phase densities is established and the regions of applicability of previously reported approximate solutions are determined.

Résumé—Les équations régissant le grossissement de phase, sphériquement symétrique, dans un milieu infini, sont d'abord établies pour le cas général et simplifiées pour décrire le grossissement réglé par le transport thermique et le transport de matière. Il est tenu compte de toutes les hypothèses et limitations. Des solutions exactes des équations sont obtenues pour des conditions typiques de grossissement de bulles, dans l'ébullition sous forme de bulles :

(a) de substances pures
(b) de mélanges binaires.

L'influence de la convection radiale résultant de densités inégales est établie, et les régions d'application des solutions approchées, notées précédemment sont déterminées.

Zusammenfassung—Die Gleichungen für das kugelsymmetrische Phasenwachstum in einem ausgedehnten Medium werden zunächst allgemein formuliert und dann für jenen Fall vereinfacht, bei dem das Wachstum durch den Transport von Wärme und Stoff bestimmt ist. Alle Annahmen und Einschränkungen werden aufgezählt. Exakte Lösungen der Gleichungen werden erhalten für Bedingungen, wie für das Blasenwachstum bei Blasenverdampfung in (a) reinen Stoffen und (b) Zweistoffgemischen typisch sind. Die Einflüsse radialer Konvektion, hervorgerufen durch ungleiche Phasendichten, werden behandelt und die Bereiche bestimmt, in denen die oben erwähnten Näherungslösungen anwendbar sind.

1. INTRODUCTION

THE dynamics of vapour bubbles is of fundamental importance in nucleate boiling. The photographic evidence for this and the auspicious developments in the theory of boiling that have followed have been reviewed by WESTWATER [23]. Recently ZUBER and his co-workers [7, 14, 25] attempted to relate heat transfer in pool boiling and density transients in volume-heated boiling systems to an idealized theory of bubble growth in superheated liquids, and their results are promising. Thus study of the mechanism of bubble growth should advance our understanding of nucleate boiling heat transfer, although, to be sure, complete understanding awaits explanation of various nucleation phenomena.

This paper has twofold purpose: (a) to present a consolidated mathematical statement of the problem of spherically symmetric phase growth with sufficient generality that the connection and applicability of diverse treatments of the problem can be seen; and (b) to analyse in this setting the growth of a single vapour bubble in an unlimited body of superheated liquid when growth is controlled solely by the transport of heat and matter. Two cases are examined in

detail: bubble growth in pure liquids, and in binary solutions. Approximate solutions have been obtained by PLESSET and ZWICK [18, 26] and FORSTER and ZUBER [6, 11] for the former case, and by STERNLING [22] for the latter when one component is non-volatile. It is shown that the approximations are accurate only over restricted ranges of pressure and superheat.

Other instances of spherically symmetric phase growth controlled by diffusion have been analysed mathematically. Over the years there has been considerable interest in "Stefan-like" problems, i.e., deducing the motion of a phase-transition front controlled by transient diffusion of a single entity, most often heat energy, *when the old and new phases are of equal density*. RIECK first obtained a solution for a spherically symmetric front [12]. His result was rederived by ZENER [24], GEIST [9], and FRANK [8]; the latter also dealt with motion of the front governed by the diffusion of both heat and matter. Recently SESTINI [21] established the existence and uniqueness, in the mathematical sense, of a solution. KOLODNER [13] achieved a reduction of the problem to the solution of an integro-differential equation for the motion of the phase-transition front, in which the effect of interfacial tension is readily included. The effect of interfacial tension was also included in the approximate solutions published by EPSTEIN and PLESSET [4]. In other approximate treatments the interactions in a swarm of growing spheres have been considered [15, 20].

A transition between phases of different densities produces in the surrounding fluid a radial convective motion which modifies the concentration and temperature fields and hence the motion of the front. In their analyses of bubble growth in superheated water FORSTER and ZUBER [6, 11] and PLESSET and ZWICK [17, 18, 26] allowed for convective heat transport. Despite complexities arising from terms representing hydrodynamic and surface tension effects in their equations, the two groups obtained useful approximate solutions in fair agreement for the "asymptotic stage" of bubble growth, i.e., for growth limited by heat transfer. CHAMBRÉ [3] tried to treat the dynamics of phase growth in a two-phase system of unequal densities, but his results are vitiated by their violation of the equation of continuity throughout the fluid surrounding the growing phase*. In this paper the influence of radial convection on spherically symmetric phase growth controlled by diffusion is established.

The problem is complicated not only by radial convection, but also by the motion, unknown beforehand, of the phase-transition front, at which boundary conditions involving concentrations, temperature, and their normal gradients must be specified.

We begin by formulating, in rather general form, the equations describing spherically symmetric phase growth, including the pertinent equations of hydrodynamics. We then simplify the problem by imposing a series of restrictions and assumptions which are reasonable for bubble growth in nucleate boiling, and all of which are explicitly stated. Finally, we find particular solutions of the *resulting equations of heat and mass flow*. These solutions are exact so far as the stated assumptions are concerned. They are asymptotic solutions; they are not complete solutions for the earliest moments of bubble growth in a superheated liquid, and neither do the equations of heat and mass flow completely describe the earliest stages of growth, in which surface tension predominates and liquid inertia and viscosity may be important. However, the errors introduced by our solutions at the beginning of the growth process become negligible at later times, so that *they provide adequate descriptions of bubble growth during all but the earliest stages*. Moreover, the heat transfer associated with the *initial growth* of bubble nuclei apparently is relatively insignificant in typical nucleate boiling heat transfer (see ref. [7]).

2. FORMULATION OF THE PROBLEM

We consider a spherical vapour bubble growing in a quiescent, superheated liquid of infinite extent. The growth rate is determined by the difference between the pressure within the bubble and the ambient pressure, liquid inertia

* See equations (17)–(19), ref. [3]. For an incompressible fluid, conservation of matter requires that the product ur^K be independent of the positional co-ordinate, r.

VOL. 10 1959

and viscosity, surface tension, and transport of heat and volatile material through the liquid to the bubble surface. Under all but the most extreme conditions compressibility effects, vapour inertia and viscosity, and pressure, temperature, and concentration gradients within the vapour can be disregarded [18, 26]. Over moderate variations of temperature and composition the physical properties of liquid and vapour can be assumed constant.

For convenience, the additional restrictions and assumptions that are imposed below are collected here, together with the number of the equation(s) where each is first introduced:

Spherical symmetry	(2)
Constant fluid density	(2)
Newtonian fluid	(7)
External body forces absent	(7)
Infinite medium	(8)
Viscous dissipation negligible	(12)
Energy flow by ordinary conduction only	(12)
Constant thermal properties	(12)
Two-component system	(15)
No chemical reactions	(15)
Mass flow by ordinary diffusion only	(16)
Constant mass diffusivity	(16)
Uniform initial distributions	(20), (21)
Kinetic energy terms negligible	(25)
Surface energy term negligible	(27)
Heat of mixing negligible	(27)
Heat capacities of the two components equal	(27)
Inertial, viscous, and surface tension effects negligible	(27), (31)
Linear equilibrium relation	(29)
Dalton's law for gases	(30)
Internal heat generation absent	(36)

A. Equation of continuity

The equation of continuity*

$$\frac{D\rho}{D\theta} = -\rho \nabla \cdot \boldsymbol{V} \tag{1}$$

when written for spherical symmetry and an incompressible fluid can be integrated to give

$$ur^2 = \mathrm{f}(\theta) \tag{2}$$

where the origin of the co-ordinate system is the bubble centre, which is at rest. Since the quantity ur^2 is a function of time alone, it can be evaluated in terms of its value at any radius, say, at the bubble surface. The surface moves with velocity $\dot{R}$ while the liquid immediately adjacent moves with velocity $u(R)$; the net velocity causes a mass flow of $4\pi R^2 \rho_L [\dot{R} - u(R)]$ which must just equal the rate of vaporization of volatile material into the bubble. Thus a mass balance written for the bubble surface gives [3]

$$\frac{d}{d\theta}\left(\frac{4}{3}\pi R^3 \rho_G\right) = 4\pi R^2 \rho_L [\dot{R} - u(R)] \tag{3}$$

During bubble growth the volume increases by orders of magnitude but the vapour density changes relatively little; hence it is permissible to assume that vapour density is independent of time [18, 26], whence

$$u(R) = \dot{R}(\rho_L - \rho_G)/\rho_L = \epsilon \dot{R} \tag{4}$$

Substituting this result in equation (2), we have

$$ur^2 = \epsilon \dot{R} R^2 \tag{5}$$

as an expression of the continuity condition for the liquid.

B. Equation of motion

The motion of the liquid is governed by the Navier-Poisson equation

$$\rho \frac{D\boldsymbol{V}}{D\theta} = -\nabla \cdot \boldsymbol{\pi} + \rho \boldsymbol{F} \tag{6}$$

which for spherical symmetry, incompressible Newtonian fluid, and no external body forces reduces to [10]

$$\frac{\partial u}{\partial \theta} + u\frac{\partial u}{\partial r} = \frac{1}{\rho_L}\frac{\partial p_{rr}}{\partial r} - 2\eta \frac{\partial^2 u}{\partial r^2} \tag{7}$$

Substituting for velocity from equation (5) and integrating over radius from the bubble surface to infinity, we obtain

$$\frac{p_{rr}(\infty) - p_{rr}(R)}{\epsilon \rho_L} = R\ddot{R} + \frac{3}{2}\dot{R}^2 + 4\eta \frac{\dot{R}}{R} \tag{8}$$

The radial component of the radial stress at infinity is just the negative of the ambient pressure, while at the bubble surface it is given by

$$-p_{rr}(R) = p_v + p_i - 2\sigma/R \tag{9}$$

* The vector and tensor notation used in equations (1), (6), (11), (14), and (15) is that of BIRD [1, 2].

The equation of motion for the bubble surface is obtained in final form by substitution in equation (8); thus

$$\frac{p_v + p_i - p_\infty - 2\sigma/R}{\epsilon \rho_L} = R\ddot{R} + \frac{3}{2}\dot{R}^2 + 4\eta\frac{\dot{R}}{R} \quad (10)$$

This equation is identical with the "extended Rayleigh equation" of other writers [3, 16, 19], except that they have tacitly assumed that the density factor ϵ is unity and, in some cases, they have overlooked the viscous term, which is, admittedly, often sufficiently small that it can be neglected [11, 18, 26].

The partial pressure of volatile material in the growing bubble, p_v in equation (10), is specified by postulating thermodynamic equilibrium between vapour and liquid at the bubble surface. Hence it depends upon the temperature and composition of the liquid there, which are in turn dependent upon the rates of energy and mass transport, respectively, within the surrounding liquid. The partial pressure of any inert gas initially present also depends upon the temperature at the bubble surface; in addition, it is a function of the bubble radius. In general, then, the transport equations must be considered simultaneously with the equation of motion.

C. *Equation of energy flow*

The energy balance equation is [2]

$$\rho\frac{DE}{D\theta} = -\nabla\cdot\boldsymbol{q} - \boldsymbol{\pi}:\nabla\boldsymbol{V} + Q \quad (11)$$

which for spherical symmetry, incompressible fluid, negligible viscous dissipation, no energy fluxes other than ordinary conduction, and constant thermal properties reduces to [1]

$$\frac{\partial T}{\partial\theta} + u\frac{\partial T}{\partial r} = K\left(\frac{\partial^2 T}{\partial r^2} + \frac{2}{r}\frac{\partial T}{\partial r}\right) + \frac{Q}{\rho_L c_L} \quad (12)$$

With equation (5) for radial velocity this becomes*

$$\frac{\partial T}{\partial\theta} = K\left(\frac{\partial^2 T}{\partial r^2} + \frac{2}{r}\frac{\partial T}{\partial r}\right) - \frac{\epsilon R^2\dot{R}}{r^2}\frac{\partial T}{\partial r} + \frac{Q}{\rho_L c_L} \quad (13)$$

* The heat generation term $Q/\rho_L c_L$ in equations (13) and (22) is omitted later in the present analysis [equation (36)], but is retained here to facilitate comparison with the work of others [6, 11, 17, 18, 20, 26].

D. *Equation of mass flow*

The mass balance equation for the i-th component of a multi-component fluid is [1, 2]

$$\frac{DC_i}{D\theta} = -\nabla\cdot\boldsymbol{j}_i - C_i\nabla\cdot\boldsymbol{V} + J_i \quad (14)$$

Restricting consideration to two-component systems in which chemical reaction effects are absent and writing equation (14) for component 1, we have

$$\frac{\partial C_1}{\partial\theta} + \nabla\cdot C_1\boldsymbol{V} = -\nabla\cdot\boldsymbol{j}_1 \quad (15)$$

which for spherical symmetry, constant mass density, no mass fluxes other than ordinary diffusion, and constant diffusivity reduces to [1]

$$\frac{\partial D}{\partial\theta} + u\frac{\partial C}{\partial r} = \mathscr{D}\left(\frac{\partial^2 C}{\partial r^2} + \frac{2}{r}\frac{\partial C}{\partial r}\right) \quad (16)$$

Substituting for radial velocity, we get

$$\frac{\partial C}{\partial\theta} = \mathscr{D}\left(\frac{\partial^2 C}{\partial r^2} + \frac{2}{r}\frac{\partial C}{\partial r}\right) - \frac{\epsilon R^2\dot{R}}{r^2}\frac{\partial C}{\partial r} \quad (17)$$

E. *Initial conditions*

Initial conditions for equations (10), (13) and (17) can be formulated somewhat arbitrarily as follows:

$$R(0) = \frac{2\sigma}{p_{v0} + p_{i0} - p_\infty} + \delta \quad (18)$$

where the small displacement δ from the initial equilibrium radius may be set equal to zero if the source term is retained in equation (13), [6, 11, 18, 26].

$$\dot{R}(0) = 0 \quad (19)$$

i.e., the initial bubble growth velocity is nil.

$$T(r, 0) = T_0 \quad (20)$$

$$C(r, 0) = C_0 \quad (21)$$

i.e., the liquid is initially of uniform temperature and composition.

F. *Boundary conditions at infinity*

If the source term in equation (13) is independent of position at large distances from the origin, then

VOL. 10 1959

$$T(\infty, \theta) = T_0 + (\rho_L c_L)^{-1} \int_0^\theta Q(\infty, \theta')\, d\theta' \quad (22)$$

$$C(\infty, \theta) = C_0 \quad (23)$$

G. Boundary conditions at the bubble surface

At the bubble surface the temperature and concentration gradients in the liquid are related to the rate of bubble growth by energy and mass balances written for the open system represented by the bubble itself. The mass balance for component 1 in the bubble is, by a derivation like that of equation (3),

$$m\rho_G \dot{R} = C(R, \theta)\,[\dot{R} - u(R)] + \mathscr{D}\left(\frac{\partial C}{\partial r}\right)_{r=R}$$

$$= C(R, \theta)(1 - \epsilon)\,\dot{R} + \mathscr{D}\left(\frac{\partial C}{\partial r}\right)_{r=R} \quad (24)$$

The energy balance for the bubble, neglecting relatively unimportant kinetic energy terms, is

$$\frac{d}{d\theta}\left\{\frac{4}{3}\pi R^3 \rho_G\,[mU_1 + (1-m)\,U_2] + 4\pi R^2 \sigma\right\} + 4\pi R^2 \dot{R} p_\infty =$$

$$4R^2\left\{h_1\left[C(R,\theta)(1-\epsilon)\,\dot{R} + \mathscr{D}\left(\frac{\partial C}{\partial r}\right)_{r=R}\right] + h_2\left[(\rho_L - C(R,\theta))(1-\epsilon)\,\dot{R} - \mathscr{D}\left(\frac{\partial C}{\partial r}\right)_{r=R}\right] + k\left(\frac{\partial T}{\partial r}\right)_{r=R}\right\} \quad (25)$$

During bubble growth the changes in vapour density and internal energy are small compared to the volume increase, and the surface energy term is appreciable only for very small radii. Furthermore, the difference

$$p_v + p_i - p_\infty \equiv \rho_G \bar{H} - (\rho_G \bar{U} + p_\infty) \quad (26)$$

is negligible provided the inertia, viscous, and surface tension terms in equation (10) are negligible. If it is also assumed that the heat capacities of the two liquid components are equal and the heat of mixing is negligible, equation (25) simplifies considerably to

$$\rho_G \dot{R}\bar{H} = \rho_L h (1-\epsilon)\,\dot{R} + k\left(\frac{\partial T}{\partial r}\right)_{r=R} \quad (27)$$

Taking liquid at the initial temperature of the system as the reference state in equation (27), we have

$$\rho_G \dot{R}\{\bar{L} + c_G\,[T(R,\theta) - T_0]\}$$

$$= \rho_L c_L [T(R,\theta) - T_0](1-\epsilon)\,\dot{R} + k\left(\frac{\partial T}{\partial r}\right)_{r=R} \quad (28)$$

Finally, the partial pressure of volatile material in the bubble is determined by the assumption of thermodynamic equilibrium at the bubble surface, i.e., by specifying p_v as a function of liquid temperature and composition at the interface. It is convenient to employ the first terms of a Taylor expansion about a suitable reference, say

$$p_v = p_v(T_{sat}, C_0) + [T(R,\theta) - T_{sat}]\left(\frac{\partial p_v}{\partial C}\right) + [C(R,\theta) - C_0]\left(\frac{\partial p_v}{\partial T}\right) \quad (29)$$

The partial derivatives must be evaluated at the reference conditions from thermodynamics. The assumption of thermodynamic equilibrium also determines the vapour composition, since

$$p_v = \gamma_1 x_1 P_1 + \gamma_2 (1 - x_1) P_2 \quad (30)$$

at bubble surface conditions.

H. Over-all energy and mass balances

In addition to the foregoing boundary conditions, solutions of equations (13) and (17) necessarily satisfy the requirements of conservation of energy and mass in the system composed of the bubble and its surroundings. Provided that reasonable approximations have been made in formulating the boundary conditions, these requirements are automatically satisfied by exact solutions; they thus supply a test of assumptions made and a means of checking exact solutions, and they place definite restrictions upon approximate solutions.

I. Further simplifications

Differential equations (10), (13) and (17), together with the initial conditions given by equations (18)–(21) and the boundary conditions given by equations (22), (23), (24), (28), (29) and (30), constitute a general statement of the problem

of spherically symmetric phase growth. The problem is obviously formidable, despite the numerous assumptions and restrictions set forth above. In the present analysis the following additional simplifications, valid for conditions typical of nucleate boiling, are made:

(a) The viscous term in equation (10) is completely negligible for bubbles growing in ordinary liquids near their boiling points [11, 18, 26]. While it may be significant during the early stages of growth in a highly viscous liquid, it becomes vanishingly small as growth progresses [11]; hence it is omitted in the following.

(b) The inertia and surface tension terms in equation (10) are neglected, since they are significant only during the initial expansion of the original bubble nucleus [6, 11, 18, 26]. As the bubble grows, its growth rapidly becomes limited by the rate of arrival of volatile materials in the proper proportion and of the heat necessary for vaporization at the bubble surface.

(c) The inert gas term in equation (10) is ignored. This is permissible provided the boiling liquid is nearly free of dissolved gases; for then any small quantity of inert gas present in the original bubble nucleus becomes negligible compared to the material vaporized during growth.

(d) The heat source terms in equations (13) and (22) are set equal to zero. These terms are non-zero for a volume-heated system, but even when they are not zero, their influence on the later stages of bubble growth is usually negligible [6, 11, 18, 26].

From the additional simplifications (a)–(c) it follows that p_c *equals* p_∞ *throughout the motion*. For a one-component system the equilibrium boundary condition then reduces simply to $T(R, \theta) = T_{sat}$, a constant, while for a binary solution equation (29) yields directly a relation between liquid temperature and composition at the bubble surface; thus

$$C(R, \theta) = C_0 + [T(R, \theta) - T_{sat}]\left(\frac{\partial C}{\partial T}\right)_p \quad (31)$$

The accuracy of this linear approximation is diminished when the bubble surface temperature deviates greatly from the bulk saturation temperature. However, replacing equation (31) by a non-linear relation does not introduce undue complication. For a binary solution, it can be shown that*

$$\left(\frac{\partial C}{\partial T}\right) \cong -\frac{C_\infty L_1 [M_2 C_\infty + (\rho_L - C_\infty) M_1](1 + \alpha l)}{\rho_L R_g T_{sat}^2 (1 - \alpha)} \quad (32)$$

With simplification (c) and equation (30), the mass fraction of component 1 within the bubble is

$$m = \frac{C(R, \theta)}{C(R, \theta) + \alpha_s [\rho_L - C(R, \theta)]} \quad (33)$$

where α_s is the relative volatility at the bubble surface temperature.

For the present analysis the over-all energy and mass balance requirements are

$$\frac{4}{3}\pi R^3 \rho_G \{L + c_G [T(R, \theta) - T_0]\} + \rho_L c_L \int_R^\infty 4\pi r^2 [T(r, \theta) - T_0]\, dr = 0 \quad (34)$$

$$4\pi R^3 \rho_G (\rho_L - C_0) + \rho_L \int_R^\infty 4\pi r^2 [C(r, \theta) - C_0]\, dr = 0 \quad (35)$$

3. Growth Controlled by Heat Transfer

Initially the growth of the vapour nucleus depends very strongly on surface tension and the surrounding fluid, but in a *one-component system* the growth very quickly becomes limited by the rate at which latent heat of vaporization can be supplied at the bubble surface [6, 11, 18, 26]. Growth thereafter is governed by equations (13),

* In the derivation of equation (32) use is made of the Clausius–Clapeyron equation, and heat of mixing is neglected.

VOL. 10 1959

(20), (22), (28), (29), and (34). In terms of dimensionless temperature and parameters, these are conveniently transformed to

$$l = K\,(t_{rr} + 2r^{-1}\,t_r) - r^{-2}\,R^2\,\dot{R}\,t_r \tag{36}$$

$$t\,(r,\,0) = t\,(\infty,\,\theta) = 0 \tag{37}$$

$$t\,(R,\,\theta) = -\,\tau \tag{38}$$

$$t_r\,(R,\,\theta) = K^{-1}\,\dot{R}\,(\xi + \omega\nu\tau) \tag{39}$$

On dimensional grounds we assume as a solution $t\,(r,\,\theta) = t\,(s)$, and

$$r = 2\beta\sqrt{(K\theta)} \tag{40}$$

where

$$s = r/2\sqrt{(K\theta)} \tag{41}$$

Then equation (36) becomes

$$t_{ss} = 2t_s\,(-\,s - s^{-1} + \epsilon\,\beta^3\,s^{-2}) \tag{42}$$

which integrated once gives

$$t_s = As^{-2}\exp\,(-\,s^2 - 2\,\epsilon\,\beta^3\,s^{-1}) \tag{43}$$

and upon a second integration and application of equation (37) yields

$$t = -\,A\int_s^\infty x^{-2}\exp\,(-\,x^2 - 2\,\epsilon\,\beta^3\,x^{-1})\,dx \tag{44}$$

The constant of integration is evaluated using equation (39)

$$t = -\,(\xi + \omega\nu\tau)\,2\beta^3\exp\,(\beta^2 + 2\epsilon\beta^2)\int_s^\infty x^{-2}\exp\,(-\,x^2 - 2\epsilon\beta^3\,x^{-1})\,dx \tag{45}$$

The growth constant β is evaluated by means of equation (38):*

$$\frac{\tau}{\xi + \omega\nu\tau} = \phi\,(\epsilon,\,\beta) \equiv 2\beta^3\exp\,(\beta^3\exp\,(\beta^2 + 2\epsilon\beta^2)\int_\beta^\infty x^{-2}\exp\,(-\,x^2 - 2\epsilon\beta^3\,x^{-1})\,dx \tag{46}$$

* The analogous result for growth controlled by mass transfer (e.g., evolution of a gas bubble) is

$$\frac{\rho_L\,(C_\infty - C_{sat})}{\rho_G\,(\rho_L - C_{sat})} = \phi\,(\epsilon,\,\beta) \tag{46a}$$

in which case

$$r = 2\beta\sqrt{\mathcal{D}\,\theta} \tag{40a}$$

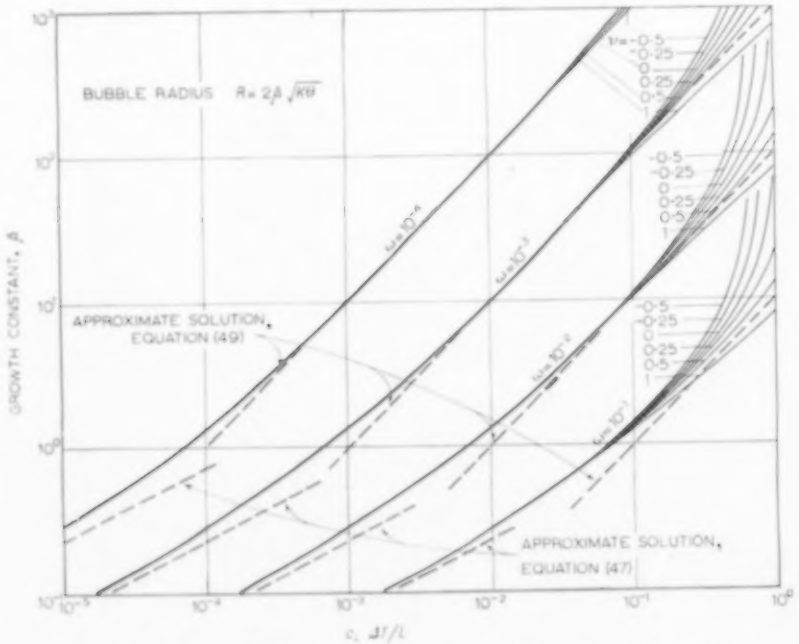

FIG. 1. Bubble growth in one-component systems. Equation (46).

Equations (45) and (46) are a particular solution of the differential equation ; together they satisfy all the boundary conditions and the conservation of energy requirement. Equation (46) may be solved by successive approximation for the growth rate constant β, given the degree of superheat and the requisite physical properties, or a plot of the equation as in Fig. 1 may be used. Figure 2 displays β for a typical case, bubble growth in

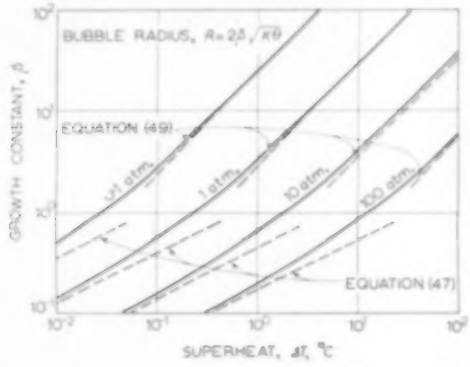

FIG. 2. Bubble growth in water. Equation (46).

superheated water at various pressures. In the Appendix it is demonstrated that for $\beta \to 0$ (e.g., small superheats), $\phi \to 2\beta^2$, whence

$$\beta = \sqrt{\left\{\frac{\Delta T}{2\left(\frac{\rho_G}{\rho_L}\right)\left[\frac{L}{c_L}+\left(\frac{c_L-c_G}{c_L}\right)\Delta T\right]}\right\}}, \quad \beta \to 0 \tag{47}$$

$$R = \sqrt{\left\{\frac{2\Delta T\, k\theta}{\rho_G\left[L+(c_L-c_G)\,\Delta T\right]}\right\}}, \quad \beta \to 0 \tag{48}$$

For larger β a good approximation is $\phi \cong \sqrt{(\pi/3)}\,\beta^3$, provided $\rho_G \ll \rho_L$ (see Appendix) ; in this case

$$\beta \cong \sqrt{\left(\frac{3}{\pi}\right)}\left\{\frac{\Delta T}{\left(\frac{\rho_G}{\rho_L}\right)\left[\frac{L}{c_L}+\left(\frac{c_L-c_G}{c_L}\right)\Delta T\right]}\right\}$$

$$\beta \gg 0, \quad \omega < 1 \tag{49}$$

$$R \cong 2\sqrt{\left(\frac{3}{\pi}\right)}\left\{\frac{\Delta T\sqrt{(\rho_L\, c_L\, k\theta)}}{\rho_G\left[L+(c_L-c_G)\,\Delta T\right]}\right\}$$

$$\beta \gg 0, \ \omega < 1 \tag{50}$$

Similar expressions have been proposed by PLESSET and ZWICK [18, 26] and FORSTER and ZUBER [6, 11] as approximate solutions for the entire range of β. From Fig. 1 and 2 it is seen that equation (49) is an accurate approximation only when $\rho_G \ll \rho_L$ and the dimensionless superheat $c_L\,\Delta T/L$ is sufficiently large.

If there is no change in density accompanying phase transition, i.e., $\rho_G/\rho_L = 1$ and $\epsilon = 0$, there is no convective motion in the system and the solution simplifies to

$$l = (\xi + \nu\tau)\,2\beta^2 e^{\beta^2}\left[\sqrt{(\pi)}\left\{\operatorname{erfc}(s) - s^{-1}e^{-s^2}i\right\}\right] \tag{51}$$

$$\frac{\tau}{\xi+\nu\tau} = \phi\,(0,\beta) \equiv 2\beta^2\left[1-\sqrt{(\pi)}\left\{\beta\, e^{\beta^2}\operatorname{erf} c(\beta)\right\}\right] \tag{52}$$

This result is essentially the same as that obtained by FRANK [8] and ZENER [24].

4. GROWTH CONTROLLED BY HEAT AND MASS TRANSFER

The treatment of the preceding section is easily extended to the growth of a vapour bubble in a *binary solution*. In addition to the set of equations considered there, the growth is also governed by equations (17), (21), (23), (24), (31), (33) and (35). In terms of dimensionless temperature, concentration, and parameters, these become

$$\dot{l} = K\,(t_{rr} + 2r^{-1}t_r) - \epsilon r^{-2}R^2\,\dot{R}\,t_r \tag{53}$$

$$t\,(r,0) = t\,(\infty,\theta) = 0 \tag{54}$$

$$t_r\,(R,\theta) = K^{-1}\,\dot{R}\left[\xi - \omega v t\,(R,\theta)\right] \tag{55}$$

$$\dot{c} = \mathscr{D}\,(c_{rr} + 2r^{-1}c_r) - \epsilon r^{-2}R^2\,\dot{R}\,c_r \tag{56}$$

$$c\,(r,0) = c\,(\infty,\theta) = 0 \tag{57}$$

$$c_r\,(R,\theta) = \mathscr{D}^{-1}\,\dot{R}\left[m\zeta - \omega - \omega c\,(R,\theta)\right] \tag{58}$$

$$c\,(R,\theta) = \mu t\,(R,\theta) + \mu\tau \tag{59}$$

$$m = \frac{\omega[\,1 + c\,(R,\theta)]}{\omega\left[1+c(R,\theta)\right] + \varkappa_s\left[\zeta - \omega - \omega c(R,\theta)\right]} \tag{60}$$

Particular solutions are obtained in the same manner as above ; thus

$$t = -\frac{\xi}{1-\omega\nu\phi\,(\epsilon,\beta)}\,2\beta^2 \exp(\beta^2 + 2\epsilon\beta^2)\int_s^\infty x^{-2}\exp(-x^2 - 2\epsilon\beta^3 x^{-1})\,dx \tag{61}$$

VOL. 10 1959

$$c = -\frac{m\zeta - \omega}{1 - \omega\phi(\epsilon, \lambda\beta)} 2\lambda^3\beta^3 \times \exp(\lambda^2\beta^2 + 2\epsilon\lambda^2\beta^2) \int_{\lambda s}^{\infty} x^{-2} \times \exp(-x^2 - 2\epsilon\lambda^3\beta^3 x^{-1})\, dx \quad (62)$$

The surface concentration is

$$c(R, \theta) = -(m\zeta - \omega)\,\psi(\epsilon, \lambda\beta);\ \psi(\epsilon, \lambda\beta) \equiv \frac{\phi(\epsilon, \lambda\beta)}{1 - \omega\phi(\epsilon, \lambda\beta)} \quad (63)$$

This result, with equation (60), leads to a quadratic equation for vapour composition m:

$$m^2\omega\zeta(1 - \alpha_s)\psi - m\left[\zeta(\alpha_s + \omega\psi) + \omega(1 - \alpha_s)(1 + \omega\psi)\right] + \omega(1 + \omega\psi) = 0 \quad (64)$$

These equations imply that vapour composition and surface concentration and temperature remain constant throughout the growth process.

The growth constant β is evaluated by means of equation (59)*

$$\tau = \frac{\xi\phi(\epsilon\ \beta)}{1 - \omega\phi(\epsilon, \beta)} + \frac{(\omega - m\zeta)\,\phi(\epsilon, \lambda\beta)}{\mu\left[1 - \omega\phi(\epsilon, \lambda\beta)\right]} \quad (65)$$

Actually equations (64) and (65) must be solved simultaneously for m and β.

It is evident, by comparison of equations (46) and (65), that the influence of mass transfer on bubble growth is represented by the second term of equation (65), which can be broken down into two factors

$$\frac{\phi(\epsilon, \lambda\beta)}{1 - \omega\phi(\epsilon, \lambda\beta)}$$

where $\lambda = \sqrt{(K/\mathscr{D})}$, and

$$\frac{\omega - m\zeta}{\mu} = -\frac{\rho_G(m\rho_L - C_\infty)}{\rho_L T_\infty (\partial C/\partial T)_p} \cong \frac{(m\rho_L - C_\infty)\rho_G R_g T_{sat}^2 (1 - \alpha)}{C_\infty L_1\left[M_2 C_\infty + (\rho_L - C_\infty) M_1\right] T_\infty (1 + \alpha l)} \quad (66)$$

where equation (32) has been used to obtain the latter. As expected, the lower the concentration of volatile material or the mass diffusivity, the greater is the superheat required to attain a given bubble growth constant. Equation (65) reduces to the heat transfer-controlling case for a one-component system or for infinite mass diffusivity of the solute.

From equation (65) and the limiting form of $\phi(\epsilon, \beta)$ there follows a simplification which is useful for small superheats:

$$\beta \cong \sqrt{\left\{\frac{\Delta T}{2\left(\frac{\rho_G}{\rho_L}\right)\left[\frac{L}{c_L} - \frac{(m\rho_L - C_\infty) K}{(\partial C/\partial T)_p \mathscr{D}}\right]}\right\}},\ \beta \to 0 \quad (67)$$

for equation (65), corresponding to which ψ in equation (64) is

$$\psi \cong \left(\frac{K}{\mathscr{D}}\right) \frac{\Delta T}{\left(\frac{\rho_G}{\rho_L}\right)\left[\frac{L}{c_L} \frac{(m\rho_L - C_\infty) K}{(\partial C/\partial T)_p \mathscr{D}}\right]},\ \beta \to 0 \quad (68)$$

Substituting equations (32) and (67) in equation (40) for bubble radius as a function of time, we obtain

$$R \cong \sqrt{\left\{\frac{2\Delta T\, k\, \theta}{\rho_G\left(L - \frac{k(m\rho_L - C_\infty) R_g T_{sat}^2 (1 - \alpha)}{\mathscr{D} C_\infty L_1\left[M_2 C_\infty + (\rho_L - C_\infty) M_1\right](1 + \alpha l)}\right)}\right\}},\ \beta \to 0 \quad (69)$$

Another set of simplified equations, useful for higher superheats, results from the approximation for $\beta > 0$ with $\rho_G < \rho_L$, i.e., from $\phi(\epsilon, \beta) \cong \sqrt{(\pi/3)}\,\beta$:

$$\beta \cong \sqrt{\left(\frac{3}{\pi}\right)}\left\{\frac{\Delta T}{(\rho_G/\rho_L)\left[L/c_L - (m\rho_L - C_\infty)\sqrt{(K/\mathscr{D})}/(\partial C/\partial T)_p\right]}\right\},\ \beta > 0,\ \omega < 1 \quad (70)$$

$$\psi \cong \sqrt{\left(\frac{K}{\mathscr{D}}\right)}\left\{\frac{\Delta T}{(\rho_G/\rho_L)\left[L/c_L - (m\rho_L - C_\infty)\sqrt{(K/\mathscr{D})}/(\partial C/\partial T)_p\right]}\right\},\ \beta > 0,\ \omega < 1 \quad (71)$$

In this case we have for bubble radius as a function of time

* The use a of a non-linear equilibrium relation in place of equations (31) and (59) merely results in a more unwieldy expression for β at equation (65).

$$R \cong 2\sqrt{\left(\frac{3}{\pi}\right)}\left\{\frac{\Delta T\sqrt{(\rho_L\, c_L\, k\theta)}}{\rho_G\left\{L + \frac{(m\rho_L - C_\infty)R_g\, T_{sat}{}^2\,(1-\alpha)}{C_\infty\, L_1\,[M_2\, C_\infty + (\rho_L - C_\infty)\, M_1]\,(1+\alpha l)}\sqrt{\left(\frac{\rho_L\, c_L k}{\mathscr{D}}\right)}\right\}}\right\} \tag{72}$$

Equations (70–(72) are valid neither at high pressures where the vapour density is no longer small compared with the density, nor at extremely high superheats.

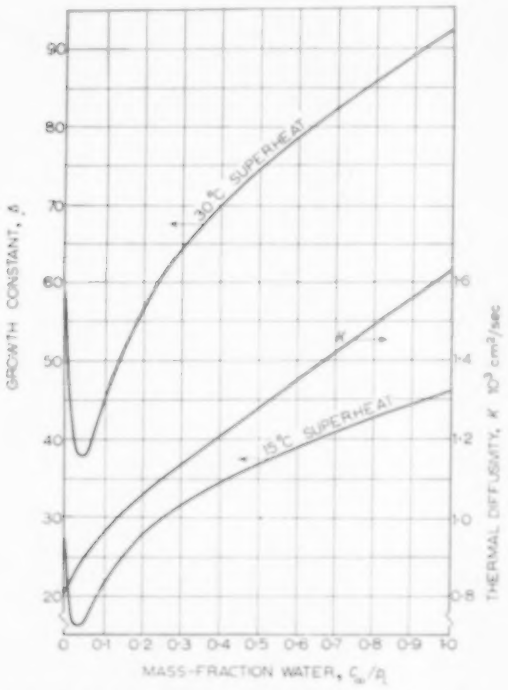

FIG. 3. Bubble growth in water–ethylene glycol solutions at 1 atm. Equations (32) and (70).

Figure 3 shows the dependence of the growth constant on liquid composition for a representative system, water–ethylene glycol, at atmospheric pressure. Fig. 3 is based on the above set of simplified equations and on equation (32). Water–ethylene glycol mixtures display very nearly ideal solution behaviour over their atmospheric boiling range, 100 to 197°C. The latent heats are about 540 and 225 cal/g, and the molecular weights are 18 and 62, respectively.

If one component of the binary mixture is non-volatile, say component 2, a further simplification can be made since the bubble then contains only component 1, $m \equiv 1$ ($\alpha \equiv 0$), and equation (64) can be dispensed with. Figure 4 shows the dependence of the growth constant on liquid composition and superheat for the system, water–glycerol, at atmospheric pressure. For Fig. 4 it is assumed that the glycerol is non-volatile.

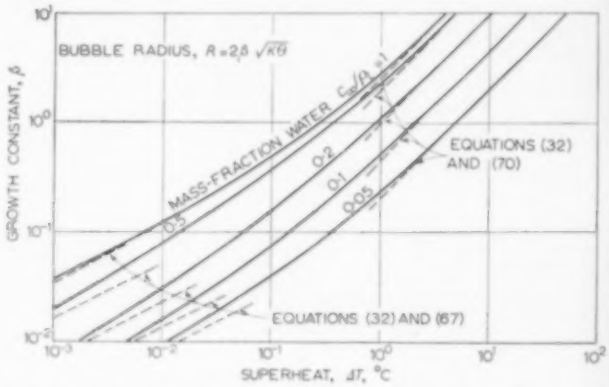

FIG. 4. Bubble growth in water–glycerol solutions at 1 atm. Equations (32) and (65).

If there is no change in density accompanying phase transition, i.e., $\epsilon = 0$, the solution simplifies to

$$t = \frac{\xi}{1 - \nu\phi\,(0,\beta)}\, 2\beta^3 e^{\beta^2}\left[\sqrt{(\pi)}\{\mathrm{erfc}(s) - s^{-1}e^{-s^2}\}\right] \tag{73}$$

$$c = \frac{m\zeta - 1}{1 - \phi\,(0,\lambda\beta)}\, 2\lambda^3\,\beta^3\, e^{\lambda^2\beta^2} \times \left[\sqrt{(\pi)}\,\mathrm{erfc}\,\{(\lambda s) - (\lambda s)^{-1}\, e^{-\lambda^2 s^2}\}\right] \tag{74}$$

$$\tau = \frac{\xi\phi\,(0,\beta)}{1 - \nu\phi\,(0,\beta)} + \frac{(1 - m\zeta)\,\phi(0,\lambda\beta)}{\mu\left[1 - \phi\,(0,\lambda\beta)\right]} \tag{75}$$

This result supersedes the less complete one reported by FRANK [8].

5. CONCLUDING REMARKS

Accurate asymptotic solutions, the first with radial convection accounted for, have been obtained for the problem of spherically symmetric phase growth. They apply to growth controlled by heat and mass transport, which is characterized

VOL. 10 1959

Table 1. *The function*

$\omega = 1 - \epsilon$

β \ ω	0	10^{-4}	$2{\cdot}5 \times 10^{-4}$	10^{-3}	$2{\cdot}5 \times 10^{-3}$	10^{-2}	$2{\cdot}5$
1×10^{-2}	0·0001965						
1·5	0·0004383						
2	0·0007726						
3	0·001709						
4	0·002987						
6	0·006504						
8	0·01120						
1×10^{-1}	0·01697						
1·5	0·03546						
2	0·05881						
3	0·1166						
4	0·1850						
6	0·3420						
8	0·5152						
1×10^{0}	0·6977			0·6974	0·6970	0·6950	
1·5	1·175			1·174	1·173	1·167	
2	1·668			1·666	1·664	1·651	
3	2·671			2·666	2·660	2·628	
4	3·683			3·675	3·662	3·601	
6	5·719			5·698	5·668	5·521	
8	7·760			7·722	7·666	7·397	
1×10^{1}	9·803	9·797	9·788	9·743	9·654	9·228	
1·5	14·91	14·90	14·88	14·78	14·57	13·61	1
2	20·03	20·00	19·97	19·78	19·41	17·72	1
3	30·26	30·20	30·11	29·69	28·86	25·23	1
4	40·49	40·39	40·23	39·47	38·02	31·88	2
6	60·96	60·72	60·37	58·67	55·48	43·02	2
8	81·42	81·00	80·38	77·38	71·87	54·90	3
1×10^{2}	101·9	101·2	100·3	95·61	87·28	59·65	3
1·5	153·1	151·6	149·4	139·2	121·9	71·65	3
2	204·2	201·6	197·8	180·2	151·7	79·53	3
3	306·6	300·7	292·2	254·8	199·9	88·20	3
4	408·9	398·5	383·6	321·0	236·5	92·48	3
6	613·6	590·3	558·0	431·9	286·8	96·27	3
8	818·2	777·3	721·7	520·3	318·2	97·80	3
∞	∞	10,000	4,000	1,000	400	100	4

ion $\phi(\epsilon, \beta)$

$2{\cdot}5 \times 10^{-2}$	10^{-1}	$2{\cdot}5 \times 10^{-1}$	$7{\cdot}5 \times 10^{-1}$	9×10^{-1}	1
	0·0001965	0·0001965	0·0001965	0·0001965	0·0001965
	0·0004383	0·0004383	0·0004383	0·0004382	0·0004382
	0·0007725	0·0007724	0·0007723	0·0007723	0·0007723
	0·001709	0·001709	0·001708	0·001707	0·001707
	0·002987	0·002986	0·002984	0·002983	0·002983
	0·006503	0·006500	0·006489	0·006485	0·006483
	0·01120	0·01119	0·01115	0·01114	0·01114
	0·01695	0·01693	0·01684	0·01684	0·01682
	0·03539	0·03530	0·03497	0·03488	0·03482
	0·05864	0·05837	0·05748	0·05723	0·05706
	0·1159	0·1148	0·1114	0·1104	0·1097
	0·1832	0·1805	0·1719	0·1694	0·1678
	0·3357	0·3264	0·2981	0·2903	0·2852
	0·5066	0·4797	0·4186	0·4025	0·3923
0·6908	0·6706	0·6328	0·5273	0·5068	0·4842
1·155	1·098	0·9959	0·7428	0·6864	0·6525
1·627	1·513	1·320	0·8921	0·8067	0·7572
2·565	2·285	1·851	1·069	0·9392	0·8673
3·483	2·975	2·255	1·162	1·003	0·9184
5·244	4·137	2·806	1·247	1·059	0·9610
6·901	5·062	3·146	1·282	1·080	0·9774
8·459	5·805	3·366	1·300	1·091	0·9854
11·96	7·110	3·659	1·318	1·102	0·9934
14·98	7·921	3·791	1·325	1·106	0·9962
19·86	8·808	3·900	1·329	1·109	0·9983
23·55	9·242	3·942	1·331	1·110	0·9991
28·62	9·625	3·974	1·332	1·111	0·9996
31·79	9·780	3·985	1·333	1·111	0·9998
33·86	9·850	3·990	1·333	1·111	0·9998
36·65	9·933	3·996	1·333	1·111	0·9999
37·94	9·962	3·998	1·333	1·111	1·000
39·01	9·983	3·999	1·333	1·111	1·000
39·42	9·991	3·999	1·333	1·111	1·000
39·74	9·996	4·000	1·333	1·111	1·000
39·85	9·998	4·000	1·333	1·111	1·000
40	10	4	4/3	10/9	1

by uniform pressure throughout the system and by position of the phase boundary asymptotically proportional to the square root of time. The dependence of the proportionality constant on several system parameters is complicated. For bubble growth in pure liquids at normal pressures and moderate superheats, the formula of FORSTER and ZUBER [6, 11] is in fair agreement and that of PLESSET and ZWICK [18, 26] is in substantial agreement not only with equations (40) and (46) above, but also with the published experiments of DERGARABEDIAN (see [6, 18]) and of FANEUFF *et al.* [5] with superheated water. From the new solutions it appears, however, that for small superheats and for large vapour densities the earlier approximate formulae are in considerable error; the latter give, for example, values of the growth constant about 50 per cent lower for water superheated 0·1°C at atmospheric pressure or 10°C at 100 atm. In order to confirm the new theoretical results, measurements of bubble growth are needed in pure liquids at extreme conditions, particularly at high pressures, and especially in liquid mixtures.

Acknowledgement—The author is indebted to C. V. STERNLING and C. H. BARKELEW for critical advice.

APPENDIX

The function $\phi(\epsilon, \beta)$ is defined in equation (46):

$$\phi(\epsilon, \beta) = 2\beta^3 \exp(\beta^2 + 2\epsilon\beta^2) \int_{\beta}^{\infty} x^{-2} \exp(-x^2 - 2\epsilon\beta^2 x^{-1})\, dx$$

The change of variable $y = 1 - \beta x^{-1}$ leads to a form more convenient for numerical evaluation,

$$\phi(\epsilon, \beta) = 2\beta^2 \int_0^1 \exp\{-\beta^2[(1-y)^{-2} - 2\epsilon y - 1]\}\, dy$$

The function can be expressed as a series, which is particularly convenient for small values of β:

$$\phi(\epsilon, \beta) = 2\beta^2 e^{2\epsilon\beta^2} \sum_{n=0}^{\infty} \frac{(-1)^n (2\epsilon\beta^2)^n}{(n+1)!} I_n$$

$$I_0 = 1 - \sqrt{(\pi)}\,(\beta\, e^{\beta^2}\,\mathrm{erfc})\,(\beta)$$

$$I_1 = 1 + \beta\, e^{\beta^2}\, Ei(-\beta^2)$$

$$I_n = 1 - 2\frac{n+1}{n-1}\beta^2 I_{n-2}$$

Thus

$$\lim_{\beta \to 0} \phi(\epsilon, \beta) = 2\beta^2 - 0(\beta^3)$$

For large values of β the principal contribution to the integral is in the neighbourhood of $x = \beta$; hence the saddle point method can be used to obtain an asymptotic form:

$$\phi(\epsilon, \beta) \sim \sqrt{(\pi/3)}\,[\beta\, e^{\omega^3\beta^3/3}\,\mathrm{erfc}(\omega\beta/\sqrt{3})], \quad \omega = 1 - \epsilon$$

$$\sim \frac{1}{\omega}\left[1 - \frac{3}{2\omega^2\beta^2} + 0(\omega^{-4}\beta^{-4})\right]$$

A useful expression results from an asymptotic expansion of $\phi(1, \beta)$:

$$\phi(1, \beta) \sim \sqrt{(\pi/3)}\,[\beta - 4/9 + 0(\beta^{-1})]$$

This provides a reasonably accurate approximation for $\phi(\epsilon, \beta)$ provided ϵ is not too different from unity and β is large but not too large (see Fig. 5).

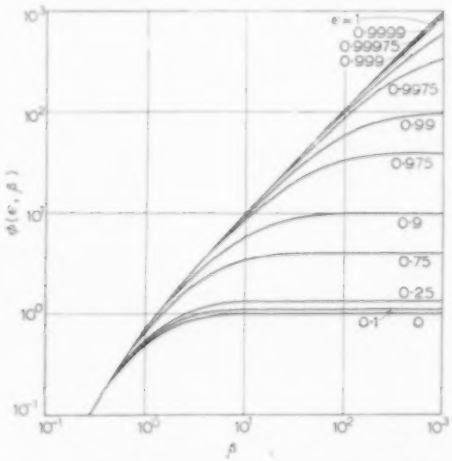

Fig. 5. The function $\phi(\epsilon, \beta)$. Equation (46).

For a given value of ϵ there is a broad intermediate range of β over which neither the series nor asymptotic representations are convenient for evaluating ϕ, which must then be computed by numerical quadrature. Machine computations have been performed for values spanning the range of potential application; the results are presented in Table 1 and Fig. 5.

NOTATION

(*Dimensions in the* MLØTH *system*)

A = constant of integration, dimensionless
$c = (C - C_\infty)/C_\infty$, reduced concentration, dimensionless
= (with subscript) specific heat $[HM^{-1}T^{-1}]$
C = mass concentration $[ML^{-3}]$
D = substantial derivative operator

$\mathscr{D}$ = mass diffusivity $[L^2\theta^{-1}]$
E = internal energy $[HM^{-1}]$
$\boldsymbol{F}$ = vector body force per unit mass $[L\theta^{-2}]$
h = liquid enthalpy $[HM^{-1}]$
H = vapour enthalpy $[HM^{-1}]$
$\boldsymbol{j}$ = vector mass flux $[ML^{-2}\theta^{-1}]$
J = rate of chemical reaction $[ML^{-3}\theta^{-1}]$
k = thermal conductivity $[HL^{-1}\theta^{-1}T^{-1}]$
K = thermal diffusivity $[L^2\theta^{-1}]$
$l = L_2(\rho_L - C_\infty)/L_1 C_\infty$, dimensionless
L = latent heat of vaporization $[HM^{-1}]$
m = mass fraction in vapour, dimensionless
M = molecular weight $[M(\text{mole})^{-1}]$
p_i = partial pressure of inert gas $[ML^{-1}\theta^{-2}]$
p_{rr} = radial component of radial stress $[ML^{-1}\theta^{-2}]$
p_v = partial pressure of volatiles $[ML^{-1}\theta^{-2}]$
p_∞ = ambient pressure $[ML^{-1}\theta^{-2}]$
P = vapour pressure $[ML^{-1}\theta^{-2}]$
$\boldsymbol{q}$ = vector energy flux $[HL^{-2}\theta^{-1}]$
Q = heat generation per unit volume $[HL^{-3}\theta^{-1}]$
r = radial co-ordinate $[L]$
R = bubble radius $[L]$
R_g = gas constant $[HT^{-1}(\text{mole})^{-1}]$
$s = r/2\sqrt{(K\theta)}$, dimensionless co-ordinate
$t = (T - T_\infty)/T_\infty$, reduced temperature, dimensionless
T = temperature $[T]$
u = radial velocity $[L\theta^{-1}]$
U = vapour internal energy $[HM^{-1}]$
$\boldsymbol{V}$ = vector velocity $[L\theta^{-1}]$
$\alpha = \gamma_2 P_2/\gamma_1 P_1$, relative volatility, dimensionless
β = growth constant, dimensionless
γ = activity coefficient, dimensionless
$\Delta T = T_\infty - T_{sat}$ $[T]$
$\epsilon = 1 - \rho_G/\rho_L$, dimensionless
$\zeta = \rho_G/C_\infty$, dimensionless
η = kinematic viscosity $[L^2\theta^{-1}]$
θ = time co-ordinate $[\theta]$
$\lambda = \sqrt{(K/\mathscr{D})}$, dimensionless
$\mu = (\partial c/\partial)_p$, dimensionless
$\nu = (c_L - c_G)/c_L$, dimensionless
$\xi = \rho_G L/\rho_L c_L T_\infty$, dimensionless
π = pressure tensor $[ML^{-1}\theta^{-2}]$
ρ = density $[ML^{-3}]$
σ = surface tension $[M\theta^{-2}]$
$\tau = (T_\infty - T_{sat})/T_\infty$, dimensionless
ϕ = function defined by equation (46), dimensionless
ψ = function defined by equation (63), dimensionless
$\omega = 1 - \epsilon = \rho_G/\rho_L$, dimensionless

Subscripts

0 = initial value
∞ = value at large r
s = value at R
sat = value at saturation
G = gas
L = liquid
1 = solute
2 = solvent

Overbar indicates a mass average

References

[1] Bird R. B. Theory of Diffusion, Chapter in *Advances in Chemical Engineering*, Vol. 1. Academic Press, New York 1956.

[2] Bird R. B. *Chem. Engng. Sci.* 1957 **6** 123.

[3] Chambré P. L. *Quart. J. Mech.* 1956 **9** 224.

[4] Epstein P. S. and Plesset M.S. *J. Chem. Phys.* 1950 **18** 1505.

[5] Faneuff C. E., McLean E. A. and Scherrer V. E. *J. Appl. Phys.* 1958 **29** 80.

[6] Forster H. K. and Zuber N. *J. Appl. Phys.* 1954 **25** 474, 1067.

[7] Forster H. K. and Zuber N. *Amer. Inst. Chem. Engrs. J.* 1955 **1** 531.

[8] Frank F. C. *Proc. Roy. Soc.* 1950 **A201** 586.

[9] Geist D. *Proc. Phys. Soc.* 1951 **A64** 208.

[10] Goldstein S. *Modern Developments in Fluid Dynamics*, Vol. 1. Clarendon Press, Oxford 1938.

[11] Greenfield M. L., Lipkis R. L., Liu C. and Zuber N. *A.E.C.U.-2950* Technical Information Service, U.S. Atomic Energy Commission, Oak Ridge, Tenn. 1954.

[12] Huber A. Z. *Angew. Math. Mech.* 1939 **19** 1 (summary of Rieck's analysis).

[13] Kolodner I. I. *Commun. Pure Appl. Math.* 1956 **9** 1.

[14] Lipkis R. P., Liu C. and Zuber N. *Chem. Engng. Progr. Symp. Ser. No.* 18 1956 **52** 105.

[15] Luborsky F. E. *J. Phys. Chem.* 1957 **61** 1336.

[16] Plesset M. S. *J. Appl. Mech.* 1949 **16** 277.

[17] Plesset M. S. and Zwick S. A. *J. Appl. Phys.* 1952 **23** 95.

[18] Plesset M. S. and Zwick S. A. *J. Appl. Phys.* 1954 **25** 493.

[19] Poritsky H. *Proc. First U.S. Nat. Congr. Appl. Mech.* (*Amer. Soc. Mech. Engrs.*) 1951 813.

[20] Reiss H. and La Mer V. K. *J. Chem. Phys.* 1950 **18** 1.

[21] Sestini G. *Riv. Mat. Univ. Parma* 1955 **3** 3, 103.

[22] Sternling C. V. unpublished notes, Shell Development Company, 1954.

[23] Westwater J. W. Boiling of Liquids. Chapter in *Advances in Chemical Engineering*, Vol. I. Academic Press, New York 1956.

[24] Zener C. *J. Appl. Phys.* 1949 **20** 950.

[25] Zuber N. *Amer. Inst. Chem. Engrs. J.* 1957 **3** 3, 98 (communication to the editor).

[26] Zwick S. A. *Hydrodynamics Lab. Rep. No.* 21-19 Californian Institute of Technology, Pasadena 1954.

Chemical Engineering Science, 1959, Vol. 10, pp. 14 to 21. Pergamon Press Ltd. London. Printed in Great Britain

The frequency response of some illustrative models of porous media

Experiments and computations with two artificial packed beds to illustrate a method of determining parameters of the bed

G. A. Turner

Chemical Engineering Department, College of Science and Technology, and the University, Manchester

(*Received* 23 *May* 1958)

Abstract—This paper amplifies and extends a previous one in which a method was put forward of determining the flow structure or physical structure of any given packed bed or porous solid.

The measured harmonic response of physical models similar to the postulated ones is reported ; as an illustration of the method, these results are used for the calculation of a distribution of some appropriate parameter of the (artificial) bed. The calculated quantities were reasonably close to the actual ones.

The demands and the limitations of the method are pointed out.

Résumé—Dans un article précédent l'auteur a donné une méthod pour la détermination du mode d'écoulment, ou la structure physique d'un garnissage quelconque ou d'un solide poreux.

Il a mesuré la réponse harmonique de modèles physiques analogues à ceux du Ier article. Afin d'illustrer la méthode l'auteur utilise ces résultats pour le calcul de la répartition de paramètres appropriés au lit artificiel de garnissage. Les valeurs calculées concordent assez bien avec les valeurs réeells.

Exigences et restrictions de la méthode sont mises en évidence.

Zusammenfassung—Diese Arbeit ist die Fortsetzung und Erweiterung einer früheren [1], in der eine Methode mitgeteilt war, um das Strömungs oder das physikalische Verhalten eines gegebenen Festbettes oder porösen Körpers zu bestimmen.

Das gemessene harmonische Verhalten physikalischer Modelle, die den verlangten ähnlich sind, wird beschrieben ; zur Illustration der Methode werden Verteilungen einiger geeigneter Parameter des (künstlichen) Bettes berechnet. Die berechneten Grössen stimmen vernünftig mit den wirklichen überein.

Voraussetzungen und Grenzen der Methode werden diskutiert.

Introduction

In an earlier paper [1] a method is given whereby the flow structure or physical structure of a packed bed or porous medium may be analysed in terms of models chosen to be representative of the bed and to allow mathematical analysis of their frequency response. Linear simultaneous equations have to be solved, whose roots give the distribution by volume of some parameter of the bed ; the parameters of the two models of [1] were depth of pocket and length of channel respectively. The roots can be calculated if the coefficients of the equations are known ; this paper describes a method of obtaining these coefficients – by trial – and, by way of illustration, quotes the results obtained by experiments on physical models which closely resembled the postulated ones.

The Coefficients*

In [1] the linear simultaneous equations (19.1) to (19.n), relating to model 1, are

*Symbols are explained in [1].

coupled with the statement that "the values of β_r corresponding to $l_r\,(r = 1 \ldots n)$ may be found by setting up the determinants of the coefficients." This is of course true, but presupposes that the coefficients, and hence values of l_r, be known. The latter may be found, directly if the geometry of the system be known, or by a method, to be described, which enables values of l_r to be chosen such that at least a rough picture of the distribution is provided. The following argument, involving β, will also apply to the equations associated with model 2 of ref. [1] involving ϵ, viz. $\sum^{r} \eta_r\, \epsilon_{jr} = \mu_j$; both β and ϵ are ratios of volumes.

Let it be desired to find values of the distribution β of some property of the bed defined by a length l_r, namely depth of pocket or length of channel in models 1 or 2 respectively. If r ranges from 1 to n then the $2n$ quantities l_r, β_r require $2n$ equations all told, i.e.,

$$\eta_{11}\,\beta_1 + \ldots\ldots + \eta_{1n}\,\beta_n = \mu_1 \qquad (1.1)$$

$$\eta_{2n\,1}\,\beta_1 + \ldots\ldots + \eta_{2n\,n}\,\beta_n = \mu_{2n}, \qquad (1.2n)$$

in each of which the constant term μ is known (experimentally) at any given value of the angular frequency ω_j. Neither η nor β is known in any of these equations but the coefficients $\eta = f(\omega_j, l_r)$ are such that the choosing of n values of l_r to put numerical values on η_{11} to η_{1n} will also put numerical values on the rest of the coefficients η for the particular values of ω_j already stipulated; that is to say since $\eta = f(\omega, l)$ then $\eta_{jr} = F(\eta_{1r}, \omega)$. The numerical values of η are calculated from analytical response functions exemplified in [1].

Now a condition that n roots can be found for $\beta_1 \ldots \beta_n$ is given by the eliminant: if the first n equations are taken and combined with the $(n+1)$ th, $(n+2)$ th $\ldots$, $2n$th equation in turn then altogether n independent eliminants exist, which means that n relations can be written down, each involving the coefficients and the constant terms of the first n equations together with the coefficients and the constant term of one of the remaining equations (numbered $n+1$ to $2n$). All the μ's are known experimentally, and if n values of l_r are chosen then all the $\eta_{jr}\,(j = 1 \ldots 2n : r = 1 \ldots n)$ may be calculated; the problem is to choose values of l_r which allow these n eliminants to be satisfied simultaneously. In the examples given in [1], the relationship between the coefficients $\eta_{jr}\,(j = 1 \ldots 2n, r = \text{constant})$ is such that the choice must be made by trial and error.

The total relative volume may be found independently of the above computation. For model 2 the total voidage $\bar{\epsilon} = \sum \epsilon_r$ and can be measured with more or less accuracy. For model 1 $\bar{\beta} = \sum \beta_r$ and is the ratio of the total volume of pockets to the total volume of the channels. The volume of the channels may be found either by one of the methods mentioned in [1] p. 162 or, if apparatus for generating and measuring impulsive inputs of concentration is available, by arranging conditions in the channel so that flow is laminar and the effect of diffusion is small (the pockets then have little effect on the distribution of concentration) and using an impulse. If t is the time at which the output concentration falls to half its maximum value (see TAYLOR [4]), when the volumetric flow-rate is V, the total volume of the channels is given by Vt and the total volume of the pockets (for this flow regime) is given by the difference between this volume and the total void volume.

The above physical condition can be written in place of (say) the nth equation so that set of equations becomes

$$\eta_{11}\,\beta_1 + \ldots\ldots + \eta_{1n}\,\beta_n = \mu_1 \qquad (2.1)$$

$$\ldots\ldots\ldots\ldots\ldots$$

$$\eta_{n-1\,1}\,\beta_1 + \ldots\ldots + \eta_{n-1\,n}\,\beta_n = \mu_{n-1} \qquad (2.n-1)$$

$$\beta_1 + \ldots\ldots + \beta_n = \bar{\beta} \qquad (2.n)$$

$$\ldots\ldots\ldots\ldots\ldots$$

$$\eta_{2n\,1}\,\beta_1 + \ldots\ldots + \eta_{2n\,n}\,\beta_n = \mu_{2n} \qquad (2.2n)$$

and the eliminant is simplified somewhat, becoming

$$\Delta \equiv \begin{vmatrix} \eta_{11} & \ldots & \eta_{1n} & \mu_1 \\ \eta_{n-1\,1} & \ldots & \eta_{n-1\,1} & \mu_{n-1} \\ \eta_{p1} & \ldots & \eta_{pn} & \mu_p \\ 1 & \ldots & 1 & \bar{\beta} \end{vmatrix} = 0 \;(p = (n+1) \ldots 2n)$$

A further value μ_{2n+1} will yield an equation which will not, in general, be consistent with the previous equations; the inconsistency will be most probably due to experimental errors in μ and cannot be used to disprove the assumption of exactly n values of l_r. (For a discussion of the simultaneous equations met with in an experimental science see, for example, LANCZOS [8]).

If n becomes infinite there arises the integral equation $\int_0^\infty \beta(l)\,\eta(l, \omega')\,dl = \mu(\omega')$, where $\beta(l)$ is the relative volume of pockets of length between $(l - \frac{1}{2}dl)$ and $(l + \frac{1}{2}dl)$ and $\eta(l, \omega') = Q(2l\omega')/2l\omega'$.

To test the method physical models resembling the postulated ones were made; their dimensions were known, but the method was applied as if it were required to determine them experimentally. The results are reported below.

EXPERIMENTAL

(*a*) *Apparatus*

Kerosene containing nitrobenzene in sinusoidal concentration flowed steadily through the model under test, at such a rate that the flow was laminar and that all conditions specified elsewhere were satisfied. Analysis of concentration was by the change in dielectric constant.

The liquid flowed through inlet and outlet cells, of $\frac{1}{4}$ in. bore tube, $2\frac{1}{4}$ in. long, having a central insulated electrode $\frac{1}{8}$ in. diam. The change in capacitance was measured and recorded. The meter reading varied linearly with all concentration above 8 per cent (w/w) and both bridges gave the same meter reading for the same concentration; the recorded values were thus used as direct measures of the concentration. The sinusoidal concentration was generated by suspending two similar capillary tubes C, one at each end, from a beam D pivoted at its centre (Fig. 1). Liquid flowed from each of two Marriotte bottles A, containing solutions of different concentrations, through its connected capillary via a flexible tube B. The beam was rocked about its central shaft by a crank F (driven by a synchronous electric motor), connected to it by a long connecting rod F, so that the head of each liquid varied sinusoidally. By means of the Hagen-Poiseuille law and the assumption of constant viscosity it can easily be shown that, with this device, the total flow-rate is constant and that the output concentration is truly sinusoidal. Thus it contrasts in both respects with the method whereby a solution is injected at a sinusoidally varying rate into a steady stream of liquid, a method which produces harmonics. Furthermore, concentrated solutions are not required by the generator used in this work.

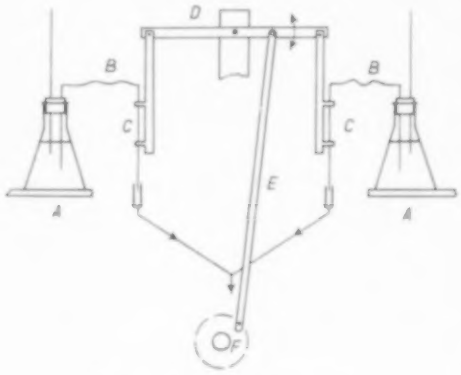

FIG. 1. Sine-wave generator.

The physical models (1). The channel was a narrow rectangular slit (dimensions below) and rows of blind holes, $\frac{3}{32}$ in. diam. and of three different depths, communicated with it along its length, as shown in Fig. 3.

(2). Two identical headers were coupled to precision-bore glass capillary-tubes; there were two different tube diameters in all and three different lengths of tube for each diameter.

(*b*) *Procedure*

Since these experiments were considered to be exploratory no special effort was made to keep the temperature constant; in any case, the temperature-dependence of the dielectric constant of these solutions was small – much less than that of electrolytic conductivity, for example.

When either model was in use the flow-rate was kept constant and measured by measuring-vessel and stop-watch. The attenuation and phase angle were measured at a number of different frequencies.

The portion of the total response which was due to headers and measuring cells was found. The cells (model 1) or headers and cells (model 2) were detached from the appropriate system and connected together by short tubes; their responses were found at the same frequencies and flow-rates as obtained in the main experiments.

The system is linear and hence the response of the whole is the product of the responses of its parts; the fact that

the transfer functions are complex means that the magnitude of the resulting transfer function is the product of those of its parts and that its phase-angle is the sum of those of its parts. Hence, if E is a ratio of (absolute) amplitudes and ϕ a phase-angle (subscripts identifying the component, as in Fig. 2),

$$E_A = E_1 E_2 E_3,$$
$$E_B = E_1 E_3.$$

Therefore $E_2 = \dfrac{E_A}{E_B}$.

Again, $\phi_A = \phi_1 + \phi_2 + \phi_3$,

$$\phi_B = \phi_1 + \phi_3.$$

Therefore $\phi_2 = \phi_A - \phi_B$.

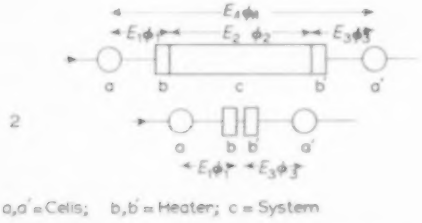

FIG. 2. Method of correcting for response of headers and cells.
(1) Complete system
(2) Headers and cells connected together

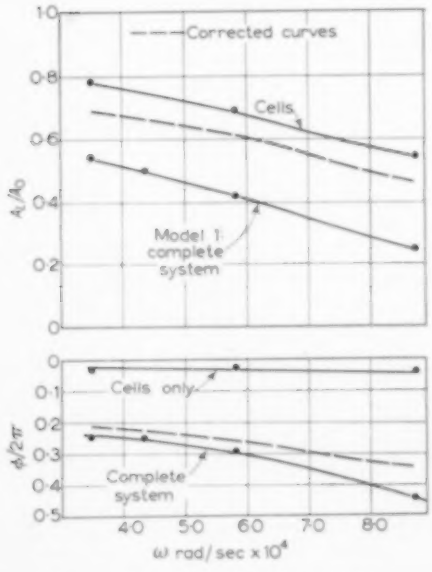

FIG. 3. Response curves of model 1.

Measured and corrected values of amplitude ratio and phase-angle are given in Figs. 3 and 4.

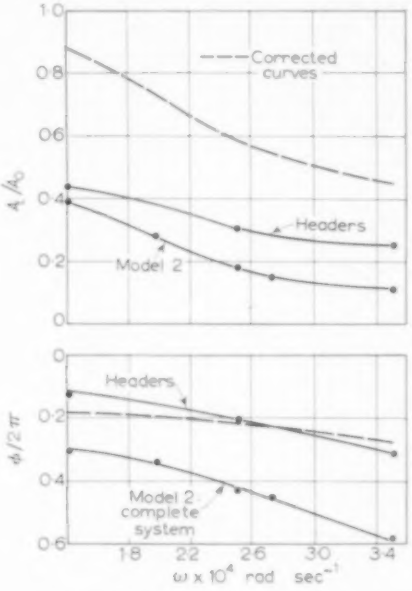

FIG. 4. Response curves of model 2.

CALCULATIONS

For model 1 the effective longitudinal diffusivity $\bar{D}$ in the narrow channel must be calculated. An expression for this may be obtained in a way based on the method reported by TAYLOR [2] in dealing with flow in a circular capillary; the equations are of exactly the same form, only numerical quantities being different. The expression is:

$$\bar{D} = D + \frac{2}{105}\frac{b^2\bar{U}^2}{D}, \qquad (2)$$

where

$\bar{U}$ = average velocity in the channel, D = molecular diffusivity and $2b$ = defined in Fig. 5; provided

$$4\frac{l}{b} > \frac{b\bar{U}}{D} > 7{\cdot}3, \qquad (3)$$

where l is the length of channel containing the change in concentration.

The above analysis is based on the assumption that the velocity distribution in the channel is the same as that between two infinitely wide flat plates. This is nearly true here, for, if the expression given by ALLEN [3] (quoting CORNISH) be used, it is found that, b/a being

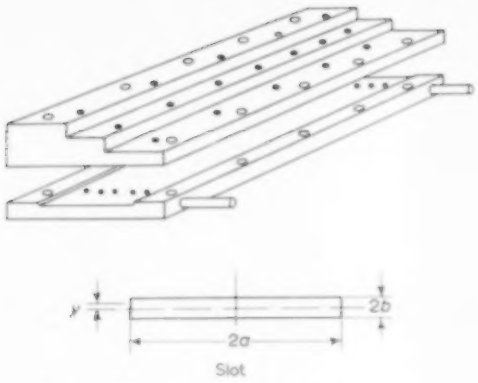

FIG. 5. Constructional details of model 1.

equal to 45, $\frac{U_0}{\overline{U}} = 1{\cdot}014\left(\frac{3}{2}\right)$, whilst for infinite flat plates $\frac{U_0}{\overline{U}} = \frac{3}{2}$, and $\frac{U}{U_0} = \left[1 - \left(\frac{y}{b}\right)^2\right]$, where U_0 = maximum velocity and $\overline{U}$ = mean velocity in the channel, and U = velocity at distance y from the long axis (Fig. 5).

Again, the theory postulates that the concentration be uniform across the channel, normal to the flow. Diffusion in the b direction (Fig. 5) will make it so if condition (3) holds ; it is necessary to find whether it is reasonably uniform in the a direction. It is assumed that area $e\,f\,g\,h$ (Fig. 6 – to scale) has concentration C_0 at $t = 0$. If the logic of TAYLOR [4] be applied it is found that the time necessary for the concentration at $x = 0$ to fall by half its value is given by t, such that $\text{erf}\, 1/2\sqrt{(Dt/h^2)} = \frac{1}{2}$, provided that $2\sqrt{(Dt/h^2)} < 3$. Hence $t = 1{\cdot}09\,h^2/D$. Now the conditions desired (cf. TAYLOR) is that the time of decay, t, is less than the time in which effects of convective transport appear ; that is, the time in which the concentration would change due to its flow down the channel and it seems logical to take this as half the cycle-time, T. Thus the condition for the actual case to approximate to the postulated one is that $T > 2\left(1{\cdot}09\,\frac{h^2}{D}\right)$. Derived from numerical quantities, the condition is that $T > 2{\cdot}14$ hr,

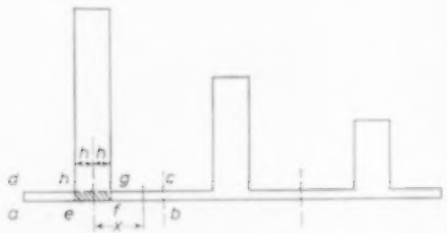

FIG. 6. Cross-section of model 1 (to scale).

and this was satisfied in the experiments but only by a small margin.

Another condition to be satisfied for model 1 is that $2\omega' l < 10$, otherwise the sine-waves do not penetrate to the bottom of the pocket [5] [6].

It is necessary to find lengths and radii of tubes for model 2 which allow the effective longitudinal diffusivity to be calculated by TAYLOR's treatment [2]. They can be found by using the conditions stipulated in that paper, together with the condition obtained from Fig. 3 of KRAMERS and ALBERDA [7] – this refers to flow without diffusion but it should give the order of magnitude. It is that, for $E < 0{\cdot}8$ (say), $L/\overline{U} > 1{\cdot}8/\omega$. TAYLOR's conditions involve a length of tube " in which the greater part of the change in concentration takes place." Here this length is identified with half a wavelength ($= 2\pi\,\overline{U}/\omega$) If ratios of 10 : 1 in TAYLOR's inequalities and 1 : 1 in the condition derived from KRAMERS and ALBERDA be used and if the Hagen-Poiseuille law be introduced then elimination of ω gives the conditions

$$L > (\tfrac{1}{4}\sqrt{gp/\pi\mu\, D})\, R^2 \qquad (4)$$

and

$$L < (gp/552\,\mu\, D)\, R^3 \qquad (5)$$

A convenient value of p and appropriate values for the other variables enable the limits of length for a given value of the radius to be found.

RESULTS

For both models ; $\mu = 1{\cdot}323$ cp, D (mean of eight) $= 4 \times 10^{-6}$ cm^2/sec, $\rho = 0{\cdot}822$ gm/cm^3.

Model 1.

In order that (2) may be used to calculate the effective longitudinal diffusivity, the inequalities given by (3) must be satisfied. Here the conditions are $l > 5{\cdot}8$ cm ; $\overline{U} > 9{\cdot}2 \times 10^{-3}$ cm/sec, corresponding to $V > 6$ cm^3/hr. In the experiments, $V = 6$ cm^3/hr ; $l = 33$ cm at the highest frequency used.

$L = 27{\cdot}94$ cm, $2a = 2{\cdot}8575$ cm, $2b = 0{\cdot}0635$ cm, V (measured) $= 6$ cm^3/hr, $\overline{D} = 4{\cdot}045 \times 10^{-4}$ cm^2/sec, $\beta = 0{\cdot}8716$.

Since $F^* = \left(\frac{S^* + F^*}{2}\right) - \left(\frac{S^* - F^*}{2}\right)$ it follows from equations (17) and (18) in [1] that

$$\sum \beta_r = \frac{(\ln E/L)^2 - 2\,(U/2\overline{D})\ln E/L - (\phi_L/L)^2}{\omega_j/\overline{D}}$$

Substitution of the above quantities gives the results in Table 1.

Table 1.

j	ω_j rad/sec $\times 10^4$	ω_j'	$\sum \beta\,(Q/\sigma)$
1	3·491	13·20	0·3469
2	4·364	14·76	0·3202
3	5·8185	17·06	0·2741

Calculations

The four equations

$$\left.\begin{aligned} 0{\cdot}3469 &= (Q/\sigma)_{11}\,\beta_1 + (Q/\sigma)_{12}\,\beta_2, \\ 0{\cdot}3207 &= (Q/\sigma)_{21}\,\beta_1 + (Q/\sigma)_{22}\,\beta_2, \\ 0{\cdot}2741 &= (Q/\sigma)_{31}\,\beta_1 + (Q/\sigma)_{32}\,\beta_2, \end{aligned}\right\} \quad (11)$$

$$0{\cdot}8716 = \beta_1 + \beta_2, \quad (12)$$

containing two unknown relative volumes (β_1 and β_2), can be written down. Elimination of β_1 and β_2 from (12) and two at a time from equations (11) gives

$$\left.\begin{aligned} &[0{\cdot}398 - (Q/\sigma)_{12}]/[0{\cdot}367 - (Q/\sigma)_{22}] \\ &= [(Q/\sigma)_{11} - (Q/\sigma)_{12}]/[(Q/\sigma)_{21} - (Q/\sigma)_{22}] \end{aligned}\right\} \quad (13)$$

$$\left.\begin{aligned} &[0{\cdot}398 - (Q/\sigma)_{12}]/[0{\cdot}315 - (Q/\sigma)_{32}] \\ &= [(Q/\sigma)_{11} - (Q/\sigma)_{12}]/[(Q/\sigma)_{31} - (Q/\sigma)_{32}]. \end{aligned}\right\} \quad (14)$$

$$\text{Also, } \sigma_1 = \frac{\sigma_2}{1{\cdot}118} = \frac{\sigma_3}{1{\cdot}291}. \quad (15)$$

The relationship between $(Q/\sigma)_{r1}$ and $(Q/\sigma)_{r2}$ is shown by line A, and the relationship between $(Q/\sigma)_{r1}$ and $(Q/\sigma)_{r3}$ by line B, in Fig. 7. Shown also are typical eliminants, obtained by putting trial values of $(Q/\sigma)_{11}$ (and hence of $(Q/\sigma)_{21}$) into (13) and (14). The intersection of the related two curves gives the roots. By trial [and by using (15)], values of $(Q/\sigma)_{11}$ and $(Q/\sigma)_{12}$ were found which satisfied (13) – these are shown by line 1 in Fig. 7 (inset). Also, values of $(Q/\sigma)_{11}$ and $(Q/\sigma)_{12}$ were found which satisfied (14); these are shown by line 2 in Fig. 7 (inset). These lines intersect at $(Q/\sigma)_{11} = 0{\cdot}395$; $(Q/\sigma)_{12} = 0{\cdot}414$, corresponding to $\sigma_1 = 2{\cdot}70$; $\sigma_2 = 2{\cdot}40$. Hence, by using the fact that $2\omega' = 13{\cdot}2$ and by substitution in (11), the measured values were found to be those of Table 2.

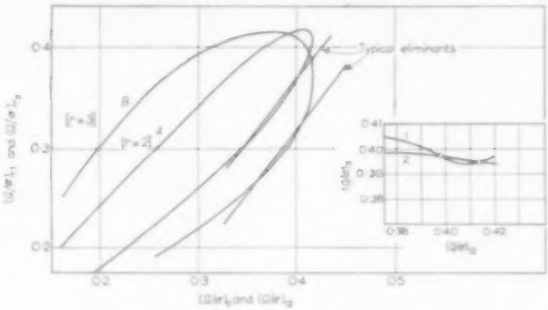

FIG. 7. Model 1: relations between coefficients.

Table 2.

Relative volume (cm³/cm³)	*Depth of pocket* (cm)
0·138	0·182
0·734	0·204
0·872 Total	
whilst the actual values are:	
0·1366	0·476
0·3408	0·794
0·2183	1·270
0·6957 Total	

Table 3.

j	ω rad/sec $\times 10^4$	$\frac{V\,\xi\,\mu}{P}\left(\frac{A_L}{A_0}\right)\cos\phi = \mu \times 10^6$
1	1·4	1·0172
4	2·3	0·4670
5	2·6	0·2697

Model 2.

Volume of "pore-space" (by calculation): 12·861 cm³; p (mean): 0·1805 dynes/cm²; V: 17 cm³/hr; $\xi = 8$ (for c.g.s. units).

From this there arises the values of $(V\xi\mu/p)\,(A_L/A_0)\cos\phi$ given in Table 3 (values corrected for effect of headers).

Calculations

(Here ϵ stands for a volume and not for a voidage as it does in ref. [1]).

The equations

$$\epsilon_1 + \epsilon_2 = 12{\cdot}861 \qquad (15)$$

$$\left.\begin{aligned} \eta_{111}\,\epsilon_1 + \eta_{221}\,\epsilon_2 &= 1{\cdot}0172 \\ \eta_{114}\,\epsilon_1 + \eta_{224}\,\epsilon_2 &= 0{\cdot}4670 \\ \eta_{115}\,\epsilon_1 + \eta_{225}\,\epsilon_2 &= 0{\cdot}2697 \end{aligned}\right\} \qquad (16)$$

can be written down (η incorporates a factor of 10^6). Two independent eliminants may be formed from equations (15) and (16). For both, values of η were calculated for various values of l; (see equation (36) of ref. [1] and below). For any particular values of R and l, η depends on ω_j; the relationships between l and η_{1r1} and η_{1r3} are shown in Fig. 8. Similar curves were drawn for η_{2r1} and η_{2r3}, η_{1r1} and η_{1r4} and η_{2r1} and η_{2r4}.

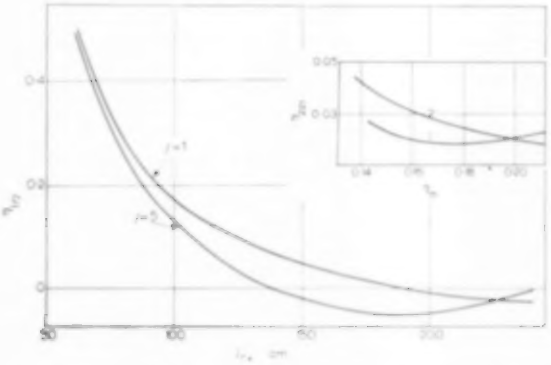

FIG. 8. Model 2; relations between coefficients and lengths of tubes.

By trial, the values of l_1 and l_2 were chosen so as to enable the eliminants to be satisfied; the coefficients which satisfy one eliminant are shown by line 1 in Fig. 8 (inset), the coefficients which satisfy the other by line 2. Their point of intersection gives the only coefficients satisfying both eliminants simultaneously; they are: $\eta_{111} = 0{\cdot}20$, $\eta_{221} = 0{\cdot}02$. From Fig. 8 – η_{111} and η_{115} versus l_1 — the values of l_1 and η_{115} were found. From the corresponding graph of η_{211} and η_{215} versus l_2 (not reproduced) the values of l_2 and η_{225} were similarly found. From the knowledge of the values of η_{111}, η_{221}, η_{115} and η_{225} the simultaneous equations (16) were solved for ϵ_1 and ϵ_2.

The values thus found of l_1, ϵ_1 and l_2, ϵ_2 are given in Table 4.

Table 4.

Radius (cm)	*Length l* (cm)	*Volume ε* (cm³)	*Total volumes* (cm³)	
Actual				
0·044	72·5	1·323		
0·044	82·5	1·505	4·790	
0·044	107·5	1·962		12·861
0·050	92·5	2·180		
0·050	117·5	2·769	8·071	
0·050	132·5	3·122		
Measured:				
0·044	94	4·22	4·22	12·861
0·050	195	8·64	8·64	

The numerical values of the coefficients

The tedium of the calculations may be reduced by suitable approximations. The coefficients appertaining to model 2 are, in general, to be calculated from equation (36) of ref. [1], but in the present example $(\omega/12\,D)^2\,R^4 \ll 1$. It follows, from the binomial theorem, that the exponential term approximates to

$$\exp\left[-(Ml^2/8)\,(\omega/12\,D)^2\right] \doteq \left[1 - (Ml^2/8)\,(\omega/12\,D)^2\right]$$

and that the cosine term approximates to

$$\cos\left[(l^2/2R^2)\,(N/M)\right].$$

DISCUSSION

For both models the calculated values of the parameters were in the region of the actual values. It could not be hoped, when using the existing apparatus, to get them closer to one another. The agreement may be fortuitous for it was found that the calculated values were appreciably influenced by variations in μ, that is small errors, especially in the amplitude ratios and phase angles, have a large effect. The number of significant figures employed in the calculations was for the purpose of getting out an answer; the measurements did not merit this apparent degree of accuracy. The trial-and-error calculations were laborious (although experience has reduced the effort) and, for this reason and because

the accuracy of the measurements was suspect, only two values of the appropriate parameter were found for each model. Further values could have been calculated if each one were based on a preceding–and rougher–approximation. It was realised later that the highest frequency used for model 1 was too high to allow penetration of the sine-wave into the full depth of the larger pockets; this may explain the low values obtained for the depths of the pockets.

Conclusions

The method suggested in ref. [1], and amplified here in its details, appears able to give information which would be difficult or impossible to obtain in any other way. For this information to be valid it is necessary for measurements of some of the variables to be made to within 0·1 per cent; others are less exacting. The relative importance of the variables might best be found from a calculation which used estimated values of sufficient parameters to yield the harmonic response.

The computational labour might be reduced by graphical solutions on large-scale graphs, or by using a computer. Thought is being given to the design of an analogue computer for this purpose.

In practice the greatest use of the method may be for comparative purposes, because results will be in terms of simplified models and also because it might be difficult to correct for the effect of the headers on a piece of industrial equipment as was done in these experiments.

Acknowledgements—The author is indebted to Dr. O. E. Potter for the suggestion from which the sine-wave generator developed, and to Messrs. J. Toft and W. Newton for making some of the apparatus. The advice and comments of the referee have been of the greatest assistance. The capacitance meter and recorder were Fielden 'Proximity Meter' and 'Servograph' respectively; the precision-bore capillary tubing was Chance's 'Veridia'; the synchronous motor was by Sangamo-Weston.

Notation

E = ratio of (absolute) amplitudes

f, F = function

T = cycle time

β = total volume

Remainder of the symbols as in ref. [1].

References

[1] Turner G. A. *Chem. Engng. Sci.* 1958 **7** 156.

[2] Taylor G. I. *Proc. Roy. Soc.* 1954 **A225** 473.

[3] Allen J. *Phil. Mag.* 1934 **18** 488.

[4] Taylor G. I. *Proc. Roy. Soc.* 1953 **A219** 186.

[5] Carslaw H. S. and Jaeger J. C. *Conduction of Heat in Solids* p. 89, Oxford University Press, London 1947.

[6] Jakob M. *Heat Transfer.* Vol.1, p. 301. Chapman & Hall, London 1949.

[7] Kramers H. and Alberda G. *Chem. Engng. Sci.* 1953 **2** 173.

[8] Lanczos C. *Applied Analysis* § 25, Chap. 2, Pitman, London 1957.

Chemical Engineering Science, 1959, Vol. 10, pp. 22 to 30. Pergamon Press Ltd. London. Printed in Great Britain

On heat transfer between vapour bubbles in motion and the boiling liquid from which they are generated

E. RUCKENSTEIN

Bucharest Polytechnical Institute, Rumanian People's Republic

(*Received* 26 *June* 1958)

Abstract—In this paper the mechanism of heat transfer between a boiling liquid and vapour bubbles in motion is discussed. FRITZ' and ENDE's experimental results regarding this problem are interpreted.

Résumé—L'auteur discute dans cet article le mécanisme de transfert de chaleur entre un liquide en ébullition et les bulles de vapeur en mouvement. Il interprète les résultats expérimentaux de FRITZ et ENDE concernant ce problème.

Zusammenfassung—In dieser Arbeit wird der Mechanismus der Wärmeübertragung zwischen einer siedenden Flüssigkeit und sich bewegenden Dampfblasen behandelt. Die Versuchsergebnisse von FRITZ und ENDE zu dieser Frage werden interpretiert.

EXPERIMENTAL research concerning the boiling of water in conditions of free convection leads, among others, to the following conclusions [1], [2], [3]:

(a) The liquid is superheated and the vapours have the saturation temperature.

(b) The greatest part of the heat quantity given to the system is taken directly by the liquid and transmitted by evaporation to the vapour bubbles.

From these experimental facts one may conclude that the greatest part of the heat is transmitted directly to the liquid which, due to superheating by an amount Δt, transmits it to the surface of the bubbles.

The aim of this paper is to analyse the mechanism of the heat transmission from the liquid to the moving bubbles, and to interpret FRITZ' and ENDE's [4] experimental results regarding this problem.

A vapour bubble cannot spontaneously originate in a saturated liquid. Boiling begins if there exists finite curvatures (for example, those of the surface irregularities) on the heating surface and at a superheating $\Delta t'$ of the liquid given by

$$\Delta t' \approx \Delta p \left(\frac{dt}{dp}\right)_s, \tag{1}$$

where

$$\Delta p = \frac{2\sigma}{R}\frac{\gamma'}{\gamma' - \gamma''} \tag{2}$$

and

$$\left(\frac{dp}{dt}\right)_s = \frac{Jr_c}{T_s(1/\gamma'' - 1/\gamma')} \tag{3}$$

Here σ is the surface tension of the liquid with respect to the vapour, R the bubble radius, γ' the specific gravity of the liquid, γ'' the specific gravity of the vapours, r_c the latent vaporization heat, T_s the saturation temperature in °K and J the mechanical equivalent of heat.

A given irregularity of the heating surface, characterized by a linear dimension l, can become an active centre if the superheating Δt of the liquid in the vicinity of the surface is sufficiently large, so that

$$l = \frac{2\sigma}{\Delta t}\frac{T_s}{\gamma'' r_c J}. \tag{4}$$

Let it be considered that on the heating surface which, for the case analysed is horizontal, there exists such active centres. On them, vapour bubbles will form, which detach themselves when the diameter of a sphere having the same volume as the bubble becomes equal to D_0.

$$D_0 = 0{\cdot}02\,\theta'\left(\frac{\sigma}{\gamma' - \gamma''}\right)^{1/2}. \tag{5}$$

Here θ' represents the contact angle between the bubble and the solid surface when the bubble detaches itself from the solid surface.

In this paper, the mechanism of heat transfer between the bubble and the liquid will be analysed, starting with the moment when the bubble detaches itself from the active centre.

Mechanism of Heat Transfer Between a Liquid and Bubbles in Motion

The mechanism of heat transfer between a liquid and bubbles in motion will depend, in the first place, on the possibility to consider or not, that the bubbles behave like independent bubbles, therefore, on whether it may be considered that both the motion of the bubble and that of the liquid are, or are not, affected by the surrounding bubbles. What is meant by practically independent bubbles may be specified by comparing the distance L between the centres of two consecutive bubbles, with the distance L' from the centre of an independent bubble to the spot where the velocity of the liquid is a sufficiently small fraction of the velocity of the bubble. Denoting by f the frequency by which bubbles are generated on an active centre, and by U the velocity of the bubble (considered as being practically constant), there results that $L = U/f$. The distance L' will be estimated with the help of the expression valid for the case of a potential flow (this may be done on account of the fact that fairly large distances from the bubble surface are involved) which, for the case of a spherical bubble, is of the form*

$$|v| \lesssim \left(\frac{R}{r}\right)^3 U,$$

r being the distance to the centre of the bubble. By putting $r = 3R$ one obtains for the velocity v of the liquid $v \lesssim \frac{1}{27} U$, therefore a relatively small fraction of U. The bubbles may be considered as being practically independent if

$$L \geqslant 2L' = 6R. \qquad (6)$$

Condition (6) must be fulfilled on the vertical. In order that it be possible to consider the bubbles as being independent, condition (6) must be completed by a condition, valid this time on the horizontal, namely, that the distance between the active centres be sufficiently large.

1. Let one consider in the first place, the case of an independent bubble. The mechanism of the heat transfer between the liquid and the bubble depends essentially on the value of the Reynolds number $\left(\frac{2RU}{\nu}\right)$. Up to $\frac{2RU}{\nu} \approx 1600$–$1800$, experience shows that the gas bubbles maintain an almost spherical shape and have a rectilinear motion, whereas for larger Reynolds' numbers the bubbles deform themselves to a greater extent, they begin to vibrate, and their rectilinear ascension is replaced by a spiral ascension [6].

Let those bubbles be considered, which have sufficiently small Reynolds number to permit their shape to be spherical. On such a bubble, a liquid layer forms, in which the temperature T of the liquid satisfies the equation [6]

$$\frac{\partial T}{\partial t} + v_r \frac{\partial T}{\partial r} + \frac{v_\theta}{r} \frac{\partial T}{\partial \theta} = \frac{a}{r^2} \frac{\partial}{\partial r}\left(r^2 \frac{\partial T}{\partial r}\right), \qquad (7)$$

r being the distance to the centre of the bubble, θ, the angle of the vector radius with the vertical (the latter pointing upwards), v_r and v_θ, the components of the liquid velocity with respect to the centre of the bubble, a, the thermal diffusivity and t, the time, measured from the moment of detachment from the active centre. The first term in the left member of the equation appears especially† on account of the fact that the radius R of the bubble grows as the bubble rises, and this affects both the velocity and the temperature distribution. If, however, the rate of increase of the radius of the bubble is sufficiently low in comparison to the velocity of the bubble, one may proceed as if R were constant (therefore

*In the case of a bubble moving in a pure liquid and for Reynolds' numbers of the order of 10^3, the separation of the liquid from the bubble occurs at points very near to the rear stagnation point [6]. The wake behind the bubble is practically non-existent. A discussion regarding the validity—for this case—of the assumption of potential flow, even in the vicinity of the bubble, is given in Section 1.

†The time is very short in which the stationary state of the liquid flow on a constant radius bubble is realized.

the first term of the left member of equation (7) may be neglected and, especially, one may proceed as if the bubble surface constituted a fixed boundary and not a moving boundary). An additional approximation will be made in connection with equation (7), namely, the right member will be expressed by $a \frac{\partial^2 T}{\partial r^2}$. Since $\frac{\partial^2 T}{\partial r^2}$ is of the same order of magnitude as $\frac{\Delta T}{\delta^2}$ and $\frac{2}{r}\frac{\partial T}{\partial r}$ of the same order of magnitude as $\frac{2\Delta T}{(R+\delta)\,\delta}$, this approximation is possible if $R > \delta$ (it shall be shown later that this condition is satisfied if Péclet's number (Pe) is much larger than unity).

For $Re > 1$, but not quite large enough for the bubble to begin deforming itself appreciably, the velocity components v_r and v_θ will be approximated by the expressions valid for an ideal fluid. The only argument in support of this approximation is the fact that, in opposition to the case of a solid sphere, the tangential component of the velocity at the interface is not equal to zero in the case of a spherical bubble, a condition which is also fulfilled by the tangential component of the velocity of an ideal fluid. Since $Re > 1$ the difference between the actual velocity and the velocity of an ideal fluid is not too great [6]. The velocity components v_r and v_θ of an ideal fluid are given by the expressions

$$v_r = -U\left[1 - \left(\frac{R}{r}\right)^3\right]\cos\theta \tag{8}$$

$$v_\theta = U\left[1 + \frac{1}{2}\left(\frac{R}{r}\right)^3\right]\sin\theta \tag{9}$$

For $\frac{r-R}{R} \equiv \frac{y}{R} < 1$,

$$v_r \approx -3\,U\frac{y}{R}\cos\theta \tag{8'}$$

$$v_\theta \approx \frac{3}{2}U\sin\theta. \tag{9'}$$

The boundary conditions for the temperature T are

$$T = T_0 \text{ for } r = \infty \tag{10}$$

$$T = T_i \text{ for } r = R. \tag{11}$$

Since for $\frac{y}{R} < 1$ $\frac{v_\theta}{r}\frac{\partial T}{\partial \theta} \approx \frac{v_\theta}{R}\frac{\partial T}{\partial \theta}$, by using the above mentioned approximations, equation (7) becomes

$$-3\,U\frac{y}{R}\cos\theta\frac{\partial T}{\partial r} + \frac{3}{2}\frac{U}{R}\sin\theta\frac{\partial T}{\partial \theta} = a\frac{\partial^2 T}{\partial r^2}. \tag{7'}$$

With these approximations the problem becomes analogous to the diffusion problem treated by LEVICH [6], and the solution of equation (7') is therefore

$$\frac{T - T_i}{T_0 - T_i} = \frac{2}{\sqrt{\pi}}\operatorname{erf}\frac{\frac{3}{2}URy\sin^2\theta}{2\sqrt{\frac{3}{2}UR^3a\left(\frac{2}{3} - \cos\theta + \frac{1}{3}\cos^3\theta\right)}} \tag{12}$$

For the heat quantity q, transmitted in the unit time, on an unit surface, the normal to which makes an angle θ with the vertical, one obtains

$$\frac{q}{c_p\gamma} = (T_0 - T_i)\times \frac{\frac{3}{2}URa\sin^2\theta}{\sqrt{\frac{3}{2}\pi\,aUR^2\left(\frac{2}{3} - \cos\theta + \frac{1}{3}\cos^3\theta\right)}} \tag{13}$$

The heat quantity transmitted to the bubble in the unit time is therefore given by the expression

$$Q = 2\pi R^2\int_0^\pi q\sin\theta\,d\theta = 8\,(T_0 - T_i)\,\lambda\left(\frac{\pi}{2}\right)^{1/2}\left(\frac{U}{Ra}\right)^{1/2}R^2. \tag{14}$$

For the heat transfer coefficient, defined by the equation

$$Q = \alpha\,4\pi\,R^2\,(T_0 - T_i), \tag{15}$$

one obtains

$$\alpha = \left(\frac{4}{\pi}\right)^{1/2}\lambda\left(\frac{U}{2\,Ra}\right)^{1/2} \tag{16}$$

Equation (16) may also be written in the form*

*By estimating δ with the help of the expression $\alpha = \frac{\lambda}{\delta}$, there results $\frac{\delta}{R} = \pi^{1/2}\,Pe^{-1/2}$ and therefore the inequality $\frac{\delta}{R} < 1$ is satisfied if $Pe > 1$.

VOL. 10 1959

$$Nu \equiv \frac{2\,\alpha\,R}{\lambda} = \left(\frac{4}{\pi}\right)^{1/2}\left(\frac{2\,RU}{a}\right)^{1/2} \equiv \left(\frac{4}{\pi}\right)^{1/2} Pe^{1/2}. \quad (16')$$

It must be noted, in the first place, that the term $v_r \frac{\partial T}{\partial r}$ of equation (7) cannot be neglected in comparison to the term $\frac{v_\theta}{r}\frac{\partial T}{\partial \theta}$. If, nevertheless, this term would be neglected and putting $v_\theta \sim U$, it is easy to prove that equation (16′) is again obtained, providing a certain value would be chosen for the proportionality constant.

It is also to be noted that the so-called penetration theory [7], [8], [9], equally suggests (16′) to be used for Nusselt's number and that KARMAN'S approximate method, recently used by POTTER [10] in connection with the mass transfer between two phases flowing in co-current, could be used to solve this problem.

If Reynold's number is larger than 1600–2000, the bubbles deform themselves to a greater extent and begin to vibrate.

A computation, analogous to that used for the case of a sphere, is at present under study for a vapour bubble having the shape of an oblate spheroid and will be published subsequently.

If the independence criterion is not satisfied (the active centres are nevertheless considered to be far enough from each other to prevent the chain of bubbles from influencing each other) but the distance between the bubbles is still sufficiently large, the velocity-field influence of the bubbles in a chain of bubbles, originating from the same active centre, on one of the bubbles in the chain, can be estimated by making use of the equations valid in the case of the flow of an independent bubble. As a first evaluation, the influence of the more distant neighbours will be neglected and the velocity value which corresponds to the centre of the bubble will be taken as an approximation for the average value of the velocity induced in the liquid on the surface of the bubble by the two neighbouring bubbles. The upper bubble induces an absolute velocity $U\left(\frac{R}{L}\right)^3$, directed in the sense of the bubble motion, and the lower one, an absolute velocity $U\left(\frac{R}{L}\right)^3$, also directed in the same direction, U being the velocity of one of the bubbles in the chain. These effects therefore add and give the liquid a velocity directed in the sense of the bubble motion, equal to $2\,U\left(\frac{R}{L}\right)^3$. Hence the bubble moves in the liquid with a relative velocity $U' \approx U\left[1 - 2\left(\frac{R}{L}\right)^3\right]$. In order to bring back this case to the one previously examined it may be considered that one has to deal with a quasi-independent bubble which moves in the liquid with a velocity $U\left[1 - 2\left(\frac{R}{L}\right)^3\right]$. In a paper in preparation concerning mass transfer in a liquid in the case of bubbling, the author will use a somewhat less approximate computation concerning the above problem.

2. If the bubbles can no longer be considered as being practically independent, that is in the case of a group of non-independent bubbles, the movement of the liquid through which a bubble has passed does not die away before the arrival of the subsequent bubble and intense turbulent motions may appear in the liquid. KISHINEVSKY and PAMFILOV [11] have used, in the course of their investigations regarding the absorption mechanism in intensely mixed systems, a model for which they consider that, owing to turbulence, the contact surface between the liquid and the bubble is constantly renewed, each volume element of liquid remaining at the interface for a certain short time after which it mixes with the bulk of the liquid. They assume that this volume element has a turbulent structure with a sufficiently great turbulence diffusivity to make the concentrations independent of the distance to the interface. Based on this model it is easy to obtain

$$\alpha = \gamma' c_p \frac{x_0}{\tau}, \quad (17)$$

x_0 being the thickness of the liquid volume element and τ the time it remains at the interface. It is to be noted that dimensional considerations permit to obtain expressions for x_0 and τ, and therefore,

an equation for α; this same equation may however be established for α only with the help of dimensional considerations.

As a simplification, a group of uniformly distributed bubbles having the same diameter will be considered.

Taking into account the fact that the turbulence is especially caused in the system by the group of non-independent bubbles, it is necessary that besides the quantities on which α is dependent in the case of independent bubbles, a quantity should appear which characterizes this group. This quantity is the fraction γ of the volume occupied by the bubbles. If the mixing of the liquid were also due to the bubble oscillations there should equally appear, among the quantities α is dependent on, a property of the oscillating surface, namely, the surface tension. Since here the cases are considered, in which the mixing is essentially due to the group, the influence of the latter quantity is not important, except, at most indirectly, through γ (it may eventually become important for low values of γ, if the Reynolds number for a bubble is sufficiently large to permit the bubble to start oscillating).

The dimensional analysis leads to

$$Nu = F(Re, Pr, \gamma). \tag{18}$$

In sufficiently intensive turbulence conditions which among other things, require that γ should have a sufficiently large value, taking into account the fact that the interface is not solid* and therefore that the heat transfer may be essentially due to turbulence, α is not dependent on the transfer quantities which have a molecular character: η (excepting, at most indirectly, through γ, for instance) and λ. For this limiting case, which gives the asymptotic behaviour of α one obtains, from equation (18),

$$\alpha \sim \gamma' c_p U \text{ for } \gamma = \text{constant} \tag{19}$$

Equation (19) may also be written †

$$Nu \sim Pe. \tag{19'}$$

The case discussed has a limiting character and, for the time being, it is not possible to ascertain whether it can be experimentally realized. A somewhat analogous limiting case was examined by HANDLOS and BARON [15], in connection with the mass transfer in the interior of an oscillating drop. Based on a model, they obtain an expression of the same form as equation (19'), the agreement with the experiment being satisfactory.

Equation (19') was not established on the basis of a model, the only assumption which it implies being that the turbulence does not die out at the interface. The use of KISHINEVSKY's and PAMFILOV's model also leads to equation (19') since, on dimensional grounds, taking into account the intensive turbulence, one may write

$$x_0 \sim R \quad \tau \sim \frac{R}{U}.$$

It is to be noted that also other models may lead to the same result. Consider, for instance, that a turbulent diffusion occurs in the liquid volume element which has come to the interface, and that the cofficient ϵ of turbulent diffusion is independent on the distance to the interface. If during the time τ in which contact exists between this element and the bubble, the depth of penetration by thermal turbulent diffusivity is smaller than the thickness of the fluid element, then

$$\alpha = \left(\frac{4}{\pi}\right)^{1/2} \gamma' c_p \left(\frac{\epsilon}{\tau}\right)^{1/2}. \tag{20}$$

Taking into account the intensive turbulence, dimensional considerations lead to the equatiors

$$\epsilon \sim RU, \quad \tau \sim \frac{R}{U}$$

and therefore, in the end, equation (19') is again obtained.

*If active capillary substances are introduced in the liquid, they are adsorbed on the surface of the bubbles. The adsorption on the surface of the bubble may lead this surface to behave like a solid surface and therefore to the suppression of turbulence on the surface. With regard to this, the works of LEWIS [12], [13], mentioned in [14], may be consulted.

†If in equation (18) there would appear also other dimensionless groups one would obtain that $\frac{Nu}{Pe}$ is a function not only of γ but also of these new groups.

VOL. 10 1959

DANCKWERTS [16] suggested another type of renewal model, still for the case of a sufficiently intensive mixing. According to his theory, turbulence renews the volume elements at the interface, but the element itself has a non-turbulent structure (in other words, the heat or mass transfer in this volume element has a molecular character). For this reason, the model suggested in [16] also has a limiting character, being eventually valid for not too intensive turbulent conditions. If the time τ is sufficiently small so that the thermal diffusivity penetration depth is smaller than the thickness of the volume element which has come into contact with the bubble, then

$$\alpha = \left(\frac{4}{\pi}\right)^{1/2} \gamma' c_p \left(\frac{a}{\tau}\right)^{1/2}. \qquad (21)$$

The time of contact between a liquid volume element and a bubble differs for the various elements, for two reasons. In the first place, because a liquid volume element which has come into contact with the bubble in upper part may have a longer contact with it than one which, owing to a turbulent fluctuation, has come into contact with it at a lower region. In the second place, on account of the turbulence itself (DANCKWERTS' work [16] should be referred to in this connection). It can be noted, however, that this does not modify the form of equation (21) in which appears the time τ, which is not dependent on the thermal diffusivity a, but about which the theory gives no other additional information. In fact, consider as an example, that a function $A\,\psi\left(\frac{\tau'}{\tau_0}\right)d\tau'$ may be defined, which gives the liquid-bubble contact surface, for which τ is comprised between τ' and $\tau' + d\tau'$. The heat transfer coefficient should be considered as given by the average value

$$\alpha/\gamma' c_p = (4/\pi)^{1/2} a^{1/2} \int_0^\infty \tau'^{-1/2} \psi(\tau'/\tau_0)\, d\tau' \Big/ \int_0^\infty \psi(\tau'/\tau_0) d\tau'.$$

The latter equation leads to

$$\frac{\alpha}{\gamma' c_p} \sim \left(\frac{a}{\tau_0}\right)^{1/2},$$

an equation which differs from equation (21) by the fact that, instead of the time τ there appears a time τ_0 which, as may easily be shown, is proportional to the average value of τ. The time τ_0 is not dependent on the thermal diffusivity a, but theory does not provide any additional information about it.

With regard to the time of contact between a liquid element and a bubble, an information of an experimental nature was given by KISHINEVSKY and MOCIALOVA [17] who investigate the kinetics of CO_2 absorption through bubbling in aqueous Na OH solutions. For the interpretation of the experimental results obtained, they make use of an equation established on the basis of a renewal model, with the hypothesis that the mass transfer in each volume element which has come into contact with the bubble, takes place through turbulent and molecular diffusion, with a total diffusion coefficient which is independent of the distance to the interface. They reach the conclusion that the time of contact satisfies the equation $\tau = \frac{R}{U}$ and that the total diffusion coefficient is approximately ten times larger than that of molecular diffusion. It should be noted that the value obtained for τ by these researchers is of the same order of magnitude as the value used by the penetration theory for the non-turbulent case. Therefore, for the case of the experiments conducted by the above-mentioned researchers, the turbulence does not sensibly diminish the time of contact between a liquid element and a bubble, but introduces the turbulent diffusion.

INTERPRETATION OF FRITZ' AND ENDE'S EXPERIMENTAL RESULTS

Using a cinematographic method, FRITZ and ENDE [4] determined the volume increase of a bubble in motion, and they obtained for water at 100°C an average value $\alpha = 16{,}000$ kcal/m²hr°C. This value represents an average for the six bubbles studied. In the following, α shall be estimated in the first place, by using for U the mean value $U = 0{\cdot}26$ m/sec, determined experimentally in [4], and for the bubble radius, the value at the moment of its detachment from an

active centre, computed with the help of equation (5).

From Fritz' and Ende's experimental determinations there results that for a temperature in the neighbourhood of 90°C, the mean value of θ' is approximately 45°. By using this value for θ', equation (5) leads to $D_0 = 2{\cdot}3{\cdot}10^{-3}$ m.

Inequality (16) allows to establish whether the bubbles having this value for D_0 may be considered as quasi-independent. Fritz and Ende suggested an approximate relation between the frequency and the diameter,

$$fD_0 \approx K,$$

K being a quantity which, in the experimental conditions used, has a value close to 95 mm/sec. (In comparison with the experimental results of Fig. 9 in [4], this value for K leads to values for f which are too large, at small diameters, and too small at large diameters. For example, for $D_0 = 10^{-3}$ m there results $K \approx 72$ mm/sec and the only point of this figure, for which mention is made that it refers to water vapour bubbles, has $D_0 = 2{\cdot}8{\cdot}10^{-3}$ m and $K \approx 75$ mm/sec).

Therefore $L = \dfrac{UD_0}{K}$, and inequality (6) is written

$$\frac{UD_0}{K} \gtrsim 6R.$$

In the zone near the detachment point of the bubble, this inequality is satisfied if $K \approx 75$ mm/sec. It may be noted that if $K \approx 95$ mm/sec, the inequality is not satisfied; however, the difference between its right and left member is less than 10 per cent of the right member value. The Reynolds number for $D_0 = 2{\cdot}3{\cdot}10^{-3}$ m is 1800 and this bubble is therefore near to these values of the Reynolds number which separate the bubbles that do not deform themselves from those that suffer a deformation. This bubble will have at first a spherical shape and later the shape of an ellipsoid. By using equation (16) one obtains $\alpha \approx 17{,}000$ kcal/m² hr °C.

The three smaller bubbles ($D_0 \approx 1$ mm) studied by Fritz and Ende have at the moment of their detachment, and for a considerable part of their course, smaller Reynolds' numbers and they shall therefore have a spheric shape during this interval. These bubbles have an initial radius $R_0 = 0{\cdot}5{\cdot}10^{-3}$ m and after travelling over a distance of 60 mm (height of the liquid) they have a radius of $1{\cdot}8{\cdot}10^{-3}$ m (this value represents an average for the three smaller bubbles).

As ascertained experimentally [6] – and a comparison with Fritz' and Ende's experimental data do not contradict this fact – for Reynolds' numbers between 400 and 1600 the velocity of an independent bubble may be computed with the help of an expression similar to the one valid for solid spheres

$$U' = \left(\frac{8g\,(\gamma' - \gamma'')\,R}{3\,\zeta\,\gamma'}\right)^{1/2} \approx 6{\cdot}6\,R^{1/2}\ \text{m/sec} \equiv 16{,}800\,D^{1/2}\ \text{m/hr}, \quad (22)$$

the friction factor ζ having a value of about 0·6.

The velocity of these bubbles in the zone near to their detachment point is 0·15 m/sec, and near the free surface it is 0·28 m/sec; the Reynolds numbers are therefore 450 and 3,000 respectively. The latter value of the Reynolds' number exceeds the range in which the above equation is valid for U; it may be noted, however, that the recommended value [6] for the velocity U in this case, namely 0·28 – 0·3 m/sec practically coincides with the value obtained from equation (22).

Equation (16) leads to $\alpha \approx 19{,}300$ kcal/m² hr°C in the zone of detachment and to $\alpha \approx 14{,}200$ kcal/m²hr°C after the bubble has travelled over 60 mm. The mean value is 16,750 kcal/m² hr °C. As the criterion of quasi-independence, it should be stressed that this criterion is not satisfied. It may, however, be noted that, in the first place, if a somewhat weaker criterion is used, corresponding to $|v| \lesssim \dfrac{U}{10}$, it is satisfied in the vicinity of the detachment point. In the vicinity of the free surface the bubbles have an ellipsoidal shape and the criterion (6) is no longer valid. One may however also note that, from Fig. 6 in [4], where the very case of bubbles having $D_0 \approx 10^{-3}$ m is presented, there follows that the criterion (6) is satisfied. These facts suggested that one may still use equation (16), as a first approximation.

The three larger bubbles studied by Fritz

and ENDE have an initial diameter of 4·8 mm and after travelling over 60 mm, a diameter of 6·6 mm. The values shown represent an average for the three bubbles. These bubbles deformed themselves considerably, having a still more irregular shape and on account of this, equation (16) can probably no longer be used in this case. If it is nevertheless used, $\alpha \approx 12{,}000$ is obtained for the instant of detachment and $\alpha \approx 11{,}400$ after a path of 60 mm. These values are probably smaller than the actual one (FRITZ' and ENDE's experimental mean values for the three larger bubbles are 15,800, 14,900 and 22,700 but, as mentioned by the authors, they are less certain than for the smaller bubbles) because equation (16) does not take into account the considerable and rapid deformation of the bubble.

The dependence of the bubble diameter on the distance to the generation point can easily be obtained. This computation will be made in the hypothesis that the bubbles have a spheric shape, that α is given by equation (16) and that for the velocity U, equation (22) may be used. A thermal balance permits the following equation to be written

$$\gamma'' r_c \frac{\pi}{6} \frac{dD^3}{dt} = \lambda \left(\frac{4}{\pi}\right)^{1/2} \left(\frac{U}{aD}\right)^{1/2} (T_0 - T_i)\, \pi D^2 \quad (23)$$

The time t is considered as being measured from the instant of detachment from an active centre. Using equation (22) one obtains

$$\frac{dD}{dt} = \beta\, D^{-1/4}, \quad (24)$$

where

$$\beta \equiv 292\, \frac{\lambda}{\gamma''\, a^{1/2}\, r_c} (T_0 - T_i)\ \mathrm{m}^{5/4}/\mathrm{hr}.$$

By taking an average value for the superheating $(T_0 - T_i)$, one obtains by integration

$$D^{5/4} - D_0^{5/4} = \frac{5}{4} \beta t.$$

Since $U = \frac{dx}{dt}$, equation (22) and (24) lead to

$$D^{3/4} \frac{dD}{dx} = \frac{\beta}{16{,}800} \equiv \beta'.$$

Therefore

$$D^{7/4} - D_0^{7/4} = \frac{7}{4} \beta' x. \quad (25)$$

Since the conditions in which equation (25) was established are approximately fulfilled in the case of the smaller bubbles, the value of D in this case will be estimated by help of equation (25) for $x = 0{\cdot}06$ m. For $T_0 - T_i$ the value 0·4 °C [4] will be considered. One obtains $D = 4{\cdot}3 \cdot 10^{-3}$ m, a value which is near to the one obtained experimentally.

There is still an observation to be made. The velocity of the bubbles satisfies the equation for solid spheres and this fact is explained [18] by the adsorption on the bubble surface of the traces of active capillar substances present in common water. This fact suggests that the equation valid for solid spheres may be used for the computation of the heat transfer coefficient. In [3] the following equation is recommended for this case*

$$Nu = 0{\cdot}37\ Re^{0{\cdot}6}\ Pr^{1/3}. \quad (26)$$

This equation leads to values of α comprised between 10,500 and 8,000, these values being of the same order of magnitude as the ones obtained above. The experimental material used is too scarce to allow a choice to be made on its basis between equation (16) or (26).

Acknowledgements—The author is indebted to Prof. M. B. DONALD and Mr. F. HASLAM for very helpful suggestions.

*In this case the independence criterion has to be established taking into account the length of the wake behind the bubble. It should nevertheless be stressed that strictly speaking equation (26) is valid for an independent sphere. In the case studied above this condition may not always be satisfied.

NOTATIONS

a = thermal diffusivity of the liquid	m^2/hr
c_p = specific heat of the liquid	kcal/kg °C
D = diameter of the bubble	m
g = gravitational acceleration	m/hr^2
J = mechanical equivalent of heat	kg/kcal
r = distance to the centre of the bubble	m
r_c = latent heat of vaporization	kcal/kg
R = radius of the bubble	m
T_s = saturation temperature	°K
Δt = superheating of the liquid	°C
T = temperature in the liquid	°C
U = velocity of the bubble	m/hr

v = velocity of the liquid	m/hr	σ = surface tension	kg/m
α = heat transfer coefficient	kcal/m^{2}hr°C	t, τ, τ', τ_θ = time	hr
γ' = specific gravity of the liquid	kg/m^3	θ = angle of the vector radius with the vertical	degrees
γ'' = specific gravity of the vapour	kg/m^3	θ' = contact angle	degrees
ζ = friction factor		δ = average on the bubble surface of the depth of penetration by thermal diffusivity	m
λ = thermal conductivity of the liquid	kcal/mhr°C		
ν = kinematic viscosity of the liquid	m^2/hr		
η = dynamic viscosity of the liquid	kghr/m^2		

References

[1] Jacob M. *Heat transfer*, Wiley, New York 1949.

[2] Kutateladze S. S., *Teploperedacia pri kondensatii i kipenie* (Heat transfer by condensation and by boiling), Masghiz, Moskwa. 1952.

[3] Grigull V. *Die Grundgesetze der Wärmeübertragung* Springer, Berlin. 1955.

[4] Fritz W. and Ende W. *Phys. Z.* 1936 **37** 391.

[5] Fritz W. *Phys. Z.* 1935 **36** 379.

[6] Levich V. G. *Fizico-khimiceskaia ghidrodinamika* (Physico-chemical hydro-dynamics), Izdateltsvo Akademii Nank SSSR, Moskwa. 1952.

[7] Higbie R. *Trans. Amer. Inst. Chem. Engrs.* 1935 **31** 65 (quoted in [8] and [9]).

[8] Berg C., Manders M. and Switzer R. *Chem. Engng. Progr.* 1951 **47** 11.

[9] West F. B., Gilbert W. D. and Shimizu T. *Industr. Engng. Chem.* 1952 **44** 2470.

[10] Potter O. E. *Chem. Engng. Sci.* 1957 **6** 170.

[11] Kishinevsky M. H. and Pamfilov A. V. *Zh. prikl. khim.* 1949 **22** 1183

[12] Lewis J. B. *Chem. Engng. Sci.* 1954 **3** 248, 260 (quoted in [14]).

[13] Lewis I. B. and Pratt H. R. C. *Nature* 1953 **171** 1155 (quoted in [14])

[14] Christensen G. B. and Terjesen S. G. *Chem. Engng. Sci.* 1958 **7** 222.

[15] Handlos A. E. and Baron T. *Amer. Inst. Chem. Engng. J.* 1957 **3** 127.

[16] Danckwerts P. V. *Industr. Engng. Chem.* 1951 **43** 1460.

[17] Kishinevsky M. H. and Mocialova L. A. *Zh. prikl. khim.* 1956 **29** 170.

[18] Gorodetzkaia A. V. *Zh. fiz. khim.* 1949 **23** 7.

Chemical Engineering Science, 1959, Vol. 10, pp. 31 to 36. Pergamon Press Ltd. London. Printed in Great Britain

Method of calculations for the absorption accompanied with heat liberation

T. Mizushina, J. Oishi and N. Hashimoto
Department of Chemical Engineering, Kyoto University, Kyoto, Japan

(*Received* 27 *June* 1958)

Abstract—When a large quantity of heat is liberated in the absorption of gas into liquid, the heat liberated elevates the temperature of liquid and vaporizes a part of solvent into gas. The temperature of gas also changes through the apparatus. Therefore, in order to calculate the required absorption area, the variation of condition of gas through the apparatus must be known.

This paper describes the method of calculation for the absorption accompanied with heat liberation in countercurrent-type liquid–gas contactors. Enthalpy of mixed gas is defined in terms of absorption heat, and at low concentrations of solute gas and solvent vapour in mixed gas the driving force of absorption is shown to be expressed in terms of a difference of modified enthalpy of mixed gas derived from the above-mentioned enthalpy. By using the diagram of equilibrium conditions and the diagrams which show the relations among the enthalpy, modified enthalpy and temperature of mixed gas, the concentration of solute in mixed gas, the temperature of liquid and the concentration of solute in liquid, the change of condition of gas can be traced through the apparatus. The required area for the absorption can be easily calculated by this method without using the complicated method of successive analytical calculation.

Résumé—Quand l'absorption d'un gaz par un liquide libère une grande quantité de chaleur celle-ci élève la température du liquide et vaporise dans le gaz une partie du solvant. La température du gaz change elle aussi dans l'appareil. On doit donc connaître la variation de la condition du gaz dans celui-ci pour calculer la surface d'absorption nécessaire. Dans cet article les auteurs traitent les méthodes de calcul de l'absorption lorsqu'elle est accompagnée de dégagement de chaleur dans les contracteurs liquide-gaz du type contre courant. L'enthalpie du mélange gazeux est calculée en fonction de la chaleur d'absorption, et pour de faibles concentrations dans le mélange gazeux du gaz soluble et de vapeur du diluant le potentiel d'échange peut s'exprimer en fonction d'une différence d'enthalpie modifiée du gaz, cette enthalpie étante dérivé de l'enthalpie précédente. En utilisant le diagramme des conditions d'équilibre et les diagrammes qui montrent les relations entre l'enthalpie, l'enthalpie modifiée et la température du mélange gazeux, la concentration du soluté dans le liquide, la variation de condition du gaz dans l'appareil peut être décrite. L'aire nécessaire pour l'absorption peut être facilement calculée par cette méthode sans utiliser la méthode compliquée de calculs analytiques successifs.

Zusammenfassung—Wenn bei der Absorption eines Gases in einer Flüssigkeit eine grosse Wärmemenge frei wird, erhöht diese Wärmemenge die Flüssigkeitstemperatur und verdampft einen Teil des Lösemittels in das Gas. Auch ändert sich die Gastemperatur innerhalb der Apparatur. Zur Berechnung der notwendigen Absorptionfläche muss die Änderung des Gaszustandes in der Apparatur bekannt sein.

Diese Arbeit behandelt die Berechnung der Absorption mit Wärmetönung in Gegenstromgeräten mit Austausch zwischen flüssiger und gasförmiger Phase. Die Enthalpie der Gasmischung ist in Termen der Absorptionswärme definiert. Bei kleinen Konzentrationen des gelösten Gases und des lösenden Dampfes in der Gasmischung kann die treibende Kraft der Absorption in Termen einer Differenz der modifizeirten Enthalpie der Gasmischuug ausgedrückt werden, die von der oben erwähnten Enthalpie abgeleitet ist. Bei Verwendung eines Gleichgewichtsdiagramms und der Diagramme für die Beziehungen zwischen der Enthalpie, der modifizeirten Enthalpie und der Temperatur der Gasmischung, kann die Konzentration des Gelösten in der Gasmischung, die Temperatur der Flüssigkeit und die Konzentration des Gelösten in der Flüssigkeit sowie die Änderung des Gaszustandes innerhalb der Apparatur verfolgt werden. Die für die Absorption notwendige Fläche kann mit dieser Methode leicht berechnet werden ohne das komplizierte Verfahren der schrittweisen analytischen Berechnung.

Introduction

When hydrogen chloride gas is absorbed into water to produce hydrochloric acid, a large quantity of heat is liberated. By this heat water vaporizes into gas* and the temperature of acid rises. The temperature of gas also varies through the apparatus.

The process of absorption accompanied by heat liberation as mentioned above cannot be only analysed from the standpoint of mass transfer, but simultaneous heat and mass transfer must be taken into consideration.

Simultaneous heat and mass transfer may be taken into consideration by employing a difference of enthalpy of mixed gas as the driving force in a simple system such as air–water; modified enthalpy is used as the driving force in general inert gas–liquid systems. But in a complicated process, where a component of mixed gas is absorbed into liquid, many variables are encountered and the above-mentioned conventional method is not applicable for analysis.

In this paper a new method of calculation, by defining enthalpy and modified enthalpy of mixed gas, are provided.

There are two types of apparatus used in absorption with heat liberation. One is an adiabatic type in which the system is adiabatic and the heat liberated is balanced with the heat of vaporization and the sensible heat changes of liquid and gas. The other is a type with external-cooling, in which the system is cooled externally with appropriate coolant to remove the heat liberated and the absorption is carried out isothermally. These two types are extreme cases, and the actual operation is midway between them.

Adiabatic Absorption

1. *Basic equations*

Consider a liquid–gas countercurrent absorber, such as a packed tower (Fig. 1). It is assumed that the solute in gas is of low concentration and highly soluble and that the change of concentration of solute in liquid is not considerable. In such a case the rates of heat and mass transfer between liquid and gas phases may be considered to be gas-film controlled. Therefore, the temperature and the concentration of solute in liquid at the interface between two phases are equal to those in the bulk of liquid.

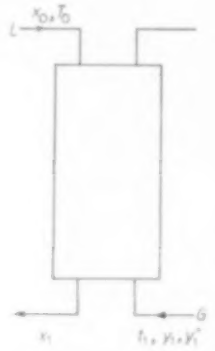

Fig. 1. Liquid–gas countercurrent absorption tower.

The material balance of solute passing differential contact area dA is

$$Ldx = Gdy \tag{1}$$

The rate of vaporization of solvent is assumed to be so small that it is neglected compared with the solvent feed rate. Hence L may be constant through the tower.

Taking the heat balance in dA, equation (2) is obtained.

$$LC_l\,dT = G\,(C_H\,dt + Q dy + Q''\,dy'') \tag{2}$$

The enthalpy of mixture of solute gas, solvent vapour and inert gas is defined as follows.

$$i = C_H\,t + Qy + Q''\,y'' \tag{3}$$

C_H, Q and Q'' may be assumed constant for the system considered*. Hence

$$di = C_H\,dt + Q dy + Q''\,dy''$$

* Vaporization of the solvent also occurs in absorption, but the vapour pressure is so low that the vaporization may be neglected.

* *For* HCl–*Water system at* 25°C *the following values of of* Q *are obtained.*

Composition of hydrochloric acid produced (wt. %)	0·13	2	9·2	16·9
Q	488	481	467	450

VOL. 10 1959

Then equation (2) becomes

$$LC_l\,dT = Gdi \tag{4}$$

The following three equations are obtained for the transfer rates. For the rate of transfer of sensible heat

$$GC_H\,dt = h_g\,(t - T)\,dA \tag{5}$$

For the rate of transfer of solute

$$Gdy = k\,(y - y_i)\,dA, \tag{6}$$

where the difference in the molal ratio of solute to inert gas is taken as the driving force.
For the rate of vaporization of solvent

$$Gdy'' = k''\,(y'' - y_i'')\,dA \tag{7}$$

Substituting equations (5), (6) and (7) in equation (2) and equating equation (4),

$$\begin{aligned} Gdi &= \{h_g\,(t - T) + Q\,k\,(y - y_i) + Q''\,k'' \\ &\quad (y'' - y_i'')\}\,dA \\ &= k\,\{(\alpha\,C_H\,t + Qy + \beta\,Q''\,y'') - \\ &\quad (\alpha\,C_H\,T + Q_i y + \beta\,Q''\,y_i'')\}\,dA, \end{aligned} \tag{8}$$

where

$$\alpha = \frac{h_g}{k\,C_H} \text{ and } \beta = \frac{k''}{k}$$

The modified enthalpy of mixed gas is defined as equation (9).

$$i' = \alpha\,C_H\,t + Qy + \beta\,Q''\,y'' \tag{9}$$

At the interface

$$\begin{aligned} i_i' &= \alpha\,C_H\,t_i + Qy_i + \beta\,Q''\,y_i'' \equiv \alpha\,C_H\,T \\ &\quad + Qy_i + \beta\,Q''\,y_i'' \end{aligned} \tag{10}$$

Then equation (8) becomes

$$Gdi = k\,(i' - i_i')\,dA \tag{11}$$

The integration of equation (11) leads to

$$A = \int dA = \frac{G}{k}\int_{i_i}^{i_a} \frac{d_i}{i' - i_i'}, \tag{12}$$

and by this equation the required absorption area can be calculated.

Generally α and β are given by the equations

$$\alpha = \frac{h_g}{k\,C_H} = \left(\frac{Sc}{Pr}\right)^n \tag{13}_1$$

and

$$\beta = \frac{k''}{k} = \left(\frac{Sc}{Sc''}\right)^n, \tag{13}_2$$

where the value of n has been reported to be $\frac{2}{3}$ [1] or $\frac{1}{2}$ [2].

i' and i_i' are functions of t, y and y'' as seen in equations (3) and (8). Hence, in order to calculate the integral of equation (12), the change of condition of gas must be known through the tower. From equations (5) and (11), equation (14) is obtained,

$$\frac{di}{dt} = \frac{k\,C_H}{h_g}\,\frac{i' - i_i'}{t - T} = \frac{1}{\alpha}\,\frac{i' - i_i'}{t - T}, \tag{14}$$

which gives a direction of the change of condition by the temperature. From equations (6) and (11),

$$\frac{di}{dy} = \frac{i' - i_i'}{y - y_i} \tag{15}$$

This equation shows a direction of the change of condition by the concentration.

Equation (1) for the material balance of the solute and equation (4) for the heat balance express the relationship between the conditions of the bulk of liquid and the bulk of gas at any height in the tower. The relationships are expressed by straight lines having the slopes of G/L and LC_l/G, i.e.

$$\frac{dx}{dy} = \frac{G}{L} \tag{16}_1$$

and

$$\frac{di}{dT} = \frac{LC_l}{G} \tag{16}_2$$

Equilibrium conditions at the interface between liquid and gas are given by the equation

$$y_i = f_1\,(x_i)_{t_i} = f_1(x)_t \tag{17}_1$$

for the concentrations of solute in gas and liquid, and by the equation

$$y_i'' = f_2\,(t)_{x_i} = f_2\,(T)_x \tag{17}_2$$

for the concentration of solvent vapour in gas and the temperature of liquid. Analytical expressions of equations $(17)_1$ and $(17)_2$ are so complicated that usually the relationships are shown diagrammatically.

2. *Method of calculations*

Diagrams are employed to trace the change of condition of gas through the tower and to calculate the absorption area by equation (12).

Diagram A is constructed with i and i' as the ordinate and t as the abscissa to show the relation between i or i' and t (Fig. 2). Diagram B is provided with i, i' and x as the ordinate and y and T as the abscissa to show the relations between i or i' and y, x and y, and i or i' and T (Fig. 3).

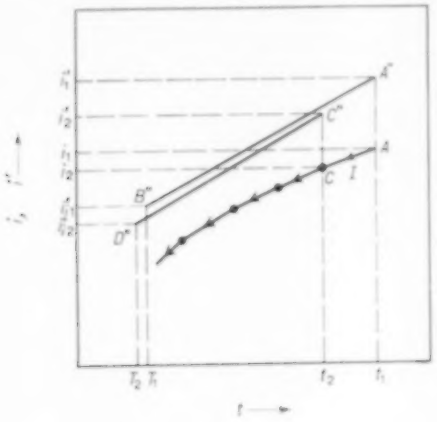

Fig. 2. Diagram A.

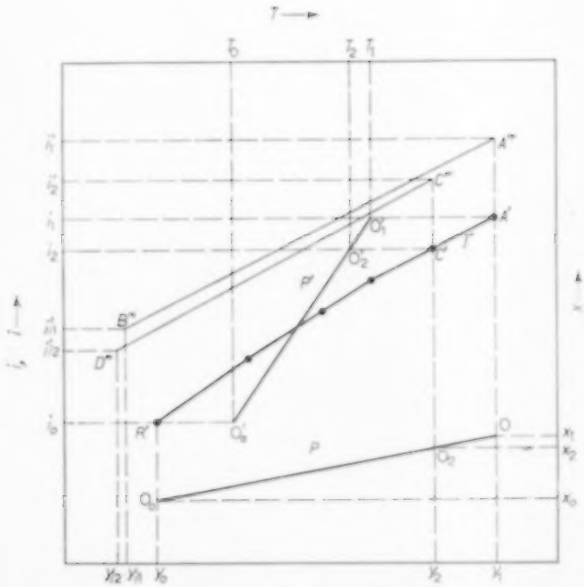

Fig. 3. Diagram B. Adiabatic condition.

It is supposed that of the conditions of gas and liquid at the inlet and outlet of the tower, the condition of gas at the inlet (i.e. at the bottom) $[t_1, y_1, y_1'']$, the condition of liquid at the inlet (i.e. at the top) $[x_0, T_0]$ and the condition of liquid at the outlet (i.e. at the bottom) $[x_1]$ are given, and L and G are known.

Point 0_1 $[y_1, x_1]$ is located on the y–x plane of Diagram B and straight line P is drawn with slope of G/L through point 0_1. Line P is an operating line for $x \sim y$ relation as shown by equation $(16)_1$. Point 0_0 lying on line P with the ordinate of x_0 expresses the operating condition at the top of tower, and y_0, the abscissa of point 0_0 gives the concentration of solute in mixed gas at the top. i_1, the enthalpy of mixed gas at the bottom is obtained by equation (3) from the condition $[t_1, y_1, y_1'']$. T_1 is assumed, and point $0_1'$ is located on the $T - i$ plane of Diagram B with the assumed T_1 and i_1. Straight line P' drawn through point $0_1'$ with the slope of LC_l/G is an operating line for $i \sim T$ relation as shown by equation $(16)_2$, and i_0, the enthalpy of mixed gas at the top is given by point $0_0'$ (T_0, i_0) on line P'.

The change of condition of gas is traced as follows, starting from the condition at the bottom.

Points A (t_1, i_1) and A'' (t_1, i_1') are located on Diagram A, where i_1' is calculated easily from $[t_1, y_1, y_1'']$ and equation (9). Since y_{i1} and y_{i1}'' are obtained by equations $(17)_1$ and $(17)_2$ respectively from the condition $[x_1, T_1]$, i_{i1}' can be calculated by substituting y_{i1} and y_{i1}'' in equation (10). Hence, point B'' (T_1, i_{i1}') can be located on Diagram A. The straight line joining points A'' and B'' has a slope of $(i_1' - i_{i1}'/t_1 - T_1)$, and from equation (14) this slope multiplied by $1/\alpha$ gives a direction of the change of condition for $i \sim T$ at point A. Therefore, straight line I drawn through point A with the slope of $(1/\alpha)$ $(i_1 - i_{i1}/t_1 - T_1)$ is a locus for the change of enthalpy of mixed gas with its temperature. Similarly, points A' (y_1, i_1), A''' $(y_1\, i_1')$ and B''' (y_{i1}, i_{1i}') can be located on Diagram B. The slope of the straight line connect-

ing point A''' with point B''' is $(i_1' - i_{i1}'/y_1 - y_{i1})$, and this slope gives a direction of the change of condition for $i \sim y$ at point A'. Hence, straight line I' parallel to line A''' B''' through point A' shows the change of enthalpy of mixed gas with the concentration of solute gas.

Point C (t_2, i_2) is located on line I of Diagram A at an infinitesimal distance from point A, and corresponding to point C, point C' (y_2, i_2) is located on line I' of Diagram B. Points C and C' give the condition of mixed gas at the position of an infinitesimal distance above the bottom of the tower. Corresponding to point C', points 0_2 (y_2, x_2) and $0_2'$ (T_2, i_2) are located on the operating lines P and P' respectively, and hence the condition of liquid are known at the position considered.

Beginning at points C and C', next conditions are obtained by the same method as above. y_2'' is calculated from the condition $[t_2, y_2, i_2]$ at points C and C' by equation (3), and hence i_2' is known by using equation (9). Point C'' (t_2, i_2') is located on Diagram A corresponding to point C, and point C''' (y_2, i_2') on Diagram B corresponding to point C'. As y_{i2} and y_{i2}'' are calculated from x_2 and T_2 of points 0_2 and $0_2'$ by employing equations $(17)_1$ and $(17)_2$, point D'' (T_2, i_{i2}') and point D''' (y_{i2}, i_{i2}') can be located on Diagram A and Diagram B respectively and these two points give a condition of liquid. The slope of straight line C'' D'' multiplied by $1/\alpha$ gives the direction of the next change of condition of gas starting from point C, and the slope of straight line C''' D''' gives the direction of the next change starting from point C'. The similar procedure is repeated until the locus reaches point R' whose abscissa is y_0. The ordinate of point R' should be i_0, the same as that of point $0_0'$, and if the ordinate is not i_0 it shows that T_1 is assumed incorrectly. Then different value must be assumed for T_1 and the procedure must be repeated until point R' having the abscissa of y_0 and the ordinate of i_0 is obtained on the locus and the assumed T_1 is shown to be correct.

In integrating equation (12) to obtain the area A, the values of i, i' and i_i' may be read at each position in the tower from the diagrams, and $1/i' - i_i'$ may be integrated with i graphically.

Absorption at External-cooling Condition

In the case that absorption occurs in the tower cooled externally, the heat balance may be expressed by equation (18) instead of equation (4)

$$LC_l\,dT = G\,di - dq \tag{18}$$

For simplification, it is supposed that the tower is cooled with a considerable amount of coolant and the temperature of coolant is kept constant. The heat transfered to the coolant is given by

$$dq = U_c\,(T - T_c)\,dA \tag{19}$$

Substituting equation (19) in equation (20),

$$LC_l\,dT = Gdi - U_c\,(T - T_c)\,dA$$

For the rate of transfer rate of heat and mass between liquid and gas, the same expressions as in the adiabatic adsorption are applicable. Dividing both sides of equation (20) by Gdi and using equation (11),

$$\frac{di}{dT} = \frac{LC_l}{G} \Big/ \left\{1 - \frac{U_c}{k}\frac{T - T_c}{i' - i_i'}\right\} \tag{21}$$

are obtained. This equation expresses an operating line for $i \sim T$ in the case of external-cooling.

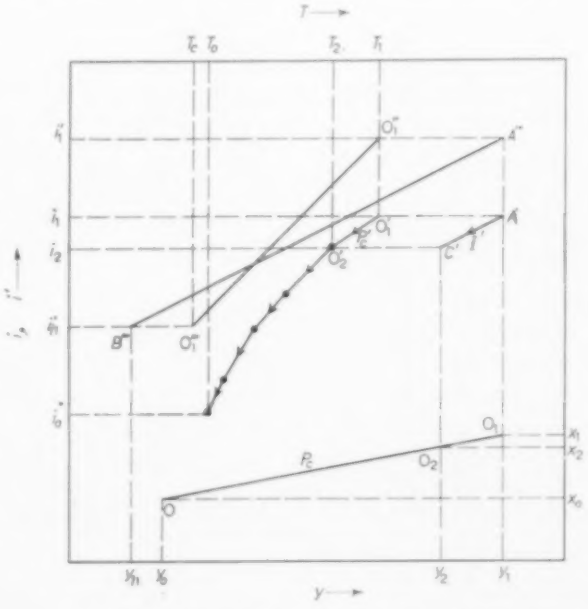

Fig. 4. Diagram B. External cooling condition.

Evidently the operating line is not a straight line joining the conditions at the inlet and outlet of the tower.

Diagram B in this case is shown in Fig. 4. On this diagram points $0_1''$ and $0_1'''$ express the conditions $[T_1,\ i_1']$ and $[T_c,\ i_{i1}']$ respectively. The slope of a straight line connecting point $0_1''$ with point $0_1'''$ is $\dfrac{i_1' - i_{i1}'}{T_1 - T_c}$. By substituting this value in equation (21), (di/dT) can be calculated. Hence, straight line P_c' drawn through point $0_1'$ with the slope of $(di/dT)_1$ now obtained may be an operating line at an infinitesimal interval from the bottom of the tower. Point $0_2'$ located on line P_c' corresponding to point C'' shows the operating condition $[T_2,\ i_2]$. The next change of condition of the gas is traced starting from point C'' and then the operating line is drawn through point $0_2'$ by the same method. The method may be repeated until the condition at the top of the tower is reached.

An examination must be made of the assumed value of T_1 in the same manner as in an adiabatic absorption.

Notation

A = absorption area, m²
C_H = specific heat of mixed gas, kcal/°C kg-inert gas
C_l = specific heat of liquid, kcal/°C kg-solvent
G = inert gas flow rate, kg-inert gas/hr
h_g = gas-film coefficient of heat transfer, kcal/m² hr °C
i = enthalpy of mixed gas, kcal/kg-inert gas
i' = modified enthalpy of mixed gas, kcal/kg-inert gas
k = gas-film coefficient of transfer of solute gas, kg/m² hr Δy
k'' = gas-film coefficient of transfer of solvent vapour, kg/m² hr $\Delta y''$
L = solvent flow rate, kg-solvent/hr
Pr = the Prandtl number of mixed gas
q = heat transferred to coolant, kcal
Q = heat liberated in absorption of solute gas, kcal/kg-solute gas
Q'' = latent heat of vaporization of solvent, kcal/kg-solvent
Sc = the Schmidt number of inert gas-solute gas system,
Sc'' = the Schmidt number of inert gas-solvent vapour system
t = temperature of mixed gas, °C
T = temperature of liquid, °C
T_c = temperature of coolant, °C
U_c = over-all coefficient of heat transfer in cooling, kcal/m² hr °C
x = concentration of solute in liquid, kg-solute/kg-solvent
y = concentration of solute in mixed gas, kg-solute/kg-inert gas
y'' = concentration of solvent vapour in mixed gas, kg-solvent vapour/kg-inert gas

Subscript :
i = interface between liquid and gas

References

[1] Chilton T. H. and Colburn A. P. *Industr. Engng. Chem.* 1934 **26** 1183.
[2] Mizushina, T. and Nakajima M. *Chem. Engng.* (*Japan*) 1951 **15** 30.

VOL. 10 1959

Chemical Engineering Science, 1959, Vol. 10, pp. 37 to 46. Pergamon Press Ltd. London, Printed in Great Britain

Pressure–temperature–density relations of pure liquids*

ALFRED W. FRANCIS

Socony Mobil Oil Company, Inc. Research and Development Laboratory Paulsboro, New Jersey

(*Received* 1 *July* 1958)

Abstract—Saturated densities of liquids are expressed as $D_s = A - Bt - C/(E - t)$ over almost the entire ranges for which data are available. The constants are presented for 130 pure substances.

Liquid density under high pressure can be calculated from saturated density by the equation, $\log (dP/dt)_V = KD - F$, whose constants are tabulated for most of the same liquids.

Résumé—Les densités de liquides saturés sont exprimées par $D_s = A - Bt - C(E - t)$ dans presque tout le domaine des résultats expérimentaux. Les constantes sont données pour 130 substances pures.

La densité liquide sous haute pression peut être calculée à partir de la densité saturée, par l'équation $\log (dP/dt)_V = KD - F$, dont les constantes sont répertoriées pour la plupart des liquides envisagés.

Zusammenfassung—Sättigungsdichten von Flüssigkeiten lassen sich durch die Gleichung $D_s = A - Bt - C/(E - t)$ über den gesamten Bereich ausdrücken, für welchen Messungen vorleigen. Die Konstanten werden für 130 reine Substanzen mitgeteilt.

Die Dichte der Flüssigkeit unter hohem Druck kann aus der Sättigungsdichte durch folgende Gleichung berechnet werden

$$\log (dP/dt)_V = KD - F$$

Die Konstanten dieser Gleichung werden für die meisten der genannten Flüssigkeiten aufgeführt.

SIMPLE equations were published recently [19] for forty-four hydrocarbons relating saturated liquid densities with temperature over wide ranges. Another equation showed a simple relation between liquid density and slopes of isochors, $(dP/dt)_V$, for compression of twenty-seven hydrocarbons and hydrogen. The same forms of equations have now been found applicable to non-hydrocarbons over even wider ranges and with deviations hardly greater than uncertainties in observations, or an average of less than 0·0008.

Constants of equation (1)

$$D_s = A - Bt - \frac{C}{E - t} \qquad (1)$$

have been derived for eighty-one non-hydrocarbons, including twenty-seven inorganic liquids, for which density observations substantially above the boiling points have been published. They are listed in Tables 1 and 2 along with pertinent properties of the liquids, the temperature ranges to which the equations are applicable, and the sources of the data. In the equations D_s is the saturated liquid density, i.e. under the vapour pressure; t is the temperature in °C; A is usually a little higher than the liquid density at low temperatures; B is a little less than the temperature coefficient of liquid density; C is a small integer (with three exceptions) which depends on the curvature; and E is a constant somewhat higher than the critical temperature.

For non-aromatic hydrocarbons the value of E in the equation [19] was usually 34° above the critical temperature. But for aromatic hydro-

*Delaware Valley Regional Meeting, A.C.S., Philadelphia, Pa., 5 February 1958; 133rd Meeting A.C.S., San Francisco, Calif., 18 April 1958.

carbons and for non-hydrocarbons it is necessary to use less uniformity in this constant, possibly because of greater diversity in polarity. This permits adjustment of the constants of equation (1) to make it applicable to the entire temperature range of experimental observations available almost to the critical temperature for each substance except water and the lower alcohols. A recalculation of the constants for hydrocarbons, with relaxation of the restriction on E, allowed a similar large extension of the ranges, as listed in Table 3.

For water the equation is supplemented by a quadratic equation covering the range 50°–230°C with high precision, thus giving substantial overlap. Table 4 presents the degree of concordance in densities of water calculated by three equations in their respective ranges, in comparison with the best selections from observations [15]. In the range 4° to 50°C the density of water is $1-0{\cdot}0000048\,t^2$ very closely. Deuterium oxide requires similar supplementary equations.

The values reported [40, 60] for methyl, ethyl, and propyl alcohols at temperatures considerably below 0°C are inconsistent with any constants for equation (1) which are valid at higher temperatures. They indicate concave curves, i.e. decreasing coefficients of density with rising temperatures. According to BRIDGMAN [9] this relation is rare at ordinary pressures. However, mercury is reported [29] to have a very slightly concave curve for density over the entire liquid range from − 39° to + 357°C. This is perhaps fortunate since it results in an almost perfectly linear plot of specific volume against temperature, thus facilitating calibration of thermometers.

The estimates for acetonitrile in the International Critical Tables [30] in the range 90°–200°C were not used because no observation in that range is published. They are about 0·004 higher than present estimates. The limit in range of equation (1) for phosgene is that of the observations of DAVIES [12], since he showed that the observations in the I.C.T. [30] are about 1 per cent high, and probably at higher temperatures also.

Several published observations on density of liquid hydrogen sulphide in the range − 83° to + 18·5°C [4, 37, 38, 45, 56] are mutually very inconsistent. Extrapolation of the equation from Table 1, which results from the observations at higher temperatures [53] agrees best with those of KLEMENC [37, 38] in the low temperature range. This is illustrated in Fig. 1. The calculations of WEST [63] are based on the observations of BAXTER and co-workers [4]. They show excessive curvature for a range so far below the critical temperature.

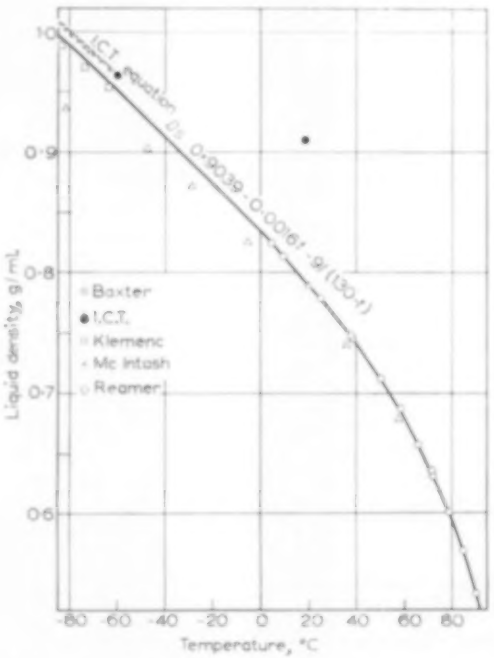

FIG. 1. Density of liquid hydrogen sulphide as a function of temperature.

Equation (2), developed for saturated densities of hydrocarbons within about 50°–100° of the critical temperatures [19], is equivalent to equation (3) published by HERZ [28]

$$(D_s - D_c)^h = G\,(t_c - t) \qquad (2)$$

$$(d - d_k)/a\,(t - t_k)^h = 1 \qquad (3)$$

(with h the reciprocal of b, and if he had used $(t_k - t)$ so as to avoid imaginary values). As in equation (1), t is the temperature in °C and D_s is the saturated liquid density. D_c and t_c are the critical density and temperature, respectively;

Table 2. Constants of equations for saturated densities of organic non-hydrocarbon liquids

Organic Liquid[a]	*Boiling Point*	*Critical temperature*		*Density*		*Equation 1*[b]						*Equation 2*[c]		
		Obs'd.	*Calc'd.*[c]	*Liquid at 20° C*	*Critical*	*A*	*B* × 10^3	*C*	*E*	*Range, °C*	*Mean dev.* × 10^4	*b*	*G* × 10^6	*Min. temp*
Acetic acid	118·1	321·6	322·8	1·0492	0·351	1·1275	91	22	385	16 to 300	7	2·6	1180	180
Acetone	56·2	235·5	236·3	0·7906	0·273	0·8555	96	12	280	− 95 to + 230	7	2·5	866	80
Acetonitrile	81·6	274·7	275·1	0·7824	0·237	0·8355	98	10	315	− 45 to + 260	7	2·5	738	212
Bromobenzene	156·1	397	—	1·4951	0·458	1·5761	117	24	430	0 to 270	4	2·35	2600	130
n-Butyric acid	164·0	355	—	0·9577	0·304	1·0531	72	36	460	0 to 300	9	2·6	870	240
Carbon disulphide [8]	46·25	279	—	1·2632	0·44	1·3743	125	25	310	− 111 to + 80	6	—	—	—
Carbon tetrachloride	76·75	283·2	284·6	1·5940	0·558	1·7022	168	23	330	0 to 270	5	2·6	3580	210
Chlorobenzene	132·0	359·2	359·8	1·1062	0·365	1·1840	91	24	425	− 45 to + 350	3	2·6	1170	240
Chlorodifluoromethane [Freon 22] [6, 50]	− 40·6	96·4	96·7	1·2123	0·525	1·4140	236	17	131	− 69 to + 87	12	2·5	5100	27
Chloroform	61·2	263·4	264·8	1·4891	0·50	1·5920	166	20	365	− 63 to + 251	7	2·7	3550	233
Chlorotrifluoroethylene [48, 50]	− 28·36	105·8	104·25	1·2411	0·55	1·4931	125	20	136	25 to 100	13	2·9	5000	25
Chlorotrifluoromethane [Freon 13] [1, 50]	− 81·4	28·8	28·9	0·9193	0·578	1·3901	300	16	59	− 142 to + 21	9	2·6	7000	− 14
Dichlorodifluoroethane [14]	46·64	222	—	1·4163	—	1·5490	163	23	270	20 to 200	10	—	—	—
Dichlorodifluoromethane [Freon 12] [7, 50]	− 30·0	111·5	111·80	1·329	0·555	1·5277	230	20	130	− 40 to + 100	11	2·6	5330	60
Dichloromonofluoromethane [Freon 21] [6, 50]	8·92	178·5	179·1	1·3781	0·522	1·5225	190	22	225	− 29 to + 158	17	2·5	4125	51
Diethylamine [59]	55·6	223	—	0·7042	0·246	0·7730	81	14	280	0 to 203	5	2·8	432	187
Ethyl acetate	77·15	250·1	250·3	0·9035	0·308	0·9658	106	12	291	− 83 to + 240	5	2·6	979	190
Ethyl alcohol	78·3	243	243·4	0·7894	0·276	0·8700	62	19	300	− 30 to 230	10	2·7	747	140
Ethylamine [30, 31, 59]	16·5	183·2	—	0·6820	0·2434	0·7518	93	10	220	− 73 to + 138	4	2·6	667	126
Ethyl bromide	38·34	230·7	231·1	1·4607	0·507	1·5738	176	20	272	− 112 to + 224	12	2·8	3220	198
Ethyl chloride [50]	12·3	187·2	—	0·8943	0·331	0·9697	130	10	222	0 to 180	8	2·6	1234	100
Ethyl ether	34·6	194	194·2	0·7135	0·264	0·7872	91	12·5	245	− 123 to + 170	4	2·6	663	120
Ethyl formate	54·15	235·3	235·7	0·9226	0·323	1·0004	108	15	284	0 to 225	6	2·6	1080	160
Ethyl mercaptan	35·05	226	—	0·8398	0·300	0·9076	102	12	270	0 to 220	7	2·9	690	170
Ethyl propionate	99·1	272·9	273·3	0·8901	0·2865	0·9520	102	12	316	0 to 265	7	2·6	870	230
Ethyl *n*-propyl ether	63·7	227·4	—	0·7612	0·280	0·7808	104	7	264	0 to 210	7	2·7	513	160
Ethyl sulphide	92·1	284	284·5	0·8360	0·279	0·8987	85	14	336	0 to 270	6	2·7	668	210
Fluorobenzene [16]	84·8	286·92	—	1·0252	0·354	1·0877	108	13	330	0 to 275	8	2·2	2020	250
Iodobenzene	188·45	448	—	1·8307	0·581	1·9212	135	30	488	0 to 270	3·5	—	—	—
*Iso*butyric acid	154·7	336	—	0·9480	0·302	1·0241	82	23	410	− 45 to + 300	5	2·6	876	250
*Iso*propyl *iso*butyrate	120·76	—	—	0·8484	—	0·9028	93	11	328	0 to 230	2	—	—	—
Methanol	64·6	240·0	240·2	0·7914	0·272	0·8497	77	11	277	0 to 232	10	2·8	719	20
Methyl acetate	57·3	233·7	234	0·9335	0·325	1·0128	108	15	280	0 to 227	9	2·6	1130	170
Methyl *n*-butyrate	102·7	281·3	281·5	0·8985	0·300	0·9610	98	13	328	0 to 270	6	2·7	761	230
Methyl chloride [50]	− 23·7	143·1	—	0·898	0·353	1·0207	146	12	180	− 40 to + 120	6	2·7	1600	100
Methyl ether	− 24·9	126·9	126·8	0·6610	0·2714	0·7480	111	8	160	− 24 to − 115	4	2·6	760	90
Methyl ethyl ether	7·6	164·7	163·6	0·700	0·272	0·7570	115	6	195	0 to 160	5	2·8	565	100
Methyl fluoride [11, 23]	− 78·414	44·6	—	0·5782	0·300	0·7939	186	10	78	− 130 to + 42	31	2·8	1140	20
Methyl formate [30]	31·6	214	214·2	0·9742	0·349	1·0616	123	15	280	0 to 200	5	2·6	1330	170
Methyl *iso*butyrate	92·4	267·6	268	0·8890	0·301	0·9504	100	12	310	0 to 260	7·5	2·6	872	220
Methyl mercaptan	5·96	196·8	197·5	0·868	0·323	0·9466	108	12	235	0 to 190	10	2·5	1240	0
Methyl propionate	79·7	257·4	257·6	0·9149	0·3124	0·9807	108	12	300	0 to 250	9	2·6	1000	150
Methyl sulphide	37·3	229·9	229·7	0·8497	0·309	0·9253	95	15	285	0 to 220	10	2·7	810	160
Perfluoro-*n*-butane [18]	− 1·7	113·3	112·9	1·47	0·63	1·715	30	30	145	20 to 85	30	2·7	7500	45
Phosgene [12]	7·56	182	182·2	1·3714	0·520	1·5100	190	20	220	− 20 to + 60	5	2·7[d]	3410[d]	160
Propionic acid	141·3	339	—	0·9930	0·32	1·0650	89	20	305	0 to 280	12	2·6	890	270
Propionitrile	97·2	291·2	—	0·7818	0·240	0·8372	80	12	341	− 90 to + 280	7	2·6	617	210
n-Propyl acetate	101·53	276·2	276·5	0·8884	0·296	0·9513	98	13	323	0 to 266	6	2·7	758	220
n-Propyl alcohol	97·2	264	264·3	0·8035	0·273	0·9032	55	28	340	0 to 250	8	2·7	704	200
n-Propyl formate	80·85	264·9	265·5	0·9038	0·309	0·9785	98	16	320	0 to 250	5	2·6	928	190
Trichloromonofluoromethane [Freon 11] [6, 50]	23·77	198·0	198·3	1·4877	0·554	1·6200	193	21	240	− 40 to + 191	11	2·6	4310	71
Trichlorotrifluoroethane [Freon 113] [6]	47·57	214·1	214·45	1·5760	0·576	1·7322	184	30	270	− 30 to + 192	6	2·6	4800	80
Triethylamine [59]	89·35	259	257	0·7280	0·231	0·7704	84	7	293	0 to 245	5	2·5	614	233
Trimethylamine [13, 59]	2·87	160·1	—	0·6331	0·233	0·6845	102	5	182	0 to 158	3	2·5	710	150
											8			

a—References in addition to [24, 30, 40, 61]

b—Equation (1), $D_s = A - Bt - \dfrac{C}{E - t}$

c—Equation (2), $(D_s - D_c)^b = G\,(t_c - t)$

d—Densities for phosgene from this equation may be about 1 per cent high (cf. [12])

Table 1. Constants of equations for saturat

Inorganic liquid[a]	*Boiling point*	*Critical temperature*		*Density*		
		Obs'd	*Calc'd*[c]	*Liquid at 20°*	*Critical* [39]	*A*
Ammonia [35, 50]	− 33·35	132·3	132·8	0·6103	0·235	0·7048
Argon	− 185·7	− 122	− 122·2	—	0·5308	0·5857
Carbon dioxide [34, 36, 44, 50, 61]	− 78·5	31·04	31·07	0·7771	0·468	1·0652
Carbon monoxide [43, 61]	− 192·0	− 140·2	− 140·3	—	0·301	0·4106
Chlorine [33]	− 33·7	144	142·5	1·524	0·573	1·6060
Deuterium oxide [26, 27]	101·43	371·5	371·6	1·1048	0·363	1·2409
Helium [43]	− 268·9	− 267·9	—	—	0·0693	4·8086[e]
Hydrogen [43]	− 252·7	− 239·9	—	—	0·0326	− 0·0028
Hydrogen bromide [57]	− 67·0	90	—	1·800	—	2·035
Hydrogen chloride	− 83·7	51·4	53·4	0·831	0·42	1·0765
Hydrogen cyanide [20, 61]	26	183·5	184·5	0·6876	0·195	0·7560
Hydrogen sulphide [4, 37, 38, 45, 53, 56]	− 61·8	100·4	100·2	0·8720	0·3488	0·9039
Krypton [43, 46]	− 151·8	− 63·8	− 63·7	—	0·908	1·737
Neon [43]	− 245·9	− 228·7	− 228·5	—	0·484	− 1·266
Nitrogen [43, 50]	− 195·8	− 147	− 146·3	—	0·311	0·1800
Nitrogen dioxide [52]	21·3	158·22	157·8	1·4415	0·550	1·5850
Nitrosyl chloride	− 5·5	167	—	1·3000	—	1·40
Nitrous oxide [22, 43]	− 89·5	36·5	37·3	0·784	0·457	1·0835
Oxygen [43, 50]	− 183·0	− 118·4	—	—	0·41	0·5400
Ozone [43, 55]	− 111·9	− 5	—	—	0·537	1·2860
Perchloryl fluoride [17, 31]	− 46·76	95·17	95·36	1·4475	0·637	1·6844
Phosphine	− 87·4	51·3	53	0·566	0·30	0·7798
Stannic chloride	114·1	318·7	319·1	2·2262	0·742	2·3604
Sulphur dioxide [43, 50]	− 10·0	157·5	156·8	1·3829	0·524	1·5660
Sulphur trioxide [64]	44·8	218·2	219·3	1·9225	0·633	2·008
Water [15]	100·0	374·15	—	0·99816	0·32	1·1258
Xenon [43, 49, 62]	− 109·1	16·59	17	1·987(0)	1·105	2·6709

a—References in addition to 24, 30, 39, 40.

b—Equation (1), $D_s = A - Bt - \dfrac{C}{E - t}$

c—Equation (2), $(D_s - D_c)^h = G\,(t_c - t)$.

d—Equation (6) (deuterium oxide) $D_s = 1{\cdot}1132 - 0{\cdot}0002\,t - 0{\cdot}00^{\circ}003t^2$. Range 50° to 140°C. Mean deviation 2×10^{-4}.

e—Equation (1) for helium using °K. $D_s = 0{\cdot}2666 + 0{\cdot}0158\,T - 1{\cdot}2/(10 - T)$.

f—Equation (5) for water $D_s = 1{\cdot}0064 - 0{\cdot}00025t - 0{\cdot}0^{\circ}0^{\circ}023t^2$. Range 50° to 230°C. Mean deviation $1{\cdot}4 \times 10^{-4}$.

urated densities of inorganic liquids

	Equation 1[b]					Equation 2[c]		
	$B \times 10^5$	C	E	*Range*, °C	*Mean Dev.* $\times 10^4$	h	$G \times 10^6$	*Min. temp.*
48	98	12	180	− 78 to + 120	4·6	2·35	876	− 40
57	500	10	− 101	− 189 to − 131	32	2·5	10170	− 161
52	318	7	+ 51	− 56 to + 22	5	2·6	4286	0
06	265	10	− 112	− 205 to − 147	9	2·5	3100	− 190
60	216	28	+ 200	− 100 to + 130	13	2·6	4500	90
09	80	30	440	140[d] to 350	9	2·6	1495	140
86[e]	− 1660	1·3	− 263	− 271 to − 268·5	2	3·3	76·3	− 270·84
28	36	0·4	− 230	− 258 to − 246	3	2·7	12·8	− 258
35	380	17	130	− 80 to + 60	24	—	—	—
65	225	13	85	− 85 to + 50	4	2·5	3400	− 20
60	116	9	220	− 13 to + 160	2	2·0	2040	160
39	160	9	130	4 to + 90	8	2·4	1720	0
7	580	25	− 35	− 147 to − 71	13	2·7	27400	− 92
6	1080	5	− 219	− 248 to − 234	4	2·4	26700	− 249
90	360	5	− 129	− 210 to − 150	21	2·5	3480	− 196
50	143	20	190	21 to 149	11	2·7	5820	88
	220	10	200	− 6 to + 40	—	—	—	—
35	240	11	64	− 90 to + 20	8	2·5	4000	− 90
00	390	10	− 93	− 210 to − 128	18	2·5	6300	− 168
50	269	13	+ 7	− 183 to − 25	5	2·0	8590	− 183
44	267	20	130	− 142 to + 90	22	2·9	6200	54
98	72	20	120	− 87 to + 40	4	3·0	610	− 20
04	228	30	363	0 to 280	9	2·5	7930	180
50	194	27	205	− 50 to 145	11	2·4	5000	0
8	450	—	—	+ 12 to 180	43	2·6	5970	150
58	67	32	451	180[f] to 340	3	2·56	1200	190
09	560	33	48	− 67 to + 10	$\frac{48}{9}$	3·3	36400	0

Table 3. Constants of equations for saturated densities of hydrocarbons nearly to their critical temperatures.

Hydrocarbon	*A*	*B* × 10⁵	*C*	*E*	*Range*, °C	*Mean dev. from Eq. 1**
Methane	0·3254	94	6	− 48	− 180 to − 90	3
Ethane	0·4976	100	6	64	− 180 to + 27	4
Ethylene	0·5000	112	7	45	− 170 to 0	7
Acetylene	0·5061	122	7	69	− 81 to + 25	4
Propane	0·5757	95·7	6	128	− 150 to + 90	5
Propylene	0·5995	103	7	127	− 160 to + 80	7·4
n-Butane	0·6379	87	7	186	− 140 to + 146	9
*Iso*butane	0·6344	85	10	186	− 80 to + 121	8·7
1-Butene	0·6574	96	7	180	− 110 to 125	4·6
2-Butene (*trans*)	0·6897	81	13	208	− 40 to + 25	1
*Iso*butene	0·6566	95	7	179	− 50 to 130	2
Butadiene	0·7000	91	11	206	− 109 to 140	4
n-Pentane	0·6853	79	10	243	− 136 to 185	9·4
*Iso*Pentane	0·6738	83	8	231	− 158 to 175	5
Neopentane	0·6493	88	7	195	− 20 to 150	5
2-Pentene (*cis*)	0·7382	72	15	240	− 70 to + 80	4
2-Pentene (*trans*)	0·7277	72·5	15	250	− 70 to + 80	4
2-Methyl-2-butene	0·7822	56	25	250	− 70 to + 80	3·3
n-Hexane	0·7154	75	11	285	− 100 to 220	4
2-Methylpentane	0·7022	79	8	260	− 10 to 220	5
3-Methylpentane	0·7248	74·6	12	283	− 10 to 220	1
2, 2-Dimethylbutane	0·7058	75·5	10	260	0 to 210	4
2, 3-Dimethylbutane	0·7163	77	10	274	− 10 to 210	4·5
n-Heptane	0·7333	74	10	308	− 90 to 238	5
3-Ethylpentane	0·7478	75·4	10	310	− 120 to + 90	1
2, 2-Dimethylpentane	0·6979	83	2	280	− 120 to + 80	0·7
2, 3-Dimethylpentane	0·7448	73·5	10	307	0 to 246	6·3
2, 4-Dimethylpentane	0·7150	80	7	282	0 to 230	8
n-Octane	0·7486	72	10	339	− 60 to 290	6
2, 5-Dimethylhexane	0·7440	72	11	326	− 20 to 260	4·6
2, 2, 4-*Tri*methylpentane	0·7403	72·5	10	316	− 110 to 260	4·5
2, 2, 3, 3-Tetramethylbutane	0·7672	72	10	340	20† to 230	10
n-Nonane	0·7681	68	13	378	− 50 to 240	7
2, 2, 5-*Tri*methylhexane	0·7528	75	9	334	20 to 285	8
n-Decane	0·7822	65·8	15	408	− 30 to 325	4
n-Dodecane	0·8057	61·2	20	467	− 10 to 370	3·8
*Cyclo*Pentane	0·8057	79·4	15	297	0 to 225	4·4
Methyl*cyclo*Pentane	0·8010	84	10	302	0 to 255	9·5
Ethyl*cyclo*Pentane	0·8201	81	12	347	20 to 285	7·7
*Cyclo*hexane	0·8286	85	10	324	7 to 273	6·6
Methyl*cyclo*hexane	0·8244	74	13	352	− 95 to 285	8
Benzene	0·9360	93	12	334	0† to 280	5·1
Toluene	0·9371	77	20	386	− 23 to 305	4
o-Xylene	0·9632	67	30	452	− 30 to 336	11
m-Xylene	0·9296	72·5	20	415	− 50 to 330	10
p-Xylene	0·9272	73	20	411	10 to 340	11
Ethylbenzene	0·9078	82	9	390	− 90 to 140	2
Naphthalene	1·0810	74	20	550	70† to 430	5·4
Biphenyl	1·0786	72	18	588	60† to 520	8
						6

*Equation (1), $D_s = A - Bt - \frac{C}{E - t}$ †Subcooled

Table 4. Saturated density of water as a function of temperature (observed vs. calculated)

Temp.	Calculated			Observed[d]	Temp.	Calculated		Observed[d]
	Eq. 1[a]	Eq. 2[b]	Eq. 5[c]			Eq. 1[a]	Eq. 2[b]	
50			0·9881	0·9881	270	0·7682	0·7672	0·7679
60			0·9831	0·9832	280	0·7511	0·7497	0·7507
70			0·9776	0·9777	290	0·7327	0·7314	0·7323
80			0·9717	0·9718	300	0·7129	0·7117	0·7125
90			0·9653	0·9653	310	0·6911	0·6905	0·6908
100			0·9584	0·9583	320	0·6671	0·6669	0·6670
110			0·9511	0·9510	330	0·6402	0·6405	0·6405
120			0·9432	0·9431	340	0·6097	0·6101	0·6095
130			0·9350	0·9349	350		0·5737	0·5725
140			0·9263	0·9261	355		0·5521	0·5531[e]
150			0·9171	0·9169	360		0·5265	0·5245
160			0·9075	0·9074	365		0·4946	0·4960[e]
170			0·8974	0·8974	366		0·4870	0·4882[e]
180	0·8871		0·8869	0·8869	367		0·4788	0·4801[e]
190	0·8759	0·8774	0·8759	0·8760	368		0·4703	0·4708[e]
200	0·8643	0·8654	0·8644	0·8647	369		0·4601	0·4608[e]
210	0·8523	0·8529	0·8523	0·8528	370		0·4490	0·4482
220	0·8399	0·8403	0·8401	0·8403	371		0·4359	0·4354
230	0·8269	0·8272	0·8272	0·8273	372		0·4205	0·4200
240	0·8133	0·8133		0·8136	373		0·3993	0·3997
250	0·7991	0·7986		0·7992	374		0·3574	0·358
260	0·7841	0·7832		0·7840	374·15	Critical Point		0·323

[a] $D_s = 1{\cdot}1258 - 0{\cdot}00067\ t - 32/(451 - t)$

[b] $(D_s - D_c)^{2\cdot56} = 0{\cdot}0012\ (t_c - t)$

[c] $D_s = 1{\cdot}0064 - 0{\cdot}00025\ t - 0{\cdot}0000023\ t^2$

[d] Reciprocals of selections of specific volumes in DORSEY [15] 592.

[e] Reciprocals of selections of specific volumes in DORSEY [15] 583.

h is an exponent, usually between 2 and 3; and G is another constant.

HERZ applied equation (3) to five substances over so great a range in temperature as to introduce discrepancies over 2 per cent for each substance. In the ranges here applied the uncertainty is usually less than one tenth as great. SUGDEN's somewhat similar equation [58] is explicit for neither liquid nor vapour densities in absence of the other; and it is inaccurate for "associated liquids," and for "unassociated liquids" close to the critical temperatures.

Equation (2) is less convenient than equation (1) because of the decimal exponent; and its range of reliability is more limited. However, its constants have been evaluated for all but the six liquids in Tables 1 and 2 which lack observations near the critical temperatures. The equation furnishes an excellent means of correlation of density observations in the critical region, which are more erratic than those at lower temperatures.

In several cases the value of G in equation (2) calculated from the liquid density observation nearest the critical temperature is higher than that from the others. In a few cases it is lower. Since

it is perfectly in line for water and very close for the other best-studied substances, it seems possible that the discrepancies in other cases are due to inaccuracies in observation. An adjustment of a few tenths of one degree in the critical temperature or that of the other observation in each case will almost eliminate the discrepancy. Consistency in this respect is evidence of the validity of the observations. Some suggested critical temperatures which would improve it are included in column 4 in Tables 1 and 2 when these differ from the observations of column 3. However, this relation cannot provide an accurate calculation of critical temperatures unless the critical densities are known accurately.

Figures 2 and 3 illustrate the degree of concordance of many investigations on the density of liquid carbon dioxide. Observations are plotted on a large vertical scale as deviations from values calculated by equations (1) and (2) respectively. Increased weight is assigned to the more recent observations, points L, M and Curve 5. Curve 1 is preferred up to 22°C; and Curve 2 is valid from 0° to the critical temperature, 31·04°C. Between 0° and 22°C either equation is satisfactory. Similar methods were used with the other substances, though usually without such a wealth of observations.

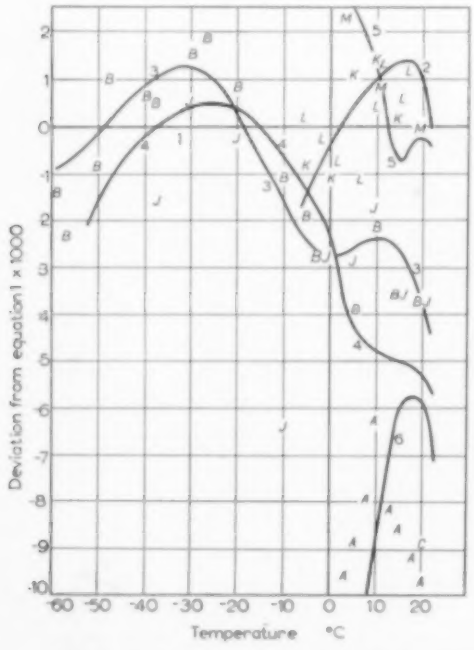

Fig. 2. Density of liquid carbon dioxide.

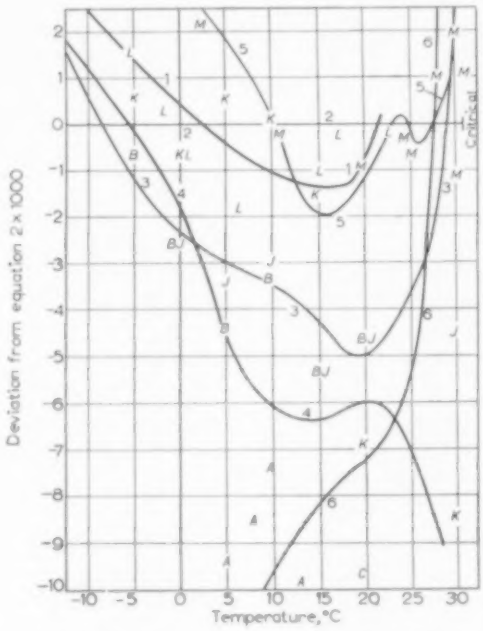

Fig. 3. Density of liquid carbon dioxide.

It is doubtful if consistent correlation of the constants in the tables with structure is yet possible because they were derived empirically. Trifling revisions in observations selected could make large changes in the constants. Two equations with quite different constants might reproduce the observations almost equally well because of mutual compensation.

Thus the observations on ethyl ether from − 123° to + 170°C are reproduced equally well by equations with the following constants:

A	B	C	E	Av. deviation
0·7872	0·00091	12·5	245	0·0004
0·7889	0·000905	13	247	0·0004
0·7924	0·000896	14	250	0·0004

If the range were shortened to − 123° to + 60°C, the average deviation of the observations (given to five decimal places) is only 0·00007 for each

of the above three equations. It is because of the relatively better observations on this substance, and the wide range, that the extra decimal place in B or C is justified.

The negative values of A for hydrogen and neon, and the large value for helium have no physical significance, and are due merely to the low densities and low temperatures involved. PATTERSON and co-workers [49] called attention to the high critical density of xenon. It indicates that close to the critical temperature and pressure it should be possible to have bubbles of xenon gas *sinking* in liquid water, perhaps a unique phenomenon.

The larger average deviations for argon, xenon, and sulphur trioxide are due, of course, to erratic observations (which are understandable because of rarity, difficulty in purification, or hygroscopicity). Observations on sulphur trioxide do not justify an equation more complex than a linear one. The relatively larger deviations for several of the fluorine compounds may be due not to less accurate observations, but to the probability that observations on most of the longer known substances have been smoothed previously in other ways.

Some industrially important liquids such as 2-butanone (methyl ethyl ketone) and acetic anhydride are omitted from the Tables because no density data above their boiling points are published.

Original references are omitted from Tables 1 and 2 unless they give data not included in the compilations [24, 30, 39-42, 61]. Critical data are mostly those from KOBE and LYNN [39]. Most of the boiling points and densities used in Table 2 are listed in TIMMERMANS [61]. References and the physical properties of the hydrocarbons and their equation (2) constants, are omitted from Table 3 because they are given in the earlier paper [19].

ISOCHORS

BRIDGMAN [9] and others maintained that isochors or lines of constant volume are not straight. Although there are numerous slight irregularities at high pressures, these are nearly random in direction of curvature. At least the assumption of straight isochors gives a useful correlation. The slopes of the isochors are related to the densities by equation (4).

$$\log S = \log (dP/dt)_V = KD - F \qquad (4)$$

Constants for this equation are evaluated for sixty-nine non-hydrocarbon liquids in Table 5. Data for most of these substances are from BRIDGMAN's work [8, 9, 30, 42] and that of AMAGAT [3], and extend up to 12,000 atm.

This relation is illustrated in Fig. 4 for carbon dioxide. Only for hydrogen [19] and for water (below 2000 atm in each case) are the isochors noticeably curved. The former are slightly convex, and the latter slightly concave. At temperatures above 50°C or at high pressures the water isochors are satisfactorily straight.

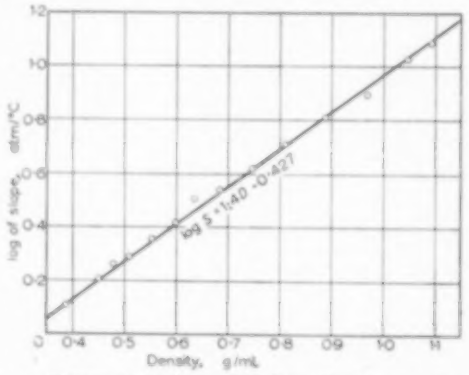

FIG. 4. Slopes of isochors of carbon dioxide as a function of density.

As many isochors as possible, usually about twelve, were calculated for each substance. In general their slopes are $(P_2 - P_1)/(t_2 - t_1)$ in which P_1 and P_2 are two listed pressures, t_2 is one of the higher listed temperatures, and t_1 is the temperature at P_1 corresponding to the same relative volume as that at P_2 and t_2, as found by interpolation or short extrapolation. In order to get isochors over as long a range as possible, and thus improve the accuracy of their slopes, P_1 was taken as one atmosphere when densities were known at sufficiently low temperatures, sometimes as low as -100°C. This method permitted calculations of isochors when relative volumes were given at only one temperature under pressure, as in the cases of isoprene [19] and carbon tetrachloride, eugenol, and glycerol.

Table 5.

Constants of isochors for compression of non-hydrocarbon liquids[a]

Substance	*K*	*F*	*References*
Acetic acid[b]	2·0	1·048	30
Acetone	1·5	0·11	8, 20, 30, 42
Allyl alcohol	1·9	0·552	3
Ammonia	2·2	0·16	35
Aniline[b]	2·1	0·882	30
Bromobenzene	0·9	0·213	8, 9, 42
Bromoform	0·6	0·682	8, 9, 42
n-Butyl alcohol	1·6	0·240	8, 9
n-Butyl bromide	1·1	0·407	8, 42
n-Butyl chloride	1·4	0·218	8, 42
n-Butyl iodide	1·0	0·561	8, 42
n-Butyl phthalate	1·2	0·117	8, 42
Capric acid[b]	3·0	1·628	30, 40
Carbon dioxide	1·4	0·427	34
Carbon disulphide	1·1	0·326	9, 21, 30, 42
Carbon tetrachloride	1·3	1·034	8, 9, 21, 42
Chlorobenzene	1·5	0·52	8, 9, 21, 42
Chloroform[b]	1·4	0·979	21, 40, 42
Chlorotrifluoromethane (Freon 13)	1·1	− 0·308	1
Dichlorodifluoroethane	1·3	0·86	14
Diethylene glycol	1·7	0·673	8, 42
Diphenylamine[b]	2·1	1·118	30, 40
Ethyl acetate[b]	2·3	0·993	30, 40
Ethyl alcohol	1·5	0·142	9, 21, 30, 42
Ethyl bromide	0·8	0·094	9, 30
Ethyl *n*-butyrate[b]	2·2	0·863	30, 40
Ethyl chloride	1·5	0·391	9, 30
Ethyl dibenzylmalonate	2·0	1·03	8, 42
Ethylene chloride[b]	1·6	0·844	30, 40
Ethylene glycol	1·4	0·311	8, 42
Ethyl ether	1·1	0·289	8, 9, 21, 30, 42
Ethyl iodide	0·7	0·365	9, 30
Eugenol	1·9	0·783	8, 42
Fluorobenzene	1·95	0·936	16
Glycerol	1·5	0·601	8, 42
n-Hexyl alcohol	2·3	0·874	8, 9, 42
Hydrogen (above 2,000 atm)	22·0	0·885	19

Table 5. (Continued)

Substance	*K*	*F*	*References*
Hydrogen sulphide	1·7	0·38	53
*Iso*amyl alcohol	1·9	0·533	8, 30
*Iso*butyl alcohol	2·1	0·713	9, 30
*Iso*propyl alcohol	1·7	0·272	8, 9, 42
Mercury	0·15	0·398	9
Methanol	1·6	0·192	8, 9, 21, 30, 42
Methyl acetate[b]	2·4	1·129	30, 40
Methyl *n*-butyrate[b]	1·6	0·32	30, 40
3-Methyl-1-heptanol	1·8	0·369	8, 42
2-Methyl-3-heptanol	1·8	0·403	8, 42
6-Methyl-3-heptanol	1·9	0·437	8, 42
3-Methyl-4-heptanol	1·9	0·527	8, 42
Methyl oleate	2·5	1·075	8, 42
Nitrobenzene[b]	2·2	1·433	30
Nitrogen dioxide	0·7	− 0·15	52
3-Octanol	1·9	0·498	8, 42
Palmitic acid[b]	3·0	1·642	30, 40
Phosphorus trichloride	1·0	0·525	9, 30
n-Propyl alcohol	2·2	0·765	9, 30, 42
n-Propyl bromide	1·0	0·33	8, 42
n-Propyl chloride	1·8	0·621	8, 42
Propylene glycol	1·9	0·765	8, 42
n-Propyl iodide	0·7	0·175	8, 42
Tetrachloroethylene[b]	1·1	0·638	8, 30
Thymol[b]	2·0	0·858	30, 40
p-Toluidine[b]	1·8	0·59	30, 40
o-Tolyl phosphate	1·0	− 0·03	8, 42
Triacetin	1·2	0·169	8, 42
Tricaproin	1·6	0·488	8, 42
Triethanolamine	2·0	1·103	8, 42
Trimethylene glycol	2·2	1·126	8, 42
Water (above 50°C *or* 2,000 atm)	2·2	1·11	8, 9, 30

a—Log $(dP/dt)_V = KD - F$ Slope in atm/°C.
Applicable to densities above the critical density.
b—Calculated from compressibility coefficients (21, 30, 40, 41).

Use of the isochor equations would normally employ the reverse procedure. That is, an isochor would be selected, by trial if necessary, having the same density or specific volume as that at saturated pressure and some lower temperature [e.g. by equation (1)] or at some other temperature and pressure. Examples are given of methods of calculation in the earlier paper [19].

Isochors can be calculated also by dividing the relative expansion coefficient, dV/Vdt, by the compressibility coefficient, $\beta = \left(\frac{-10^6}{V}\frac{dV}{dP}\right)$ at the same temperature and minimum pressure range. The latter is given [30, 40, 41] for several substances. Derivation of equation (4) requires at least two isochors at widely different densities (or temperatures). Precision of isochors is believed to approach that shown for carbon dioxide (Fig. 4), except for those marked *b* [40] in Table 5.

Errata in Reference 19.
Figure 2 (ordinate) change °C to $G/M1$.
Figure 5 change title to "*Slopes of hydrogen isochors.*"

Notation

P = pressure, atmospheres
t = temperature, °C.
t_c = critical temperature
V = volume, ml.
D = liquid density, g/ml.
D_s = saturated density, (under vapour pressure)
D_c = critical density
β = compressibility coefficient, $\left(\frac{-10^6}{V}\frac{dV}{dP}\right)_t$
S = slope of isochor, $(dP/dt)_V$
A, B, C, E = empirical constants of equation (1)
b, G = empirical constants of equation (2)
F, K = empirical constants of equation (4)

Curves
1. Equation 1. $D_s = 1{\cdot}0632 - 0{\cdot}00318t - 7/(51 - t)$. (Horizontal line in Fig. 2 ; valid only up to 22°C).
2. Equation 2. $(D_s - D_c)^{3{\cdot}6} = 0{\cdot}004286\ (t_c - t)$. Horizontal line in Fig. 3 ; valid only above 0°C.
3. Selections of International Critical Tables [31].
4. Selections of Refrigerating Data Book [50, 54].
5. Observations of Kendall and Sage [34].
6. Selections of Handbook of Chemistry and Physics [25].

Points
A Amagat [2, 41].
B Behn [5, 41].
C Cailletet [10, 41].
J Jenkin [32, 41].
K Keyes and Kenny [36, 44].
L Lowry and Erickson [44, 61].
M Michels and co-workers [47, 61].

Several other points, *A*, *C* and *K* are too low to appear on the graph.

References

[1] Albright L. F. and Martin J. J. *Industr. Engng. Chem.* 1952 **44** 188.
[2] Amagat E. H. *C. R. Acad. Sci., Paris.* 1892 **114** 1093.
[3] Amagat E. H. *Ann. Chim. Phys.* 1913 **28** 5.
[4] Baxter J. P., Burrage L. J. and Tanner C. C. *J. Soc. Chem. Ind.* 1934 **53** 410T.
[5] Behn U. *Ann. Phys.* 1900 (4) **3** 733.
[6] Benning A. F. and McHarney R. C. *Industr. Engng. Chem.* 1940 **32** 814.
[7] Bichowsky F. R. and Gilkey W. K. *Industr. Engng. Chem.* 1931 **23** 366.
[8] Bridgman P. W. *Proc. Amer. Acad. Arts Sci.* 1931 **66** 185-233 ; 1932 **67** 1-27 ; 1933 **68** 1-25.
[9] Bridgman P. W. *The Physics of High Pressure*, 128-30 136 138-9 Bell, London 1949.
[10] Cailletet L. P. and Mathias E. *C. R. Acad. Sci., Paris* 1886 **102** 1202.
[11] Cawood W. and Patterson H. S. *J. Chem. Soc.* 1932 2180.
[12] Davies C. N. *J. Chem. Phys.* 1946 **14** 48.
[13] Day H. O. and Felsing W. A. *J. Amer. Chem. Soc.* 1950 **72** 1698.
[14] Deviney M. L. Jr. with Felsing W. A. *J. Amer. Chem. Soc.* 1957 **79** 4915.
[15] Dorsey N. E. *Properties of Ordinary Water Substance* 583, 592 Reinhold, New York 1940.
[16] Douslin D. R., Moore R. T., Dowson J. P. and Waddington G. *J. Amer. Chem. Soc.* 1958 **80** 2031.
[17] Engelbrecht A. and Atzwanger H. *J. Inorg. Nuclear Chem.* 1956 **2** 348.
[18] Fowler R. D. *et al. Industr. Engng. Chem.* 1947 **39** 375.
[19] Francis A. W. *Industr. Engng. Chem.* 1957 **49** 1779.
[20] Fredenhagen K. and Dahmlos J. *Z. anorg. Chem.* 1929 **179** 77.
[21] Freyer E. B., Hubbard J. C. and Andrews D. H. *J. Amer. Chem. Soc.* 1929 **51** 766.
[22] Golding B. H. and Sage B. H. *Industr. Engng. Chem.* 1951 **43** 160.

[23] Grosse A. V., Wacker R. C. and Linn C. B. *J. Phys. Chem.* 1940 **44** 275.

[24] *Handbook of Chemistry and Physics* (2th ed.) 1760-80. Chemical Rubber Publishing Co., Cleveland Ohio 1944.

[25] *Handbook of Chemistry and Physics* (28th ed.) p. 1819 Chemical Rubber Publishing Co., Cleveland Ohio 1944. (also in all recent editions).

[26] Hebert G. M., McDuffie H. F. and Secoy C. H. *J. Phys. Chem.* 1958 **62** 431.

[27] Heiks J. R., Barnett M. K., Jones L. V. and Orban E. *J. Phys. Chem.* 1954 **58** 488.

[28] Herz, W. *Z. Electrochem.* 1927 **33** 348.

[29] *International Critical Tables* Vol. II 458. McGraw-Hill, New York 1927.

[30] *International Critical Tables* Vol. III 22-9, 35-42, 2(3-4, 228-246, McGraw-Hill, New York 1928.

[31] Jarey R. L. *J. Phys. Chem.* 1957 **61** 498.

[32] Jenkin C. F. *Proc. Roy. Soc.* 1920 **A98** 170.

[33] Johnson F. N. G. and McIntosh D. *J. Amer. Chem. Soc.* 1909 **31** 1138.

[34] Kendall B. J. and Sage B. H. *Petroleum* 1951 **14** 184.

[35] Keyes F. G. *J. Amer. Chem. Soc.* 1931 **53** 965.

[36] Keyes, F. G. and Kenny A. W. *J. Amer. Soc. Refrig. Engng.* 1916 **3** 48.

[37] Klemenc A. *Z. Elektrochem.* 1932 **38** 592.

[38] Klemenc A. and Bankowski O. *Z. anorg. allgem. Chem.* 1932 **208** 350.

[39] Kobe K. A. and Lynn R. E. Jr. *Chem. Rev.* 1953 **52** 117.

[40] Landolt-Börnstein-Roth Scheel *Tabellen Hauptwerke* Erg. I 94, 271-84, 452. Julius Springer, Berlin 1923.

[41] Landolt-Börnstein-Roth Scheel *Tabellen Hauptwerke* Erg. I 56, 1931. Julius Springer, Berlin 1923.

[42] Landolt-Börnstein-Roth Scheel *Tabellen Hauptwerke* Erg. IIa 88-95, Julius Springer, Berlin 1935.

[43] Little Arthur D. Inc., *Boiling Points of Gases* 1958.

[44] Lowry H. H. and Erickson W. R. *J. Amer. Chem. Soc.* 1927 **49** 2729.

[45] McIntosh D. and Steele B. D. *Proc. Roy. Soc.* 1904 **A73** 450.

[46] Mathias E., Crommelin C. A. and Meihuizen J. J. *C. R. Acad. Sci., Paris* 1937 **204** 632.

[47] Michels A., Blaisse B. and Michels C. *Proc. Roy. Soc.* 1937 **A160** 358.

[48] Oliver G. D., Grisard J. W. and Cunningham C. W. *J. Amer. Chem. Soc.* 1951 **73** 5719.

[49] Patterson H. S., Cripps R. S. and Whytlaw-Gray R. *Proc. Roy. Soc.* 1912 **A86** 584.

[50] Perry J. H. *Chemical Engineers' Handbook* (3rd Ed.) 250-275 McGraw-Hill 1950.

[51] Pohland E. and Mehl W. *Z. phys. Chem.* 1933 **A164** 48.

[52] Reamer H. H. and Sage B. H. *Industr. Engng. Chem.* 1952 **44** 185.

[53] Reamer H. H., Sage B. H. and Lacey W. N. *Industr. Engng. Chem.* 1950 **42** 140.

[54] *Refrigerating Data Book* (5th Ed.) American Society of Refrigerating Engineers, New York 1942.

[55] Riesenfeld E. H. and Schwab G. M. *Z. Phys.* 1922 **11** 16.

[56] Steele B. D., McIntosh D. and Archibald E. H. *Z. phys. Chem.* 1906 **55** 141.

[57] Strunk W. G. and Wingate W. H. *J. Amer. Chem. Soc.* 1954 **76** 1025.

[58] Sugden S. *J. Chem. Soc.* 1927 1780.

[59] Swift E. Jr. *J. Amer. Chem. Soc.* 1942 **64** 115.

[60] Timmermans J. *Bull. Chim. Soc. Belg.* 1912 **26** 205 ; *ibid.* 1923 **32** 299.

[61] Timmermans J. *Physical Constants of Pure Organic Compounds.* Elsevier, New York 1950.

[62] Weinberger M. A. and Schneider W. G. *Canad. J. Chem.* 1951 **30** 431.

[63] West J. R. *Chem. Engng. Progr.* 1948 **44** 287.

[64] Westrink R. *Acad. Proefschrifft Univ. Amsterdam*; *Chem. Abstr.* 1942 **36** 696.

Chemical Engineering Science, 1959, Vol. 10, pp. 47 to 56. Pergamon Press Ltd. London. Printed in Great Britain

The absorption and the chemisorption of ammonia in a jelly

P. M. HEERTJES, M. H. VAN MENS and M. BUTAYE

Laboratory of Chemical Engineering of the Technical University, Delft

(*Received* 1 *July* 1958)

Abstract—In jellies consisting of a solution of carboxy methyl cellulose in water the absorption and chemisorption of ammonia has been studied. The reacting component was acetic acid. The concentration of ammonia and of free acetic acid has been measured as a function of the distance from the plane surface, for so called semi-infinite layers. It has been found, that for jellies containing 4% by weight of carboxy methyl cellulose, the equations derived and given in the literature for absorption and for chemisorption, in the case of an infinite fast reaction, in semi-infinite layers of a stagnant liquid, were valid, for the distribution of ammonia in the jelly, as well as for the amount of ammonia sorbed.

Résumé—Les absorptions, physique et chimique de l'ammoniac dans les gels preparés à partir d'une solution de carboxy-methyl-cellulose dans l'eau ont été étudiées.

Le composé réactif était l'acide acétique. La concentration en ammoniac et en acide acétique libre ont été mesurées pour ce qu'on appelle des couches semi-infinies en fonction de la distance á la surface plane. Il a été trouvé que pour des gels contenant 4% en poids de carboxy-methyl-cellulose, les équations données dans la littérature pour les absorptions physique et chimique dans le cas d'une réaction instantanée et pour des couches semi-infinies d'un liquide stagnant, étaient valables, aussi bien pour la distribution de l'ammoniac dans le gel que pour la quantité d'ammoniac absorbée.

Zusammenfassung—Die Absorption und Chemisorption von Ammoniak wurde in Gelen untersucht, die aus wässrigen Lösungen von Karboxymethylzellulose bestanden. Die Reaktionskomponente war Essigsäure. Die Konzentration von Ammoniak und freier Essigsäure wurden als Funktion des Abstandes von der ebenen Oberfläche gemessen, in sogenannten halbunendlichen Schichten. Für Gele, die 4 Gewichtsproenzt Karboxymethylzellulose enthielten, bestätigten die Messungen jene Gleichungen für die Absorption und Chemisorption, die für unendlich schnelle Reaktion in halbunendlichen Schichten einer ruhenden Flüssigkeit abgeleitet und in der Literatur mitgeteilt sind. Das galt sowohl für die Verteilung des Ammoniaks in dem Gel als auch für den Betrag des absorbierten Ammoniaks.

INTRODUCTION AND THEORY

As far as the present authors know no direct illustration of the validity of the equations, derived for the sorption of a component in a stagnant liquid of infinite thickness has been published in the literature. The purpose of the research to be described in this paper was to give such an illustration. The equations used will be given first.

Consider a stagnant liquid with a flat surface, of an infinite thickness, measured perpendicular to that surface. The liquid contains no component A, or a component with which A can react. At the time zero in the liquid at the interface suddenly a concentration C_A^* of component A is created. If this concentration with time (θ) is kept constant and if the diffusion coefficient ($\mathfrak{D}_A$) is constant, the concentration of component A (C_A), at the distance x from the surface will be expressed by [1]:

$$C_A = C_A^* \left[1 - \operatorname{erf}\left(\frac{x^2}{4\,\mathfrak{D}_A\,\theta}\right)^{\frac{1}{2}}\right] \qquad (1)$$

The same equation will be valid for the absorption of component A in a stagnant liquid of finite thickness for any time for which the concentration at the greatest distance from the surface remains zero.

The total amount of component A *absorbed* in the time θ per unit of surface is given by

$$(\phi_A)_{\text{abs.}} = -\mathfrak{D}_A \int_0^\theta \left(\frac{\partial C}{\partial x}\right)_{x=0} d\theta.$$

From this equation and equation (1) as given by Higby [2] it follows that:

$$(\phi_A)_{\text{abs.}} = 2\,C_A^\bullet \left(\frac{\mathfrak{D}_A\,\theta}{\pi}\right)^{\frac{1}{2}} \qquad (2)$$

If, under the same conditions as described above, the stagnant liquid contains a component B of a uniform concentration $C_B^\bullet$ and if the components A and B can react chemically, the liquid will take up component A by absorption and by chemisorption. If the second-order reaction between A and B is infinitely fast, in the liquid, after a certain time, two zones can be distinguished divided by a reaction-front parallel to the surface of the liquid, at which the concentration of A as well as of B is zero. The distance (r) of this reaction-front from the surface is a function of the time and given by:

$$r^2 = 4\alpha\,\theta \qquad (3)$$

The quantity α which appears in (3) is a function of both the diffusion coefficients $\mathfrak{D}_A$ and $\mathfrak{D}_B$ and of the concentrations $C_A^\bullet$ and $C_B^\bullet$, as expressed by equation (4):

$$\frac{C_A^\bullet \cdot (\mathfrak{D}_A)^{\frac{1}{2}} \cdot \exp(-\alpha/\mathfrak{D}_A)}{\operatorname{erf}(\alpha/\mathfrak{D}_A)^{\frac{1}{2}}} = \frac{C_B^\bullet\,(\mathfrak{D}_B)^{\frac{1}{2}} \exp(\alpha/\mathfrak{D}_B)}{\operatorname{erf}(\alpha/\mathfrak{D}_B)^{\frac{1}{2}}} \qquad (4)$$

For the zone between the reaction front and the surface, transportation of A takes place in a liquid which contains an amount of $C_B^\bullet$ of component AB by diffusion only. The relation between C_A, x and θ in this zone is:

$$C_A = C_A^\bullet \left[1 - \frac{1}{\operatorname{erf}(\alpha/\mathfrak{D}_A)^{\frac{1}{2}}} \cdot \operatorname{erf}\left(\frac{x^2}{4\,\mathfrak{D}_A\,\theta}\right)^{\frac{1}{2}}\right] \qquad (5)$$

The *total amount* of component A sorbed by the liquid in the time θ is given by:

$$(\phi_A)_{\text{tot.}} = 2C_A^\bullet \frac{1}{\operatorname{erf}(\alpha/\mathfrak{D}_A)^{\frac{1}{2}}} \left(\frac{\mathfrak{D}_A\,\theta}{\pi}\right)^{\frac{1}{2}}\Bigg] \qquad (6)$$

as found from: $(\phi_A)_{\text{tot.}} = -\mathfrak{D}_A \int_0^\theta \left(\frac{\partial C_A}{\partial x}\right)_{x=0} d\theta,$

in which [equation (5)] $\left(\frac{\partial C_A}{\partial x}\right)_{x=0} = \frac{C_A^\bullet}{\operatorname{erf}(\alpha/\mathfrak{D}_A)^{\frac{1}{2}}} \cdot \frac{1}{(\pi\,\mathfrak{D}_A\,\theta)^{\frac{1}{2}}}$.

The amount *chemisorbed* in the time θ is given by:

$$(\phi_A)_{\text{chem.}} = 2C_A^\bullet \cdot \frac{1}{\operatorname{erf}(\alpha/\mathfrak{D}_A)^{\frac{1}{2}}} \cdot \left(\frac{\mathfrak{D}_A\,\theta}{\pi}\right)^{\frac{1}{2}} \cdot e^{-\alpha/\mathfrak{D}_A} \qquad (7)$$

as found from: $(\phi_A)_{\text{chem.}} = -\mathfrak{D}_A \int_0^\theta \left(\frac{\partial C_A}{\partial x}\right)_{x=r} d\theta,$

in which [equation (5)] and by combination with equation (3):

$$\left(\frac{\partial C_A}{\partial x}\right)_{x=r} = -\frac{C_A^\bullet}{\operatorname{erf}(\alpha/\mathfrak{D}_A)^{\frac{1}{2}}} \cdot \frac{1}{(\pi\,\mathfrak{D}_A\,\theta)^{\frac{1}{2}}} \cdot e^{-\alpha/\mathfrak{D}_A}.$$

If the range of concentrations of A in the stagnant liquid is chosen such that the diffusion coefficient of A remains substantially constant at constant concentration of component AB, proof of the equations presented can be given by measuring the concentration of A and eventually of B as a function of the distance from the surface and as a function of time. The experimental difficulty lies in the choice of such conditions, that convective movements in the liquid to be used, can be sufficiently suppressed.

Because in a watery jelly convective movements will anyhow be strongly restricted as compared with water, to the authors it seemed possible to prepare a jelly of such a consistency that convective movements would for all practical purposes be absent at all. As far as the results of the experiments to be described below seem to indicate, the attempt to find such a jelly has been successful.

Experimental

As component A and B respectively ammonia and acetic acid have been chosen. In water the reaction between these two components seems to be very fast.

The jelly finally chosen was a solution of carboxymethylcellulose (4 g) in water (110 g),

VOL. 10 1959

The jelly was contained in a cylindrical stack of fourteen rings. Each ring had a diameter of 4 cm and a height of $\sim$ 4·4 mm. The rings were finely ground at the upper and under surfaces so that they fitted water-tight on each other. Nevertheless a small amount of silicone grease was applied between the touching surfaces, to promote easy sliding of the rings. With the help of two diametrically placed glass rods the pile was fastened in a plastic holder in a vertical position. A slight pressure in a vertical direction was exerted by means of two indiarubber pieces of elastic fastened over the rods.

By placing the pile and support *C* quickly in an exsiccator *B* (See Fig. 1) through which a stream of air with a constant partial pressure of ammonia was circulated, a sudden and constant boundary concentration of ammonia could be created in the jelly. The partial coefficient of transfer of ammonia in the flowing gas is such, as compared with the diffusion coefficient in the jelly, that the surface concentration of the jelly quickly attains and maintains the equilibrium concentration with the gas. To obtain a gas stream with a constant ammonia content, a closed circuit was used. The air from the exsiccator was circulated by means of a pump D through three vessels containing a solution of ammonia in water. The first and largest of these (A_1) was placed in the air (as was the exsiccator) which was kept at a constant temperature of 20 $\pm$ 0·5 °C. The two smaller vessels, A_2 and A_3 were placed in a water bath, provided with a heating and cooling system, which kept the temperature of the bath at 20 $\pm$ 0·1 °C. The air, coming from the last vessel was returned to the exsiccator. Because the amounts of ammonia sorbed by the jelly are very small as compared with the ammonia contained in the vessels an air stream of constant ammonia content was guaranteed and moreover many experiments could be done with one charge. The contents of the vessels were regularly controlled as to their density. Before starting an experiment the empty apparatus was run for several hours to ensure stationary conditions.

At the end of each experiment the pile was

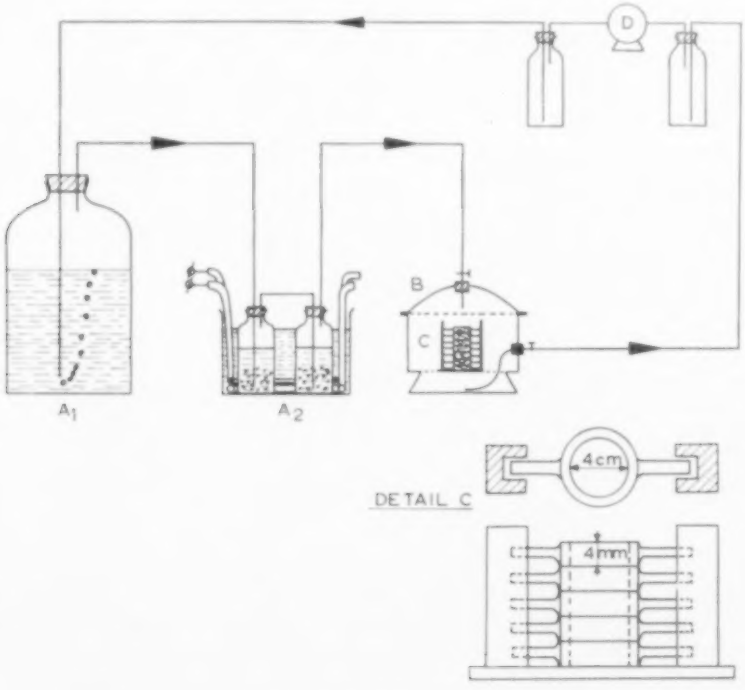

Fig. 1. Sketch of the apparatus.

taken from the exsiccator, each ring slipped off quickly and carefully and brought into a weighed amount of water. From the total weight and the weight of each ring the amount of jelly was then known. After dissolving the jelly the amount of free ammonia and free acetic acid were determined by potentiometric titration. In this manner mean concentrations in moles/g of jelly (C'') could be calculated. C'' is equal to $\frac{C'}{\rho}$ if C' in the concentration in moles/cm² and ρ is the density of the jelly in g/cm³. The density of the jelly has not been determined because the amounts of ammonia absorbed were small enough to neglect the differences in the densities caused by sorption.

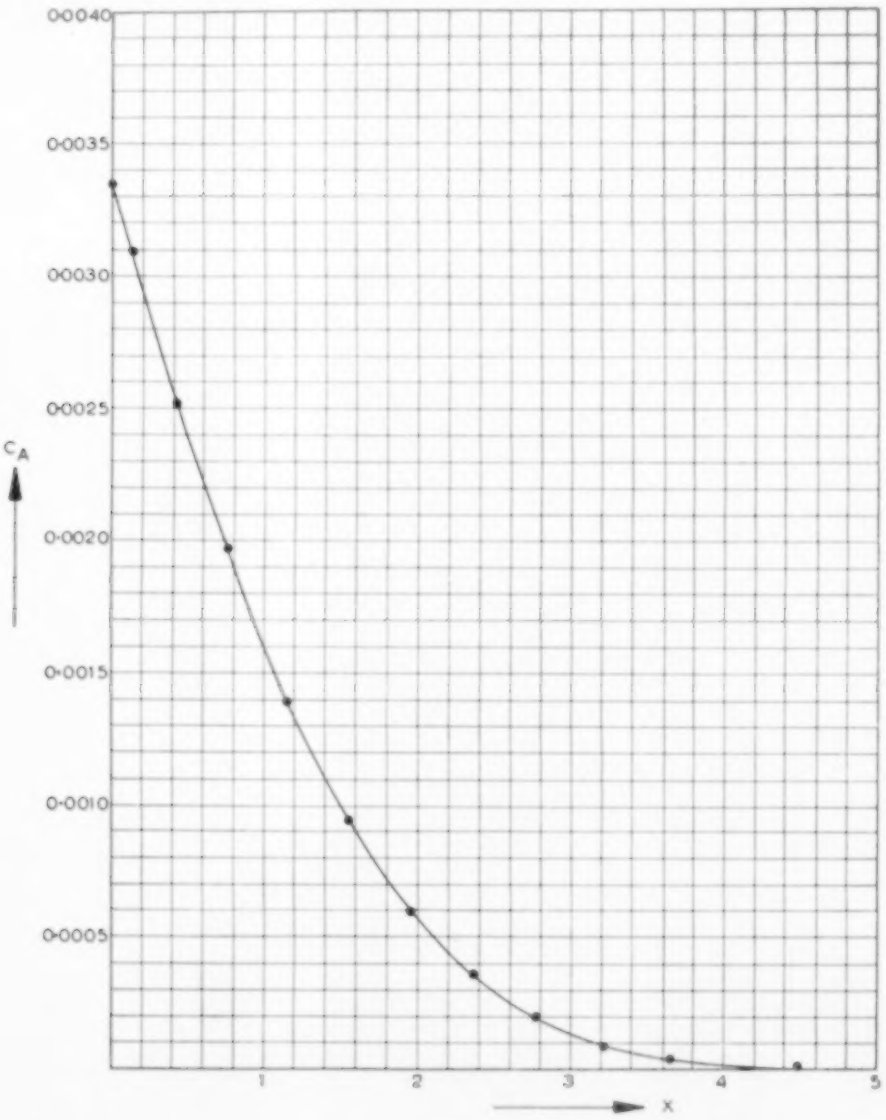

Fig. 2. The concentration of ammonia as a function of the distance of the surface.

The concentration found was taken as the concentration at half the height of the ring. The height of the ring was taken as the mean value from four places, measured with a micrometer, around the circumference of the ring. The deviation of these four heights was in the order of a few thousands of a millimeter.

The concentration at the interface C_A^* was determined by placing a few rings so long (several weeks) in the apparatus, that all the rings showed the same concentration of ammonia. This concentration was taken as C_A^*.

Results and Discussion

Two series of experiments have been carried out. In the first series the absorption of ammonia in jellies, containing different amounts of ammonium acetate has been measured; in the second series the sorption of ammonia in jellies containing different amounts of acetic acid has been studied.

Some of the data obtained in the *first series* have been given in Table 1. The amount of ammonium acetate in the jelly has been marked as C_B^*, the equilibrium concentration of ammonia in the jelly (C_A^*), as determined separately, has been taken up in the table as the concentration at the distance zero.

One of the experiments has been presented graphically in Fig. 2. From the data collected for each point measured the diffusion coefficient has been calculated, by division of $\frac{x^2}{4\mathbb{D}\theta}$, obtained from equation (1) via the known C_A and C_A^*, on $\frac{x^2}{4\theta}$, obtained directly from x and θ. The resulting values have been included in Table 1.

A *mean* value of D_A has been obtained by plotting on rectangular co-ordinates the values of $\frac{x^2}{4\mathbb{D}\theta}$ versus those of the corresponding $\frac{x^2}{4\theta}$. If $\mathbb{D}_A$ is independent of C_A the points will lie on a straight line, passing the origin, of slope $1/\mathbb{D}_A$.

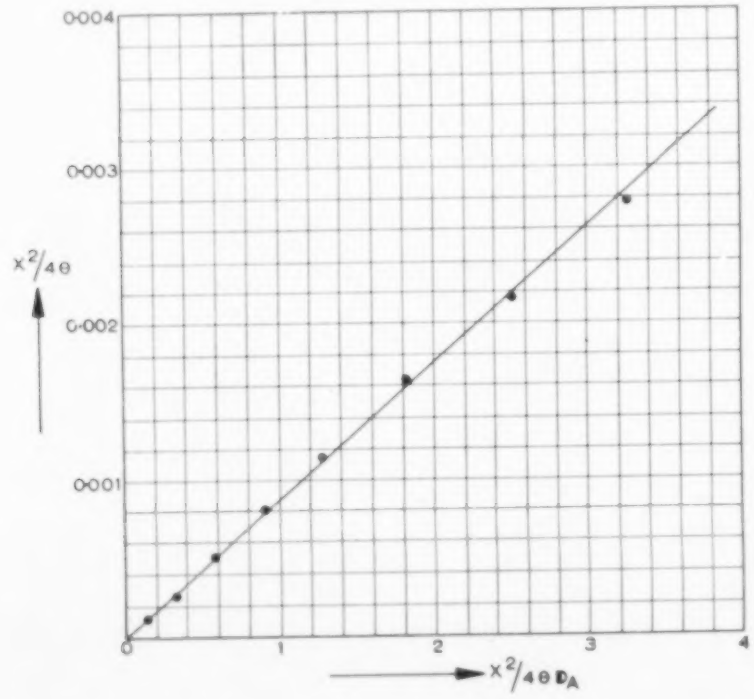

Fig. 3. $\frac{x^2}{4\theta}$ as a function of $\frac{x^2}{4\theta\mathbb{D}_A}$

Table 1. Data of the absorption experiments

I : $C_B^*/\rho = 0{\cdot}000$				II : $C_B^*/\rho = 0{\cdot}553 \times 10^{-3}$				III : $C_B^*/\rho = 1{\cdot}130 \times 10^{-3}$			
θ	x	C_A/ρ $\times 10^3$	$\mathfrak{D}_A$ $\times 10^4$	θ	x	C_A/ρ $\times 10^3$	$\mathfrak{D}_A$ $\times 10^4$	θ	x	C_A/ρ $\times 10^3$	$\mathfrak{D}$ $\times 10^4$
(a) 283	0	1·43	—	1051	0	3·44	—	1201	0	3·35	—
	0·216	1·10	9·5		0·154	3·14	9·4		0·138	3·09	9·0
	0·654	0·56	10·5		0·443	2·59	9·2		0·421	2·58	8·8
	1·094	0·21	10·1		0·782	2·00	9·4		0·761	2·00	8·3
	1·534	0·05	9·9		1·182	1·38	9·4		1·159	1·38	8·4
	1·965	0·01	10·1		1·589	0·91	9·6		1·562	0·94	8·8
					2·000	0·54	9·4		1·962	0·60	8·8
(b) 382	0	1·40	—		2·404	0·30	9·4		2·371	0·36	9·0
	0·197	1·14	9·3		2·821	0·13	9·2		2·794	0·21	9·0
	0·602	0·68	9·8		3·249	0·07	9·4		3·228	0·08	8·6
	1·046	0·34	10·4		3·671	0·03	9·3		3·655	0·05	8·5
	1·496	0·11	9·5								
	1·932	0·03	9·2								
	2·367	0·01	9·6								
(c) 963	0	1·47	—								
	0·231	1·38	10·1								
	0·670	1·02	11·0								
	1·101	0·68	10·1								
	1·537	0·40	9·2								
	1·960	0·25	10·0								
	2·382	0·12	9·6								
	2·811	0·02	9·3								

In all cases investigated no other tendency than that of a straight relationship has been detected. The straight line through the points, including the origin, has been calculated by means of the method of the least squares. As an example, the result for the experiment presented above in Fig. 2, has been given in Fig. 3.

A third method to calculate a mean value of $\mathfrak{D}_A$ is to determine the amount $(\phi_{A/ab})$ by graphical integration of the $C_A - x$ line (see later Table 5). By means of equation (2) $\mathfrak{D}_A$ can then be calculated.

In Table 2 the results of the three methods used have been collected taking the arithmetic mean value for method I.

Comparing all the values of $\mathfrak{D}_A$ obtained, it can be concluded that no tendency is found that the diffusion coefficient depends on the place of measurement. Therefore apparently in the concentration regions used the diffusion coefficient is constant. Moreover, convective movements in the jelly seem to be absent and the theory as given can be used. The most accurate values are taken to be those obtained with method II. Method III gives somewhat too high values, probably caused by a too high value of $(\phi_A)_{ab.}$ (see later).

The diffusion coefficient appears to be a function of the amount of ammonium acetate in the jelly.

Table 2. The diffusion coefficients of ammonia for jellies with different amounts of ammonium acetate

C_B^*/ρ	0	$0{\cdot}553 \times 10^{-3}$	$1{\cdot}130 \times 10^{-3}$
Method I	$9{\cdot}8 \times 10^{-4}$	$9{\cdot}4 \times 10^{-4}$	$8{\cdot}7 \times 10^{-4}$
Method II	$9{\cdot}9 \times 10^{-4}$	$9{\cdot}3 \times 10^{-4}$	$8{\cdot}6 \times 10^{-4}$
Method III	$10{\cdot}0 \times 10^{-4}$	$9{\cdot}6 \times 10^{-4}$	$8{\cdot}7 \times 10^{-4}$

VOL. 10 1959

An increase of the amount of this component causes a decrease in $\mathcal{D}_A$. As can be seen from Fig. 4, where $\mathcal{D}_A$ has been plotted as a function of the amount of ammonium acetate, in the region investigated the relation is almost straight.

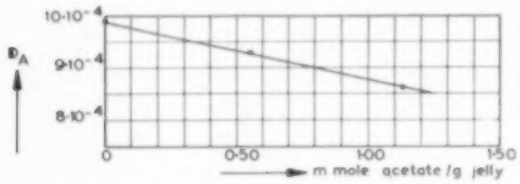

FIG. 4. The diffusion coefficient of ammonia as a function of the concentration of ammonium acetate.

The results of the *second series* are given in Table 3. As an example for the experiments VII*a*, *b* and *c*, C_A and C_B (not presented in Table 3) have been plotted as a function of x in Fig. 5. It can be concluded that a sharp reaction-front, for which $C_A = C_B = 0$ seems indeed to exist. However, it is theoretically possible that the amounts of ammonia and acetic acid as titrated do not represent the actual situation in the jelly. If the reaction is not infinitely fast it is possible that e.g. in zone I (between the surface and the reaction front) still free acetic is present, because by titration only the excess of ammonia over acetic acid is found. Although this is not likely in view of the very long times of sorption as compared with the time necessary for titration which depends on the same type of reaction, and in view of the time interval between the end of the experiment and the time of titration, another criterion ought to be applied.

According to the theory in zone I ammonium acetate of a constant concentration equal to C_B^* should be present and free ammonia of a concentration C_A; in zone II ($x = r$ to $x = \infty$) free acetic acid of a concentration C_B and ammonium acetate of a concentration $C_B^* - C_B$.

If the reaction between ammonia and acetic acid is infinitely fast, the data obtained for zone I must fulfil equation (5). The inspection of these data has been carried out in the following manner. Through the points as plotted in Fig. 5 smooth lines have been drawn. By extrapolation the intersection of these lines with the x axis, gives the value of r (see later: Table 6). From r, by means of equation (3) the value of α has been calculated. From α and from $\mathcal{D}_A$ corresponding to C_B^* (see Fig. 4) the value of $\mathrm{erf}\,(\alpha\sqrt{\mathcal{D}_A})^{\frac{1}{2}}$ has been found. This enables to determine the value of $\mathrm{erf}\left(\frac{x^2}{4\mathcal{D}_A\theta}\right)^{\frac{1}{2}}$ (equation 5) and the corresponding value of $\mathcal{D}_A$. These have been inserted in Table 3. Their arithmethic

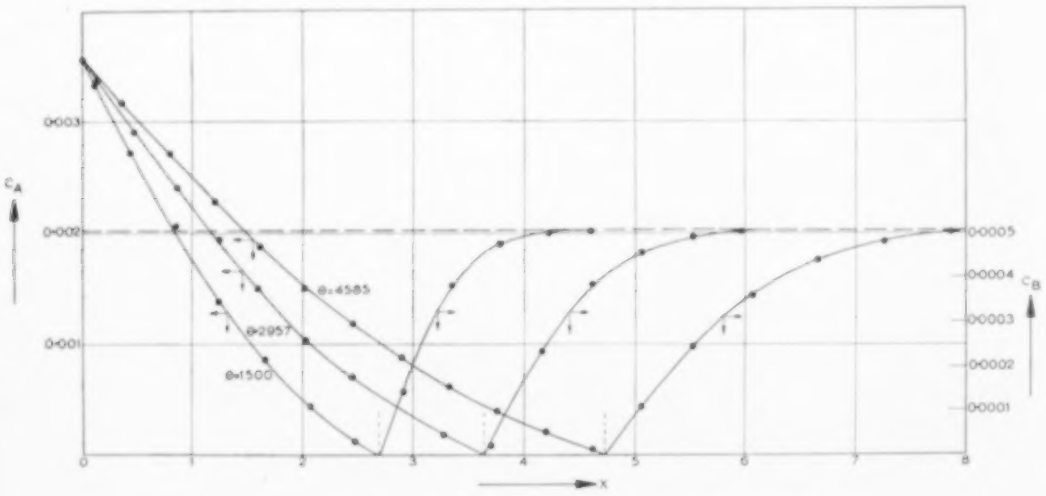

FIG. 5. Concentration profiles of ammonia and acetic acid at different times.

Table 3. Data on the sorption of ammonia in the presence of acetic acid

IV : $C_A^*/\rho = 0{\cdot}107 \times 10^{-3}$				V : $C_B^*/\rho = 0{\cdot}271 \times 10^{-3}$				VI : $C_B^*/\rho = 0{\cdot}450 \times 10^{-3}$				VII : $C_B^*/\rho = 0{\cdot}517 \times 10^{-3}$			
θ	x	$C_B/\rho \times 10^3$	$\mathfrak{D}_A \times 10^4$	θ	x	$C_A/\rho \times 10^3$	$\mathfrak{D}_A \times 10^4$	θ	x	$C_A/\rho \times 10^3$	$\mathfrak{D}_A \times 10^4$	θ	x	$C_A/\rho \times 10^3$	$\mathfrak{D}_A \times 10^4$
1054	0	3·68	—									(a) 1500	0	3·55	—
	0·149	3·37	9·9	(a) 1197	0	3·60	—	1093	0	3·56	—		0·114	3·34	9·8
	0·300	2·65	9·7		0·153	3·29	9·4		0·150	3·22	8·8		0·440	2·72	9·2
	0·906	1·89	9·6		0·509	2·59	9·3		0·438	2·51	8·5		0·855	2·06	9·6
	1·312	1·25	9·5		0·914	1·91	10·0		0·786	1·86	8·6		1·254	1·38	9·3
	1·713	0·76	9·5		1·319	1·27	9·7		1·195	1·20	9·2		1·662	0·86	9·4
	2·119	0·43	9·6		1·725	0·76	9·5		1·604	0·62	9·6		2·071	0·43	9·3
	2·537	0·19	9·5		2·133	0·39	9·5		2·022	0·22	9·0		2·481	0·12	9·2
	2·959	0·05	9·5		2·549	0·14	9·5					(b) 2957	0	3·55	—
				(b) 1496	0	3·60	—						0·123	3·38	8·9
					0·148	3·34	9·7						0·456	2·90	8·2
					0·491	2·71	8·9						0·874	2·41	9·4
					0·889	2·06	9·4						1·239	1·94	9·2
					1·298	1·46	9·4						1·604	1·49	9·9
					1·701	0·95	9·1						2·020	1·04	8·5
					2·102	0·55	9·0						2·448	0·71	8·8
					2·529	0·31	9·5						2·862	0·46	9·3
					2·956	0·09	9·4						3·271	0·17	8·7
												(c) 4585	0	3·55	—
													0·055	3·49	10·2
													0·352	3·17	9·3
													0·792	2·71	9·5
													1·194	2·29	9·3
													1·605	1·89	9·3
													2·024	1·51	9·2
													2·446	1·19	9·4
													2·885	0·88	9·6
													3·326	0·61	9·5
													3·764	0·39	9·6
													4·199	0·20	9·6
													4·629	0·04	9·5

Table 4

C_B^*/ρ	$0{\cdot}107 \times 10^{-3}$	$0{\cdot}271 \times 10^{-3}$	$0{\cdot}450 \times 10^{-3}$	$0{\cdot}517 \times 10^{-3}$
$\mathfrak{D}_A$ from Fig. 4	$9{\cdot}7 \times 10^{-4}$	$9{\cdot}5 \times 10^{-4}$	$9{\cdot}3 \times 10^{-4}$	$9{\cdot}2 \times 10^{-4}$
$\mathfrak{D}_A$ from equation (5)	$9{\cdot}6 \times 10^{-4}$	$9{\cdot}4 \times 10^{-4}$	$9{\cdot}0 \times 10^{-4}$	$9{\cdot}4 \times 10^{-4}$

means have been collected in Table 4, together with the $\mathfrak{D}_A$ values as read from Fig. 4.

The agreement between the values is sufficient to warrant the conclusion that the experiments satisfy equation (5).

Several other inspections of the data given and obtained have been made.

With the aid of equation (4) the values of the diffusion coefficient of acetic acid ($\mathfrak{D}_B$) in the jelly can be calculated. An approximation of equation (4) has been used, by assuming that $\exp(x/\mathfrak{D}_B - x/\mathfrak{D}_A) = 1$, because $\mathfrak{D}_B \approx \mathfrak{D}_A$. The values obtained are given in Table 5. The error in these values is such that no dependency

Table 5. The diffusion coefficients of acetic acid

C_B^*/ρ	$0{\cdot}107 \times 10^{-3}$	$0{\cdot}271 \times 10^{-3}$	$0{\cdot}450 \times 10^{-3}$	$0{\cdot}517 \times 10^{-3}$
$\mathfrak{D}_B$	$9{\cdot}9 \times 10^{-4}$	$9{\cdot}9 \times 10^{-4}$	$9{\cdot}8 \times 10^{-4}$	$9{\cdot}8 \times 10^{-4}$

Table 6. Collected data of the sorption experiments

Nr	θ	$C_A^*/\rho \times 10^3$	$C_B^*/\rho \times 10^3$	$\mathfrak{D}_A \times 10^4$	r	$\alpha \times 10^3$	$\alpha/\mathfrak{D}_A$	erf $(\alpha/\mathfrak{D}_A)^{\frac{1}{2}}$	$(\phi_A)_{abs}/\rho \times 10^3$	p $(\phi_A)_{chem}/\rho \times 10^3$	q $(\phi_A)_{tot}/\rho \times 10^3$	s $(\phi_A)_{tot}/\rho$ calc $\times 10^3$	s/q	p/q	t $e^{-\alpha/\mathfrak{D}_A}$ from r	u $e^{-\alpha/\mathfrak{D}_A}$ from slopes $C_A - x$ line	error in r in % +	$\frac{p/q}{t}$	$\frac{p/q}{u}$
I-a	283	1·43	0	9·9	—	—	—	—	0·860	—	0·860	0·854	0·99	—	—	—	—	—	—
-b	382	1·40	0	9·9	—	—	—	—	0·961	—	0·961	0·972	1·01	—	—	—	—	—	—
-c	963	1·57	0	9·9	—	—	—	—	1·66	—	1·66	1·62	0·97	—	—	—	—	—	—
II	1051	3·44	0·353	9·3	—	—	—	—	3·91	—	3·91	3·74	0·95	—	—	—	—	—	—
III	1201	3·35	1·130	8·6	—	—	—	—	3·86	—	3·86	$\frac{3{\cdot}84}{\text{mean}}$	$\frac{0{\cdot}99}{0{\cdot}98}$	—	—	—	—	—	—
IV	1054	3·68	0·107	9·7	3·25	2·51	2·59	0·977	3·87	0·38	4·25	4·30	1·01	0·090	0·075	0·083	2·7	1·20	1·08
V-a	1197	3·60	0·271	9·5	2·91	1·77	1·86	0·946	4·00	0·87	4·87	4·59	0·95	0·179	0·156	0·191	2·7	1·15	0·94
-b	1496	3·60	0·271	9·5	3·24	1·75	1·84	0·945	4·48	0·98	5·46	5·13	0·94	0·181	0·159	0·185	2·7	1·14	0·98
VI	1093	3·56	0·450	9·3	2·40	1·32	1·42	0·908	3·23	1·20	4·43	4·48	1·01	0·271	0·247	0·254	2·5	1·10	1·07
VII-a	1500	3·55	0·517	9·2	2·71	1·22	1·33	0·894	3·78	1·60	5·38	5·26	0·98	0·297	0·266	0·283	2·9	1·12	1·05
-b	2957	3·55	0·517	9·2	3·66	1·22	1·33	0·894	5·02	2·19	7·21	7·39	1·02	0·304	0·265	0·317	3·2	1·15	0·96
-c	4585	3·55	0·517	9·2	4·74	1·23	1·34	0·894	6·77	2·92	9·69	9·21	0·95	0·301	0·276	0·331	2·6	1·09	0·91
												mean :	0·98			mean :	2·8	mean :	1·00

The experiments I have been carried out with a lower ammonia concentration in the gas-phase than the other experiments.

of $\mathfrak{D}_B$ of the concentration of ammonium acetate can be deduced.

The total amount of ammonia sorbed and the amount chemically bound can be calculated by means of the equations (6) and (7). These amounts can also be obtained by graphical integration from the curves showing C_A and C_B as a function of x. The ratio between $(\phi_A)_{\text{chem.}}$ $(= p)$ and $(\phi_A)_{\text{tot.}}$ $(= q)$ as follows from the equations is equal to $e^{\alpha/\mathfrak{D}_A}$; A comparison can also be made between the ratio $\frac{p}{q}$ and the value of $e^{\alpha/\mathfrak{D}_A}$; calculated either via α obtained via r as described before $(= t)$, or from the ratio of the slopes $\left(\frac{dC_A}{dx}\right)_{x=0}$ and $\left(\frac{dC_A}{\partial x}\right)_{x=r}$ of zone I $(= u)$. This second method for the calculation of $e^{\alpha/\mathfrak{D}_A}(= u)$, although less accurate than the first, may be advantageous. As has been remarked the diffusion coefficients as calculated with method III from $(\phi_A)_{\text{abs}}$ (see Table 2) were larger by ~ 1 per cent than those obtained with the other methods. This might indicate a systematic error in x. If this should be true an error of ~ 2 per cent in r is to be expected, which signifies an error of about 4 per cent in α, and a corresponding error in $e^{\alpha/\mathfrak{D}_A}(= t)$; in the second method the error in x cancels out. It may be remarked that a systematic error in x will not influence the value of $\mathfrak{D}_A$ as found with the methods I and II.

In Table 6 some data as calculated for the different experiments of both series have been collected.

Comparison of the values of the ratio p/q with the two values t and u $\left(\text{see } \frac{p/q}{t} \text{ and } \frac{p/q}{u}\right)$ enables the conclusion that $e^{\alpha/\mathfrak{D}_A}$ as calculated from the slopes of the $C_A - x$ lines, gives correct results. The error, however, is relatively large.

As demonstrated by the ratio $\frac{p/q}{t}$, the values of $e^{\alpha/\mathfrak{D}_A}$ as calculated from r are too small, although a relatively much smaller error is made. Therefore α as used is too large. The error in α must be attributed to an error in r. This error has been calculated and introduced in Table 6. It appears that in all the experiments the error is almost the same (mean value $+$ 2·8 per cent). It seems not likely that this systematic error is caused by an incorrect extrapolation only. It will be assumed that the error in r is caused by a systematic error in x. In that case the amounts of ammonia taken up by the jelly as found by integration of the curves will be too large by $\sim 2{\cdot}8$ per cent. Keeping in mind that an error of 2·8 per cent. in r corresponds to 5·6 per cent in α, but only to $\frac{1}{2}$ per cent in erf $(\alpha/\mathfrak{D})^{\frac{1}{2}}$, a support in favour of the supposition made is, that the amounts of ammonia taken up calculated from equations (2) and (6) are 2 per cent smaller than the values determined by graphical integration.

The systematic error in x is not caused by the use of a faulty micrometer. A possible explanation might be the observation that slipping off of the rings, by nature of the jelly, caused a small inward displacement of the jelly into the remaining rings. This was possible because the jelly was so viscous that small air bubbles were always present in the jelly. The result will be that the distance as taken will be larger than compared with the original situation.

Conclusions

A jelly containing ~ 4 per cent of carboxy methylcellulose behaves like a stagnant "liquid." The equations derived for the absorption of a component in such a liquid are valid. For ammonia as the absorbing component in the concentration regions used this diffusion coefficient is independent of the ammonia concentration, but decreases with increasing amount of ammonium acetate.

The reaction between ammonia and acetic acid dissolved in the jelly is infinitely fast as compared with the diffusion process.

For jellies containing acetic acid the sorption of ammonia in the jelly entirely agrees with the equations derived for the absorption and chemisorption, with an infinitely fast second-order reaction.

Notation

C_A	= concentration of component A	mole cm^{-3}
C_A^*	= interface concentration of component A	mole cm^{-3}

C_B	= concentration of component B	mole cm^{-3}
C_B^*	= initial concentration of component B, or concentration of component AB	mole cm^{-3}
$\mathfrak{D}_A$	= diffusion coefficient of component A	cm^2 min^{-1}
$\mathfrak{D}_B$	= diffusion coefficient of component B	cm^2 min^{-1}
p	= $(\phi_A)_{\text{chem}}$ as determined graphically	mole cm^{-2}
q	= $(\phi_A)_{\text{tot}}$ as determined graphically	mole cm^{-2}
r	= distance of reaction front from the surface	cm
s	= $(\phi_A)_{\text{tot}}$ as calculated from the equations	mole cm^{-2}
t	= $c^2/\mathfrak{D}_A$ as calculated from r	no dimension
u	= $c^2/\mathfrak{D}_A$ as calculated from the slope of the $C_A - x$ lines	no dimension
x	= distance from the surface	cm
z	= integration constant	cm^2 min^{-1}
ρ	= density	g cm^{-3}
θ	= time	min
$(\phi_A)_{\text{abs.}}$	amount of component A absorbed per unit of surface in time θ	mole cm^{-2}
$(\phi_A)_{\text{chem.}}$	amount of component A chemisorbed per unit of surface in time θ	mole cm^{-2}
$(\theta_A)_{\text{tot.}}$	amount of component A sorbed per unit of surface in time θ	mole cm^{-2}

$$\operatorname{erf}(z) = \frac{2}{\sqrt{\pi}} \int_0^z e^{-\beta^2}\, d\beta$$

References

[1] Sherwood T. R. and Pigford R. L. *Absorption and Extraction* 328 (2nd Ed.) McGraw Hill, New York.

[2] Higby J. *Trans. Amer. Inst. Chem. Engrs.* 1935 **31** 365.

VOL. 10 1959

Chemical Engineering Science, 1959, Vol. 10, pp. 57 to 67. Pergamon Press Ltd. London. Printed in Great Britain

Kinetics of pentaerythritol-production reactions

M. S. Peters and C. R. Cupit*

Chemical Engineering Division, University of Illinois, Urbana, Illinois

(*Received* 11 *July* 1958)

Abstract—The kinetics of the reactions involved in the formation of pentaerythritol were investigated. The results show that the aldol condensations leading to pentaerythrose are very rapid and the rate-limiting step is the pentaerythrose–formaldehyde Cannizzaro reaction. The rate equations for both the pentaerythrose–formaldehyde and the direct formaldehyde Cannizzaro reactions are shown to be represented satisfactorily as third order. Activation energies and rate-constant expressions are presented for the Cannizzaro reactions with sodium hydroxide as the base.

Résumé—Les auteurs ont étudié la cinétique des réactions mises en jeu dans la formation du pentaerythritol. Les résultats montrent que les condensations d'aldol conduisant au pentaerythrose sont très rapides, la réaction de Cannizaro pentaerythrose – formaldehyde limitant la vitesse. Les équations de vitesse pour les réactions pentaerythrose – formaldehyde et formation directe de formaldehyde par la réaction de Cannizaro sont représentées de façon satisfaisante par une réaction d'orde 3. Les expressions des énergies d'activation et des constantes de vitesse sont données pour les réactions de Cannizaro avec la soude comme base.

Zusammenfassung—Die Kinetik der bei der Bildung von Pentaerythrit auftretenden Reaktionen wurde untersucht. Die Ergebnisse zeigen, dass die Aldol-Kondensationen, die zu Pentaerythrose führen, sehr schnell verlaufen und dass der geschwindig keitsbestimmende Schritt die Pentaerythrose – Formaldehyd-Cannizaro-Reaktion ist. Die Gleichungen für die Geschwindigkeit der Pentaerythrose – Formaldehyd und der direkten Formaldehyd-Cannizaro-Reaktion lassen sich befriedigend durch die dritte Ordnung wiedergeben. Aktivierungsenergien und Ausdrücke für die Geschwindigkeitskonstante werden für die Cannizaro-Reaktionen mit Natriumhydroxyd als Base angegeben.

Pentaerythritol is an important intermediate in the plastics, paint, dye, and explosives industries. A large amount of information relating to methods of commerical production is available in the form of patents and in the general literature [3, 9, 11]; however, due to the complexity of the reactions that may be involved, very little information has been published on the kinetics or mechanisms of the reactions [2, 12].

In the commercial process, pentaerythritol is produced in an aqueous alkaline medium of formaldehyde and acetaldehyde. Sodium hydroxide or calcium hydroxide are the alkalies most frequently used. The general reaction steps are well understood from the standpoint of organic reactions. The α-hydrogen atoms of an aldehyde are very reactive, and, in a basic medium, they can undergo the aldol condensation reaction with any aldehyde present provided steric hindrance does not rule out the reaction. If there are no α-hydrogen atoms present on the aldehyde molecule, it can undergo the Cannizzaro reaction in which two molecules of aldehyde yield a molecule of an organic acid and an alcohol molecule. The reaction steps of formaldehyde with acetaldehyde are summarized in the following equations:

Aldol condensation reactions,

$$HCHO + CH_3CHO \xrightarrow{(OH^-)} HOCH_2CH_2CHO \quad (a)$$

$$HCHO + HOCH_2CH_2CHO \xrightarrow{(HO^-)} (HOCH_2)_2CHCHO \quad (b)$$

* Present Address: Research Division, Shell Oil Company, Houston, Texas.

$$HCHO + (HOCH_2)_2CHCHO \xrightarrow{(OH^-)} (HOCH_2)_3CCHO \quad (c)$$
Pentaerythrose

Cannizzaro reaction,

$$HCHO + (HOCH_2)_2CCHO + OH^- \xrightarrow{k_1} (HOCH_2)_4C + HCOO^- \quad (d)$$
Pentaerythritol

The only significant side reaction involving formaldehyde and hydroxyl ion is the formaldehyde Cannizzaro reaction

$$2HCHO + OH^- \xrightarrow{k_2} HCOO^- + CH_3OH \quad (e)$$

In the production of pentaerythritol, this side reaction and the formaldehyde reaction to form glycollic aldehyde are only of major importance at high formaldehyde concentrations or at temperatures above 50–60°C. Side reactions resulting in the formation of ethers or formals of pentaerythritol may also occur if the unneutralized mixture is allowed to stand for an extended period of time or if the reaction is carried out at an elevated temperature.

The product pentaerythritol is recovered from the reaction mixture by crystallization. Since the presence of formaldehyde increases the solubility of the product in the reaction liquor, various methods, such as the promotion of reaction (e) by increasing the temperature, have been proposed to remove any excess formaldehyde remaining at the end of the primary reactions.

In this study, the kinetics of the primary reactions leading to pentaerythritol were investigated with sodium hydroxide as the alkali. The experimental tests were carried out at concentration and temperature levels such that all side reactions were relatively unimportant; however, in order to obtain the kinetics of the primary reactions, it was necessary to correct for the small consumption of hydroxyl ion and formaldehyde caused by the formaldehyde Cannizzaro reaction.

Analysis of the Kinetics of the Reactions

The results of this investigation show that, below 10°C, the aldol condensation reactions are rapid relative to the pentaerythrose Cannizzaro reaction. Consequently, by carrying out the initial steps of the reaction batchwise at a temperature near 0°C, it is possible to convert the acetaldehyde to pentaerythrose before any appreciable amount of pentaerythritol is formed. After all the pentaerythrose is formed, it is assumed that formaldehyde concentration and temperature are such that only the Cannizzaro reactions (d) and (e) occur. Under these conditions, the following reaction-rate equations can be written:

$$-\frac{dC}{dt} = k_1 ABC \quad (1)$$

$$-\frac{dA}{dt} = k_1 ABC + k_2 (B)(A)^2 \quad (2)$$

$$-\frac{dB}{dt} = k_1 ABC + \frac{k_2}{2}(B)(A)^2 \quad (3)$$

where A = formaldehyde concentration
B = sodium hydroxide concentration
C = pentaerythrose concentration

The preceding rate equations are expressed in the general empirical form normally assumed for Cannizzaro reactions [1, 3, 6, 8]. They are applicable when changes are considered with respect to concentration [5, 6]. In this work, the initial concentrations used were approximately constant in the range normally encountered in the industrial production of pentaerythritol, and the applicability of equations (1) to (3) is shown by the agreement with the experimental results.

A study of the side reaction reveals that it is is very slow relative to the pentaerythrose-formaldehyde Cannizzaro reaction and can be neglected over the time interval used to study the pentaerythrose–formaldehyde reaction. Under these conditions, $dA = dB = dC$, and equation (1) can be integrated by using the method of partial fractions to give the following result:

$$\frac{1}{(A_0 - B_0)(B_0 - C_0)(C_0 - A_0)} \times \ln \left(\frac{A}{A_0}\right)^{(B_0 - C_0)} \left(\frac{B}{B_0}\right)^{(C_0 - A_0)} \left(\frac{C}{C_0}\right)^{(A_0 - B_0)} = k_1 t \quad (4)$$

where A_0, B_0, and C_0 refer to the concentrations

VOL. 10 1959

of the respective components at the start of the time interval. Letting

$$a = B_0 - C_0 \qquad X = \left(\frac{A}{A_0}\right)^a \left(\frac{B}{B_0}\right)^b \left(\frac{C}{C_0}\right)^c$$

$$b = C_0 - A_0 \qquad N = \frac{1}{abc}$$

$$c = A_0 - B_0$$

equation (4) becomes

$$N \ln X = k_1 t \tag{5}$$

A plot of ln X versus t should yield a straight line with a slope of k_1/N for any given set of initial concentrations of this kinetic analysis corresponds to the actual process.

To determine the influence of the formaldehyde Cannizzaro reaction on the hydroxyl and formaldehyde concentrations, it is necessary to evaluate k_2. This can be accomplished by considering the formaldehyde side reaction alone. After all the pentaerythrose has reacted, the aldehyde concentration of the reaction mixture should follow the kinetics of the formaldehyde Cannizzaro reaction, and equation (2) can be written as

$$-\frac{dA}{dt} = k_2 (B)(A)^2 \tag{6}$$

In a manner similar to that used for obtaining equation (5), equation (6) can be integrated to give

$$P = Kt + S \tag{7}$$

where $P = \dfrac{1}{A} + \dfrac{1}{2B_0 - A_0} \ln \dfrac{A}{B}$

$$K = \frac{k_2}{2}(2B_0 - A_0)$$

$$S = \frac{1}{A_0} - \frac{1}{2B_0 - A_0} \ln \frac{B_0}{A_0}$$

A plot of P versus t should give a straight line with a slope of $\dfrac{k_2}{2}(2B_0 - A_0)$ for any given set of initial concentrations if these kinetics are followed. If $A = 2B$, as is essentially the case for some of the experimental runs reported in this work, the integrated result for equation (6) is

$$\frac{1}{B^2} = 4k_2 t + \frac{1}{B_0^2} \tag{8}$$

and a plot of B^{-2} versus t should be straight line with a slope equal to $4k_2$.

Experimental Equipment and Procedure

Experimental data, which followed the course of the reaction, were obtained using an ice bath and a constant-temperature bath. The condensation reactions were carried out in the ice bath and the pentaerythrose–formaldehyde Cannizzaro reaction was performed in the constant-temperature bath.

The reagents were added to an agitated, 1l. Erlenmeyer flask located in the ice bath, and the solution temperature was maintained below 10°C. The mixture was formed by adding sodium hydroxide to a homogeneous solution of acetaldehyde and formaldehyde. After the initial mixing, the temperature of the reaction mixture dropped to almost 0°C in about 30 min. After one hour of reaction time in the ice bath, the reaction mixture was introduced into an agitated, three necked, 1l. flask in the constant-temperature bath. A high rate of agitation was maintained to give a homogeneous mixture and kinetic results that were independent of the agitation rate. About 6 min were required for the cold reaction mixture to reach the bath temperature. Samples were taken periodically by introducing 25 ml pipette into one of the side necks, and the temperature of the reaction mixture was determined by means of a thermometer inserted in one of the side necks.

The samples were placed in 300 ml Erlenmeyer flasks containing an excess of 1N HCl above that required to neutralize the uncombined NaOH, thus stopping all aldol condensations and Cannizzaro reactions. The samples were than titrated with 1N NaOH to the phenolphthalein end-point. From this titration, the NaOH concentration of the reaction mixture was calculated. Following the NaOH titration, the samples were titrated with a $NaHSO_3 - Na_2SO_3$ solution that had previously been standardized against a standard formaldehyde solution. This sodium bisulphite solution was approximately 1·7 N relative to HCHO and contained a small amount of ethanol to inhibit oxidation. The total aldehyde (i.e., $-CHO$) concentration of

the reaction mixture was calculated from the results of the sodium bisulphite titration. This procedure gives accurate quantitative results for formaldehyde and acetaldehyde. Careful checks of the analytical procedure for determination of —CHO on pentaerythrose indicates that it gives slightly low results; however, the procedure gives a reasonably accurate method for following over-all changes in —CHO concentration with time.

All the pentaerythritol runs were made using a 5 to 1 molal ratio of formaldehyde to acetaldehyde and an 8 per cent excess of sodium hydroxide. The excess sodium hydroxide was based on the theoretical amount needed for complete conversion of acetaldehyde to pentaerythritol and complete removal of remaining formaldehyde by reaction (e). Considering only the total weight of water and formaldehyde initially present, the amount of formaldehyde used was 13 per cent by weight. These values were used because they were recommended by earlier investigators [3, 4, 7, 10, 11, 13] and are compatible with those used in commercial processes. The concentrations, expressed in terms of initial moles/l. were approximately 1·30 M in NaOH, 0·797 M in acetaldehyde, and 1·14 M in methanol. The methanol was introduced with the formaldehyde because commercial formalin was used. The pentaerythrose–formaldehyde reaction was studied at temperatures of 0°C, 24°C, 31·0°C, and 41°C.

The formaldehyde side reaction alone was studied at temperatures ranging from 0°C to 70°C. In these tests, formalin, water and sodium hydroxide were mixed thoroughly in a volumetric flask and placed in the constant-temperature bath. Samples were taken and treated in the same manner as those in the pentaerythritol runs.

Results and Discussion

The basic experimental data are presented in Tables 1 and 2. Figs. 1 and 2 show a graphical representation of the data for typical runs. The fast initial decrease in (—CHO) content at low temperature due to the rapid aldol condensation reactions is illustrated in Figs. 1 and 2. The theoretical analysis of the results is based on dividing the concentration versus time plots into three distinct sections. In the first section, corresponding to a reaction temperature less

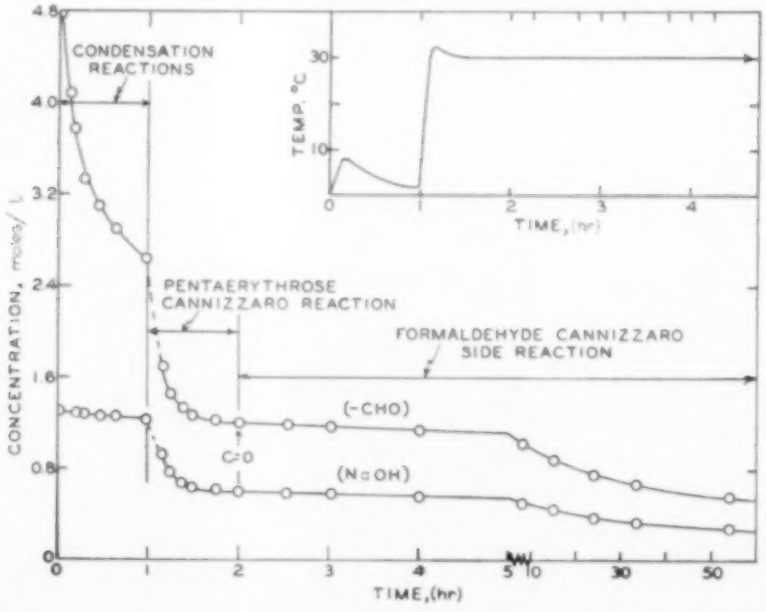

Fig. 1. Variation of concentration and temperature with time for pentaerythritol formation at 30°C (Run No. 3).

VOL. 10 1959

Table 1. *Experimental data for pentaerythritol runs*

Run No. 1

Time (hr)	(min)	*Temp.* (°C)	NaOH moles/l.	(— CHO) moles/l.
0	0·0	0	(1·30)	(4·7808)
0	7·5	10	1·3004	3·7627
0				
0	13·25	8	1·2904	3·1244
0	16·25	7	1·2840	2·9564
0	22·0	5	1·2660	2·7347
0	30·0	3	1·2596	2·6204
0	50·5	1	1·2272	2·4189
1	20·0	1	1·2008	2·2509
2	0·0	0	1·1560	2·1367
2	13·0	0	1·1420	1·9822
3	0·0	0	1·1136	1·9284
14	45·0	0	0·7436	1·2766
20	0·0	0	0·6784	1·1893
26	15·0	0	0·6380	1·1557
40	0·0	0	0·6012	1·1086
50	0·0	0	0·5908	1·0952
63	0·0	0	0·5868	1·0851
73	30·0	0	0·5808	1·0808
382	30·0	1	0·5176	0·9440
575	0·0	1	0·4837	0·9096

Run No. 2

Time (hr)	(min)	*Temp.* (°C)	NaOH moles/l.	(— CHO) moles/l.
0	0·0	0	(1·30)	(4·7808)
0	8·0	8	1·2344	4·2499
0	12·0	8	1·2256	3·8224
0	20·0	6	1·2204	3·3730
0	30·0	4	1·2100	3·1802
0	40·1	3	1·2000	2·9894
0	50·0	2	1·1876	2·8758
0	57·5	2	1·1796	2·8464
1	0	(Put in 23·5°C bath – 6 min required to reach 23·5°C).		
1	10·25	25·1	1·0120	1·9696
1	16·0	24·8	0·8884	1·7200
1	26·75	24·3	0·7388	1·5183
1	35·0	24·0	0·6736	1·4362
1	48·25	23·8	0·6144	1·3473
2	3·0	23·6	0·5760	1·2994
2	32·5	23·5	0·5480	1·2584
3	8·75	23·5	0·5400	1·2378
4	2·0	23·5	0·5316	1·2242
6	15·0	23·5	0·5204	1·1968
8	0·0	23·5	0·5097	1·1729
22	0·0	23·5	0·4651	1·0874
79	0·0	23·5	0·3460	0·8481

Run No. 3

Time (hr)	(min)	*Temp.* (°C)	NaOH moles/l.	(— CHO) moles/l.
0	0·0	0	(1·30)	(4·7808)
0	8·12	8	1·2976	4·0946
0	11·25	8	1·2932	3·7889
0	17·37	6	1·2872	3·3314
0	27·37	5	1·2732	3·1173
0	39·62	3	1·2568	2·8971
0	58·50	2	1·2364	2·6470
1	0·0	(Put in 30·2°C bath – 6 min required to reach 30°C).		
1	9·25	32·5	0·9320	1·7098
1	14·25	32·0	0·7804	1·4738
1	21·62	30·7	0·6816	1·3371
1	29·62	30·4	0·6452	1·2789
1	45·0	30·2	0·6172	1·2379
2	0·0	30·2	0·6092	1·2174
2	32·0	30·2	0·5956	1·1968
3	1·0	30·2	0·5940	1·1763
4	0·0	30·2	0·5674	1·1558
8	0·0	30·2	0·5134	1·0293
15	0·0	30·2	0·4450	0·8920
24	0·0	30·2	0·3906	0·7728
33	30·0	30·2	0·3442	0·6873
54	0·0	30·11	0·2846	0·5676
124	30·0	30·2	0·1935	0·3830
151	0·0	30·2	0·1749	—
193	0·0	30·2	0·1544	—

Run No. 4

Time (hr)	(min)	*Temp.* (°C)	NaOH moles/l.	(— CHO) moles/l.
0	0·0	0	(1·30)	(4·7808)
0	23·0	6	1·2844	3·0776
1	24·5	1	1·2174	2·3527
1	48·0	(Put in 40°C bath).		
1	55·1	41·5	0·8346	1·3199
1	58·5	41·0	0·6861	1·1627
2	1·5	40·0	0·6582	—
2	4·5	40·3	0·6281	—
2	8·5	40·0	0·6251	1·0806
2	14·5	40·0	0·6154	—
2	20·0	40·0	0·6098	1·0532
2	29·5	40·0	0·6009	—
2	47·0	40·0	0·5756	1·0088
3	7·0	40·0	0·5577	—
4	45·0	40·0	0·4670	0·8446
7	38·0	40·0	0·3963	—
11	16·0	40·0	0·3431	—
21	16·0	40·0	0·2623	—
32	53·0	40·0	0·2177	—
46	8·0	40·0	0·1823	—

than 8°C and the first hour in Fig. 1, it is assumed that the aldol condensation reactions go to completion to form pentaerythrose and a small amount of pentaerythritol. In the second section, corresponding to the second hour and an average reaction temperature of 31°C in Fig. 1, the pentaerythrose-formaldehyde Cannizzaro reaction occurs, and the pentaerythrose concentration is

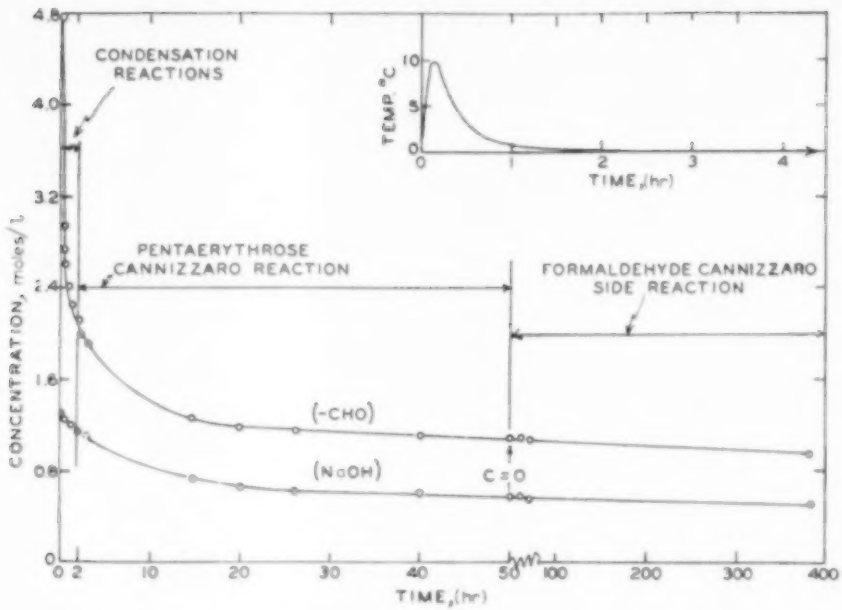

Fig. 2. Variation of concentration and temperature with time for pentaerythritol formation at 0°C (Run No. 1).

assumed to be zero at the end of this section. The last section corresponds to the occurrence of only the formaldehyde Cannizzaro reaction to give a slow, but steady, decrease in (— CHO) and hydroxyl content.

Formaldehyde side reaction

The kinetics of the formaldehyde Cannizzaro reaction was investigated extensively at various concentrations and a temperature of 30°C. In agreement with the work of other investigators, it was found that the rate constant was a constant with respect to time but was dependent upon initial concentrations. Consequently, in order to obtain rate constants that would be applicable in the balance of this work, the kinetics of the formaldehyde Cannizzaro reaction was established on the basis of the experimental data obtained in the third section of the concentration-time plots.

Equation (7) or (8) can be used to establish the kinetics of the formaldehyde side reaction. Examination of the experimental data for the pentaerythritol run presented in Fig. 1 shows that the concentration of formaldehyde was essentially twice the concentration of the sodium hydroxide when the pentaerythrose reaction was completed; therefore, equation (8) applies in this case and a plot of $(B)^2$ versus t should be a straight line. The reaction rate constant k_2 can be determined from the slope of the line. Figure 3 is such a plot for the pentaerythritol mixture at 30·2°C. Similar plots, based on equation (7) or (8), were made for the other temperatures at which the reaction was studied, and straight lines equally as good as that in Fig. 3 were obtained. Reaction-rate constants were evaluated from the slopes of the straight lines, and the results are presented in Table 3. Figure 4 (line 1) presents an Arrhenius-type plot for the reaction rate constants determined from the data obtained with the pentaerythritol mixture. The activation energy for the side reaction is 23,645 cal/g mole as evaluated from Fig. 4. The resulting equation for k_2 is

$$k_2 = 4{\cdot}85 \times 10^{15} \exp\left[-\frac{23{,}645}{RT}\right] l^2 \text{ moles}^{-2}\text{hr}^{-1} \quad (9)$$

Rate constants for the formaldehyde Cannizzaro reaction were also obtained at various initial concentrations and temperatures with no pentaerythritol present. In every case, using both

Table 2. Experimental data for formaldehyde Cannizzaro single-reaction runs

Na^+ = 1·2901 M
H_2O = 43·9 M

CH_3OH (initial) = 1·14 M
HCHO (initial) = 3·98 M

Time (hr)	(min)	*Temp.* (°C)	NaOH moles/l.	HCHO moles/l.	k_2 l^2 moles^{-2} hr^{-1}
0	0	0·7	1·1725	(3·7448)	
15	16	0·8	1·1333	(3·6664)	0·000324
41	40	0·7	1·0795	(3·5588)	
94	20	0·7	0·9782	(3·3562)	
0	0	30	1·1663	(3·7018)	
1	33·5	30	0·9389	(3·2470)	
3	19·5	30	0·7383	(2·8458)	0·0220
6	20·5	30	0·6080	2·5852	
10	14·5	30	0·4777	(2·3246)	
23	2·0	30	0·2750	1·8876	
0	0	40	1·0154	(3·3277)	
0	26	40	0·8334	(2·9637)	0·0837
1	47·5	40	0·5484	2·3937	
3	46·5	40	0·3722	(2·0413)	
0	0	50	0·7135	(2·7652)	
0	52	50	0·3619	2·0620	0·249
1	39·5	50	0·2151	(1·7684)	
3	40·5	50	0·1199	1·5523	

equations (7) and (8) for the analysis, the activation energy was the same, but the frequency factor depended upon the initial concentration. The results of experimental tests at identical initial concentrations, with the exception that no pentaerythritol or initial acetaldehyde was present, are shown in Fig. 4 (line 2) for comparison to the case when pentaerythritol was present. The fact that the expected kinetics for the formaldehyde side reaction is obeyed and the

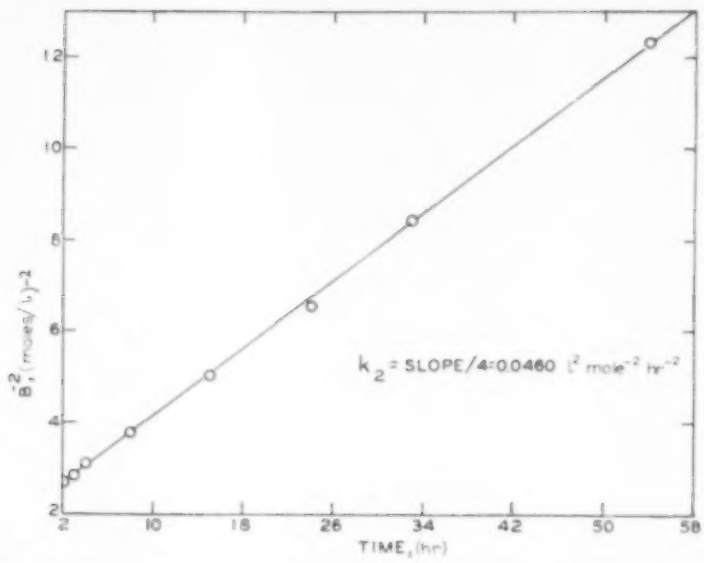

Fig. 3. Kinetic analysis of data from pentaerythritol run at 30·2°C showing applicability of equations (6) and (8) for formaldehyde Cannizzaro reaction.

activation energy is independent of concentration supports the assumption that only the formaldehyde Cannizzaro reaction takes place in the last section of the concentration-time plots.

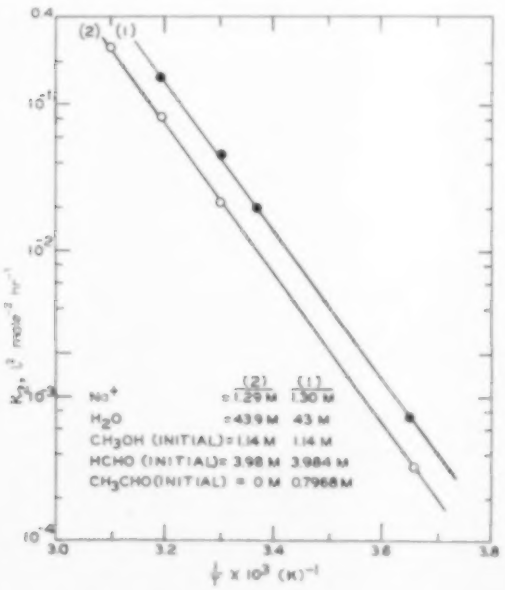

Fig. 4. Arrhenius plot for formaldehyde Cannizzaro reaction.

Table 3. Experimental values of reaction rate constants for pentaerythrose-formaldehyde Cannizzaro reaction (k_1) *and formaldehyde Cannizzaro reaction* (k_2).

Na^+ = 1·30 M
H_2O = 43 M
CH_3OH (initial) = 1·14 M
HCHO (initial) = 3·9840 M
CH_3CHO (initial) = 0·7968 M

Temp. (°C)	k_1 (l^2 moles^{-2} hr^{-1})	*Temp.* (°C)	k_2 (l^2 moles^{-2} hr^{-1})
0	0·0978	1	0·000703
24·0	2·802	23·5	0·01958
31·0	7·446	30·2	0·0460
41·0	23·544	40·0	0·1506

Pentaerythritol-formation reaction

The pentaerythrose-formaldehyde Cannizzaro reaction was found to be the rate-controlling step in the formation of pentaerythritol. Consequently, no attempt was made to evaluate rate constants for the rapid aldol condensation.

The kinetic analysis for the pentaerythritol-formation reaction is based on the application of equation (5). To use this equation, it is necessary to evaluate A, B and C at various times during

the second section of the concentration-time plot. The value of B is given directly from the experimental data at time t. The rate constant k_1 is much larger than k_2, and the effect of the formaldehyde Cannizzaro reaction can reasonably be neglected during most of the pentaerythrose reaction ; however, the formaldehyde side reaction must be considered in evaluating C, because C approaches a limit of zero. Accordingly, the following procedure can be used to determine the instantaneous values of C and A :

Combining equations (1), (2) and (3), and expressing the result in difference form gives

$$\Delta C = \Delta B + \frac{k_2}{2}(BA^2)_{avg}\,\Delta t \qquad (10)$$

$$\Delta A = \Delta B - \frac{k_2}{2}(BA^2)_{avg}\,\Delta t \qquad (11)$$

Because ΔA is small relative to A at any time, equation (11) can be simplified to $\Delta A = \Delta B$. Under these conditions, the values of A, B and C at any given time can be calculated by the stepwise procedure illustrated in Table 4, and a plot of ln X versus t, in accordance with equation (5), can be prepared. A plot of this type for a reaction temperature of 31·0°C is presented in Fig. 5. It can be seen that the expected straight-line relationship is obtained.

Plots similar to Fig. 5 were prepared for the pentaerythritol reaction at other temperatures, and values of the reaction rate constant k_2 were determined from these plots. The results are

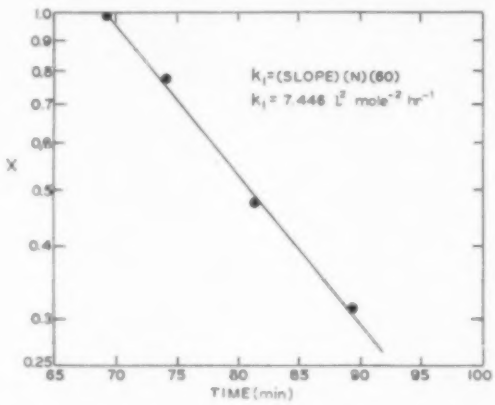

Fig. 5. Kinetic analysis of data for pentaerythrose-formaldehyde Cannizzaro reaction at 31°C showing applicability of equations (1) and (5).

tabulated in Table 3. The Arrhenius-type plot of the resultant values of the rate constants is presented in Fig. 6. From Fig. 6, the activation energy for the pentaerythrose-formaldehyde

Table 4. Method for evaluation of concentrations and terms in equation (5) based on run 3. Temperature = 31°C $k_2 = 7{\cdot}5 \times 10^{-4}$ l² moles^{-2} min^{-1}.

t (min)	B moles/l.	$-\Delta B$ moles/l.	Δt (min)	A moles/l.	$\frac{k_2}{2}(BA^2)_{avg}\,\Delta t$	$-\Delta C$ moles/l.	C mules/l.	X
69·25	0·9320			1·5402			0·3018	1·0000
		0·1516	5·00		0·0035	0·1481		
74·25	0·7804			1·3886			0·1537	0·7740
		0·0988	7·37		0·0036	0·0952		
81·62	0·6816			1·2898			0·0585	0·4750
		0·0364	8·00		0·0032	0·0332		
89·62	0·6452			1·2534			0·0253	0·3128
		0·0280	15·38		0·0056	0·0224		
105·00	0·6172			1·2254			0·0029	0·0856*
		0·0080	15·00		0·0051	0·0029		
120·00	0·6092			1·2174			0	

$A_0 = 1{\cdot}5402$ $B_0 = 0{\cdot}9320$ $C_0 = 0{\cdot}3018$ $N = -2{\cdot}1067$

*This point is not included on Fig. 5 because C is close to zero and equation (5) does not apply for this condition.

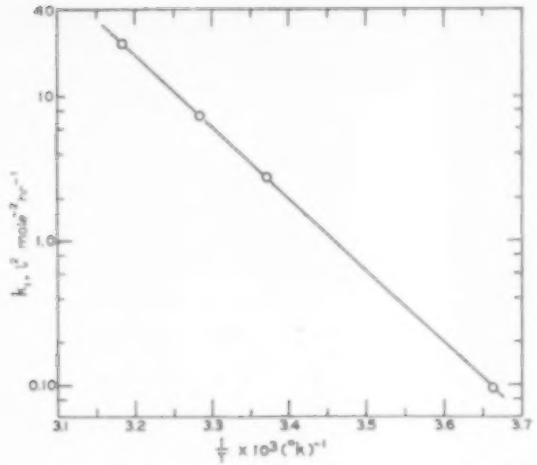

Fig. 6. Arrhenius plot for pentaerythrose–formaldehyde Cannizzaro reaction.

Cannizzaro reaction is 22,800 cal/mole and the equation for the rate constant is

$$k_1 = 1{\cdot}82 \times 10^{17} \exp\left[-\frac{22{,}800}{RT}\right] \text{l}^2\text{moles}^{-2}\text{hr}^{-1} \quad (12)$$

Yields

By observing the change in hydroxide concentration and making a correction for the formaldehye side reaction, the yield of pentaerythritol in solution can be calculated. On the basis of the experimental data for Run 3, the corrected change in NaOH concentration is 1·300–0·6092–0·0210 = 0·670 from time zero to the time indicated by $C = 0$ in Fig. 1. The per cent conversion of initial acetaldehyde to pentaerythritol therefore is (0·670/0·7968) 100 = 84·1 per cent. Approximately the same yields (± 0·5 per cent) were obtained for all runs in which the reaction mixture was held at 0°C until the pentaerythrose was formed.

The similar yields obtained for different pentaerythrose reaction temperatures indicates that side reactions involving acetaldehyde, with a resultant decrease in ultimate yield, occur during the aldol condensation steps. One possibility is the acetaldehyde aldol condensation with itself. This possibility was checked by making several runs in which the acetaldehyde was added slowly to a mixture of formaldehyde and sodium hydroxide at 0°C. After the pentaerythrose-formation reaction was complete, the final Cannizzaro reaction to produce pentaerythritol was carried out at 30°C. The calculated yield in solutions under these conditions of continuous low acetaldehyde concentration was 90·6 per cent. The observed increase in yield supports the proposal that some of the yield losses in the production of pentaerythritol can be due to side reactions in the rapid aldol condensation reactions.

Summary

Investigation of the kinetics of pentaerythritol-formation reactions shows that the rate of the aldol condensations leading to pentaerythrose is very rapid and the rate-limiting step is the pentaerythrose–formaldehyde Cannizzaro reaction. Under concentration conditions equivalent to those used in industrial operations, the rate of the pentaerythrose–formaldehyde reaction to produce pentaerythritol can be represented as

$$\frac{d\left[(\text{HOCH}_2)_4\right]\text{C}}{dt} = k_1\,(\text{HCHO})\,(\text{NaOH})\left[(\text{HOCH}_2)_3\,\text{CCHO}\right]$$

and the rate of the formaldehyde Cannizzaro reaction can be expressed as

$$\frac{-d\,(\text{HCHO})}{dt} = k_2\,(\text{HCHO})^2\,(\text{NaOH})$$

Experimental data verify the preceding equations. The observed values of the rate constants show that the reaction producing pentaerythritol is much faster than the formaldehyde Cannizzaro reaction even at low concentrations of pentaerythrose. Analysis of the "in solution" yields of pentaerythritol based on the amount of acetaldehyde charged indicates that side reactions during the rapid aldol condensation reactions can be one of the causes for yield losses in the production of pentaerythritol.

Acknowledgement—Part of this study was supported by a grant from the National Science Foundation. A fellowship from the American Oil Company, under which a portion of the work was conducted, is also gratefully acknowledged.

VOL. 10 1959

Notation

A = formaldehyde concentration (subscript 0 refers to start of time interval), moles/l.

B = sodium hydroxide concentration (subscript 0 refers to start of time interval), moles/l.

C = pentaerythrose concentration (subscript 0 refers to start of time interval) moles/l.

$a = B_0 - C_0$ moles/l.

$b = C_0 = A_0$ moles/l.

$c = A_0 - B_0$ moles/l.

k_1 = reaction rate constant for pentaerythrose-formaldehyde Cannizzaro reaction $l^2/moles^2$ hr

k_2 = reaction rate constant for formaldehyde Cannizzaro reaction $l^2/moles^2$ hr

$$K = \frac{k_2}{2}(2B_0 - A_0)$$

$$N = 1/abc$$

$$P = \frac{1}{A} + \frac{1}{2B_0 - A_0} \ln \frac{A}{B}$$

R = perfect gas law constant, cal/mole°K

$$S = \frac{1}{A_0} - \frac{1}{2B_0 - A_0} \ln \frac{B_0}{A_0}$$

t = time

T = temperature

$$X = \left(\frac{A}{A_0}\right)^a \left(\frac{B}{B_0}\right)^b \left(\frac{C}{C_0}\right)^C$$

References

[1] Alexander E. R. *Ionic Organic Reactions*. John Wiley, New York 1950.

[2] Barth R. H., Snow J. E. and Wood E. H. Paper presented at Amer. Chem. Soc. North Jersey Section Meeting-in-Miniature 8th January, 1951.

[3] Berlow E., Barth R. H. and Snow J. E. *Amer. Chem. Soc.* Monograph Series No. 136 Reinhold, New York 1958.

[4] Burghardt R. F. and Barth R. H. (Assrs. to Heyden Chemical Corp.) U.S. patent 2401749 June 11 1946.

[5] Cupit C. R. *Ph.D. Thesis* University of Illinois, 1958.

[6] Martin R. J. L. *Austral. J. Chem.* 1954 **7** 335.

[7] Peters M. S. and Quinn J. A. *Industr. Engng. Chem.* 1955 **47** 1710.

[8] Pfeil E. *Chemie.* 1951 **84** 229.

[9] Salkind M., Ahern H. F. and Albert A. A. *Industr. Engng. Chem.* 1958 **50** 1106

[10] Sherwood P. W. *Petrol. Refin.* 1956 **35** No. 11 171.

[11] Walker J. F. *Formaldehyde* (2nd ed.) Reinhold, New York 1953.

[12] Wawzonek S. and Rees D. A. *J. Amer. Chem. Soc.* 1948 **70** 2433.

[13] Wyler J. A. (Assr. to Trojan Powder Co.) U.S. patent 2170624 August 22 1939.

Chemical Engineering Science, 1959, Vol. 10, pp. 68 to 79. Pergamon Press Ltd. London. Printed in Great Britain

Absorption of iodine vapour by aqueous solutions

R. F. Taylor

Atomic Energy Research Establishment, Harwell.

(*Received* 11 *July* 1958)

Abstract—Absorption of iodine vapour into several aqueous absorbents has been studied using a disc-type laboratory column. The absorption rate was found to be completely gas-phase controlled, under all conditions investigated, for absorbents containing the sodium salts of thiosulphate, hydroxide, or iodide. With the other liquids used, namely water, sodium tetrathionate and sodium sulphate solutions, appreciable liquid-phase resistance to transfer was apparent.

The data obtained are of direct value in the design of equipment for which the operation characteristics are known in terms of phase coefficients.

Résumé—L'absorption de vapeur d'iode par différents absorbants aqueux a été étudiée en utilisant une colonne à disques de laboratoire. La vitesse d'absorption est contrôlée par la phase gazeuse, dans toutes les conditions considérées, pour les absorbants contenant les thiosulfates, hydroxide ou iodure de sodium. Pour les autres liquides utilisés, à savoir, eau, solutions de tétrathionate de sodium et de sulfate de sodium, la phase liquide produit une résistance au transfert appréciable. Les données obtenues sont directement utilisables au calcul de l'appareillage pour lequel les caractéristiques opérationnelles sont connues, en fonction des coefficients des phases.

Zusammenfassung—In einer Laborkolonne vom Scheibentyp wurde die Absportion von Joddampf in verschiedenen wässerigen Absorbenten untersucht. Die Absorptions geschwindigkeit ergab sich bei allen Versuchsbedingungen als nur von der Gasphase abhängig, wenn die Absorbenten die Natriumsalze von Thiosulfat, Hydroxyd oder Jodid enthielten. Bei Verwendung anderer Flüssigkeiten wie Wasser, Natriumtetrathionat- und Natriumsulfatlösungen, wurde ein beträchtlicher Übergangswiderstand in der flussigen Phase gefunden.

Die Ergebnisse sind direkt anwendbar zur Berechnung von Apparaten, deren Arbeitsbedingungen in Ausdrücken der Phasenkoeffizienten bekannt sind.

Introduction

Iodine absorption and desorption is of interest in nuclear reactor technology from at least three aspects. Iodine 131 is widely used as a biological tracer and methods of recovering it from irradiated uranium metal have been described [1, 2]. Emission of radio-active iodine 131 and 134 vapours into the atmosphere must be kept to low limits owing to the tendency of this element to concentrate in the thyroid gland. Cases therefore arise where it is necessary to scrub iodine out of gaseous effluents with a high degree of efficiency. Also, since iodine 135 is a precursor of xenon 135, one of the most serious of the thermal reactor "poisons," the removal of this isotope from nuclear reactor systems employing liquid fuels may become important [3, 4].

For some applications, where the iodine is a nuisance material to be eliminated from the gas stream, reaction with solid beds has been used [5, 6]. In the extraction of iodine 131 from uranium fuel elements, the following methods of absorbing iodine vapour have been used : bubbling through sodium hydroxide [1] and sodium thiosulphate solutions [8], contacting with refrigerated water in bubble-cap towers, and scrubbing with sodium hydroxide solutions [1].

Iodine is extracted from oil-well brines by a process based upon the desorption of iodine liberated from the brine into air, followed by absorption into hydriodic/sulphuric acid solutions [9]. Absorption into sodium hydroxide or carbonate has also been proposed [10].

Thus, a certain amount of practical experience is available on the absorption and desorption of iodine vapour by aqueous solutions, but there

appears to be no published information on the fundamental behaviour of these processes. The results of the present investigation provide some basic data for such systems.

I. Experimental Methods

(*a*) *Choice of absorber*

In the scrubbing of active iodine from gaseous effluents the activity level may be very high and the operating conditions corrosive, so that plant with the simplest of working parts is favoured. Packed towers are suitable equipment from this point of view. For small-scale studies, however, it is not possible to build models which behave in a manner exactly analogous to that of full-scale packed towers [11]. Moreover the effective absorbing surface area of packed towers cannot be measured directly, and it varies between wide limits even when elaborate precautions are taken [12]. Stephens and Morris devised the disc-column [13] in which liquid undergoes some degree of mixing as it proceeds down the column and thus approximates to the behaviour in a packed tower. This apparatus has the following advantages; the absorption area is known and is essentially constant; the coefficients obtained are independent of column length; relatively small phase throughputs are required; and it is particularly suitable for studying absorption with chemical reaction.

(*b*) *Calibration of absorber*

Full details of the calibration of the present disc-column have been given previously [14] as the results were of some interest in themselves. Relevant dimensions of the column used are: chain of 60 roughened pyrophyllite disc (0·574 in. diam., 0·175 in. thick) of total area 0·348 ft²; mean perimeter for liquid flow: 0·121 ft; chain held centrally in a 1 in. diam. gas channel; equivalent diam. [13] for gas flow: 0·050 ft. Absorption of carbon dioxide into water was used for determining the liquid-phase characteristics of the column, and absorption of dilute ammonia gas into water for the gas-phase characteristics (allowance being made in this latter case for a small liquid-phase resistance).

In contrast to the results of Stephens and Morris [13] a break-point, coincident with the inception of rippling of the liquid on the disc-edges, was found in the liquid-phase coefficient (k_L) versus liquid rate (Γ) correlation; this was expressed in terms of the general relationship of Sherwood and Holloway:

$$\frac{k_L}{D_M} = \alpha \left(\frac{4\Gamma}{\mu}\right)^m \left(\frac{\mu}{\rho\, D_M}\right)^{0.5} \ldots \text{ft}^{-1} \qquad (1)$$

where, for $\Gamma < 155$ lb/hr ft; $\alpha = 58{\cdot}0$; $m = 0{\cdot}4$

and for $\Gamma > 155$ lb/hr ft; $\alpha = 1{\cdot}94$; $m = 1{\cdot}0$

For gas-phase behaviour the results are best correlated in terms of the relative velocity between phases rather than the absolute gas velocity [13]; data for both counter- and co-current flows may be satisfactorily incorporated in relationships similar to those of Morris [15]

$$\frac{M_M k_G P_{BM}}{v \cdot \rho} = \beta \left(\frac{v \cdot d \cdot \rho}{\mu}\right)^{-0.33} \left(\frac{\mu}{\rho\, D_M}\right)^{-0.5} \qquad (2)$$

where, for $\Gamma < 155$ lb/hr ft; $\beta = 0{\cdot}151$

and for $\Gamma > 155$ lb/hr ft; $\beta = 0{\cdot}043\ \Gamma^{0.25}$

The calibration curves have been reproduced as lines in Figs. 10, 11 and 12 for comparison with the present investigation (though they have been adjusted by the diffusivity factors indicated in the figures in order to simplify the presentation of the iodine data).

(*c*) *Iodine absorption assembly*

Aqueous solvent flowed from a reservoir, through control valve, rotameter, and tube heater, into the column. After flowing down the absorption element the liquid passed through the sampling point and flow measuring point to an active-waste carboy. From feed vessel to sampling point the liquor lines were of glass, with stainless steel control valve and tube heater of nickel.

For the gas stream, air at room temperature was metered through a calibrated rotameter and passed into a mixing vessel where it was saturated with water vapour and, if necessary, heated. For the runs at higher temperatures a considerable volume of water vapour was introduced and the gas flow rates were calculated allowing for this, and for the increase of volume with temperature rise. The air temperature was reduced to the required value by control of the cooling water feed-rate to a condenser and the precipitated water removed from the gas stream in a cyclone separator. Pressure drop through the wet

sintered discs in the generator and in the cleaning trains was considerable, so that in order to retain atmospheric pressure in the column it was necessary to apply appreciable pressure on the inlet side and vacuum on the outlet side.

From the cyclone to the absorption trains the gas channel was of glass and was heated to the required temperature, along the lines by electric heating tape and in the column by water jacket. As the jacket walls were of glass the working of the column could be kept under observation at all temperatures. On leaving the cyclone the gas stream passed through the iodine generator and counting chamber, and into the column. Having traversed the column the gas proceeded through one of two iodine trapping trains. The first merely disposed of active iodine as a safety measure; the second train was switched in for a timed interval to provide an analysis of the outlet gas stream under equilibrium conditions.

(d) Iodine generator

Elemental iodine spiked with ^{131}I was liberated chemically at a predetermined rate in the iodine generator and was swept away with the air stream passing through. Check was kept on the iodine content of the gas entering the column by means of a gamma scintillation counter, working a "No. 1021" radiation monitor. This system provided a visual means of showing that the iodine content was being maintained at a steady value of the correct order.

The method of generation was to feed aqueous solution of potassium iodide at constant rate into a solution of iodic acid and dilute sulphuric acid. Iodine liberated by the reaction:

$$5I^- + IO_3^- + 6H^+ \rightarrow 3H_2O + 3I_{2\,(aq)},$$

(giving a 6 : 5 dilution ratio of isotope), was then removed from solution by the air stream bubbling through. The iodide–iodate reaction in acid solution is known to be rapid and the isotopic exchange between iodine and iodate ion extremely slow [16], so that the iodide activity introduced to the generator is immediately carried out with the iodine vapour without the complication of side-reactions. The iodide feed mechanism consisted of a pipette piston driven by a weight falling at a controlled rate. Iodine concentration in the vapour was calculated from that of the potassium iodide feed solution and it was therefore necessary to demonstrate that the two were exactly proportional under operating conditions. The feed mechanism was found always to expel liquid at the rate of $1{\cdot}20 \pm 0{\cdot}01$ ml/min irrespective of time and the position of the piston in the cylinder.

For the generator to run under steady-state conditions with respect to its free iodine content, no solid iodine could be permitted to precipitate out from solution. This requirement might have severely limited the range of iodine gas concentrations available. With the generator containing 100 ml of water, 6 g of iodic acid and 3 ml of sulphuric acid, it was found that, under all the conditions of gas rate and temperature used here, iodine was not precipitated if its concentration in the air stream did not exceed one fourth of saturation value. The generator system came to equilibrium within one to three minutes under the present working conditions. One run was attempted at an iodine vapour concentration of $7{\cdot}8 \times 10^{-7}$ v/v and in this case about half of the liberated iodine remained in the generator. The rate of transfer of generator liquid to the column in the form of mist was found to be 0·0017 ml/min at the highest gas rate, which would have insignificant effect on the absorption process.

(e) Iodine trapping and analysis

The iodine generator and the sintered-disc absorbers were of similar basic components with different fittings. They consisted of cylindrical glass vessels about 14 in. high with 90 mm diameter sintered glass discs placed an inch above the bottom. With 50 ml of trapping solution in one of these absorbers, fed with a gas stream containing iodine, the material passing forward from the trap (probably largely as spray) was a follows:

Gas rate, ft^3/hr:	12·7	17·0	51	74	119
% feed material passing through trap	0·02	$< 0{\cdot}1$	0·2	0·3	1·0

Two absorbers in series thus provide a quantitative trap at all these gas rates.

After each run the contents and washings of the quantitative absorbers on the gas outlet stream were separately made to 100 ml and counted for beta-gamma activity. This was performed on exactly 10 ml of solution using a Geiger-type liquid counter (halogen filled). The usual count-rate corrections were made and the necessary allowance made for the influence of high solute concentrations upon the count-rate as determined experimentally. Counting the activity of the iodide feed to the generator gave the relationship between count-rate and iodine concentration. From this equivalence the iodine concentrations in the solvent and gas outlet streams could be derived. From these data an iodine balance across the system was made and an over-all absorption coefficient evaluated.

(f) Operating procedure

Potassium iodide solution spiked with ^{131}I was made up to the required concentration and drawn up into the iodine feed reservoir. The active iodine used was IBS.1 of the Radiochemical Centre [8], in which carrier-free ^{131}I is in the form of sodium iodide in 0·01M sodium thiosulphate, and as less than 0·1 ml was used per run the influence of the thiosulphate on the generator system was negligible.

With the apparatus completely assembled and charged, the air flow was started and the outlet gas passed through the iodine disposal train. Solvent feed was turned on and the air flow gradually increased while the column pressure

was maintained at 1–2 cm of water gauge above atmospheric. The various supplies were now adjusted to the required settings and the iodide feed mechanism turned on. Readings were taken periodically on the various meters. Towards the end of the 30 min running time, which permitted many complete throughputs of both phases at even the lowest flow rates, a liquid sample was taken, followed by a gas outlet sample and two more liquid samples. The gas outlet was sampled by switching to the analytical train for an exactly timed interval. To keep trapping liquid on the sintered discs a by-pass switch was just cracked to maintain the necessary gas pressure. After sampling, the run was closed down.

(g) *Physical data on iodine systems*

Iodine vapour in air behaves as an ideal gas to within ½% [17]: its viscosity is given as 136 μp at 20°C [18]. The molecular diffusivity of iodine in air has been determined [19] as being 0·080 cm^2/sec at 20°C which agrees with values determined in nitrogen [20] and values predicted by the empirical correlations of Morris and Jackson [13] and that of Gilliland.

The solubility of iodine in water is low [17] and considerably less again in concentrated solutions of sodium sulphate [21]. Very little information is available on the molecular diffusivity of iodine in pure water. Euler [22] gave a value of $0{\cdot}6 \times 10^{-5}$ cm^2/sec at 12°C for 0·1 molar solution presumably containing alkali iodide, and Miller [23] derived a value of $0{\cdot}96 \times 10^{-5}$ cm^2/sec at 20°C.

Hydrolysis of iodine in water is so small [24] that in contrast to the case of chlorine the available driving force for absorption is not influenced significantly. Iodine dissolved in aqueous alkali iodide solutions gives rise to tri-iodide ions and the equilibrium constant $k = \dfrac{[I^-] \times [I_2]}{[I_3^-]}$ has been determined [25].

Iodine back-pressure from the iodide solutions used here was only just significant. In homogeneous reaction the rate of consumption of iodine in sodium hydroxide solutions is proportional to its concentration but is decreased by the presence of excess alkali [26]. Under present conditions the mechanism of the complex reactions taking place does not enter explicitly into the results obtained. Reaction between iodine and thiosulphate ion is so fast that it may be regarded as virtually instantaneous in the present context, though its kinetics have been studied in some detail [26]. Although tetrathionate ion is usually regarded as an end-product of this reaction it does react very slowly with iodine [27].

No information on the equilibrium distribution of iodine between air and water could be found in the literature so the data were determined experimentally as follows.

(h) *Iodine equilibrium determinations*

If checked by approaching equilibrium composition from both sides, the dynamic method is capable of producing accurate results and was chosen as being convenient for the present work.

The equipment used was based on the sintered disc contactors mentioned previously. One was used as the equilibrium cell in which air was drawn slowly through the aqueous inactive iodine solution and its iodine content determined by total trapping and chemical analysis. In some runs the air was taken straight from atmosphere, in others it passed first through another contactor containing a similar iodine solution at twice the concentration. By this means equilibrium contacting was performed with iodine-weak gas in some runs and with iodine-rich gas in others, and if, in fact, equilibrium was not attained in the main chamber the values obtained by the two methods would differ. Results given in Fig. 1 and Table 1 show that no significant difference exists; so that the data may be accepted as equilibrium values. Temperatures were maintained at 20·0 ± 0·5°C and the gas volume drawn through is considered to be known within 0·2 per cent. The gas drawn through was 1 l/hr and at this flow rate the gas pressure in the cell was 11 mm Hg below atmospheric.

A check made on spray carry-over, using ^{131}I in a non-volatile form, indicated that the amount of iodine transferred by spray to the trap was 0·25 per cent of that transported as vapour. Transfer and sampling of volatile iodine solutions were made under pressure to minimize iodine losses to atmosphere. Similar equilibrium determinations were made using as the absorbent 182 g/l. A.R. grade sodium sulphate in water. Despite previous checks it was found during preliminary equilibrium runs that free iodine at low concentrations was being destroyed

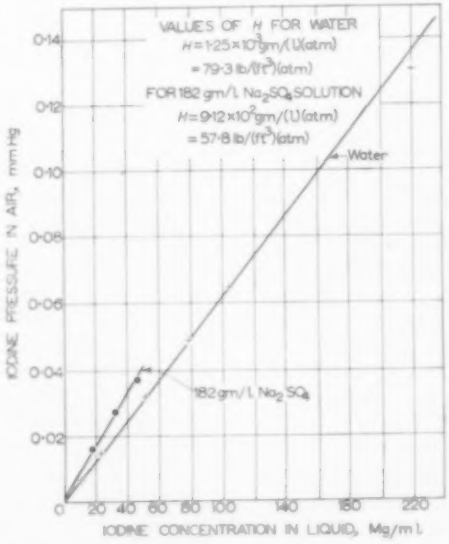

Fig. 1. Equilibrium curves for distribution of iodine between air and aqueous liquids.

Table 1. *Equilibrium data for the distribution of iodine between air and aqueous liquids.*

1. *Water*

Presaturator used	*Mean temp.* (°C)	*Working press.* (mm Hg)	*Iodine conc. in liquid* mg I/l. *End*	*Iodine conc. in liquid* mg I/l. *Mean*	*Vol. air passed* (l.)	*Iodine in trap* (mg)	*Press. iodine in air* (mm Hg)	H (g)/(l.) (atm)
No	20·0	762	219	221	2·00	3·62	0·130	$1·29 \times 10^3$
No	20·4	761	104	105	2·00	1·81	0·0655	$1·22 \times 10^3$
Yes	20·2	749	79·9	79·2	2·00	1·39	0·0495	$1·22 \times 10^3$
Yes	20·0	748	24·6	24·4	1·94	0·388	0·0142	$1·30 \times 10^3$
No	20·3	746	8·50	8·66	4·00	0·322	0·0058	$1·14 \times 10^3$
No	20·2	743	31·1	31·8	4·00	1·85	0·0321	$1·23 \times 10^3$

2. *Sodium sulphate solution* (182 g/l.)

No presaturator used	*Mean temp.* (°C)	*Working press.* (mm Hg)	*Iodine conc. in liquid* mg I/l. *End*	*Iodine conc. in liquid* mg I/l. *Mean*	*Vol. air passed* (l.)	*Iodine in trap* (mg)	*Press. iodine in air* (mm Hg)	H (g)/(l.) (atm)
	20·3	759	45·3	45·6	1·00	0·512	0·0368	$9·42 \times 10^2$
	19·8	758	18·5	18·6	1·20	0·253	0·0158	$8·94 \times 10^2$
	19·7	742	31·8	32·0	1·00	0·385	0·0271	$8·98 \times 10^2$

by such solutions. This behaviour was first noticed with a sulphate solution (182 g/l.) which had stood in a stoppered glass bottle for several weeks and in solution with iodine for 2 days; it appeared to consume approximately 40 mg iodine/l. The fresher solutions used for absorption runs were checked and found to consume 1·5 mg iodine/l.; newly made solutions consumed 0·8 mg iodine/l. For these reasons the sodium sulphate solutions were made up and mixed with iodine solutions immediately before use. The capacity of the fresh sulphate solutions appears to be too small to influence the equilibrium determinations markedly, and in the absorption work, where the period of exposure is short, the effect should be negligible.

For the equilibration work on such solutions (in which the solubility of iodine is very low) active iodine was used and a modified procedure adopted, both in order to associate a known concentration of iodine with a certain level of activity without introducing contaminants (such as KI), and to reduce to a minimum the time that iodine and sodium sulphate were in solution together before use. Liberated iodine activity was introduced to the mixed solutions by vapour-phase diffusion from a cup suspended for a certain time in limited air space above the solution in a sealed flask (Fig. 2). A sample of the resulting solution was counted and the activity level taken as a measure of the total iodine concentration. The calculated concentration had an error $> -0·2$ per cent due to iodine carrier in the diffusion cup, and an error $> +1·0$ per cent arising from iodine loss to air space in the mixing flask, but no correction was made for these; the equilibrium data are based on comparative measurements of vapour and liquid activities derived from the same original solution, and as the equilibrium curves are linear this type of error is not reflected in the final results. The equilibrium data obtained are given in Table 1 and Fig. 1.

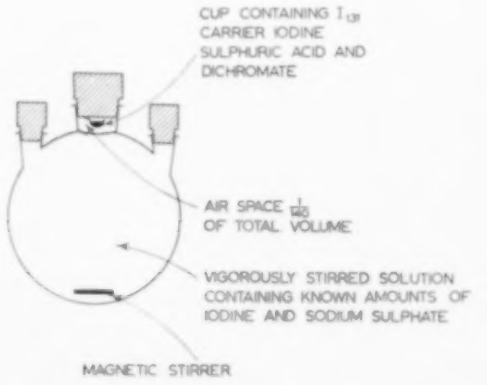

Fig. 2. Method of introducing iodine activity, free of extraneous matter.

(i) Physical properties of absorbent solutions

Of the various solutions used, those containing up to: 20 g/l. of thiosulphate, 12·1 g/l. NaI, 3·2 g/l. NaOH, or 3·5 g/l. of $Na_2S_4O_6$, have specific gravities and viscosities within 1 per cent of that of water. Relevant properties of the other solutions used were determined as necessary.

II. Experimental Results

Iodine vapour was absorbed into several aqueous solutions, as shown in Table 2.

Reagents were of analytical reagent grade and the water was demineralized and distilled. Sodium thiosulphate at 20 g/l. of pentahydrate was taken as an arbitrary standard absorbent. The hydroxide and iodide solutions were used at molar concentrations bearing a simple relationship to that of the thiosulphate.

The solutes used fall into two distinct groups as indicated in Table 2 above. In the first group solute was present which reacted rapidly with iodine, whereas in the second very little, if any, reaction took place. This distinction is reflected in the results shown in the histogram of Fig. 3, where over-all absorption coefficients for the various solutions are compared under effectively standard conditions. The influence of the indicated variations in wetting rate was negligible; solvent (9) was used at 27 °C and is more directly evaluated below.

Anticipating results given below, absorption into solvents of the first group (1 to 9 in Fig. 3) exhibited purely gas-phase control and the value of the absorption coefficient was essentially constant. Absorption into solvents of the second group (Nos. 10 to 13) was considerably slower and showed signs of appreciable liquid-phase resistance to transfer. In terms of the standard relationship:

$$\frac{1}{K_G} = \frac{1}{k_G} + \frac{1}{Hk_L} \qquad (3)$$

solvents of the first group have negligible liquid-phase resistance, so that $1/Hk_L = 0$ and $K_G = k_G$: solvents of the second group have values of k_L of practical importance, and this coefficient is used in the presentation of results.

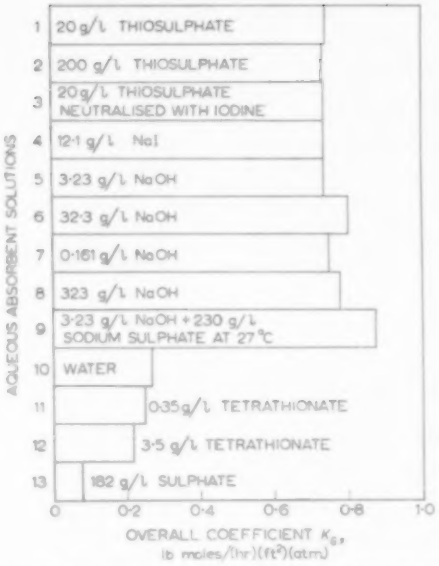

Fig. 3. Histogram showing influence of solvent used on overall coefficient.
Temperature 20 °C except (9) 27 °C.
Gas feed 7·8 × 10^{-3} % I_2
Gas velocity 7·25 ft/sec.
Values corrected to relative velocity 8·4 ft/sec.
Liquid rate Γ 274 lb/hr ft except (2) Γ = 301
(8) Γ = 346
(9) Γ = 328

(a) Solvents exhibiting purely gas-phase control

Dependence of the overall coefficient (K_G) upon liquid rate was found to be very small for absorption into

Table 2. Absorbent solutions.

Solute	*Concentration in water* (g/l.)	*Temperature* (°C)	*Gas feed conc.* (% $I_2 \times 10^{-4}$)
Sodium thiosulphate	20 and 200	20, 32, 50	(0·078 to 78·0)
Sodium hydroxide	0·16 to 323	20	7·8
Sodium iodide	12·1	20	7·8
Sodium hydroxide	3·2	27	7·8
Sodium sulphate	230		
Sodium thiosulphate exhausted with iodine	20	20	7·8
Water		20	7·8
Sodium tetrathionate	0·35 and 3·5	20	7·8
Sodium sulphate	180	20	7·8

thiosulphate, hydroxide and iodide solutions. This suggests that most of the resistance to transfer lay in the gas phase and this was confirmed by a dependence on relative velocity between phases the same as that for k_G in the calibration work. Fig. 4 shows the small influence of liquid rate upon the over-all coefficient for these solvents (the values are adjusted to eliminate the additional influence of the relative velocity between phases). A plot of the present results in the manner suggested by HASLAM [28] confirms that the liquid-phase resistance was extremely small compared with that of the gas phase [31].

Dependence of the over-all coefficient upon relative velocity between phases is demonstrated in Fig. 5. MORRIS and JACKSON [13] recommend for packed towers that the relative velocity between phases should not be taken as greater than 1·3 times the gas velocity, in order to allow for non counter-current conditions of flow at very low gas velocities caused by back-mixing. This procedure is adopted here and in the final correlation (Fig. 10) it applies for a few counter-current runs at the lowest gas rates. In the present curve the slopes and the break-point agree with those found in the k_G calibration plot (see Fig. 10).

Data in Figs. 10 and 11 show that the dependence of the coefficient upon T and v was the same at 50°C as at 20°C. The influence of temperature upon the absolute value of

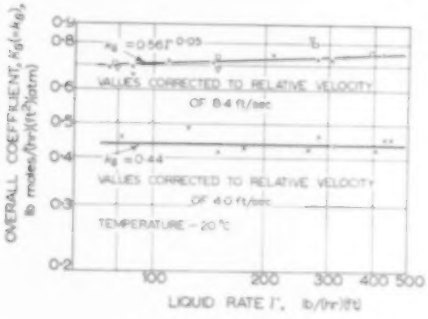

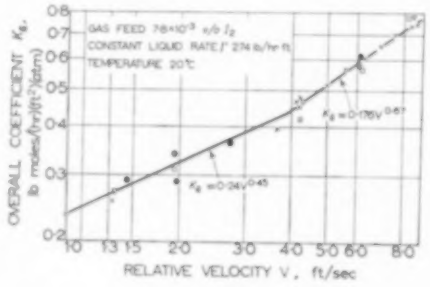

FIG. 4 and FIG. 5. Absorption into thiosulphate, hydroxide and iodide Solutions.

Fig. 4. Over-all coefficient vs. liquid rate.

× ● sodium thiosulphate (all concentrations)
▽ sodium hydroxide (3·2 g/l.)

Fig. 5. Over-all coefficient vs. relative velocity.

□ ■ sodium iodide (12·1 g/l.)
Solid symbols: co – current flow

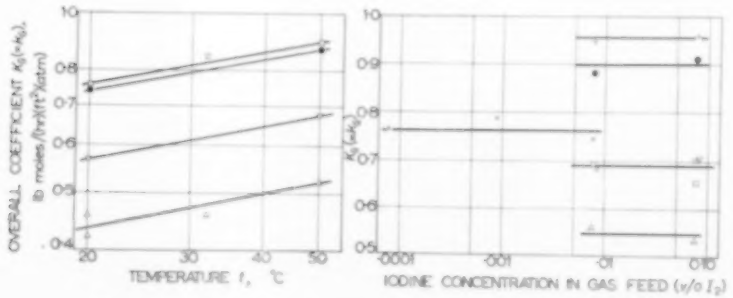

FIG. 6 and FIG. 7. Absorption into 20 g/l. thiosulphate.

FIG. 6.

Effect of temperature on over-all coefficient.
20 g/l. sodium thiosulphate sol.
gas feed 7·83 × 10^{-3} v/o I_2
Relative velocity 8·4 ft/sec ×
" " 8·4 ft/sec ●
" " 5·7 ft/sec ▽
" " 4·0 ft/sec △
Points on any one line corrected to a common velocity.
For all lines $k_G \propto t^{0.18}$

FIG. 7.

Influence of gas composition.
20°C Γ = 274, relative velocity = 8·4 ft/sec ×
50°C Γ = 434 " " = 9·1 ft/sec +
50°C Γ = 274 " " = 8·4 ft/sec ●
50°C Γ = 274 " " = 4·5 ft/sec △
50°C Γ = 274 " " = 5·9 ft/sec □
50°C Γ = 80 " " = 7·9 ft/sec ▽

k_G is shown in Fig. 6, where data determined under a variety of operating conditions are given. To allow for the influence of temperature and other factors upon phase velocities, the points plotted on any one line are corrected to a common relative velocity. Between 20°C and 50°C the coefficient increases by a factor 1·19 and the curves represent the relationship: $k_G \propto f^{0.18}$. This is to be contrasted with the prediction of MORRIS and JACKSON [13] that across the same temperature rise k_G will decrease by 5 per cent.

At 20°C the highest practicable concentration of iodine in the gas feed was $7{\cdot}8 \times 10^{-3}$ v/v, about one fifth saturation value. At 50°C it was possible to use $78{\cdot}3 \times 10^{-3}$ v/v, and in addition runs were performed at 20°C using feeds of $0{\cdot}78 \times 10^{-3}$ and $0{\cdot}078 \times 10^{-3}$ v/v. Results are presented in Fig. 7, where only those points bearing the same symbol are directly comparable. Variation in gas composition over the thousand-fold range from 0·00008 to 0·08 v/v iodine has no detectable effect on k_G.

(b) Solvents exhibiting some liquid-phase control

As absorption into solutions containing either sodium thiosulphate, iodide, or hydroxide was found to be controlled solely by gas-phase conditions, it was decided to see if the liquid-phase resistance became significant for absorption into pure water. The solubility of iodine in water is low, the degree of hydrolysis very low, and the rate of hydrolysis is unknown. MORRIS and JACKSON's [13] criterion, $\left(\frac{\rho}{HP}\right)$, has a value of $8{\cdot}9 \times 10^{-3}$, which lies in the range where they suggest the resistance of both phases may be significant. Iodine solubility in the water used, was found to be 0·298 g/1000 g at 21·2°C which agrees with values in the literature.

A few runs were made using a solution of sodium tetrathionate in water because slow reaction between this material and iodine has been reported [29]. The rate constants are so low [27] however that absorption theories predict no difference from physical absorption [30]. This prediction is borne out by the experimental results, (calculations were based on the assumption that equilibrium data are as for water, which is reasonable in view of negligible reaction and the low concentration of electrolyte). Laboratory reagent grade sodium tetrathionate was used containing 1·6 per cent water and no thiosulphate.

Results of the pure water and the tetrathionate runs are very similar and they have been plotted together (Fig. 8). From the experimental value of K_G and the value of k_G under comparable conditions, Hk_L was derived (equation 3), and with H known (Fig. 1), k_L was evaluated. Fig. 8 shows a plot of k_L versus Γ, where the break point at $\Gamma = 155$, and the exponents of 0·4 and 1·0 upon Γ, agree with those in the calibration plot for purely liquid-phase control (see Fig. 12).

(c) Concentrated electrolyte solutions

High concentrations of electrolyte in solution will increase the liquid-phase resistance and perhaps influence the overall coefficient, by lowering the physical solubility of the gas and by reducing its diffusivity in the liquid. However, absorption into concentrated thiosulphate and hydroxide solutions gave results very similar to that into dilute solutions. To check upon this matter a few runs were made using a solution of saturated sodium sulphate as inert electrolyte with dilute sodium hydroxide as reactant. Some results of these runs are given in the plot of Fig. 9 which shows that the values of the coefficient (k_G) are enhanced, not lowered, by the addition of sodium sulphate. The difference between the solvents increases with rising liquid rate.

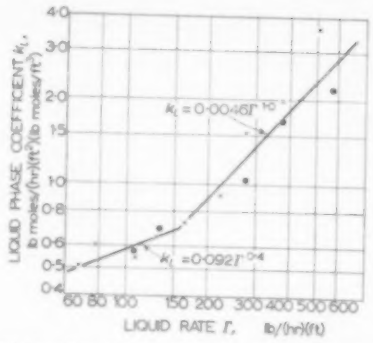

FIG. 8. Absorption into water and tetrathionate solution. Effect of liquid rate on liquid phase coefficient.
gas feed $7{\cdot}8 \times 10^{-3}$ v/v I_2
gas velocity 7·25 ft/sec
× = water
● = 3·5 gm/l. sodium tetrathionate
20°C

This increase in the gas-phase coefficient may arise from the higher density of the sodium sulphate solution. The rippling [14] of a liquid of high density may well create greater turbulence in the gas phase and higher transfer rates. Elevated values of k_G were not obtained with concentrated sodium hydroxide solution of density 1·3

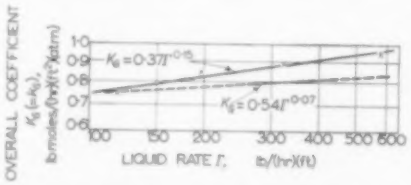

FIG. 9. Absorption into solution of 3·23 g/l. sodium hydroxide plus 230 g/l. sodium sulphate.
Overall coefficient vs. liquid rate
gas velocity 7·25 ft/sec
temperature 27°C
all values corrected to relative velocity 8·4 ft/sec
Broken line derived from combined data for thiosulphate, NaOH, and NaI at 20°C corrected to 27°C by factor 1·07.

but here the very high viscosity (7·5 cp.) may have an overriding effect.

In view of these results it was thought desirable to examine absorption into solutions containing sodium sulphate alone. For this series of runs at 20°C, an unsaturated solution of sodium sulphate was used, containing 182 g/l. Equilibrium data were taken from Fig. 1 and k_G values from the sulphate–hydroxide runs. Results of these are included in the final correlation of Fig. 12. In terms of a plot of k_L versus Γ, the coefficients are much less than those for absorption into pure water, the ratio being about 2·7. Thus, whereas the addition of high concentrations of sodium sulphate to dilute sodium hydroxide increases the overall coefficient to a small but significant extent, in the case of water alone the sulphate addition causes a very marked decrease in this coefficient.

III. Correlation of Experimental Results

(*a*) *Gas-phase coefficients*

Absorption into solvents of the first group (Nos. 1 to 9 in Fig. 3) gives over-all coefficients equal to the gas phase coefficient k_G. Dependence of these coefficients upon relative velocity and liquid rate therefore shows the same general features as the ammonia/water calibration curves. With suitable allowance for the physical properties of the two gases, an exact correlation between the k_G values for ammonia and iodine might be expected. The general relationship (equation 2) indicates that, for dilute gases in air at one temperature, the only factor of difference between the two systems is the molecular diffusivity of the solute gas in air. Thus a plot of $k_G/D_M^{0.5}$ versus flow rate for the two systems should be coincident.

This type of plot is shown in Fig. 10, where, to simplify the presentation, k_G for iodine has been given directly and the ammonia results adjusted by the required factor $(D_I/D_A)^{0.5}$. Corrections for variations in temperature and liquid rate have been made according to the correlations given above. Agreement between the iodine data and the calibration curve is precise enough to use the latter as the basis of a general correlation. Under the conditions studied:

$$k_G = \gamma . v^m \left(\frac{l}{20}\right)^{0.18} \left(\frac{\Gamma}{27{\cdot}4}\right)^{0.07} \text{lb moles/(hr)(ft}^2\text{)(atm)}$$

where for $v < 3{\cdot}6$; $\gamma = 0{\cdot}23$ and $m = 0{\cdot}45$

and for $v > 3{\cdot}6$; $\gamma = 0{\cdot}18$ and $m = 0{\cdot}67$

A similar over-all correlation of results showing the dependence of k_G upon liquid rate is given in Fig. 11. Variations in relative velocity are allowed for by use of the relationship $k_G \propto v^{0.67}$, and in order to use this simple form the few results at $v < 3{\cdot}6$ ft/sec have not been included. The data are correlated by the relationship:

$$k_G = 0{\cdot}49\ \Gamma^{0.07} \left(\frac{l}{20}\right)^{0.18} \left(\frac{v}{8{\cdot}4}\right)^{0.67} \text{lb moles/(hr)(ft}^2\text{)(atm)}$$

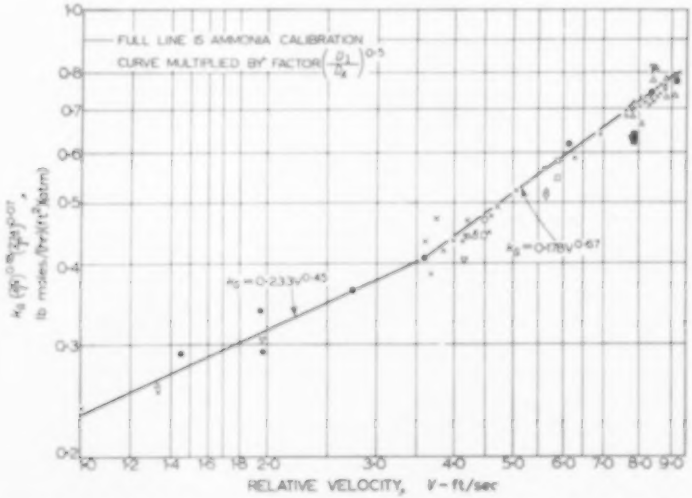

Fig. 10. General correlation of experiments on effect of relative velocity on gas-phase coefficient.

VOL. 10 1959

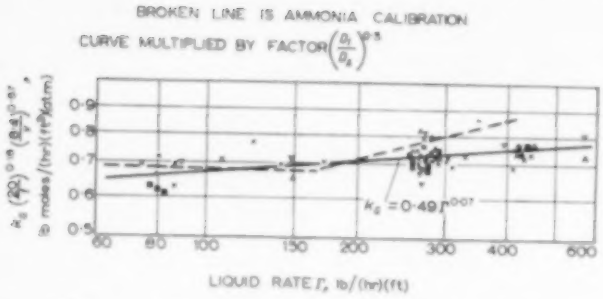

FIG. 11. General correlation showing influence of liquid rate on gas-phase coefficient.

Key to Fig. 11.

System	*Temp.* C	*Flow*	*Symbol*
Thiosulphate all concentrations	20	counter	×
	32	counter	⊗
	50	counter	⊠
	20	co-	●
NaOH all concentrations	20	counter	△
	20	co-	▲
NaI all concentrations	20	counter	▽
	20	co-	▼

This curve diverges from the ammonia calibration plot at the higher liquid rates—in this particular case the iodine curve is probably the better established.

For $v > 3{\cdot}6$ ft/sec the iodine results at 20°C and the ammonia calibration data may both be correlated in terms of the general dimensionless expression of equation (2), where, using the mean of the results for both systems, the value of the constant may be taken as:

$$\beta = 0{\cdot}102\ \Gamma^{0{\cdot}09}$$

(*b*) *Liquid-phase coefficients*

Plots of k_L data should fall on the corresponding calibration curve if the necessary adjustment for physical properties is made. For the dilute absorbents the adjustment is a simple one analogous to that used for the k_G correlation.

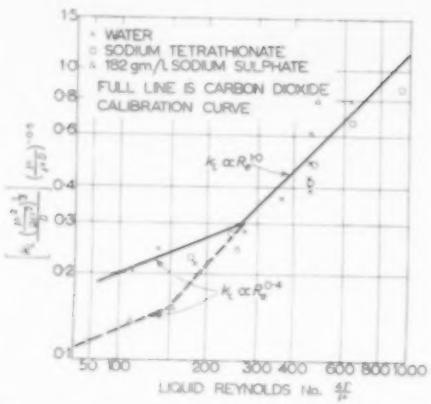

FIG. 12. General correlation of liquid phase coefficients for iodine systems with carbon dioxide calibration curves.

Inspection of equation (1) shows that for such solutions at one temperature the values of k_L for the physical absorption of iodine and carbon dioxide should differ by the factor $(D_I/D_C)^{0{\cdot}5}$, where D represents the diffusivity of the solute in water (MILLER's value being taken for iodine). This type of plot is effectively represented in Fig. 12.

The correlation used is based on the dimensionless relationship of VAN KREVELEN and HOFTIJZER [7], which corresponds to a generalized form of equation (1) modified by the inclusion of a length term.

$$k_L \left(\frac{\mu^2}{g\rho^2}\right)^{1/3} = C \left(\frac{4\Gamma}{\mu}\right)^n \left(\frac{\mu}{\rho D_M}\right)^{0{\cdot}5} \qquad (4)$$

This term represents the thickness of a falling film in laminar flow, and is included here to allow for the differences in flow behaviour between the water-like liquids and the concentrated Na_2SO_4 solution.

Correlation of the water and tetrathionate data with the calibration curve (full line) is reasonable, allowing for the multiplication of experimental errors in deriving k_L data from overall coefficients. As the falling film thickness does not differ between these systems equation (1) is obeyed, the break-point being at *Re* 260.

Correlation of the sodium sulphate results is less straightforward; the data appear to lie on a

related curve, dependent again on $Re^{0.4}$ at low flow rates and $Re^{1.0}$ at higher ones, but displaced towards the "origin," finally joining the upper part of the calibration curve.

If the water, tetrathionate and pure sodium sulphate results are plotted in terms of k_L versus Γ, two independent curves are obtained. The water and tetrathionate data fall on a curve having slopes of 0·4 and 1·0, with a break point at $\Gamma = 155$; the sulphate curve appears to have a break at the same value of Γ and to be parallel to the first curve. Values of k_L for sulphate are considerably less than for pure water, the ratio being about 2·7.

(*c*) *Overall coefficients*

Calculation of over-all coefficients is straightforward for most of the absorbents used here, for thin-film type of absorbers when the gas and liquid-phase characteristics are known. For absorbents Nos. 1 to 9 the over-all and gas-phase coefficients are identical and may be derived from k_G data for other dilute gases in air by means of factors similar to the one used in Figs. 10 and 11. For water, pure or containing low concentrations of inert electrolyte, the liquid-phase coefficient may be calculated directly from the equipment phase-characteristics and compounded with k_G by use of equation (3) to give the over-all coefficient. With a high viscosity liquor in a system exhibiting some liquid-phase control (as in the pure sodium sulphate runs) an empirical factor may be necessary in estimating k_L at the lower liquid rates.

(*d*) *Disc-column absorber*

The general correlations of k_G for iodine absorption given here can be regarded as a substantial confirmation of the gas-phase characteristics of the column as determined previously [14, 15]. On liquid-phase coefficients the data obtained are not extensive and the iodine system is not conducive to precise results. However, for dilute aqueous solutions the dependence of k_L upon $Re^{0.4}$ and $Re^{1.0}$, with a break-point at $Re = 260$, as found in the calibration work, has been confirmed. There is some difficulty in correlating results satisfactorily when absorption into liquids of high viscosity is included. This arises from the influence of liquid properties upon the inception of rippling [14] and therefore upon the break-point in the k_L versus flow rate curve. To elucidate this type of behaviour fully would require much work and it might be preferable to modify the column so as to move the break point outside the flow rates of practical interest [30].

IV. Applications to Process Design

With regard to the absorption rate of iodine, absorbents containing alkali thiosulphate, hydroxide, or an appreciable concentration of iodide are equally efficient. Reaction with thiosulphate is extremely rapid and the absorbed iodine exists entirely in the state of iodide ion, but the solutions tend to precipitate sulphur on standing. In sodium hydroxide solutions the iodine is not all in one form though it should be quantitatively liberated on acidification. Under the conditions used the gas- and liquid-phase coefficients were of the same order for absorption into pure water. Therefore, if any substance is added to the water giving an irreversible reaction with iodine, of reasonable rate and with non-volatile products, a tendency to gas-phase control will result.

The vapour pressure of iodine in solutions containing excess alkali iodide is rather low but in most absorption applications the back pressure is required to be zero, and the formation of poly-iodide ions avoided, though there are important exceptions [9]. For other solvents in which the solubility of iodine is very much greater than in water, for example many organic liquids, the absorption rate would be expected to be gas-phase controlled.

Decrease of iodine vapour concentration will tend to further gas-phase control and will therefore not influence those systems already solely controlled by that phase. In applications where much higher concentrations of iodine arise in the gas, there is the possibility, with any of the absorbents, of the liquid-phase resistance becoming significant. At 100°C the solubility of iodine in air is about one hundred times the highest concentration used here. However, the present work shows that the liquid-phase resistance is negligible even when increased several-fold by the addition of high concentrations of electrolyte. It therefore appears that, for the absorption of iodine from saturated air at 100°C into a fast reactant of requisite concentration, the gas-phase resistance will probably be significant and perhaps still controlling.

Although the vapour pressure of iodine over its pure aqueous solutions is considerable, water can still be a valuable absorbent in some circumstances [1]. The apparent interaction between iodine and concentrated sodium sulphate solution could be of some relevance to the operation of desorbing low concentrations of iodine from electrolyte solutions [3, 4].

Notation

d = diameter of gas channel, ft
D_A = molecular diffusivity of ammonia in air, ft²/hr
D_C = molecular diffusivity of carbon dioxide in water, ft²/hr
D_I = molecular diffusivity of iodine in air, or in water, according to context, ft²/hr
D_M = molecular diffusivity, ft²/hr
H = solubility coefficient, lb/(ft³) (atm)
k_G = gas-phase absorption coefficient, lb moles/(hr) (ft²) (atm)
k_L = liquid-phase absorption coefficient, lb moles/(hr) (ft²) (lb mole/ft³) = ft/hr
K_G = over-all mass-transfer coefficient, on gas-phase concentration basis, lb/moles/(hr) (ft²) (atm)
m, n = empirical constants
M_m = mean molecular weight of gas mixture
p = partial pressure, atmospheres
P_{BM} = logarithmic mean partial pressure of inert component in gas phase, atmospheres
Re = Reynolds number, $(4\ \Gamma/\mu)$, dimensionless
Sc = Schmidt number, $(\mu/\rho\ D_M)$, dimensionless
t = temperature, °C
v = relative velocity, ft/sec
$v/_0$ = volume percentage
α, β, γ = coefficients
Γ = liquid wetting rate, lb/(hr) (ft of wetted perimeter)
μ = molecular dynamic viscosity, lb/(hr) (ft)
ρ = density, lb/ft³

References

[1] Rupp A. F. *Progress in Nuclear Energy* Series 3 Vol. I. Process Chemistry. Pergamon Press, London 1956.
[2] Arrol W. J. and Chadwick J. *Progress in Nuclear Energy* Series 3, Vol. I. Process Chemistry. Pergamon Press, London 1956.
[3] Porter W. H. L. *A.E.R.E.* M/M. 121 1956.
[4] Bruce F. R. *Chem. Engng. Progr.* 1956 **52**, 347.
[5] Silverman L. *Int. Conf. Peaceful Uses At. Energy* Paper 571 1955. UNO 1956.
[6] Progress Reports. Nos. 2037 and 2222. Oak Ridge National Laboratory.
[7] Van Krevelen D. W. and Hoftojzer P. J. *Rec. Trav. Chim. Pays-Bas* 1947 **66** 49.
[8] *Isotope Specification* No. 1. Radio-Chemical Centre U.K. AEA. Amersham 1955.
[9] Sawyer F. G., Ohman F. G. and Lush F. E. *Industr. Engng. Chem.* 1949 **41** 1547.
[10] Jones C. W. and Grebe J. G. U.S. Pat. Spec. 1853621. 1932.
[11] Hoftojzer P. J. and Van Krevelen D. W. *Trans. Inst. Chem. Engrs.* 1954 S32 60.
[12] Vener R. E. *Chem. Engng.* 1956 **63** 175.
[13] Morris G. A. and Jackson J. *Absorption Towers.* Butterworth, London 1953.
[14] Taylor R. F. and Roberts F. *Chem. Engng. Sci.* 1956 **5** 168.
[15] Stephens E. J. and Morris G. A. *Chem. Engng. Progr.* 1951 **47** 232.
[16] Coryell C. D. and Sugarman N. *Nat. Nucl. Energy Series*, Series 4, **9**, Book I p. 210.
[17] Kirk R. E. and Othmer D. *Encyclopaedia of Chemical Technology* 7 942. Van Nostrand, New York 1956 ; Gerry J. D. and Gillespie L. J. *Phys. Rev.* 1932 **40** 269.
[18] Perry J. H. *Chemical Engineers' Handbook* (3rd Ed.) p. 371. McGraw-Hill, New York 1950.
[19] Topley B. and Whytlaw-Gray R. *Phil. Mag.* 1927 **4** 873.
[20] Mullaly J. M. and Jaques H. *Phil. Mag.* 1924 **48** 1105.
[21] Carter J. S. *J. Chem. Soc.* 1928 Part II 2227.
[22] Euler H. *Wied Ann. Phys.* 1897 **63** 273.
[23] Miller C. C. *Proc. Roy. Soc.* 1924 **106** 724.
[24] Allen T. K. and Keefer R. M. *J. Amer. Chem. Soc.* 1955 **77** 2957.
[25] Katzin L. I. and Gebert E. *J. Amer. Chem. Soc.* 1955 **77** 5814 ; Jones G. and Kaplan B. B. *J. Amer. Chem. Soc.* 1928 **50** 1845.
[26] Morgan K. *J. Quart. Rev. Chem. Soc. Lond.* 1954 **8** 123.
[27] Awtrey A. D. and Connick R. E. *J. Amer. Chem. Soc.* 1951 **73** 4546.
[28] Haslam R. T., Ryan N. and Webster F. *Trans. Amer. Inst. Chem. Engrs.* 1923 **15** 177.
[29] Awtrey A. D. and Connick R. E. *J. Amer. Soc.* 1951 **73** 1341.
[30] Taylor R. F. M.Sc. Dissertation, University of London 1957.
[31] Taylor R. F. M.Sc. Thesis, University of London 1957.

Chemical Engineering Science, 1959, Vol. 10, pp. 80 to 87. Pergamon Press Ltd. London. Printed in Great Britain

Diffusion and reaction in flow systems of Turner's structures

R. Aris
The Mathematical Institute, University of Edinburgh*

(*Received* 20 *August* 1958)

Abstract—It is shown here how Turner's analysis of flow structure may be extended to a generalized model in which the dead-water pocket length is continuously distributed. A solution of the integral equation is given in the form of a definite integral of which the integrand may be constructed graphically. The Péclet number for the two models is then calculated. In Model 1 its reciprocal is the sum of one term due to the diffusion in the pockets and another to diffusion in the lowing channels. In Model 2 the two terms are due to diffusion in the lowing channels and to the mixing of streams of different flow rate. Finally simultaneous diffusion and first-order reaction are considered in the two models and it is shown how the yield can be calculated.

Résumé—L'auteur a montré comment l'analyse de Turner, de la structure d'un écoulement peut être étendue à un modèle généralisé dans lequel la longueur de la poche d'eau stagnante est répartie d'une façon uniforme. Une solution de l'intégrale est donnée sous forme d'une intégrale définie où l'intégrant peut être construit graphiquement. Le nombre de Péclet est ensuite calculé pour deux modèles. Dans le modèle I son inverse est la somme d'un terme dû à la diffusion dans les poches et d'un autre dû à la diffusion dans les canaux qui les suivent. Dans le modèle 2 les deux termes sont dus à la diffusion dans ces canaux et au mélange courants d'un débit différent. Finalement la diffusion simultanée et une réaction du Ier ordre sont considérées dans les 2 modèles et il est montré comment le rendement peut être calculé.

Zusammenfassung—Es wird gezeigt, wie man die Analyse eines Strömungbildes nach Turner auf ein verallgemeinertes Modell ausdehnen kann, in dem die Länge eines Totwasser-Bezirkes kontinuierlich verteilt ist. Eine Lösung der Integralgleichung wird in Form eines bestimmten Integrals angegeben, dessen Integrand graphisch dargestellt werden kann. Wieterhin wird die Pécletzhal der beiden Modelle berechnet. Im Modell 1 ist ihr reziproker Wert die Summe zweirer Ausdrücke, von denen der eine von der Diffusion im Totwasser-Bereich und der andere eine der Diffusion in den folgenden Kanälen herrührt. Im Modell 2 stammen die beiden Ausdrücke von der Diffusion in den folgenden Kanälen und von der Mischung der Stromlinien verschiedener Geschwindigkeit. Schliesslich wird das gleichzeitige Auftreten von Diffusion und einer Reaktion 1. Ordnung in den beiden Modellen betrachtet und es wird gezeigt, wie man die Ausbeute berechnen kann.

G. A. Turner [4] has recently shown how the frequency response technique may be used to analyse the flow structure in a packed bed in terms of simplified models. His Model 1 assumes that connected with each flow channel is a certain distribution of dead-water in which diffusion but no flow takes place. It is shown that the proportion of dead-water attributable to pockets of given length may be calculated from the frequency response. His Model 2 is a distribution of channels of different radii and length in which diffusion and flow take place and again the volume attributable to given radii and lengths may be found. The frequency response of any bed may be so analysed though the bed itself may appear very different in structure from either model. The analysis will be valuable to the extent to which the lengths and radii have been realistically chosen, and it may then be used for prediction of other properties of the system.

The purpose of this paper is threefold. Firstly, it is shown how the arbitrariness in the choice of the lengths of dead-water pockets in Model 1 may be removed, by generalizing this model slightly and solving the resulting integral equation. Secondly, the apparent diffusion coefficient of a

*Present address: Department of Chemical Engineering, Institute of Technology, University of Minnesota, Minneapolis 14, Minnesota, U.S.A.

bed with generalized TURNER flow structure is calculated. Thirdly, the problem of simultaneous diffusion and first-order reaction in these models is considered.

1. A GENERALIZATION OF TURNER'S MODEL 1

In his paper, TURNER considered that associated with unit length of the channel of cross-sectional area a there is a volume α_r of dead-water pocket of length l_r. If $\beta_r = \alpha_r/a$, β_r is clearly the volume of dead-water in pockets of length l_r $(r = 1, \ldots n)$ per unit volume of channel. We will suppose here that the relative volume attributable to pockets of length between l and $l + dl$ is $\beta(l)\,dl$. Then

$$\beta = \int_0^\infty \beta(l)\,dl \qquad (1)$$

is the ratio of the total dead-water volume to that of the channels.

The frequency response of this system may be analysed in exactly the same way as on pages 158–160 of TURNER'S paper save that the β_r occurring is replaced by $\beta(l)\,dl$ and summations with respect to r by integrations with respect to l. Then with the same notation as TURNER (which is given at the end of this paper) we have in place of his simultaneous equations (19) the integral equation

$$\mu(\omega') = \int_0^\infty \beta(l)\,\eta(l, \omega')\,dl \qquad (2)$$

where $\omega' = (\omega/2D)^{\frac{1}{2}}$,

$\omega' =$ angular frequency of sinusoidal input,

$D =$ diffusion coefficient in the pockets,

$\mu =$ a function determined from the phase-lag and amplitude decay,

$$\eta(l, \omega) = \frac{1}{2\omega' l}\,\frac{\sinh 2\omega' l - \sin 2\omega' l}{\cosh 2\omega' l + \cos \omega' l} \qquad (3)$$

One method of obtaining an approximate solution of this integral equation would indeed be to convert it to the simultaneous equations of TURNER'S paper. It happens however that his equation can be solved and β obtained from μ in the form of an integral. The derivation is somewhat mathematical but for practical purposes the solution may be reduced to the following formula.

$$l\,\beta(l) = \int_0^\infty \{M(v)\,\Sigma(v, l) - N(v)\,T(v, l)\}\,dv \qquad (4)$$

where

$$C(v) + i\,S(v) = \int_{-\infty}^{\infty} e^{2z}\,\mu(\tfrac{1}{2}e^z)\{\cos vz + i \sin vz\}\,dz \qquad (5)$$

$$\Sigma(v, l) + i\,T(v, l) = \{C(v) + i\,S(v)\}\{\cos(v \log \pi/l) + i \sin(v \log \pi/l)\} \qquad (6)$$

and

$$M(v) + i\,N(v) = \frac{\cosh \pi v/4}{\zeta(2 + iv)}\,\frac{3\cos(\tfrac{1}{2}v \log 2) - i\,5 \sin(\tfrac{1}{2}v \log 2)}{17 - 8\cos(v \log 2)} \qquad (7)$$

$\zeta(s) = \sum_{n=1}^{\infty} n^{-s}$ is RIEMANN'S zeta function.

The order in which these functions are listed is the order in which they must be obtained for only M and N are known beforehand; this sequence also lends itself to graphical evaluation. Firstly from the experimentally determined function μ the cosine and sine integrals in (5) may be calculated for a number of values of v. These can best be plotted as complex numbers in a diagram in which $C(v)$ and $S(v)$ are abscissa and ordinate: it will have the form shown in Fig. 1. In the same diagram a circle of unit radius about the origin is drawn and the second factor in (6) is a point on this circle subtending an angle $v \log \pi/l$: $\beta(l)$ being evaluated for given l so that this point can be found for any v. The point (Σ, T) may be found graphically as follows. If O is the origin, D the point (1, 0), $A(C(v), S(v))$ and $B(\cos \pi/v \log l, \sin v \log \pi/l)$, draw a line OE through O making the angle BOD with OA; draw a circle with centre O through A and to meet this line in the point E. E is (Σ, T) since in (6) the second factor has unit modulus and argument $v \log \pi/l$ and this construction has simply increased the argument of $C + iS$ by this amount. If the curve $M(v)$, $N(v)$ is also drawn in this plane the integrand can also be constructed

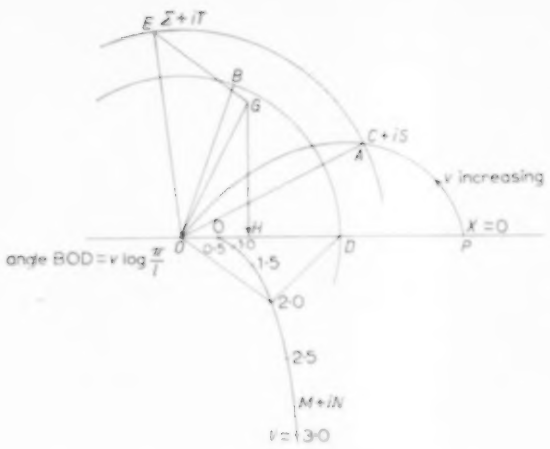

FIG. 1. Construction for the integrand in (4).

graphically. Let F be the point of this curve with the same value of v. Join FD. Draw OG so that GOE = FOD and EG so that GEO = FDO. Drop the perpendicular GH from G on to the real axis then OH is the value of the integrand in (4).

2. DIFFUSION IN TURNER'S MODELS

In this section we calculate the Péclet number for packed beds of TURNER's models. This is defined as $Pe = UL/D^*$ where U = mean velocity of flow, L = length of bed, D^* is the apparent diffusion coefficient. This apparent diffusion coefficient will be calculated by the following theoretical experiment. An infinitesimally short burst of tracer is fed into the bed and the resulting concentration-time curve at the exit is calculated. It is well-known, see for example [2] or [3], that the mean of residence time is L/U and the variance of residence times $2D^* L/U^3$. Thus if $c(L, t)$ is the concentration at the outlet and $\int_0^\infty c(L, t)\, dt = 1$, then

$$\mu_1 = \int_0^\infty t\, c(L, t)\, dt = L/U = L/U,$$

$$\mu_2 = \int_0^\infty (t - L/U)^2\, c(L, t)\, dt = 2D^* L/U^3 \quad (8)$$

and
$$Pe = 2\,\mu_1^2/\mu_2 \quad (9)$$

Moreover these quantities may be easily calculated from the Laplace transform

$\bar{c}(L, p) = \int_0^\infty e^{-pt} c(L, t)\, dt$, as is shown in [2].

Model 1

The concentration $c(z, t)$ at a distance z from the inlet and at time t is governed by the following equations. For diffusion and flow in the main channel we have

$$D \frac{\partial^2 c}{\partial z^2} - U \frac{\partial c}{\partial z} = \frac{\partial c}{\partial t} + \beta \frac{\partial q}{\partial t} \quad (10)$$

where q = average concentration in the pockets. For the pocket of length l we have the equation for $\gamma_l(y, t)$, the concentration at a distance y from the mouth

$$D \frac{\partial^2 \gamma_l}{\partial y^2} = \frac{\partial \gamma_l}{\partial t} \quad (11)$$

$$\frac{\partial \gamma_l}{\partial y} = 0 \text{ at } y = l,\ \gamma_l = c \text{ at } y = 0 \quad (12)$$

At zero time there is no tracer in the system so

$$c(z, 0) = \gamma_l(y, 0) = 0 \quad (13)$$

and for the bed as a whole we have the inlet conditions

$$-\frac{D}{U}\frac{\partial c}{\partial z} + c = \delta(t) \text{ at } z = 0 \quad (14)$$

$$\frac{\partial c}{\partial z} = 0 \text{ at } z = L \quad (15)$$

Taking the Laplace transformation of these equations and denoting this by a bar, i.e. $\bar{c}(z, p) = \int_0^\infty e^{-pt} c(z, t)\, dt$, we have for $\bar{\gamma}_l$

$$\frac{d^2\bar{\gamma}_l}{dy^2} = \frac{p}{D}\bar{\gamma}_l$$

$$\frac{d\bar{\gamma}_l}{dy} = 0 \text{ at } y = l,\ \bar{\gamma}_l = \bar{c} \text{ at } y = 0$$

whence $\bar{\gamma}_l = \bar{c} \cosh \sqrt{\frac{p}{D}}(l - y)/\cosh \sqrt{\frac{p}{D}}\, l$ (16)

The average value of $\bar{\gamma}_l$ over the whole pore is thus

$$\bar{c} \tanh \varpi / \varpi \text{ where } \varpi = l\sqrt{p/D}$$

and since a volume $\beta(l)\,dl$ is of pockets of this length the mean concentration in the pockets is

$$\beta \bar{q} = \bar{c} \int_0^\infty \beta(l) \frac{\tanh \varpi}{\varpi} dl = \bar{c}\, \Omega(p) \qquad (17)$$

Substituting this in equation (10) gives

$$D \frac{d^2\bar{c}}{dz^2} - U \frac{d\bar{c}}{dz} - p\bar{c}\{1 + \Omega(p)\} = 0 \qquad (18)$$

The main features of this equation will best be seen if we consider first the case of a very long bed, for as $L \to \infty$ the transformed conditions (14) and (15) may be taken to be

$$\bar{c}(0, p) = 1,\ \bar{c}(z, p) \to 0 \text{ as } z \to \infty \qquad (19)$$

With these conditions the solution of (18) is

$$\bar{c}(L, p) = \exp \frac{UL}{2D}\left[1 - \left\{1 + \frac{4D}{U^2} p(1 + \Omega)\right\}^{\frac{1}{2}}\right] \qquad (20)$$

It is shown in [2] that this equation yields the required moments immediately by expansion of the exponent as a function of p. In fact

$$-\mu_1 p + \tfrac{1}{2}\mu_2 p^2 - \cdots =$$

$$\frac{UL}{2D}\left[1 - \left\{1 + \frac{4D}{U^2} p\,[1 + \Omega(p)]\right\}^{\frac{1}{2}}\right] \qquad (21)$$

$$= -\frac{L}{U}(1 + \beta) p + \tfrac{1}{2} p^2$$

$$\left[\frac{2DL}{U^3}(1 + \beta)^2 + \frac{2U}{3DL}\int_0^\infty \beta(l)\, l^2\, dl\right] - \cdots$$

Whence

$$Pe = (1 + \beta)^2 \left\{\frac{D}{UL}(1 + \beta^2) + \frac{U}{3DL}\int_0^\infty \beta(l) l^2 dl\right\}^{-1} \qquad (22)$$

$$\text{or} \quad \frac{1}{Pe} = \frac{D}{UL} + \frac{U}{3DL(1 + \beta)^2}\int_0^\infty \beta(l)\, l^2\, dl \qquad (23)$$

This shows that it is the mean square length of pocket which alone affects the overall diffusion in the bed.

We also have from (21) that the mean time of residence is $(L/U)(1 + \beta)$ so that a measurement of the mean and variance of the exit concentration will give β and the mean square length of pocket. Naturally from two measurements only two quantities can be calculated, so that this method of analysis is not as complete as the frequency response. This analysis can be made very rapidly and accurately however and yields two quantities of interest. The solution of the equations under the conditions (14) and (15) yields the following result. Again $\mu_1 = L(1 + \beta)/U$ but writing $\overline{Pe}$ for UL/D the formula (23) for the Péclet number must be corrected slightly

$$Pe^{-1} = \overline{Pe}^{-1} + \frac{U}{3DL(1 + \beta)^2}\int_0^\infty \beta\, l^2\, dl - \overline{Pe}^{-2}(1 - e^{-\overline{Pe}}) \qquad (24)$$

This correction term is never greater than $\frac{1}{2}$, and it tends to zero more rapidly than the main terms as $L \to \infty$.

Model 2

This model will also be generalized slightly. Let the parallel channels be of different shapes denoted by a suffix s ($s = 1, 2, \ldots s$) and of the s^{th} shape let there be $n_s(l, r)\,dl\,dr$ channels whose lengths are between l and $l + dl$ and whose areas are between πr^2 and $\pi(r + dr)^2$; r is thus the radius of the circle with the same area. If P is the pressure difference between the two ends of any one channel the mean velocity of Poiseuille flow is

$$U = U_s(r, l) = \frac{r^2}{l\,\xi_s}\frac{P}{\mu} \qquad (25)$$

where μ is the mean viscosity and ξ_s a shape factor defined below. The longitudinal diffusion coefficient in the channel will be taken to be the Taylor diffusion coefficient

$$D = \kappa_s \frac{U^2 r^2}{D} = \left(\frac{P^2}{D\mu^2}\right)\frac{\kappa_s}{\xi_s^2}\frac{r^6}{l^2} \qquad (26)$$

where D is the molecular diffusion coefficient;

the additional term D established in [1] is usually negligible, though it might be included at the expense of a little extra labour.

The shape factors ξ_s and κ_s may be calculated as follows. Let A denote the area of the cross-section of the channel of shape s and C be its boundary. If x and y (temporarily) denote the co-ordinates in the domain B of the cross-section rendered dimensionless by dividing by $r = \sqrt{A/\pi}$ then $u(x, y)$ satisfies the equation $u_{xx} + u_{yy} = -r^2 P/l\mu$ in B and $u = 0$ on C. (P/l is the pressure gradient). Thus if ψ satisfies the equations $\nabla^2\psi = -1$ in B, $\psi = 0$ on C then $u(x, y) = (r^2 p/l\mu)\psi(x, y)$. Hence by averaging u we have $\xi_s^{-1} = A^{-1}\int\int_B \psi\, dA = A^{-1}\int\int_B (\nabla\psi)^2\, dA$ by Gauss' theorem. For κ it is shown in [1] that if ϕ satisfies the equation $\nabla^2\phi = \xi_s$ in B $\nabla^2\phi = 1$, $\partial\phi/\partial\nu = 0$ on C then $\kappa_s = A^{-1}\int\int_B \phi\, dA = A^{-1}\int\int_B (\nabla\phi)^2\, dA$. These are constants depending only on the geometry of the cross-section: for the circle $\xi = 8$, $\kappa = 1/48$.

The volume of all channels of length l, radius r and shape s is $n_s(l, r)\,\pi r^2 l\, dr dl$ so that the fraction these contribute to the voidage of the bed is

$$\epsilon_s(r, l)\, dr\, dl = \frac{\pi}{H} n_s(r, l)\, r^2 l\, dr\, dl \tag{27}$$

where H denotes the total volume of the packed bed. The total voidage

$$\epsilon = \frac{\pi}{H}\sum_{s=1}^{s}\int_0^\infty dr\int_0^\infty dl\, n_s(r, l)\, r^2 l \tag{28}$$

The volume rate of flow through channels of this species is

$$\begin{aligned} V_s(r, l)\, dr\, dl &= n_s(r, l)\, dr\, dl\, \pi r^2 U_s(r, l) \\ &= \frac{\pi P}{\mu}\frac{1}{\xi_s}\frac{r^4}{l} n_s(r, l)\, dr\, dl \\ &= \frac{HP}{\mu}\frac{1}{\xi_s}\frac{r^2}{l^2}\epsilon_s(r, l)\, dr\, dl \end{aligned} \tag{29}$$

so that the total volume flowing is

$$\begin{aligned} V &= \frac{\pi P}{\mu}\sum_{s=1}^{s}\frac{1}{\xi_s}\int_0^\infty dr\int_0^\infty dl\,\frac{r^4}{l} n_s(r, l) \\ &= \frac{HP}{\mu}\sum_{s=1}^{s}\frac{1}{\xi_s}\int_0^\infty dr\int_0^\infty dl\,\frac{r^2}{l^2}\epsilon_s(r, l) \end{aligned} \tag{30}$$

For channels of the single species (s, r, l) we have to solve the following equations for the

$$D\frac{\partial^2 c}{\partial z^2} - U\frac{\partial c}{\partial z} = \frac{\partial c}{\partial t}, \quad 0 \leqslant z \leqslant l \tag{31}$$

$$\left.\begin{aligned} -D\frac{\partial c}{\partial z} + Uc &= U\,\delta(t), \quad z = 0 \\ \frac{\partial c}{\partial z} &= 0, \quad z = l \\ c &= 0, \quad t = 0 \end{aligned}\right\} \tag{32}$$

Solving these by the Laplace transform and expanding this as far as p^2 we have

$$\bar{c}(l, p) = 1 - \frac{l}{U}p + \tfrac{1}{2}p^2\left\{\frac{l^2}{U^2} + 2\frac{Dl}{U^3} - 2\frac{D^2}{U^4}(1 - e^{-Ul/D})\right\} + \cdots \tag{33}$$

If the simpler boundary conditions for a very long channel (19) are taken then the third term in the coefficient of p^2 may be neglected; this we will do for the moment and include it later.

Equation (33) applies only to the channel of one species. The total concentration is the weighted mean of such expressions the weight being the relative volume flowing in the channel. Thus writing μ_1 for the mean residence time in the whole bed and recalling that for any species

$$\frac{l}{U} = \frac{\mu}{P}\frac{l^2}{r^2}\xi_s$$

$$\begin{aligned} \mu_1 &= \sum_{s=1}^{s}\int_0^\infty dl\int_0^\infty dr\,\frac{\mu}{P}\frac{l^2}{r^2}\xi_s\frac{V_s(r, l)}{V} \\ &= \frac{H}{U}\sum_s\int\int \epsilon_s(r, l)\, dr\, dl = \frac{H\epsilon}{V} \end{aligned} \tag{34}$$

This confirms the expected result that the mean residence time is the ratio of the free volume of the bed to the flow rate.

VOL. 10 1959

The coefficient of $\frac{1}{2}p^2$ in the expansion of c the mean concentration is $\mu_2 + {\mu_1}^2$ where μ_2 is the variance, thus

$$\mu_2 + {\mu_1}^2 = \sum_{s=1}^{s} \int_0^\infty dl \int_0^\infty dr \left\{ \left(\frac{\mu}{P}\right)^2 \frac{l^4}{r^4} \xi_s^2 + \frac{2\mu}{DP} l^2 \kappa_s \xi_s \right\} \frac{HP}{V\mu} \frac{1}{\xi_s} \frac{r^2}{l^2} \epsilon_s(r, l)$$

$$= \frac{H\mu}{VP} \sum_{s=1}^{s} \xi_s \int_0^\infty dl \int_0^\infty dr \frac{l^2}{r^2} \epsilon_s(r, l) + \frac{2H}{DV} \sum_{s=1}^{s} \kappa_s \int_0^\infty r^2 \epsilon_s(r)\, dr$$

where $\epsilon_s(r) = \int_0^\infty \epsilon_s(r, l)\, dl$. Hence

$$\mu_2 = \frac{H^2}{V^2}(\epsilon_1 \epsilon_{-1} - \epsilon^2) + \frac{2H}{DV} \sum_{s=1}^{s} \kappa_s \varpi_s \qquad (35)$$

where $\epsilon_1 = \sum_1^s \xi_s \int_0^\infty dl \int_0^\infty dr \frac{l^2}{r^2} \epsilon_s(r, l)$,

$$\epsilon_{-1} = \sum_1^s (\xi_s)^{-1} \int_0^\infty dl \int_0^\infty dr \left(\frac{l^2}{r^2}\right)^{-1} \epsilon_s(r, l) \qquad (36)$$

and

$$\varpi_s = \int_0^\infty r^2 \epsilon_s(r)\, dr \qquad (37)$$

is proportional to the mean area of all channels of shape s.

Thus

$$\frac{1}{Pe} = \frac{\mu_2}{2{\mu_1}^2} = \frac{1}{2}\left\{\frac{\epsilon_1 \epsilon_{-1}}{\epsilon^2} - 1\right\} + \frac{V}{DH\epsilon^2} \sum_{s=1}^{s} \kappa_s \varpi_s \qquad (38)$$

The first term in this expression is due to the mixing of streams having different residence times, it will be small when the range of l and r is small. In fact it is zero as we should expect if there is only one size, shape and length of channel. In the second term we may replace $V/H\epsilon$ by $\bar{U}/L$ where $\bar{U}$ is the mean linear velocity of the stream calculated on the free area of the bed and L is the total length of bed. Thus this term takes the form $(\bar{U}/DL) \Sigma \kappa_s R_s^2$ where $R^2_s = \int_0^\infty r^2 \epsilon_s(r)\, dr/\epsilon$ is the mean square radius of the s^{th} shaped channels weighted according to their contribution to the free volume.

Two remarks may be made here. Firstly if there is a sensible proportion of tubes which are quite short the third term in (33) becomes significant. When this term is included the right-hand side of (38) must be diminished by

$$\frac{VP}{D^2 H \mu \epsilon^2} \sum_{s=1}^{s} \frac{\kappa_s^2}{\xi_s} \int_0^\infty dr \int_0^\infty dl \frac{r^6}{l^2} \left\{1 - \exp\left(-\frac{\mu D}{P} \frac{\xi_s}{\kappa_s} \frac{l^2}{r^4}\right)\right\} \qquad (39)$$

Secondly, we observe that Turner's model 2 is obtained from this simply by disregarding shape and setting

$$\epsilon(r, l) = \Sigma_q \Sigma_r \epsilon_{qr}\, \delta(r - R_q)\, \delta(l - l_r)$$

the double integrals then become double sums throughout. In this connection we observe that Turner's equation (29) fixes the constant κ as that for circular tubes; to be consistent this would also fix his constant ξ as 8 according to the Poiseuille Law for circular tubes.

Lastly we may mention that, were there any incentive to do so, it would be possible to combine both models.

3. Diffusion and Reaction in the Steady State

The analysis of simultaneous diffusion and reaction, when steady state conditions have been established, follows so closely the solution of the transformed equations that it is possible to give it quite briefly. We suppose that the solute of concentration c is being destroyed by a first-order reaction at a rate kc. Thus the steady state equation of flow in a channel is

$$D\frac{d^2c}{dz^2} - U\frac{dc}{dz} - kc = 0$$

which is of exactly the same form as the transformed unsteady state equation with k playing the role of p.

Model 1.

Let $A = l\sqrt{k/D}$ then the concentration γ_l in a pocket of length l satisfies

$$D\frac{d^2\gamma_l}{dy^2} = k\gamma_l$$

with the same boundary conditions as before. Hence

$$\gamma_l = c\cosh\sqrt{\frac{k}{D}}(l-x)/\cosh A$$

and since the area of opening of pockets of length l is $\beta(l)\,dl/l$ per unit volume of channel, the total rate at which the reactant is destroyed in the pockets is

$$-\int_0^\infty D\left(\frac{d\gamma_l}{dy}\right)_{y=0}\frac{\beta(l)}{l}\,dl = kc\int_0^\infty \beta(l)\frac{\tanh A}{A}\,dl$$

Setting $k^* = k\left\{1 + \int_0^\infty \beta(l)\tanh A\,dl/A\right\}$. (40)

the equation for reaction and flow in the channel is

$$D\frac{d^2c}{dz^2} - U\frac{dc}{dz} - k^*c = 0 \tag{41}$$

subject to the conditions

$$-D\frac{dc}{dz} + Uc = Uc_0, \quad z = 0 \tag{42}$$

$$\frac{dc}{dz} = 0, \quad z = L$$

Let $\lambda = k^*D/U^2$; and $Pe = UL/D$. Then equations (41) and (42) yield

$$\frac{c_L}{c_0} = \frac{(1+4\lambda)^{\frac{1}{2}}\exp\frac{1}{2}Pe}{(1+2\lambda)\sinh\frac{1}{2}Pe\,(1+4\lambda)^{\frac{1}{2}} + (1+4\lambda)^{\frac{1}{2}}\cosh\frac{1}{2}Pe\,(1+4\lambda)^{\frac{1}{2}}} \tag{43}$$

This function is shown in Fig. 2 where c_L/c_0 is plotted against Pe for various λ.

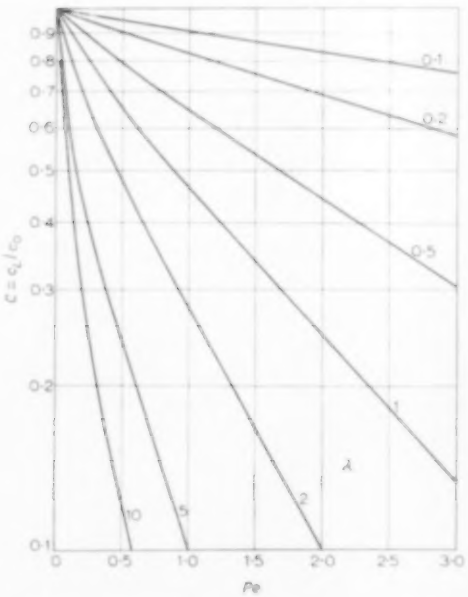

Fig. 2. Dependence of c_L/c_0 on Pe and λ.

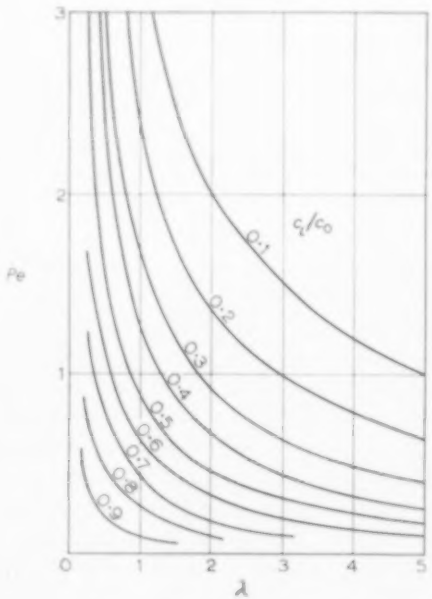

Fig. 3. Contours of c_L/c_0.

Model 2.

The problem for any one tube of length l, diffusion coefficient $\bar{D}_s$ and velocity U_s is solved by equation (43) if we put $\lambda = k\bar{D}_s/U_s^2 = (k/D)\,\kappa_s r^2$ and $Pe = U_s l/\bar{D}_s = (\mu D/P)\,\frac{\xi_s}{\kappa_s}\frac{l^2}{r^4}$. Let the result of substituting these values in (43) be a function $C_s(r, l)$, then since a volume $V_s(r, l)\,dr\,dl$ is contributed by such a tube the mean concentration at the far end is

$$\frac{c_L}{c_0} = \frac{1}{V}\sum_{s=1}^{s}\int_0^\infty dr \int_0^\infty dl\, C_s(r, l)\, V_s(r, l)$$

$$= \frac{HP}{V\mu}\sum_{1}^{s}\frac{1}{\xi_s}\int_0^\infty dr \int_0^\infty dl\,\frac{r^2}{l^2}\, C_s(r, l)\,\epsilon_s(r, l) \quad (44)$$

To assist in the evaluation of this integral (which in Turner's model would be a finite sum) Fig. 3 is given showing contours of C in the plane of the reaction number λ and the Péclet number Pe.

Notation

a = cross-sectional area of channel
c = concentration of solute
c_0 = inlet concentration
c_L = exit concentration
C = ratio c_L/c_0 for any channel
D = diffusion coefficient in pocket
$\bar{D}$ = diffusion coefficient in channel
D^* = apparent diffusion coefficient in bed
H = total bed volume
k = first-order reaction constant
k^* = modified reaction constant (40)
l = pocket length
l_r = length of r^{th} species of pocket
L = total length of bed
M, N = functions in (4)
$n_s(l, r)$ = number of channels of l, r, s species
p = Laplace transform variable
P = pressure drop across bed
$Pe = UL/D^*$
$\overline{Pe} = UL/\bar{D}$
r = equivalent channel radius $= (a/\pi)^{\frac{1}{2}}$
R_s = R.M.S. radius of s^{th} shape channel
s = suffix denoting shape of channel
S = number of shapes of channel
t = time
U = velocity in channel
$\bar{U}$ = mean velocity of stream
v = variable in (4)
V = volume flow rate through bed
$V_s(r, l)$ = volume flow rate through channel
y = length from mouth to pocket
z = length along channel
α_r = volume of pockets of length r
$\alpha_s = \epsilon R_s^2$
β = volume of deadwater/volume of channel
$\beta(l)$ = volume in pocket of length l
β_r = volume in pocket of l_r
γ_l = concentration in pocket of length l
δ = Dirac delta function
ϵ = voidage of bed
$\epsilon_s(r, l)$, $\epsilon_s(r)$ = voidage due to species of channel
ϵ_1, ϵ_{-1} = defined by (36)
ζ = Riemann's zeta function
η = function defined by (3)
κ_s = shape factor (26)
$\lambda = k^* D/U^2$
$\Lambda = l\sqrt{k/D}$
$\mu(\omega')$ = experimentally determined function
μ_1, μ_2 = mean and variance defined by (8)
μ = viscosity
$\partial/\partial\nu$ = differentiation along normal
ξ_s = shape factor in (25)
Σ, T = functions in (4)
ω = frequency of inlet concentration wave
$\omega' = (\omega/2D)^{\frac{1}{2}}$
$\varpi = l(p/D)^{\frac{1}{2}}$
$\Omega = \tanh \varpi/\varpi$

References

[1] Aris R. *Proc. Roy. Soc.* 1956 **A 235** 67

[2] Aris R. *Proc. Roy. Soc.* 1958 **A 245** 268.

[3] Titchmarsh E. C. *The Theory of Fourier Integrals.* Oxford, 1937.

[4] Turner G. A. *Chem. Engng. Sci.* 1958 **7** 156.

[5] van der Laan *Chem. Engng. Sci.* 1958 **7** 187.

[6] Jahnke E. and Emde F. *Funktiontafeln* (4th Ed.) New York, 1945.

Chemical Engineering Science, 1959, Vol. 10, pp. 88 to 104. Pergamon Press Ltd. London. Printed in Great Britain

Absorption of CO_2 in jets and falling films of electrolyte solutions, with and without chemical reaction

R. A. T. O. Nijsing, R. H. Hendriksz and H. Kramers
Laboratorium voor Fysische Technologie, Technische Hogeschool, Delft.

(*Received* 23 *August*; *in revised form* 19 *September* 1958)

Abstract—In this work the kinetics of the absorption of CO_2 by caustic solutions have been investigated. To this end, the rate of CO_2 absorption by a laminar jet and by laminar falling film was measured. In the first case, the contact times were very short which permitted to operate under conditions where the absorption can be interpreted as a diffusion of CO_2 into the liquid accompanied by a rapid pseudo first-order reaction. From these experiments the reaction velocity constant between CO_2 and OH^- ions could be derived for KOH, NaOH and LiOH solutions up to 2N at 20°C. In the experiments in the wetted wall column, the situation was approached where the absorption rate was determined by the diffusion of CO_2 and OH^- to a narrow reaction zône where a rapid second-order reaction between CO_2 and OH^- occurs. The results of these measurements agreed well with the theoretical prediction. For the correct interpretation of the measurements great care had to be taken with respect to the hydrodymanic conditions and to the values of the physical properties involved such as the "solubility" and diffusivity of CO_2 in reacting solutions and the diffusivity of OH^- ions in the liquids.

Résumé—On a étudié la cinétique d'absorption de CO_2 dans des solutions alcalines en mesurant la vitesse d'absorption de ce gaz dans un jet laminaire et dans un film tombant en régime laminaire. Dans le premier cas le temps de contact était très court, cequi permettait de réaliser des conditions, où l'absorption peut être interprétée comme diffusion de CO_2 dans le liquide accompagnée d'une réaction rapide et monomoleculaire en CO_2. On a pu obtenir de ces expériences la valeur de la constante de vitesse de la réaction entre CO_2 et OH^- pour des solutions de KOH, NaOH et LiOH ayant une concentration jusqu'à 2N à 20°C. Dans l'absorbeur à paroi mouillée de telles conditions étaient approchées que la vitesse d'absorption était déterminée par la vitesse de diffusion de CO_2 et de OH^- vers une zône étroite, où se produit une réaction rapide et bimoleculaire en CO_2 et OH^-. Les résultats de ces mesures se montraient en bon accord avec les prédictions théoriques. En particulier on s'est appliqué à obtenir les conditions hydrodynamiques correctes et à employer les valeurs justes des propriétés physiques, comme la "solubilité" et le coefficient de diffusion de CO_2 dans les solutions réagissantes et le coefficient de diffusion des ions OH^- dans ces liquides.

Zusammenfassung—In dieser Arbeit wird die Kinetik der CO_2-Absorption in alkalischen Lösungen untersucht. Hierzu wird die CO_2-Absorption durch einen laminaren Strahl und einen laminaren Rieselfilm gemessen. Im ersten Fall waren die Kontakzeiten sehr kurz, so dass man unter Bedingungen arbeitete, bei denen die Absorption als eine Diffusion von CO_2 in der Flüssigkeit unter Begleitung einer schnellen Pseudoreaktion erster Ordnung betrachtet werden kann. Aus diesen Versuchen konnte die Reaktionsgeschwindigkeitskonstante zwischen CO_2 und OH^--Ionen abgeleitet werden und zwar für KOH-, NaOH- und LiOH-Lösungen bis zu 2N bei 20°C. Bei den Versuchen in der Kolonne mit benetzter Wand werden Verhältnisse angenähert, unter denen die Absorptionsgeschwindigkeit durch die Diffusion von CO_2 und OH^--Ionen zu einer engen Reaktionszone bestimmt werden konnte, wo eine schnelle Reaktion zweiter Ordnung zwschen CO_2 und OH^- abläuft. Die Ergebnisse dieser Messungen stimmen gut mit der Vorausberechnung überein. Für die korrekte Interpretation der Messungen waren die hydrodynamischen Bedingungen und die Werte der physikalischen Einflussgrössen genau zu beachtent, nämlich die Löslichkeit und der Diffusionskoeffizient von CO_2 in den reagierenden Lösungen und der Diffusionskoeffizient der OH^--Ionen in den Flüssigkeiten.

1. Introduction

This paper is concerned with mass transfer phenomena in the liquid phase under conditions where unsteady diffusion and chemical reaction of the absorbed gas near the interface play an important part. In absorption experiments the influence of the gas phase resistance can be eliminated by the use of a pure gas; in that case the rate of absorption depends only on the conditions in the liquid phase.

Two sets of factors influencing the absorption rate of a pure gas into a liquid may be distinguished, those of physicochemical and those of hydrodynamical nature. Here, the physicochemical factors are emphasized so that the absorption experiments were performed under well defined hydrodynamic conditions with laminar falling films and laminar jets. In both cases a constant amount of fresh liquid surface is created of which each element remains in contact with the gas during the same time τ.

Under certain conditions, absorption measurements obtained with falling films and jets may be interpreted by means of the theory of unsteady state diffusion in a stagnant liquid. This "penetration" theory, as it is frequently called, has already been applied in 1877 by von Wroblewski [1] for the diffusion of a gas into a liquid. Its applications to moving liquid surfaces and its modifications as a result of chemical reaction in the liquid phase have more recently been discussed by many authors [2, 3, 4].

The present investigations are concerned with the absorption of CO_2 in inert and also in caustic solutions. The main points of the theory will be summarized in the next section.

2. Summary of Formulae used for Diffusion and Reaction in a Stagnant Liquid

Consider the transient absorption of a gas A into a semi-infinite stagnant liquid which may contain a chemical compound B reacting with A. This transient is assumed to result from a stepwise change in the concentration of A at the interface as may be brought about by suddenly contacting fresh liquid surface with a pure gas A of a given pressure provided the equilibrium at the interface is instantaneous.

For the case where the chemical reaction is irreversible with a rate proportional to the concentrations of both A and B, and under the additional assumptions:

neither B nor the reaction product are volatile,

the diffusivities of A and B are independent of concentration,

heat effects may be neglected,

the absorption process is described by the following equations:

$$\frac{\partial [A]}{\partial t} = D_A \frac{\partial^2 [A]}{\partial x^2} - k_r [A] [B] \qquad (1)$$

$$\frac{\partial [B]}{\partial t} = D_B \frac{\partial^2 [B]}{\partial x^2} - k_r [A] [B] \qquad (2)$$

The initial and boundary conditions are:

$$t = 0, x > 0, [A] = 0 \text{ and } [B] = [B]_0$$

$$x = 0, t > 0, [A] = [A^*] \text{ and } \partial [B] / \partial x = 0 \qquad (3)$$

$$x = \infty, t > 0, [A] = 0 \text{ and } [B] = [B]_0$$

A solution of (1, 2 and 3) yields the concentration distributions of A and B as a function of time. From this the rate of absorption can be calculated. Here, this rate will be expressed as the total amount of gas absorbed per unit area during the interval $0 < t < \tau$, $m(\tau)$. Since in $m(\tau)$ the amounts of gas are expressed in mass units, the formulae for $m(\tau)$ contain the equilibrium concentration of A at the interface, c^*, in mass per unit volume; c^* (and also $[A]^*$, in moles/volume) are to be considered as the "physical" solubility of A in the solution, whether or not reaction takes place.

For three particular cases relatively simple expressions for $m(\tau)$ can be obtained:

(*a*) Purely physical absorption; $[B] = 0$ and no reaction occurs:

$$m(\tau) = 2 c^* \sqrt{\frac{D_A \tau}{\pi}} \qquad (4)$$

(*b*) Pseudo first-order reaction; this is approached when the rate of diffusion of component B to the reaction zone is rapid compared with the rate at which it is removed by chemical reaction. In this case $[B] = [B]_0$ for all values of x and t. Danckwerts [5] has shown that then the following approximate relations hold:

$$m(\tau) \simeq c^* \left(\tau + \frac{1}{2k_r [B]_0}\right) \sqrt{D_A k_r [B]_0}, \quad (3)$$

provided $k_r [B]_0 \tau > 4$.

(*c*) Extremely rapid second-order reaction between A and B; both compounds diffuse towards a reaction plane where their concentrations are zero.
This case has been treated by Sherwood and Pigford [6] who showed that for $D_A = D_B$:

$$m(\tau) = 2 c^* \left(1 + \frac{[B]_0}{[A]^*}\right) \sqrt{\frac{D_A \tau}{\pi}} \quad (6)$$

For the more general case, where m molecules of A react with n molecules (or ions) of B, and D_A and D_B are not equal, it can be shown [10] that:

$$m(\tau) \simeq 2 c^* \left(\sqrt{\frac{D_A}{D_B}} + \frac{m [B]_0 \sqrt{D_B}}{n [A]^* \sqrt{D_A}}\right) \sqrt{\frac{D_A \tau}{\pi}} \quad (7)$$

This is an approximation of the more complicated exact solution; the approximation improves as the value of $m [B]_0 / n [A]^*$ is increased. For $m [B]_0 / n [A]^* = 2$ and $D_B / D_A = 2$ the value of $m(\tau)$ calculated from equation (7) is 2·7 per cent too small.

A general solution of equations (1, 2 and 3) can be presented in dimensionless form. It is convenient to use for the dimensionless amount of absorbed gas the ratio, V, of $m(\tau)$ for chemical absorption and $m(\tau)$ for physical absorption with the same values of c^*, D_A and τ. V can then be expressed as:

$$V = V\left(k_r [B]_0 \tau, \frac{[B]_0}{[A]^*}, \frac{D_B}{D_A}\right) \quad (8)$$

For the special cases discussed above we now have:

(*b*) For $[B]_0/[A]^* > 1$ combined with not too high values of $k_r [B]_0 \tau$ the depletion of B at the interface is still small and the case of absorption with pseudo first-order reaction is approached. Then:

$$V \simeq \tfrac{1}{2} \sqrt{\pi k_r [B]_0 \tau} \quad (5a)$$

Since the second term between brackets in (5) has been neglected here, equation (5a) is a good approximation only for $k_r [B]_0 \tau > 20$ or $V > 4$

(*c*) For small values of $[B]_0/[A]^*$ combined with $k_r [B]_0 \tau > 1$, the case of absorption with extremely fast chemical reaction is obtained, for which (4) and (7) give:

$$V \simeq \sqrt{\frac{D_A}{D_B}} + \frac{m [B]_0 \sqrt{D_B}}{n [A]^* \sqrt{D_A}} \quad (7a)$$

This is a good approximation for $m [B]_0 / n [A]^* > 2$ or $V > 3$ since D_A/D_B is of the order of unity.

Perry [7] and Pigford [8] have obtained numerical solutions for a number of intermediate cases and $D_A/D_B = 1$. Their results have not been given in terms of a ratio of $m(\tau)$ values but of the absorption rates after a contact time τ. However, from their results values of V can be derived; some of these have been presented in Fig. 1 which shows that no calculations were made by them for $k_r [B]_0 \tau > 6$.

In the work described in this paper the theory summarized above has been applied to the absorption of CO_2 by caustic solutions. One part deals with absorption in liquid jets of concentrated solutions under the following conditions:

$$60 < [B]_0/[A]^* < 1000 \text{ and } 3 < k_r [B]_0 \tau < 1000$$

Here, the formulae for pseudo first-order reactions [case (*b*)] can be applied, although still a correction may be necessary to account for a small depletion of reactant B near the interface.

The last part describes similar measurements with a falling film absorber under the conditions:

$$3 < [B]_0/[A]^* < 80 \text{ and } 50 < k_r [B]_0 \tau < 2500$$

VOL. 10 1959

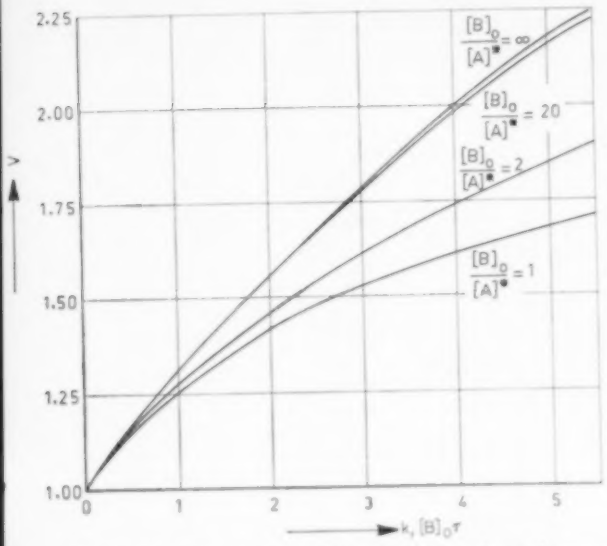

FIG. 1. The ratio Y as a function of $k_r[B]_0\,\tau$, for an irreversible second-order reaction.

Under these conditions the mechanism of absorption is intermediate between the cases (*b*) and (*c*).

Some work on the physical absorption of CO_2 in inert solutions will be presented first because it was used for testing the hydrodynamic conditions and for the determination of the diffusivity of CO_2 in electrolyte solutions.

3. Application of Theory to Absorption by Falling Films and Jets

Continuous absorption by moving liquid surfaces may be predicted if fresh surface is produced at a uniform rate $\dot{A}$ and disappears after a uniform life time τ. When there is no velocity gradient below the surface over a distance which is large with respect to the depth of penetration, the absorption rate to be expected is

$$\Phi_m = \dot{A}\, m\,(\tau) \tag{9}$$

It is known that for laminar falling films the above conditions can be satisfied [8]; for a film flowing down along the wall of a cylindrical tube over a height we have

$$\left.\begin{aligned} \dot{A} &= \pi\, d'\, v_s \\ \tau &= h/v_s \\ v_s &= \frac{3}{2}\left(\frac{g}{3\nu}\right)^{1/3}\left(\frac{L}{\pi d}\right)^{2/3} \end{aligned}\right\} \tag{10}$$

Equation (9) also may be applied to liquid jets with a uniform velocity v provided the penetration depth is sufficiently small with respect to the radius of curvature, r_0, of the jet surface. This condition amounts to $D\tau/r_0^2 \ll 1$. For a liquid jet with a flat velocity profile we then have

$$\left.\begin{aligned} \dot{A} &= 2\,\pi\, r_0\, v \\ \tau &= l/v \\ v &= L/\pi\, r_0^2 \end{aligned}\right\} \tag{11}$$

In practice, falling films may show a partially rippled surface. The ripples can be eliminated by addition of small amounts of a suitable surface active agent to the liquid without introducing an additional resistance to mass transfer. High velocity liquid jets, as used in this investigation do not show ripples at the surface.

The formation of a falling film through a slit and of a jet through a nozzle in principle introduces a deviation from the steady state relationships for the velocity given in (10) and (11) respectively. Its effect on the total contact time is negligible when the film height is greater than about 20 times the film thickness [9], or the jet length about 10 times the diameter [10]. In the latter case the jet should be formed through a bell-shaped nozzle in order to approach a flat velocity distribution at the discharge point.

Finally a falling film has a stagnant surface with a height of a few cm above the level of the receiving liquid. The contribution of this height to the absorption is negligible if the resistance on the liquid side is predominant; in that case the total film height has to be corrected by subtracting the height of this end effect. With the liquid jets used the velocities are too great for this phenomenon to occur; however, extra absorption may be measured as a result of entrainment of gas by the jet into the receiving liquid.

4. Physical Absorption of CO_2 in a Wetted Wall Column

(a) *Experimental*

Water and solutions of Na_2SO_3 and $MgSO_3$ have been used as absorbing liquids. In these liquids such a small part of the dissolved CO_2 reacts to

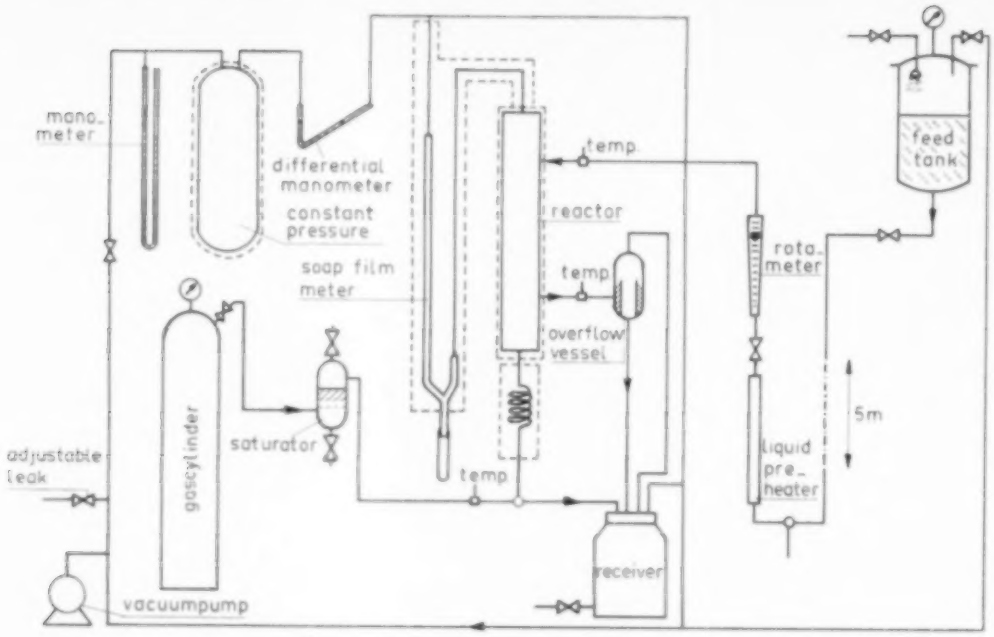

Fig. 2. Sketch of absorption equipment.

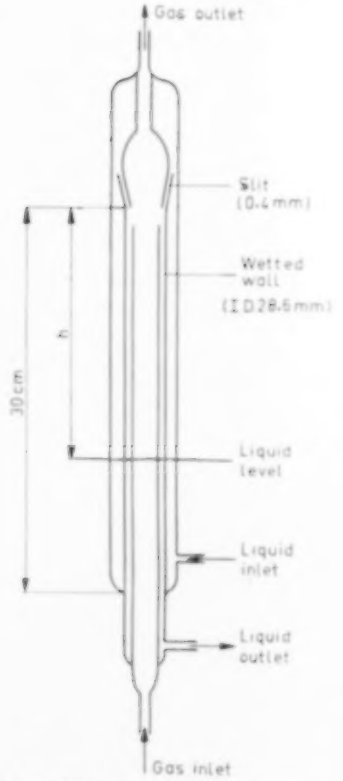

Fig. 3. The wetted wall column.

give H_2CO_3 and HCO_3^-, that the absorption may be regarded as purely physical.

In this case of physical absorption equations (4, 9 and 10) give for the total absorption rate:

$$\Phi_m = 2\,d'\,c^*\sqrt{\pi\,D\,v_s\,h} \qquad (12)$$

The absorption equipment used for the measurements reported in this paper is schematically presented in Fig. 2. The absorbing liquid contained in an overhead reservoir was fed by gravity to the absorber shown in Fig. 3. Initial to a series of measurements the liquid was degassed by spraying it into vacuum. The liquid was introduced to the wetted wall through an annular slit and flowed down into an annular liquid pool with with a small surface area. The CO_2 gas (99·8% purity, the balance being water vapour) was supplied from a pressure cylinder. It was saturated with water vapour at the experimental temperature before entering the absorber. In this equipment the experiments could be carried out at atmospheric and sub-atmospheric pressure.

For the determination of the absorption rate, Φ_m, the rate of decrease of the gas volume in the absorber at constant temperature and pressure

VOL. 10 1959

was measured as the velocity of displacement of a soap film in a calibrated tube. Apart from this determination the following data were recorded: the liquid feed rate, the gas and liquid temperatures, the pressure and the height of falling film.

(b) *Factors influencing the rate of absorption into a falling film*

(*i*) *The effect of a surface active agent.* With pure water ripples appeared on the film surface at a certain distance below the slit, depending on the liquid rate. In order to eliminate these ripples 0·02% by weight of "Lubrol W" was added to the water. Special measurements on the rate of absorption by pure water under conditions when no ripples were visible and by water with Lubrol W under the same conditions showed a complete agreement. From this it was concluded that this surface active agent at the concentration used presented no measurable additional resistance to CO_2 absorption.

(*ii*) *The influence of pressure.* It can be shown from equation (12) that under otherwise constant conditions the total CO_2 pressure does not influence the volumetric rate of absorption, provided Henry's law is valid for the system CO_2 – water and the diffusivity of CO_2 in water is independent of its concentration. Measurements between 15 and 76 cm Hg at constant liquid feed rate, film height and temperature gave the same volumetric absorption rates. Since for CO_2 – water Henry's law applies, it was concluded that the variation of the diffusivity of CO_2 in water with concentration falls within the error of the measurements.

(*iii*) *Variation of the film height h.* Results of absorption measurements in which only the film height was varied have been shown in Fig. 4. In these experiments the contact times between gas and liquid were short enough to reduce the difference between the simple penetration theory and the exact theory for diffusion in a laminar falling film with a half parabolic velocity profile, to less than 0·1 per cent. In Fig. 4 the expected linear relationship between

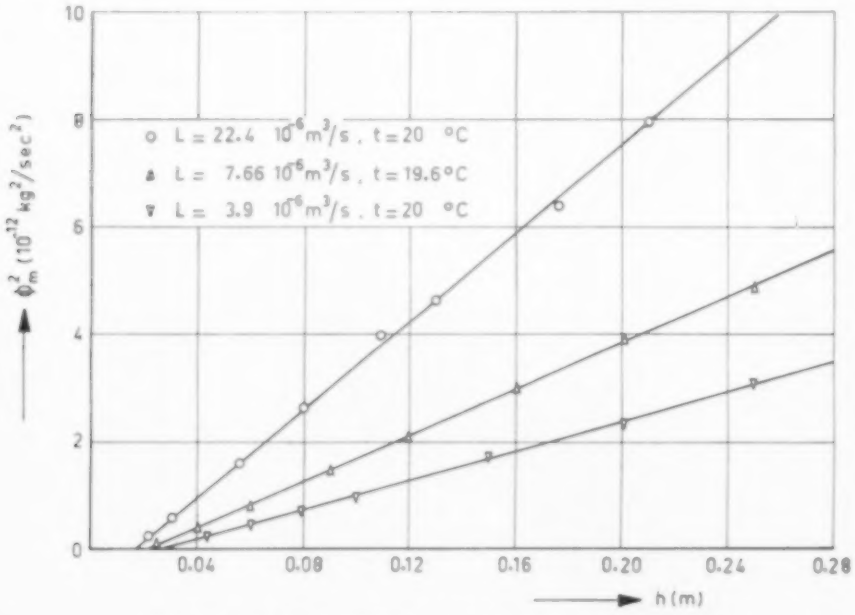

FIG. 4. Rate of absorption of CO_2 by water as a function of the film height (p_{CO_2} = 76 m Hg, wt % of Lubrol = 0·02).

Φ_m^2 and h is observed, but the extrapolated absorption rate disappears for a certain positive value of h, Δh. For all physical absorption measurements the value of Δh agrees with the visually observed height of the end effect mentioned in section 3. A quantitative agreement between theory and experiments can be obtained if the total film height h is corrected for this end effect by subtracting Δh.

In Fig. 5, for the same experiments Φ_m has been plotted against the square root of the corrected film height $h' = h - \Delta h$. From the slope of the lines $c^* \sqrt{D}$ was calculated using equations (10) and (12). The numerical results have been collected in Table 1.

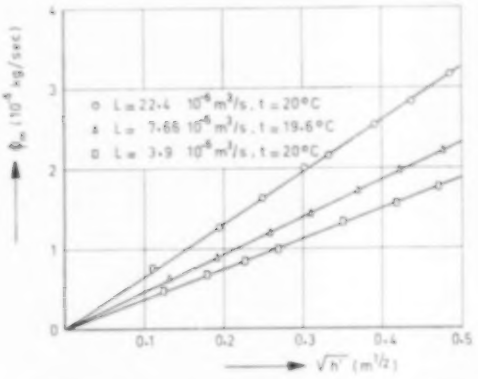

Fig. 5. Rate of absorption of CO_2 by water as a function of the corrected film height ($p_{CO_2} = 76$ cm Hg, wt % of Lubrol = 0·02)

In agreement with the theory for diffusion into a stagnant liquid the experiments at different flow rates L resulted in nearly the same values for $c^* \sqrt{D}$, with an average of $7{\cdot}1 \times 10^{-5}$ kg m^{-2} sec$^{-\frac{1}{2}}$ at 20°C and 76·0 cm Hg CO_2 presssure.

(c) *The diffusion coefficient of CO_2 in water and inert solutions*

In general, diffusion coefficients of gases in inert liquids are obtained by means of the sintered cell method [11, 12] and by measurements based on unsteady state absorption into a stagnant liquid. Both methods are time consuming and have their particular difficulties, partly of analytic nature.

A rapid and reliable determination of the product $c^* \sqrt{D}$ is possible by means of absorption rate measurements in a wetted wall column. From values of $c^* \sqrt{D}$, thus obtained, diffusion coefficients can be calculated using the separately determined values of c^*. The same method was recently published by Davidson and Cullen [13] who calculated diffusivities from absorption rates by water flowing down a sphere.

With the wetted wall column described above, we determined the diffusivity of CO_2 in water in the temperature range 6 – 30 °C. The results have been collected in Table 2. It appears that the temperature dependence can be described by means of the Nernst – Einstein relationship:

$$\frac{D\,\mu}{T} = \text{constant} \qquad (13)$$

Table 1. *Absorption of* CO_2 *in water*, $p_{CO_2} = 76{\cdot}0$ cm Hg

Wt % of Lubrol	L $\left(\frac{10^{-6}\ \text{m}^3}{\text{sec}}\right)$	*Temp* (°C)	$c^* \sqrt{D}$ $\left(\frac{10^{-5}\ \text{kg}}{\text{m}^2\ \text{sec}^{\frac{1}{2}}}\right)$	τ (sec)	c_*/ρ $\left(\frac{\text{kg}}{\text{m}^3}\right)$	D $\left(\frac{10^{-9}\ \text{m}^2}{\text{sec}}\right)$
0	4·04	19·5	7·20	0·06 – 0·3	1·75[5]	1·68
0	8·25	19·5	7·20	0·04 – 0·25	1·75[5]	1·68
0	12·5	19·5	7·24	0·04 – 0·15	1·75[5]	1·70
0·02	3·90	20·0	7·12	0·1 – 0·8	1·73	1·69
0·02	7·66	19·6	7·14	0·08 – 0·5	1·75[5]	1·66
0·02	11·0	20·5	7·11	0·05 – 0·5	1·71	1·73
0·02	14·6	20·4	7·02	0·04 – 0·3	1·71	1·69
0·02	22·4	20·0	6·99	0·03 – 0·25	1·73	1·64

†Seidell [24]

Table 2. Absorption of CO_2 *in water at different temperatures* $p_{CO_2} = 76{\cdot}0$ cm Hg, 0·02 *Wt % Lubrol in water*

L $\left(\frac{10^{-2}\ m^3}{sec}\right)$	*Temp* (°C)	$c^* \sqrt{D}$ $\left(\frac{10^{-2}\ kg}{m^2\ sec^{\frac{1}{2}}}\right)$	$c^*/\dagger$ $\left(\frac{kg}{m^3}\right)$	D $\left(\frac{10^{-9}\ m^2}{sec}\right)$	μ $\left(\frac{10^{-3}\ kg}{m\ sec}\right)$	$D\mu/T$ $\left(\frac{10^{-15}\ kg\ m}{sec^2\ °C}\right)$
7·6	6·2	8·92	2·70	·108	1·464	5·7
7·6	10·2	8·40	2·32	1·30	1·285	5·9
7,6	15,8	7·56	1·96	1·49	1·115	5,7[2]
3·9	20·0	7·12	1·73	1·69	1·0005	5·8
7·6	24·8	6·67	1·51	1·94	0·898	5·8[2]
7·6	30·0	6·26	1·31	2·26	0·801	5·9[2]

†Seidell [24]

Table 3. Absorption of CO_2 *in* Na_2SO_4 *and* $MgSO_4$ *solutions* $p_{CO_2} = 76{\cdot}0$ cm Hg, $t = 25$ °C, 0·02 wt % *Lubrol in water*

Solution	*Concentration of sulphate* $\left(\frac{kmole}{m^3}\right)$	*Liquid flow rate* $\left(\frac{10^{-6}\ m^3}{sec}\right)$	$c^* \sqrt{D}$ $\left(\frac{10^{-5}\ kg}{m^2\ sec}\right)$	$c^*/\dagger$ $\left(\frac{kg}{m^3}\right)$	D $\left(\frac{10^{-9}\ m^2}{sec}\right)$	μ ‡ $\left(\frac{10^{-3}\ kg}{m\ sec}\right)$
Na_2SO_4	0				1·95	0·89
	0·199	7·60	5·49	1·31	1·76	0·97
	0·379	7·52	4·60	1·14	1·62	1·05
	0·593	7·45	3·94	1·00	1·56	1·14
	0·785	7·37	3·30	0·88	1·41	1·26
$MgSO_4$	0				1·95	0·89
	0·564	7·46	4·22	1·07	1·56	1·25
	0·950	7·33	3·05	0·86	1·26	1·60
	1·218	7·24	2·36	0·72	1·06	1·95

†Seidell [24] ‡International Critical Tables [23].

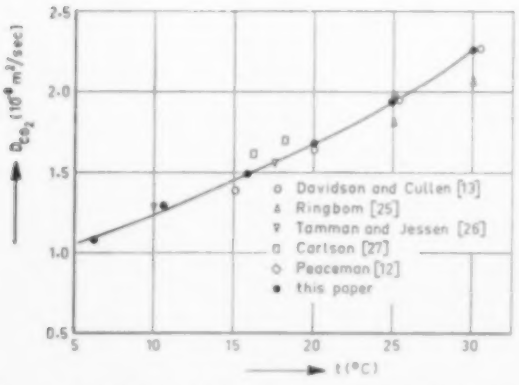

FIG. 6. Diffusivity of CO_2 in water as a function of temperature; comparison with results of other investigators.

where T is the absolute temperature. In Fig. 6 the experimental values of D_{CO_2} have been compared with those obtained by others.

In Table 3 the results of some measurements are shown on the absorption of CO_2 by Na_2SO_4 and $MgSO_4$ solutions at 25°C. These experiments were carried out in order to provide an estimate of D in electrolyte solutions, where a chemical reaction was taking place. To this end, it was assumed that the influence of a dissolved electrolyte on D could mainly be attributed to the change of viscosity with the electrolyte concentration in the solution. A relationship of the form $D\mu^a = \text{constant}$ at constant temperature was tried and it was found that

for the Na_2SO_4 solutions at $t = 25°C$

$$D\mu^{0.9} = \text{constant}$$

and for the $MgSO_4$ solutions at $t = 25°C$

$$D\mu^{0.8} = \text{constant}$$

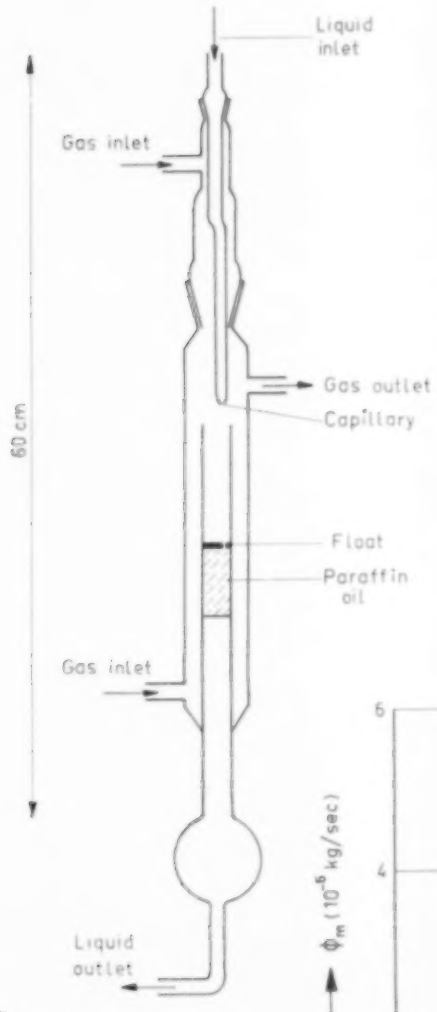

Fig. 7.
Liquid jet absorption apparatus.

Apparently the value of a is somewhat dependent on the type of electrolyte used. For the experiments on the absorption of CO_2 by caustic solutions, D was estimated from the relationship:

$$D\mu^{0.85} = \text{constant, at constant temperature} \quad (14)$$

5. Physical Absorption in Liquid Jets

In the case of physical absorption in a liquid jet of constant diameter, having a uniform velocity, equations (4, 9 and 11) predict the rate of absorption to be:

$$\Phi_m = 4\, c^* \sqrt{D L l} \quad (15)$$

provided $\dfrac{D_T}{r_0^2} \ll 1$

It was shown by Cullen and Davidson [14] that this equation is also valid for jets decreasing in thickness by the action of gravity.

The rate of absorption of SO_2 by water was measured in order to verify the hydrodynamic conditions. Because the hydration and hydrolysis reactions of SO_2 in water are very rapid relative to the contact times involved [15], this absorption may be regarded as purely physical.

The absorber has been schematically represented in Fig. 7. The experimental technique was the same as has been described in section 4. In the measurements, contact times varying between 0·001

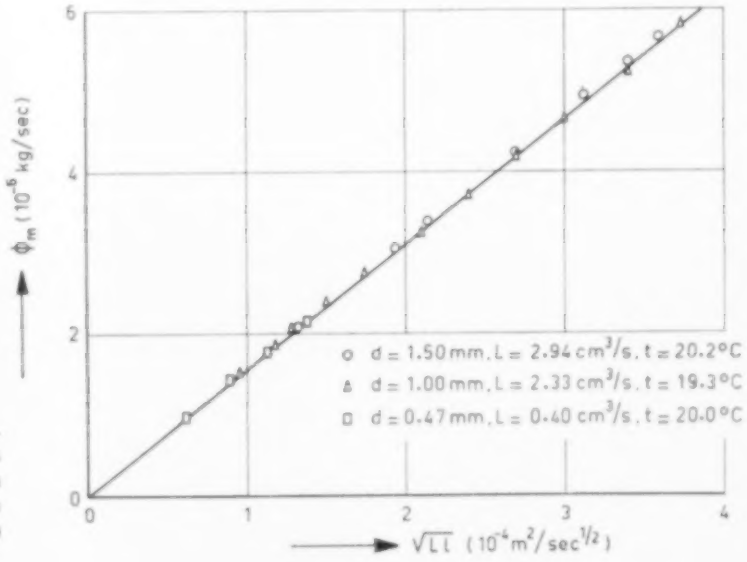

Fig. 8.
Rate of absorption of SO_2 by a liquid jet of water, as a function of liquid flow rate and jet length (p_{SO_2} = 76 cm Hg, t = 20°C.)

and 0·02 sec were used. The total rate of absorption Φ_m was determined as a function of the jet length l under otherwise constant conditions; for each series the flow rate L and the jet diameter were different.

In Fig. 8 a number of the experimental results have been shown. It appears that the observed relationship between Φ_m and $\sqrt{L\,l}$ is in close agreement with equation (15).

Thus it was concluded that the establishment of a flat velocity profile after discharge of the jet was so rapid that the assumption leading to equation (11) may be considered to be right.

The above justifies the use of equations (9) and (11) in analysing other liquid jet measurements which were performed under the same hydrodynamic conditions and which will be described in next section.

6. Absorption of CO_2 in Jets of Caustic Solutions

(*a*) *Introduction.*

Absorption of CO_2 in caustic solutions is accompanied by the following reactions which, because of the high OH^- concentrations used, may both be regarded as irreversible:

$$CO_2 + OH^- \rightarrow HCO_3^- \qquad (16)$$

$$HCO_3^- + OH^- \rightarrow CO_3^{2+} \qquad (17)$$

The second-order velocity constant k_r of the rate determining reaction (16) has been measured by Faurholt [16], Saal [15] and Pinsent *et al.* [17]. The experimental techniques of these authors, however, only can be used for dilute OH^- solutions.

The theory of ionic reactions predicts k_r, the velocity constant of a reaction between an ion and a polar molecule, to be dependent on the ionic strength [18]. The determination of the influence of ionic strength and type of ions on k_r was the purpose of our measurements. Therefore NaOH, KOH and LiOH solutions, of which the concentrations were varied, have been used to absorb the CO_2.

At sufficiently high $[OH^-]/[CO_2]$ ratios and sufficiently small contact times between gas and liquid, the reaction taking place in the liquid between CO_2 and OH may be regarded as a pseudo first-order reaction. In this case equations (5), (9) and (11) give for the total absorption rate into a jet of length l and diameter d:

$$\Phi_m = \pi\, d\, l\, c^* \sqrt{D\, k_r\, [OH^-]} \times \left(1 + \frac{1}{2\, k_r\, [OH^-]\, \tau}\right) \qquad (18)$$

A value of k_r may be obtained from measurements of Φ_m as a function of l for otherwise constant conditions, provided the value of $k_2\,[OH^-]\,\tau$ is sufficiently large to permit the neglection of the correction factor between brackets in equation (10) Furthermore, c^* and D have to be known. Because it is impossible to measure c^* and D, when the gas is reacting with a component of the solution, empirical relationships have to be used for their estimation.

Such experimental conditions were chosen that the correction, which had to be applied to equation (18) because of the depletion of OH^- ions at the gas–liquid interface, was as small as possible. The requirements for this are discussed below.

(*b*) *Selection of the experimental conditions.*

The relative depletion $\frac{\Delta\,[OH^-]}{[OH^-]_0}$ at the interface after a contact time τ is roughly:

$$\frac{\Delta\,[OH^-]}{[OH^-]_0} \simeq \frac{4\,[CO_2]^*}{[OH^-]_0} \sqrt{\frac{k_r\,[OH^-]_0\,\tau}{\pi}}, \qquad (19)$$

if it is assumed that the rate at which OH^- disappears by chemical reaction, is constant and that this chemical reaction takes place at the interface.

A low value of $\frac{\Delta\,[OH^-]}{[OH^-]_0}$ can be obtained under the following experimental conditions:

(*i*) A small CO_2 pressure, resulting in a low value of $[CO_2]^*$;

(*ii*) A short contact time τ. For this, short jets of high liquid velocity should be used. Very short jets, however, reduce the accuracy of the measurements, and in order to prevent gas entrainment in the receiving liquid the liquid velocity may not exceed a certain value.

(*iii*) A high OH^- concentration. As additional effects, balancing each other, $[CO_2]^*$ diminishes and k_r increases when the OH^- concentration is increased.

(*iv*) A low temperature. At decreasing temperature $[CO_2]^*$ increases; this effect, however, is largely outweighed by the decrease of the reaction velocity constant k_r.

The conditions chosen for the measurements were:

CO_2 pressure	= 15 cm Hg
temperature	= 20°C
liquid velocity	= 5 m/sec
jet length	= 1 – 10 cm
contact time	= 0·002 – 0·02 sec
jet diameter	= 0·66 mm

(*c*) *The results of the measurements*

In each run Φ_m was measured as a function of the jet length. As an example, the data for the absorption of CO_2 by NaOH solutions are given in Fig. 9. A linear relationship as predicted by equation (18) is observed. The rate of absorption extrapolated to zero jet length, however, retains a certain positive value. This effect has to be attributed to entrainment of CO_2 in the receiving liquid.

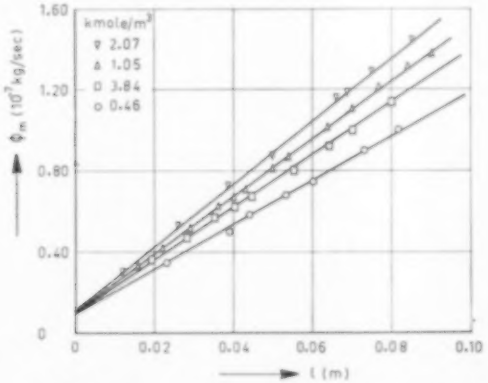

Fig. 9. Some experimental results on the absorption of CO_2 in liquid jets of NaOH solutions.

The values of $c^* \sqrt{D k_r}\,[OH^-]$ have been calculated from the slopes of the lines, such as drawn in Fig. 9.

For the computation of k_r the following properties had to be evaluated:

(*i*) The diffusivity D_{CO_2}. This was estimated by correcting for the viscosity of the solution according to equation (14).

(*ii*) The physical solubility c^*. In the calculation of c^*, an empirical formula has been used, representing the physical solubility of a gas in an electrolyte solution:

$$\log \frac{c^*}{c^*_w} = -k_s I, \qquad (20)$$

where c^* and c^*_w are the solubilities in the solution and in water respectively and I is the ionic strength ($= \frac{1}{2} \Sigma c_i z_i^2$). From a study by van Krevelen and Hoftijzer [19], it may be found that the solubilities of a gas in a hydroxyde solution and in the corresponding chloride solution are related by

$$k_{sOH^-} = k_{sCl^-} + \Delta k_s, \qquad (21)$$

where Δk_s is practically independent of the type of gas and of the temperature.

Values of Δk_s obtained from solubilities of inert gases in NaOH (KOH) solutions and in NaCl (KCl) solutions have been collected in Table 4. By correcting the LiCl solubilities of CO_2 in NaCl, KCl and solutions according to equation (21) k_{sNaOH}, k_{sKOH} and k_{sLiOH} have been calculated. Taking Δk_s to be 0·038 m³/kg ion, it was found that at 20°C:

$$k_{sNaOH} = 0{\cdot}149 \text{ m}^3/\text{kg ion},$$

$$k_{sKOH} = 0{\cdot}113 \text{ m}^3/\text{kg ion},$$

$$k_{sLiOH} = 0{\cdot}124 \text{ m}^3/\text{kg ion}.$$

Table 4. *Comparison of gas solubilities in solutions of* NaOH *and* NaCl, *resp.* KOH *and* KCl

Gas	*Temp* (°C)	Δk_s (m³/kg ion)	*Solutions compared*	
O_2	25	0·033	NaOH	NaCl
O_2	25	0·040	KOH	KCl
O_2	15	0·037	NaOH	NaCl
H_2	25	0·040	NaOH	NaCl
N_2O	25	0·038	KOH	KCl
N_2O	15	0·041	KOH	KCl

Table 5. Summary of the results of CO_2 absorption in jets of caustic solutions, $t = 20$ °C, $p_{CO_2} = 15{\cdot}0$ cm Hg

Solution	$[OH]_0$ $\left(\frac{\text{kmole}}{\text{m}^3}\right)$	$\frac{d\Phi_m}{dl}$ $\left(\frac{10^{-6}\text{ kg}}{\text{m sec}}\right)$	μ $\left(\frac{10^{-3}\text{ kg}}{\text{m sec}}\right)$	D $\left(\frac{10^{-9}\text{ m}^2}{\text{sec}}\right)$	c^* $\left(\frac{10^{-1}\text{ kg}}{\text{m}^3}\right)$	$k_r\overline{[OH^-]_r}$ $\left(\frac{1}{\text{sec}}\right)$	$\overline{[OH^-]_r}$ $\left(\frac{\text{kg ion}}{\text{m}^3}\right)$	k_r $\left(\frac{\text{m}^3}{\text{kmole sec}}\right)$
NaOH	0·46	1·10	1·10	1·55	2·91	2160	0·39[5]	5450
	1·05	1·44	1·23	1·41	2·38	6060	0·89	6200
	2·07	1·56	1·58	1·14	1·68	17700	1·97	9000
KOH	0·44	1·19	1·05	1·61	3·04	2200	0·38	5800
	0·89	1·67	1·09[5]	1·55	2·70	5720	0·82	7000
	3·14	2·56	1·44	1·23	1·55	52000	3·01	17300
LiOH	0·51	1·18	1·09	1·56	2·94	2400	0·45	5350
	1·02	1·42	1·23	1·41	2·54	5130	0·95	5400

For calculating c^* in the caustic solutions these values were used in equation (20).

(*iii*) The hydroxide concentration $[OH^-]_r$ in the reaction zone. This concentration is somewhat lower than the original one $[OH^-]_0$, due to the finite rate of diffusion of the OH^- ions. The correction to be applied was calculated in the first approximation [10] and its magnitude can be found by comparing the values of $[OH^-]_0$ and $[OH^-]_r$ in Table 5.

A summary of the experimental results and calculations has been given in Table 5. In Fig. 10 the logarithm of k_r has been plotted against the ionic strength. According to Moelwyn-Hughes [18] and Grube and Schmid [20], for dilute solutions the relationship between k_r and I would be:

$$\log k_r = \log k_{r_0} + aI \qquad (22)$$

where a is a constant depending on the system.

The results of our experiments appear to agree with such a relationship. It is observed that a is largest for KOH solutions and smallest for LiOH solutions. By extrapolation to zero ionic strength k_{r_0} is found to be about 4700 m³/kmol sec (at 20°C). This value is not much different from those obtained with entirely different experiments (4800 – 5900 m³/kmol sec) by other investigators [16, 17].

The maximum error in the value of k_r is estimated to be 15 per cent, resulting from inaccuracies in c^*, D, $[OH^-]$ and the measured absorption rates of about 1·5 per cent, 5 per cent, 2 per cent and 2 per cent respectively.

The obtained values of k_r were used for the interpretation of the measurements described below.

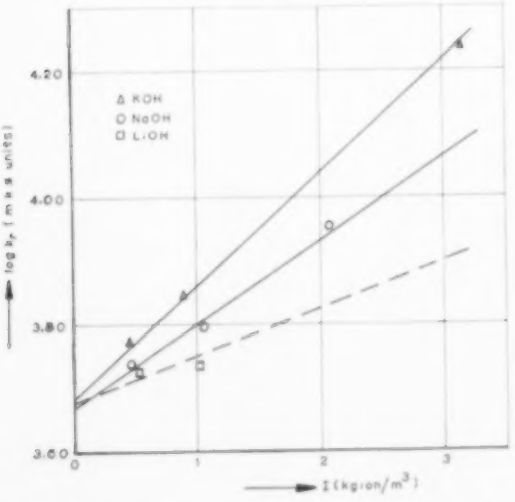

Fig. 10. The effect of ionic strength on the reaction velocity constant k_r.

7. Absorption of CO_2 in Falling Films of NaOH and KOH Solutions

(*a*) *Introduction*

With longer contact times and smaller OH^- ion concentrations than used in the jet experiments

described above, both the reaction velocity and the rate of diffusion of OH^- ions to the reaction zone determine the rate of CO_2 absorption.

If the over-all reaction

$$CO_2 + 2\,OH^- \rightarrow CO_3^{2-} + H_2O \qquad (23)$$

is assumed to be irreversible and a diffusivity D_{OH^-} can be attributed to the OH^- ion, the dimensionless relationship (8) may be used to describe the absorption process. Under the assumptions for which equation (8) may be applied we have for V:

(*i*) for large values of $\frac{[OH^-]}{[CO_2]^*}$ and small values of $k_r\,[OH^-]_0\,\tau$ according to equation (5a):

$$V = \tfrac{1}{2}\sqrt{\pi\,k_r\,[OH^-]_0\,\tau} \qquad (24)$$

(*ii*) for small values of $\frac{[OH^-]}{[CO_2]^*}$ and large values of $k_r\,[OH^-]_0\,\tau$ according to equation (7a):

$$V = \sqrt{\frac{D_{CO_2}}{D_{OH^-}}} + \frac{[OH^-]_0}{2\,[CO_2]^*}\sqrt{\frac{D_{HO^-}}{D_{CO_2}}} \qquad (25)$$

First, however, the above assumptions have to be examined in greater detail.

(*b*) *The equilibrium of the chemical reaction*

During the diffusion of CO_2 into solutions of large OH^- concentrations, for each CO_2 molecule two OH^- ions disappear according to equation (23). Down along the film the reaction zone moves inward and the OH^- concentration near the interface diminishes. At a sufficiently small value of this concentration the over-all reaction (23) may no more be regarded as irreversible and the side reaction

$$CO_2 + CO_3^{2-} + H_2O \rightarrow 2\,HCO_3^- \qquad (26)$$

occurs.

For the calculation of the additional rate of CO_2 absorption resulting from (26) Dankwerts has presented an approximative method [21]. Using this solution, it can be shown that under most unfavourable conditions of our experiments, viz.

$$[OH^-]_0 = 0{\cdot}114\ \text{kg ion/m}^3$$

$$\tau = 0{\cdot}7\ \text{sec}$$

$$p_{CO_2} = 74\ \text{cm Hg}$$

the effect of reaction (26) on the rate of absorption is smaller than 10 per cent.

(*c*) *The diffusivity* D_{OH^-}

In the reaction zone OH^- ions disappear and CO_3^{2-} ions are produced. As a result we have a counter diffusion of OH^- and CO_3^{2-} ions. An idea of the mechanism of this diffusion process may be obtained from work by Vinograd and McBain [22].

These investigators have set up equations for the rate of ionic transport in dilute solutions by steady state diffusion under the influence of a concentration gradient. From these equations it appears that the value of the " diffusivity " of an ion depends on the types, concentrations and concentration gradients of all ions present in the solution.

In our experiments concentrations and concentration gradients were transient and unknown. The Vinograd and McBain equations have been used in calculating values for D_{OH^-} on the basis of the following approximate assumptions:

(*i*) the chemical reaction occurs according to equation (23) and is irreversible;

(*ii*) the rate of reaction is very fast;

(*iii*) there is a steady state diffusion of OH^- and CO_3^{2-} ions and the ion concentrations vary linearly.

Taking for the equivalent conductivities at 20°C of Na^+, K^+, OH^- and CO_3^{2-} respectively 4·5, 6·5, 18 and 6·3 (m.k.s. units) we obtained [10] for the OH^- diffusivity in a NaOH solution:

$$D_{OH^-} = 2{\cdot}84\ 10^{-9}\ \text{m}^2/\text{sec at } 20^\circ\text{C},$$

an in a KOH solution:

$$D_{OH^-} = 2{\cdot}76\ 10^{-9}\ \text{m}^2/\text{sec at } 20^\circ\text{C}.$$

The diffusivities calculated in this manner are average values relating to very dilute solutions. When it may be assumed that the electrolyte concentration has the same effect on D_{OH^-} and D_{CO_2}, then the ratio $\frac{D_{OH^-}}{D_{CO_2}}$ is a constant which

VOL. 10 1959

amounts to $\frac{2{\cdot}8\ 10^{-9}}{1{\cdot}68\ 10^{-9}} = 1{\cdot}67$, as an average for both types of solutions.

(d) Results of the experiments

The experimental conditions have been given in Table 6. Both the OH^- concentration and CO_2 pressures were varied in order to vary the ratio $\frac{OH^-_0}{CO_2^*}$. As a result of the heat effect accompanying the absorption, the liquid temperature increased between 0·5 and 1°C. In most cases the liquid feed temperature was adjusted in such a manner, that the average of liquid in- and outlet temperature was 20°C.

In each series of measurements the rate of absorption Φ_m was determined as a function of the film height under otherwise constant conditions. For every value of τ, the appropriate value of $m(\tau)_{chem}$ was derived from Φ_m by means of equation (9).

In order to calculate the ratio V from the experiments $m(\tau)_{phys}$ had to be known. Here, $m(\tau)_{phys}$ may be considered to be the amount of gas, absorbed after a time τ in a liquid, in which no

Table 6. Experimental conditions for the absorption of CO_2 in caustic solutions in the wetted wall absorber

Solution	$[OH^-]_0$ $\left(\frac{\text{kg ion}}{m^3}\right)$	p_{CO_2} (cm Hg)	$\frac{[OH^-]_0}{[CO_2]^*}$	*Temp. liquid surface* (°C)
NaOH	0·114	15·4	14·9	20·2
		23·2	9·91	20·2
		30·4	7·51	20·2
		45·4	5·67	20·2
		74·4	3·1	20·2
	0·510	15·3	79·0	21·0
		18·0	67·4	21·2
		22·8	53·7	21·5
		30·2	41·2	22·0
		45·3	27·4	22·0
KOH	0·113	15·5	14·5[5]	20·2
		23·2	9·75	20·2
		30·3	7·45	20·2
		45·6	4·95	20·2
		74·6	3·05	20·2
	0·486	18·3	59·1	20·5
		23·0	47·0	20·5
		30·3	35·7	20·5
		45·5	24·0	20·5

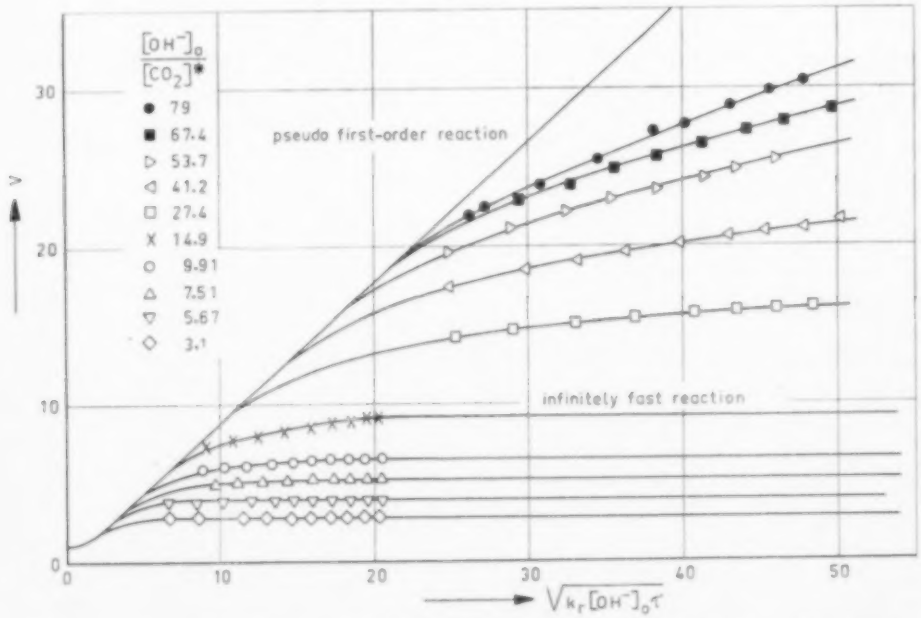

FIG. 11. The ratio V as a function of $k_r[OH^-]_0\tau$ for absorption of CO_2 by a NaOH solution.

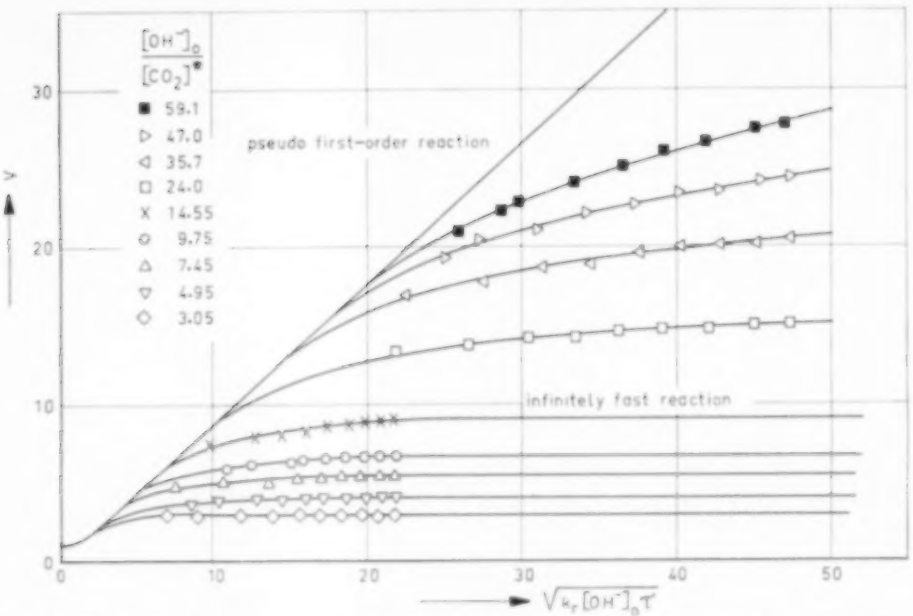

FIG. 12. The ratio V as a function of $k_r\,[OH^-]_0\tau$ for absorption of CO_2 by a KOH solution.

chemical reaction occurs, but which has the same properties as the reacting solution.

For these calculations the values of D_{CO_2} and c^* were obtained in the same manner as has been described in the previous section, at the liquid surface temperature. This temperature was estimated by means of the equation:

$$t_{\text{liquid surf.}} = \frac{t_{\text{inlet}} + t_{\text{outlet}}}{2} + \Delta T\ ^\circ\text{C},$$

where ΔT is the increase of liquid surface temperature, due to the heat effect. An expression for ΔT was derived [10] assuming that the reaction was very fast and the liquid layer infinitely thick.

For each $[OH^-]_0$ concentration k_r was taken from Fig. 10. Thus V and the corresponding values of $k_r\,[OH^-]_0\,\tau$ could be calculated. In Figs. 11 and 12 these dimensionless numbers have been plotted for NaOH and KOH solutions respectively. In Figs. 13 and 14 V has been represented as a function of $\dfrac{[OH^-]_0}{[CO_2]^*}$, for constant parameter values $k_r\,[OH^-]_0\,\tau$.

From Figs. 11 and 12 it appears that, in agreement with the theory, for large values of $k_r[OH^-]_0\tau$ and small values of $\dfrac{[OH^-]_0}{[CO_2]^*}$ V is independent of $k_r\,[OH^-]_0\,\tau$ and that for small values of $k_r[OH^-]_0\tau$ the case of a pseudo first-order reaction is approached. From Figs. 13 and 14 it was concluded

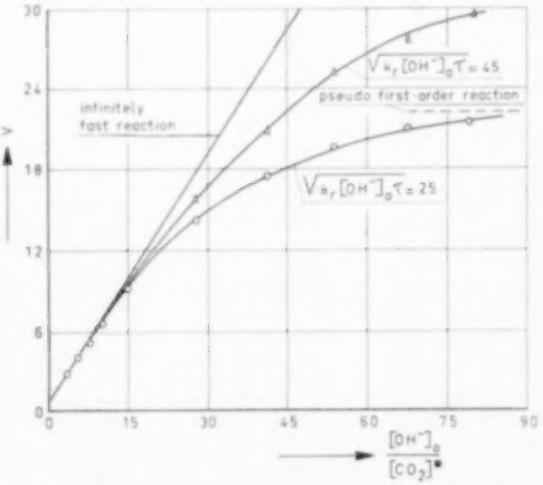

FIG. 13. The ratio V as a function of $[OH^-]_0/[CO_2]^*$ for absorption of CO_2 by a KOH solution.

VOL. 10 1959

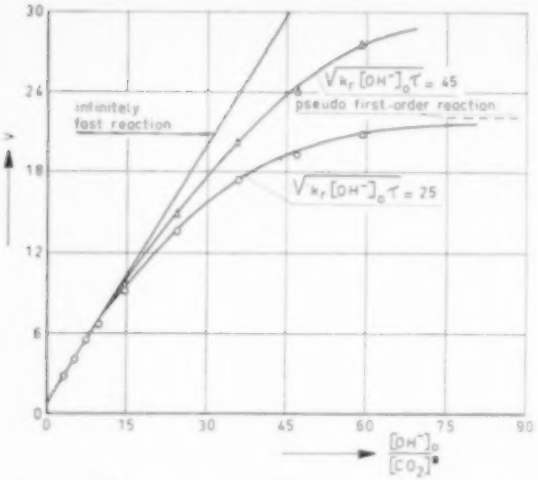

FIG. 14. The ratio V as a function of $[OH^-]_0/[CO_2]^*$ for absorption of CO_2 by a KOH solution.

that under the conditions where only diffusion of CO_2 and OH^- determines the absorption rate:

for the NaOH solution

$$V = 0{\cdot}8 + 0{\cdot}61 \frac{[OH^-]_0}{[CO_2]^*}, \qquad (27)$$

and for the KOH solution

$$V = 0{\cdot}8 + 0{\cdot}63 \frac{[OH^-]_0}{[CO_2^*]}. \qquad (28)$$

If reaction (23) is assumed to be irreversible and $\frac{D_{OH_2}}{D_{CO_2}}$ has the calculated value of 1·67, we may expect from equation (25):

$$V = 0{\cdot}77 + 0{\cdot}64 \frac{[OH^-]_0}{[CO_2]^*}. \qquad (29)$$

Hence, the agreement between the theoretical and the experimental relationship is very good.

NOTATION

$[A]$	= concentration of gas in solution	(kmole/m³)
$[A]^*$	= saturation concentration of gas in solution	(kmole/m³)
$[B]_0$	= original concentration of chemical compound in the solution	(kmole/m³)
c_i	= ion concentration	(kg ion/m³)
c^*	= saturation concentration of gas in solution	(kg/m³)
c_w^*	= saturation concentration of gas in water	(kg/m³)
d	= inner diameter wetted tube	(m)
d	= diameter liquid jet	(m)
d'	= inner diameter of cylindrical film surface	(m)
D	= coefficient of diffusion	(m²/sec)
g	= acceleration by gravity	(m/sec²)
h	= height of liquid film	(m)
Δh	= height of end effect	(m)
h'	= corrected height of liquid film $= h - \Delta h$	(m)
I	= ionic strength	(kg ion/m³)
k_r	= second-order reaction velocity constant	(m³/kmole sec)
L	= liquid flow rate	(m³/sec)
l	= length of liquid jet	(m)
$m(\tau)$	= amount of gas absorbed per unit area after contact time τ	(kg/m²)
r_0	= radius of liquid jet	(m)
t	= time	(sec)
V	= ratio $m(\tau)_{chem}/m(\tau)_{phys}$	(−)
v	= liquid velocity	(m/sec)
v_s	= surface velocity of falling film	(m/sec)
x	= co-ordinate	(m)
z_i	= ion valency	(−)
μ	= dynamic viscosity	(kg/msec)
τ	= contact time	(sec)
Φ_m	= rate of absorption	(kg/sec)

REFERENCES

[1] VON WROBLEWSKI, S. *Ann. Phys. Chem.* 1877 **2** 481.

[2] HIGBIE R. W. *Trans. Amer. Inst. Chem. Engrs.* 1935 **31** 365.

[3] DANCKWERTS P. V. and KENNEDY, A. M. *Trans. Inst. Chem. Engrs.* 1954 **32S** 54.

[4] EMMERT R. E. and PIGFORD R. L. *Chem. Engng. Progr.* 1954 **50** 87.

[5] DANCKWERTS P. V. *Trans. Faraday Soc.* 1950 **46** 300.

[6] SHERWOOD T. K. and PIGFORD R. L. *Absorption and Extraction*, p. 328. McGraw-Hill, New York 1952.

[7] PERRY R. H. *Dissert.* University of Delaware 1953.

[8] PIGFORD R. L. *Dissert.* University of Illinois 1941.

[9] LYNN S. STRAATEMEIER R. J. and KRAMERS H. *Chem. Engng. Sci.* 1955 **4** 49.

[10] Nijsing R. A. T. O. *Dissert.* Delft 1957.

[11] Hartley G. S. and Runnicles D. F. *Proc. Roy. Soc.* 1938 **A 168** 401.

[12] Peaceman D. W. *Dissert. M.I.T.* 1951.

[13] Davidson J. F. and Cullen E. J. *Trans. Inst. Chem. Engrs.* 1957 **35** 51.

[14] Cullen E. J. and Davidson J. F. *Trans. Faraday Soc.* 1956 **52** 113.

[15] Saal R. N. J. *Dissert.* University of Amsterdam 1927.

[16] Faurholt C. *J. Chim. Phys.* 1925 **22** 1.

[17] Pinsent B. R. W., Pearson L. and Roughton F. J. W. *Trans. Faraday Soc.* 1956 **52** 263.

[18] Moelwyn-Hughes E. A. *The Kinetics of Reactions in Solution.* Oxford 1947.

[19] van Krevelen D. W. and Hoftijzer P. J. *Chim. Industr., XXI*ème *Congr. Int. Chim. Industr.* 1948 168.

[20] Grube G. and Schmid G. *Z. Phys. Chem.* 1926 **119** 19.

[21] Danckwerts P. V. and Kennedy A. M. *Chem. Engng. Sci.* 1958 **8** 201.

[22] Vinograd J. R. and McBain J. W. *J. Amer. Chem. Soc.* 1941 **163** 2008.

[23] *International Critical Tables Vol. 5.* McGraw-Hill, New York 1929.

[24] Seidell A. and Linke W. F. *Solubilities of Inorganic and Organic Compounds,* Supplement to Third Edition, Van Nostrand, New York 1951.

[25] Ringbom A. *Z. Anorg. Chem.* 1938 **238** 94.

[26] Tamman G. and Jessen V. *Z. Anorg. Chem.* 1929 **179** 125.

[27] Carlson T. J. *J. Amer. Chem. Soc.* 1911 **33** 1027.

Chemical Engineering Science, 1959, Vol. 10, pp. 105 to 111. Pergamon Press Ltd. London. Printed in Great Britain

Equilibres liquide–vapeur de mélanges binaires donnant une réaction chimique : systèmes méthanol–acide acétique ; éthanol–acide acétique ; *n*-propanol–acide acétique ; *n*-butanol–acide acétique

A. Rius, J. L. Otero et A. Macarron*
Laboratoire de Génie Chimique, Faculté des Sciences, Madrid

(*Recieved* 22 *August* 1958)

Résumé—Pour déterminer les équilibres liquide–vapeur dans des systèmes susceptibles de réaction chimique, les auteurs ont mis au point un appareillage dans lequel le temps de chauffage du liquide est de l'ordre de 30 sec, en vérifiant son fonctionnement pour le mélange éthanol–eau. Ils ont étudié sous la pression atmosphérique les systèmes méthanol–acide acétique, éthanol–acide acétique, *n*-propanol–acide acétique et *n*-butanol-acide acétique, ce dernier donnant un azétrope à maximum : pour 0,518 fraction molaire d'alcool, à 120,3°C, sous 706 mm Hg. Tandis que les équations de Van-Laar et Redlich–Kister ne donnent pas pour les coefficients d'activité des résultats tout-à-fait satisfaisants, l'introduction d'un terme additif constant dans l'équation de Redlich–Kister permet l'ajustement de ces coefficients aux données expérimentales.

Abstract—To determine the liqiud – vapour equilibrium in the systems susceptible to chemical reaction, the authors have perfected an apparatus in which the heating time of the liqiud is of the order of 30 sec, in the testing of its operation for the mixture ethanol – water. They have studied under atmosphere pressure the systems methanol – acetic acid, ethanol – acetic acid, *n*-propanol – acetic acid, and *n*-butanol–acetric acid, this last giving an azetrope at maximum, for 0·518 molar fraction of alcolhol, at 120·3°C, under 706 mm Hg pressure. Whereas the equations of Van Laar and Redlich – Kister do not give completely satisfactory results for the activity coefficients, the introduction of an additive constant term in the equation of Redlich – Kister enables these coefficients to be adjusted to experimental data.

Zusammenfassung—Zur Bestimmung der Flüssigkeits-Dampf-Gleichgewichte in Systemen, die zu chemischen Reaktionen fähig sind, wurde eine Apparatur entwickelt, in der die Aufheizzeit der Flüssigkeit etwa 30 sec beträgt. Die Brauchbarkeit der Apparatur wurde am System Athanol-Wasser nachgewiesen. Unter Atmosphärendruck wurden die Systeme Methanol – Essigsäure, Athanol – Essigsäure, *n*-Propanol – Essigsäure und *n*-Butanol – Essigsäure untersucht, letzteras, das ein Azeotrop ergab, bis zu 0,518 Molenbruch Alkohol, 120,3°C unter 706 Torr. Während die Gleichungen von van Laar und Redlich – Kister für die Aktivitätskoeffizienten keine ganz befriedigenden Resultate ergaben, gelang es durch Einführung einer additiven Konstante in die Redlich – Kister-Gleichung, diese Koeffizienten an die experimentellen Ergebnisse anzupassen.

Introduction

Pour déterminer le nombre de plateaux théoriques nécessaires pour une séparation déterminée dans une colonne de rectification avec réaction chimique [1, 7, 12], plusieurs méthodes ont été proposées. Dans les quelques cas où l'on mesuré les données d'equilibre liquide–vapeur [6], ces données n'ont pas été déterminées systématiquement. Pour le système binaire alcool normal–acide acétique, étudié même en l'absence d'un catalyseur, les appareils classiques de recirculation se sont montrés inutilisables : le temps de chauffage nécessaire pour atteindre l'équilibre physique est trop grand, de telle façon que le système binaire initial devient quaternaire grâce à l'apparition de l'ester et de l'eau.

Nous nous sommes donc proposés d'étudier un appareil du type flash-distillation, ou mieux, un appareil de distillation continue avec équilibre [9].

Produits Utilises

Pour l'acide acétique, le méthanol et l'éthanol,

*Adresse actuelle : Cristalería Española, S.A. Avilés, Espagne.

nous avons employé des produits à 99,5% de la Maison "Jaber." L'acide acétique et le méthanol ont été rectifiés dans une colonne de 2 m de longueur et de 5 cm de diamètre, remplie d'anneaux Raschig de 5 mm en opérant avec un reflux voisin de l'unité. L'éthanol avait été déshydraté sur du sodium puis distillé. Les alcools *n*-propylique et *n*-butylique provenaient de l'"Union Chimique Belge." Ils ont été rectifiés dans une colonne de 3 cm de diamètre et de 0,75 m de longueur, remplie d'anneaux Fenske, en opérant avec un reflux voisin de l'unité. Le *n*-propanol passait dans un intervalle de 0,2°C. Cet intervalle était réduit à 0,1°C pour le *n*-buthanol. Les constantes physiques sont données au Tableau 1.

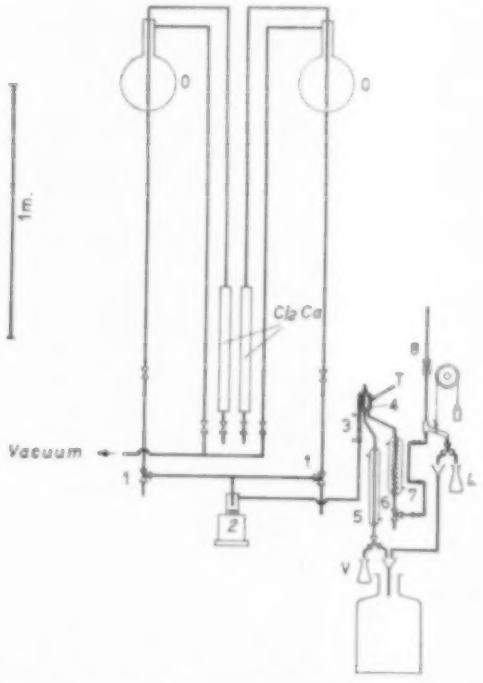

Fig. 1. Schéma de l'appareil d'équilibre.

0. Réservoirs de Mariotte, 5 l.
1. Robinets pour charger les réservoirs 0.
2. Agitateur magnétique.
3. Vaporisateur (Voir Fig. 2).
4. Séparateur adiabatique de liquide et vapeur (Voir Fig. 2).
5. Réfrigérant pour la vapeur.
6. Réfrigérant pour le liquide.
7. Bras articulé.
8. Guide fixe du bras articulé 7.
L. Enchantillon de liquide (Protegé contre l'humidité).
V. Enchantillon de vapeur (Protegé contre l'humidité).
T. Thermomètre appréciante 0,1°C (Voir Fig. 2).

Appareil d'equilibre

L'appareil (Figs. 1, 2) est entièrement construit en verre, avec des joints rodés coniques et sphériques (non représentés dans la Fig. 1, sauf les trois articulations du bras 7). Les réservoirs 0 sont remplis au moyen du vide. On place un liquide dans chaque réservoir, et en réglant les débits relatifs, l'on peut couvrir tout le domaine des

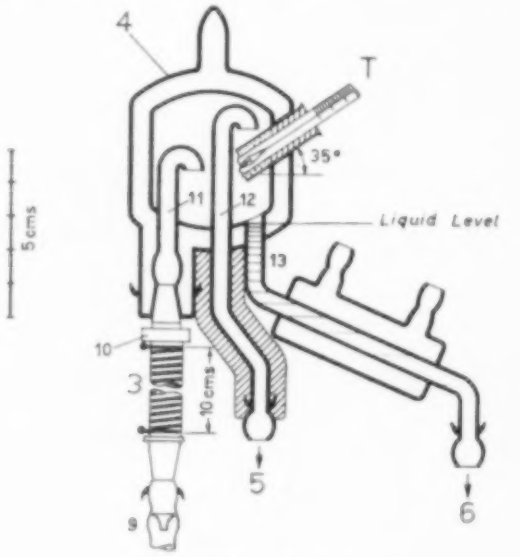

Fig. 2. Schéma du flash.

9. Embrochure, 0,5 mm diam. pour amortir les détentes de l'ébullition et empêcher le liquide de reculer.
3. Tuyau en quartz, chauffé par une résistance électrique "Kanthal D" de 9,3 Ω, connectée à une source électronique de voltage constant (125 V, 1 kVA), avec un rhéostat un série pour régler le courant.
10. Disque en asbeste.
4. Dewar avec une petite fente sans argenter pour voir directement le niveau du liquide.
11. Entrée de vapeur et liquide.
12. Sortie de vapeur, aboutissant au réfrigérant 5, isolée thermiquement.
13. Sortie de liquide, aboutissant au réfrigérant 6, munie d'un petit réfrigérant (non répresenté dans la Fig. 1) pour froidir liquide au plus tôt.
T. Thermomètre. L'espace entre la gaine de verre et le bulbe est rempli de cuivre en poudre très fin, et l'espace entre la gaine et la tige est thermiquement isolé. Ici on répresenté la gaine dans même plan que les tuyaux 11 et 12. Réellement, elle se trouve entre les deux.

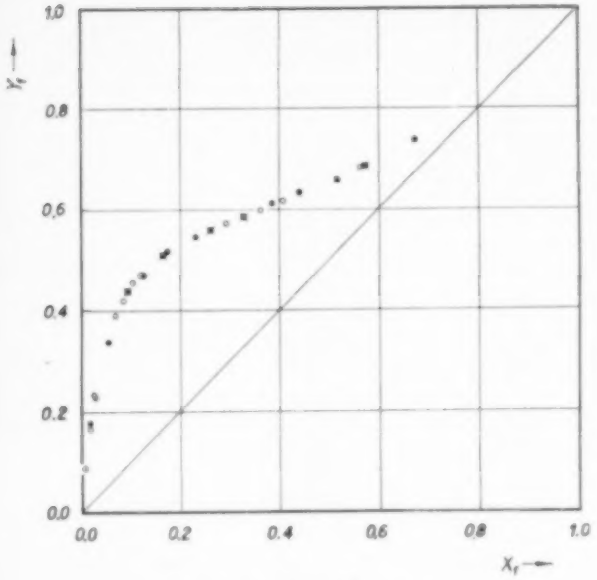

Fig. 3. Système éthanol – eau.

● Jones, Schoenborn et Colburn [4].

✖ Perry [9].

○ Travail présent.

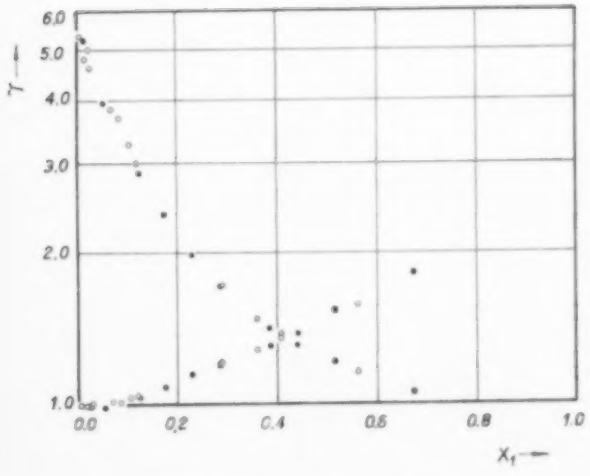

Fig. 4. Système éthanol – eau.

● Jones, Schoenborn et Colburn [4]

○ Travail présent.

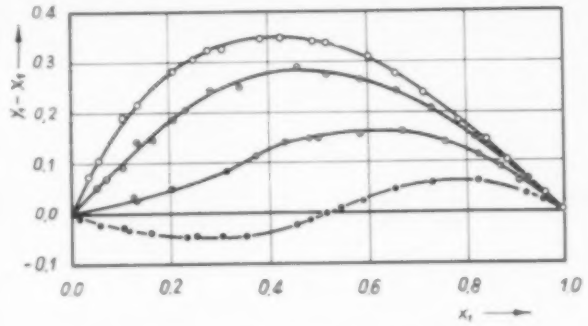

Fig. 5. ○ Système méthanol – acide acétique.

● „ éthanol – acide acétique.

○ „ *n*-propanol – acide acétique.

● „ *n*-butanol – acide acétique.

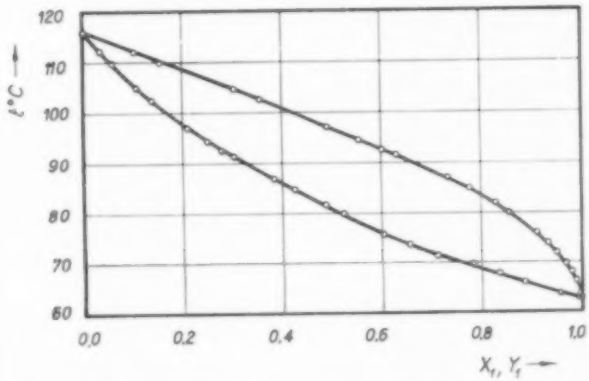

Fig. 6. Système méthanol – acide acétique.

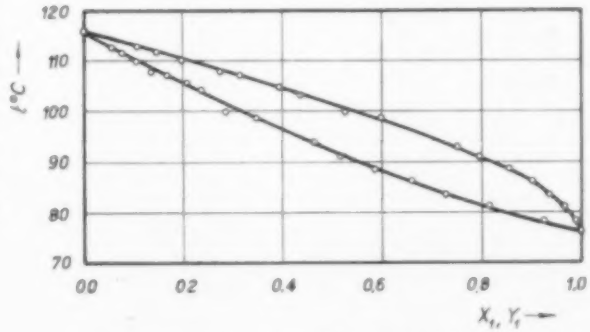

Fig. 7. Système éthanol – acide acétique.

concentrations. Etant donnée la vitesse de réaction très petite du système *n*-butanol–acide acétique, nous avons employé un seul des deux réservoirs, chargé du mélange des deux composants ; après chaque détermination, on ajoutait un peu d'un des composants pour séparer convenablement les compositions étudiées. Après trois expériences, le liquide était définitivement rejeté.

Dans le vaporisateur 3, le liquide d'alimentation subit une vaporisation partielle, et dans le séparateur 4, le liquide résiduel s'écoule par le tube 13 vers le réfrigérant 6. Le niveau de ce liquide à l'intérieur du séparateur peut être réglé en montant ou en descendant le bras articulé 7, grâce à la tige qui se déplace verticalement dans le guide tubulaire fixe 8. La vapeur se dégage par le tube 12 vers le réfrigérant 5.

Après que la température observée dans T est devenue stationnaire, on laisse fonctionner l'appareil avant prendre les échantillons L et V jusqu'au renouvellement complet du liquide occupant le réfrigérant 6 et le bras articulé 7, et dont la composition n'était pas encore celle de l'équilibre. Pour chaque système, nous avons déterminé préalablement le temps nécessaire pour laver ce volume par rinçage avec un liquide dans le cas extrême d'un remplissage initial avec l'autre, les variations de composition étant suivies au réfractomètre. Nous avons mesuré le temps nécessaire au lavage en opérant avec plusieurs débits, et la construction de la courbe temps de lavage (débit de liquide), fournit la valeur minimum du temps de lavage. On peut admettre que le liquide est pratiquement refroidi quand il a parcouru la moitié du réfrigérant 6, la durée de séjour dans la zone chaude peut être estimée à 30 sec seulement, les débits étant en général de l'ordre de 50 cm³/min. Dans les systèmes étudiés en l'absence de catalyseur, les quantités d'ester et d'eau formées dans ce temps sont négligeables. En outre, environ les deux tiers de cette durée de séjour se passent dans le réfrigérant 6, et l'ester et l'eau formés hors du contact de la vapeur n'ont plus aucune action sur l'équilibre liquide–vapeur : ils n'introduiront tout au plus qu'une erreur systématique dans la composition du liquide. Nous estimons que les données déterminées avec cet appareil correspondent très exactement aux mélanges binaires. La puissance de chauffage varie entre 300 et 600 VA. Chaque détermination prend 15 min environ.

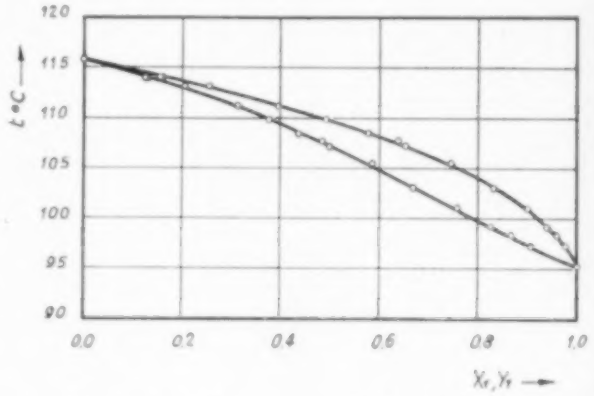

Fig. 8. Système *n*-propanol – acide acétique.

Le fonctionnement de l'appareil a été vérifié sur le système éthanol-eau (Tableau 2. Figs. 3 et 4). Lorsque le rapport en volume des phases liquide et vapeur (condensat) devient voisin de l'égalité, les températures observées dans T sont 0,2 à 0,5°C plus élevées que celles admises dans la littérature. Pour cette raison, nous avons toujours opéré avec des rapports 10/1. environ ; pour le système *n*-butanol–acide acétique, ce rapport devait être voisin de 25/1. pour éviter au maximum la surchauffe.

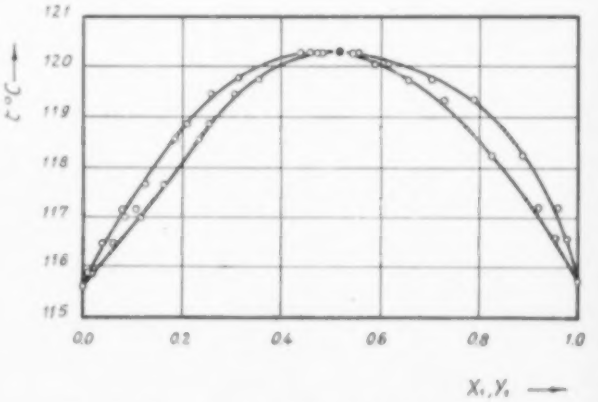

Fig. 9. Système *n*-butanol – acide acétique.

VOL. 10 1959

Analyses

Les mélanges éthanol–eau ont été anaylsés par pycnométrie en se référant aux tableaux densité-température-concentration donnés par J. H. Perry (9). Les mélanges alcool–acide acétique ont été titrés avec une solution 0,15 N de soude caustique et phenolphtaléine. Dans les mélanges *n*-butanol–acide acétique, pour solubiliser le *n*-butanol qui se sépare dans une autre phase au fur et à mesure des additions de soude caustique, on ajoutait de l'éthanol pour apprécier clairement le virage. Les titrations ont été généralement faites immédiatement après recette des échantillons, sinon, ceux-ci étaient conservés dans la glace pour ralentir l'estérification.

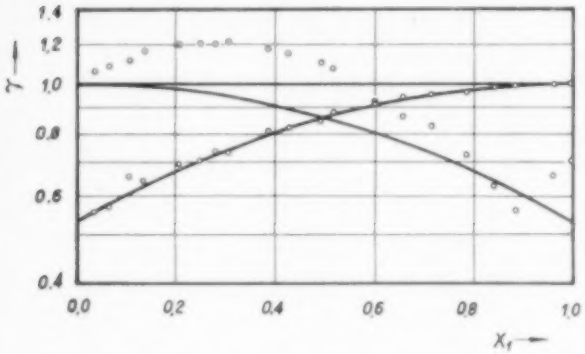

Fig. 10. Système méthanol – acide acétique : Equations de Van Laar : $A = -0{,}274$; $B = -0{,}274$.

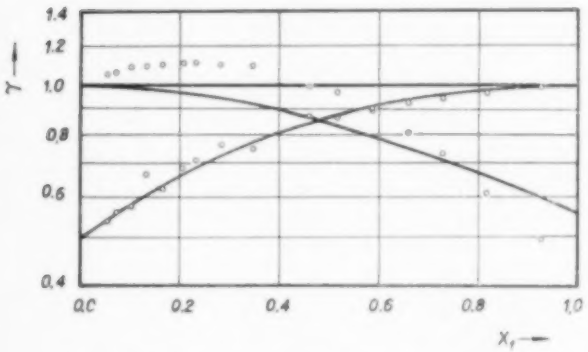

Fig. 11. Système éthanol – acide acétique : Equations de Van Laar : $A = -0{,}306$; $B = -0{,}252$.

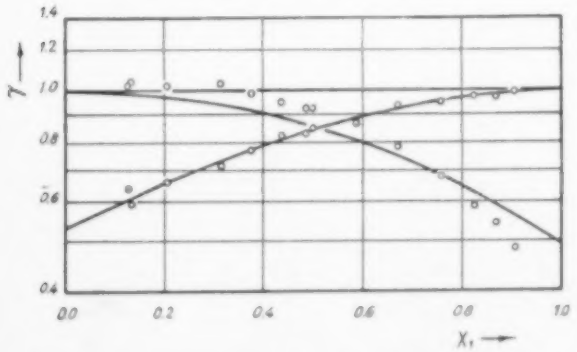

Fig. 12. Système *n*-propanol – acide acétique : Equations de Van Laar : $A = -0{,}275$; $B = -0{,}308$.

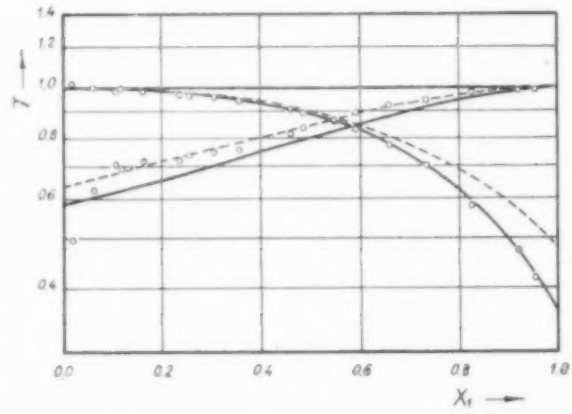

Fig. 13. Système *n*-butanol – acide acétique : Equations de Van Laar : ——— $A = -0{,}230$; $B = -0{,}440$. – – – – $A = -0{,}197$; $B = -0{,}317$.

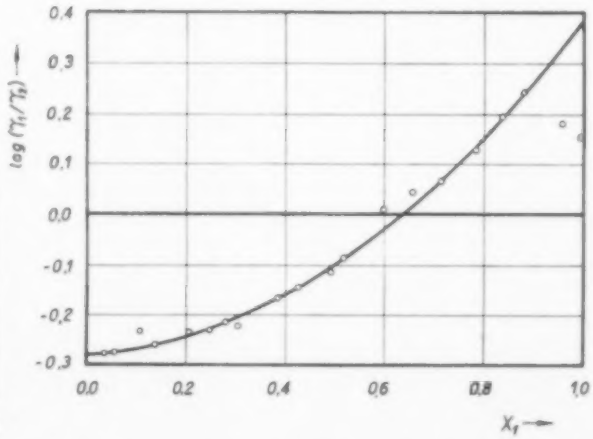

Fig. 14. Système méthanol – acide acétique : Equation de Redlich – Kister modifiée : $B = -0{,}331$; $C = -0{,}100$; $D = -0{,}003$; $K = -0{,}050$.

Correlation Des Resultats

Les Tableaux numériques 3 à 7, rassemblent nos données expérimentales sur les quatre systèmes étudiés, ainsi que les valeurs correspondantes des coefficients d'activité des deux constituants. Ces résultats sont traduits par les courbes 5 à 9.

Représentation log γ vs. X_1

Dans les systèmes méthanol–acide acétique, éthanol–acide acétique et *n*-propanol–acide acétique, la courbe log γ_2 vs. X_1 présente un maximum décroissant qui n'apparaît pas sur la courbe de log γ_1 (Figs. 10, 11 et 12). Par conséquent ces systèmes n'obéissent pas à l'equation de Gibbs-Duhem [9] valable à pression et température constantes, ni à aucune des équations qui en ont été déduites. Cependant, les points correspondant à l'alcool s'accordent avec l'équation de Van Laar sous la forme donnée par Carlson et Colburn [9].

$$\log \gamma_1 = \frac{A}{\left[1 + A/B \cdot X_1/X_2\right]^2}$$

Dans le système *n*-butanol–acide acétique, le maximum a disparu totalement (Fig. 13) : par conséquent, ce système obéit qualitativement à l'équation de Gibbs–Duhem, mais, par contre, il ne s'accorde pas aux équations de Van Laar avec les mêmes valeurs de A et B pour les deux composants. Tandis que le *n*-butanol s'accorde avec

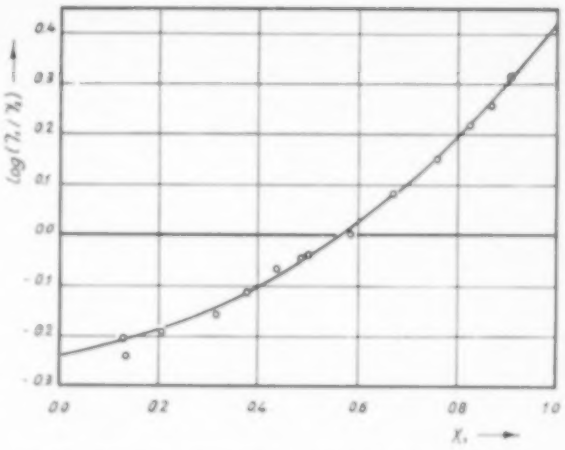

Fig. 16. Système *n*-propanol – acide acétique : Equation de Redlich – Kister :
$B = -0{,}322$; $C = -0{,}090$; $D = -0{,}008$.

les valeurs $A = -0{,}197$ et $B = -0{,}317$, les valeurs $A = -0{,}230$ et $B = -0{,}440$ permettent l'accord avec l'acide acétique.

Représentation log (γ_1/γ_2) vs. X_1

Le système *n*-propanol–acide acétique satisfait exactement à la condition de Herington [2] et l'équation de Redlich-Kister [11], (Fig. 16), tandis que les trois autres systèmes y échappent. Or, la forme géométrique de la courbe experimentale

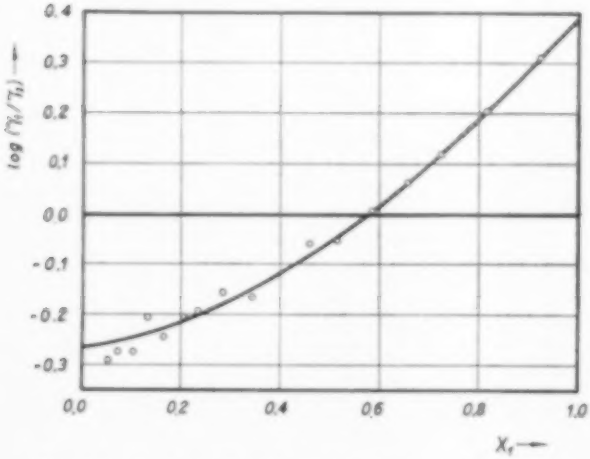

Fig. 15. Système ethanol – acide acétique : Equation de Redlich – Kister modifiée :
$B = -0{,}334$; $C = -0{,}076$; $D = +0{,}005$; $K = -0{,}015$.

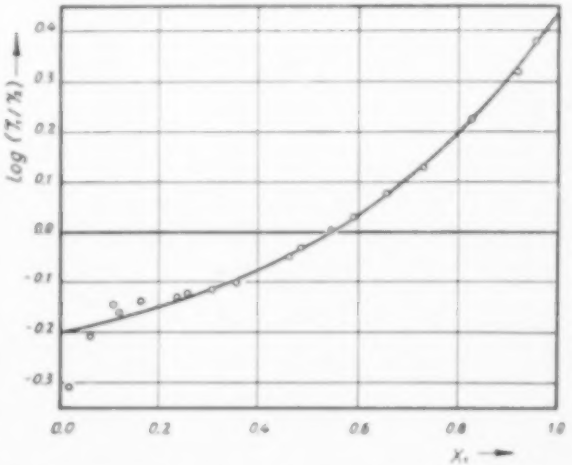

Fig. 17. Système *n*-butanol – acide acétique : Equation de Redlich – Kister modifiée :
$B = -0{,}279$; $C = -0{,}096$; $D = -0{,}021$; $K = +0{,}022$.

$\log(\gamma_1/\gamma_2)$ vs. X_1 répond à l'équation de REDLICH-KISTER (Figs. 14, 15 et 17). Il suffit d'introduire un terme constant, K, pour donner à l'equation la forme suivante :

$$\log(\gamma_1/\gamma_2) = B(1-2X_1) + C\left[6X_1(1-X_1)-1\right] + D(1-2X_1)\left[1-8X_1(1-X_1)\right] + K$$

Il faut remarquer une régularité dans les valeurs de ce terme de correction : il croît à mesure que l'on avance dans la série des alcools : — 0,050, — 0,015, 0,000, 0,022. Cette régularite ést aussi remarquable dans les données d'equilibre (Fig. 5).

Les tensions de vapeur pour calculer les coefficients d'activité ont été obtenues par interpolation linéaire de la fonction $\log P = f(1/T)$.

Les données employées sont : eau [9], méthanol [5, 9], éthanol [8, 9], *n*-propanol [5], *n*-butanol [9] et acide acétique [9].

NOTATION

t = température d'équilibre, °C.
P = pression d'équilibre, mm Hg.
X = fraction molaire dans le liquide.
Y = fraction molaire dans la vapeur.
γ = coefficient d'activité = $P.Y/P^{\circ}.X$ (P° = Tension de vapeur).
α = volatilité relative = $Y_1.X_2/X_1.T_2$.
A and B = coefficients de l'équation de VAN LAAR.
B, C and D = coefficients de l'équation de REDLICH – KISTER.
K = terme de correction de l'équation de REDLICH – KISTER.
1 (indice) = alcool.
2 (indice) = acide acétique ou eau.

REFERENCES

[1] BELCK L. H. *J. Amer. Inst. Chem. Engrs.* 1955 **1** 467.
[2] HERINGTON E. F. G. *Nature, Lond.* 1947 **160** 610.
[3] *International Critical Tables*, Vol. 3. McGraw-Hill, New York.
[4] JONES C. A. SCHOENBORN E. M. and COLBURN A. P. *Industr. Engng. Chem.* 1943 **35** 666.
[5] LANGE N. A. *Handbook of Chemistry*. Handbook Publishers, Sanduski, Ohio 1946.
[6] LEVES Ch. E. and OTHMER D. F. *Trans. Amer. Inst. Chem. Engrs.* 1945 **41** 157.
[7] MAREK J. *Coll. Trav. Chem. Tchécosl.* 1954 **19** 1055.
[8] MERRIMAN R. W. *J. Chem. Soc.* 1913 **103** 628.
[9] PERRY J. H. *Chemical Engineers Handbook* McGraw-Hill, New York 1950.
[10] POTTER A. E. and RITTER H. L. *J. Phys. Chem.* 1954 **58** 1040.
[11] REDLICH O. and KISTER A. T. *Industr. Engng. Chem.* 1948 **40** 345.
[12] ROBINSON C. S. and GILLILAND E. R. *Elements of Fractional Distillation* McGraw-Hill, New York 1950.
[13] KAISER L. *C. R. Acad. Sci. Paris* 1956 **242** 132.

Chemical Engineering Science, 1959, Vol. 10, pp. 112 to 124. Pergamon Press Ltd. London. Printed in Great Britain

Flow distributions in manifolds

A. Acrivos,* B. D. Babcock† and R. L. Pigford‡

(*Received* 15 *September* 1958)

Abstract—The division of a fluid stream into parts by means of a manifold is accompanied by fluid pressure changes owing to wall friction and to the changing fluid momentum. Friction tends to make the pressure fall while the sudden changes in direction experienced by successive portions of the stream makes the pressure rise in a " blowing " manifold and fall in a " sucking " one. As a result it is not possible to keep the fluid pressure perfectly constant inside the main channel, and there is a consequent variation in the rate of flow through identical ports.

Calculations based on one-dimensional flow equations have been carried out for channels having constant cross-sections, using computing machines. The results are applicable to a wide variety of combinations of channel dimensions, fluid velocity and physical properties, and pressure drop across the side ports. The results are summarized by charts that permit a designer quickly to estimate the non-uniformity in the flow pattern. Predicted distributions agree approximately with observed flow patterns.

Résumé—La division d'un courant fluide au moyen d'une turbulure, est accompagnée d'une variation de pression du fluide due au frottement contre les parois et à la variation de la quantité de mouvement du fluide. Le frottement tend à baisser la pression tandis que les variations brusques de direction vérifée sur des portions successives du courant font augmenter la pression dans le cas d'une tabulure à insuflation, et la fait baisser dans le cas d'une turbulure à aspiration. Il en résulte une impossibilité de rendre la pression du fluide parfaitement constante à l'intérieur du tube, et une variation dans la vitesse d'écoulement à travers les orifices identiques.

Des calculs basés sur des équations découlement à une dimension ont été effectués pour des tuyaux à section constante, à l'aide de machines à calculer. Les résultats sont applicables à un grand nombre de combinaisons de dimensions de tuyaux, vitesse du fluide et propriétés, et chutes de pression par les orifices lateraux. Les résultats sont résumes par des graphiques qui permettent de prévoir rapidement un écoulement non-uniforme. Les distributions prévues ainsi, concordent approximativement avec les écoulements obsérves.

Zusammenfassung—Die Teilung einer strömenden Flüssigkeit durch Verteiler ist von Drückänderungen in der Strömung begleitet, hervorgerufen durch Wandreibung und Impulsänderung. Reibung hat Druckabfall zur Folge, während die plötzliche Richtungsänderung, hervorgerfen durch fortlaufende Strömungsteilung, den Druck in einem " blasenden " Verteiler steigen und in einem " saugenden " Verteiler fallen lässt. Es ist daher nicht möglich, den Flüssigkeitsdruck in der Hauptströmung genau konstant zu halten, was unterschiedliche Strömungsgeschwindigkeiten in gleichgrossen Durchlässen zur Folge hat.

Ausgehend von eindimensionalen Strömungleichusgngen wurden für Kanäle konstanten Durchmessers Rechnungen mit Rechenmaschinen angestellt. Die Ergebnisse sind in einen weiten Bereich verschiedener Kombinationen von Kanalabmessungen, Strömungsgeschwindigkeiten, Stoffeigenschaften und Druckabfall über die seitlichen Durchlässe anwendbar. Die Ergebnisse sind in Diagrammen zusammengefasst, die dem Berechner die schnelle Ermittlung des ungleichförmigen Strömingsverlaufs gestatten. Berechnete Verteilungen stimmen näherungsweise mit dem beobachteten Strömungsverlauf überein.

*Department of Chemistry and Chemical Engineering, University of California, Berkeley, California.
†E.I. du Pont de Nemours and Co., Wilmington, Del.
‡Department of Chemical Engineering, University of Delaware, Newark, Delaware.

Introduction

The design of flow equipment for the division of a fluid stream into several branching streams for the formation of a single, main stream by the confluence of several smaller streams is a problem that is encountered often in chemical processing studies. The simplest device used for these purposes consists of a main, cylindrical channel to which several smaller conduits are attached at right angles. Often the object of the design is to provide for equal flow rates through the several side openings. This can be done if the fluid pressure can be kept constant throughout the main channel; otherwise, each side connection must be provided with a valve to permit adjustments to be made, compensating for the pressure variations within the main channel that would be caused by fluid friction and by the changes in the flow direction and momentum of successive portions of the stream.

As several authors have brought out previously [3, 4, 9] a uniform pressure can be maintained in the main channel by constructing it so that its cross sectional area decreases at a rate that keeps the fluid velocity nearly constant while the mass rate of flow decreases. Although this technique is a useful one it has the disadvantage that a channel designed to give uniform side-ways flow at one flow rate often does not work correctly at another rate. In any case it would appear that computations of the flow distribution to be expected from a manifold constructed from pipe uniform in diameter would be useful to the designer who wishes to provide for *nearly* although not perfectly uniform flow distribution. Frequently it is helpful to know what volume the main channel must have in order that the pressure inside the channel will not vary more than a minimum amount that produces a small but tolerable inequality in flow through the ports.

The differences in fluid pressure arise from two causes: (a) the friction of the fluid against the internal surface of the main channel makes the pressure fall in the direction of flow; and (b) the momentum of the main fluid stream flowing into a manifold tends to carry the fluid toward the closed end, where an excess pressure is produced. When the large fluid stream flows into the manifold and undergoes subdivision (a "blowing manifold") the friction and momentum effects work in opposite directions, the first tending to produce a pressure drop and the second a pressure rise. When the large stream is formed in the manifold by the combination of smaller streams and flows out of the open end of the main channel (a "sucking manifold") the friction and momentum effects reinforce each other, both tending to create lower pressures at the open end than at the closed end. Both friction and momentum effects become more pronounced when the main channel's cross section is reduced while the total quantity of fluid is kept constant. The designer often needs to know how to keep the friction and momentum effects approximately in balance in a blowing manifold and how to estimate the combined effect in a sucking manifold.

This paper describes one-dimensional fluid mechanical calculation methods and pertinent experimental data relating to manifolds of this simplest type, constructed from a main channel of constant cross section that terminates in a closed end and provided with equally spaced, uniformly sized side tubes attached to the main channel at right angles. The manifolds considered either discharge (the "blowing" case) or receive an incompressible fluid (the "sucking" case) from a region in which the pressure is uniform.

Experimental Investigation of the Branching Phenomenon

One of the two principal phenomena affecting the uniformity of fluid pressure inside the manifold is the fluid-momentum effect, which tends to produce a rise in pressure owing to the deceleration of the portion of the fluid that undergoes a change in direction in flowing through a port. The wall shear stress may be nearly the same in the non-porous sections of a manifold as in a long, straight pipe and consequently can be regarded as predictable from existing data on pipe friction. The pressure recovery phenomenon has not been investigated very widely; however, knowledge of the relation between pressure rise and velocity change is essential for the development of the one-dimensional flow theory that follows.

Consider a section of the main channel near

one of the branching outlets as shown in Fig. 1. A momentum balance can be made on the control surface indicated in the figure. If it is assumed that the fluid leaving through the branch has lost

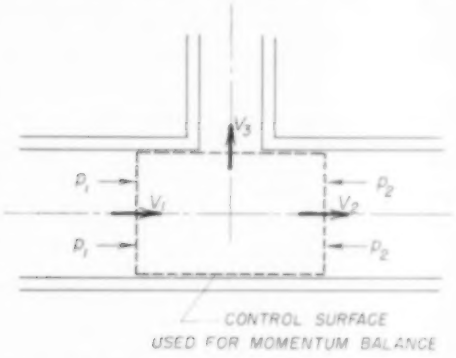

Fig. 1. Fluid pressures and velocities near a manifold port

all its longitudinal component of velocity before it crosses the control surface, the pressure rise, $p_2 - p_1$, is related to the velocity decrease by the equation

$$p_2 - p_1 = \rho\left(\frac{V_1^2 - V_2^2}{g_c}\right) \qquad (0.1)$$

Since the velocity of the side stream may not be exactly in the perpendicular direction when the stream flows through the orifice port it may be expected that the observed pressure rise will be only a fraction, k, of the expected value, so that equation (0.1) should be modified to

$$p_2 - p_1 = k\,\rho\left(\frac{V_1^2 - V_2^2}{g_c}\right) \qquad (0.2)$$

In general k is expected to be smaller than unity.

Although a calculation of the direction of fluid streamlines in the neighborhood of the orifice would permit k to be estimated theoretically, an easier course of action is to determine its value from experimentally observed pressure changes. For this purpose several experiments [1] have been carried out using a 6 ft length of 1·025 in. i.d. brass pipe to which twenty-four side ports were fastened at intervals of 3 in. The side connections were made from 9 in. lengths of 0·317 in. i.d. copper water tubing which were soldered at the top of the main tube over $\frac{1}{4}$ in. diameter holes. Fluid pressures inside the main channel were observed by means of thirty-two pressure taps that were soldered to the bottom of the main tube at 3 in. intervals, taps 5 and 27 being located half-way between side ports 1 and 2 and between 23 and 24, respectively. Connections between the pressure taps and the interior of the manifold were made by drilling $\frac{1}{8}$ in. diameter holes. A sharp-edged orifice was located at a point 28·5 in. upstream from the first side outlet and another was located 31·5 in. downstream from the last outlet. These were used to measure the quantities of air entering and leaving the manifold, respectively, and were calibrated by using a large wet-test meter. The quantity of air leaving any of the side ports could be measured by means of a small-diameter Pitot tube that was also calibrated.

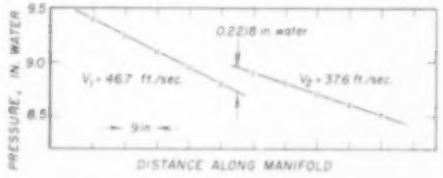

Fig. 2. Typical pressures observed near a single outlet port.

Fig. 2 shows a typical pressure profile observed with only the centre side port, number 13, open. It is seen that the fluid pressure decreases linearly in the direction of flow until the location of the side port is reached. Then a pressure rise occurs, as expected from equation (0.2), and this is followed by a second linear pressure drop. The fall in pressure before and after the port is caused by fluid friction, and the friction factors computed from the pressure gradients were found to be rather closely in agreement with the well established relations for smooth pipe. The effect of the branching flow on the wall friction was not apparent from the data taken and, if present at all, must have been confined to the region within an inch or two of the side port.

Pressure rises caused by the flow branching were calculated from the experimental observations by extrapolating the straight-line pressure profiles to the location of the port and measuring the vertical difference between the lines. When

these values of $p_2 - p_1$ were substituted into equation (0.2) the values of k shown in Fig. 3 were calculated. The fact that the numerical values are less than unity indicates that the streamlines in the diverted stream do not turn a full right angle before the stream leaves the main channel. Some of the force needed to cause the full change in flow direction is apparently produced by excess fluid pressure on the downstream side of the vertical inside surface of the outlet tube.

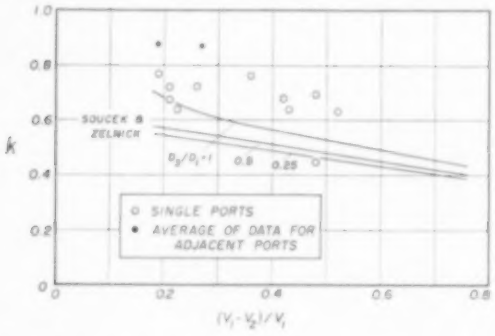

FIG. 3. Pressure recovery coefficients observed in tests of single and double outlet ports.

Fig. 3 also shows lines representing similar data on branching flow as reported by ROUSE [6], based on the work of SOUCEK and ZELNICK [7]. The experiments referred to were made on a long horizontal channel of 6 in. square cross-section through which water flowed. Short side ports were connected to a square channel at right angles. The side ports were square in cross-section and had sharp edges where they were attached to the main channel. In spite of the different geometry and the fluid properties the k-values agree satisfactorily.

A few experiments were made in which two side ports were allowed to discharge simultaneously, leading to data that are shown typically by Fig. 4. The distance between the open ports was varied from 6 in. to 36 in. but there was no significant trend of the k-values for either of the two holes with the spacing between them. The average value for each hole for six different spacings is shown on Fig. 3. The points fall higher than would have been expected from the single-port data. However, the differences between these two points and the previous data are probably not sufficient to affect the predicted flow distribution and an average of all the observations will be used in further calculations.

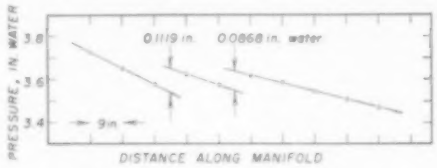

FIG. 4. Typical pressures observed near pair of outlet ports. Fluid velocities before, between and after ports are 28·5, 23·2 and 16·7 ft/sec respectively.

A manifold with a continuously porous wall is a special case of the manifolds under consideration here, in which the number of side tubes is made very large while keeping the ratio of total port area to inside tube surface constant. WEISSBERG [8] has carried out an experimental study of the pressure distribution along the axis of such a manifold through the wall of which air was pumped at a uniform rate. When the pressure loss owing to expected wall friction, using the smooth-tube formula, was subtracted from the observed pressure change, the residual pressure rise was not as large as the net rate of input of fluid momentum. Thus, if equation (0·2) were applied to WEISSBERG's data k-values less than unity would result. In the two experiments where the effect was most noticeable in WEISSBERG's work the appropriate values of k are 0·88 and 0·69, which are of the same order of magnitude as those appearing on Fig. 3.

ONE-DIMENSIONAL FLOW THEORY FOR BRANCHING CONDUITS*

The manifolds of greatest interest here consist of straight tubes with finite numbers of similar side connections spaced equally at discrete

*A more accurately descriptive two-dimensional theory is too difficult to carry out, although laminar-flow calculations can be developed for a case in which the side flow is assumed constant as shown by BERMAN [2]. For rather small side-flow velocities these computations show that the fluid pressure will rise in a "blowing" manifold, in spite of fluid friction, quite like the pressure changes predicted from the simpler, one-dimensional equations.

intervals. When the spacing between the side connections is small, however, and the number of side tubes in any small increment of length is large the manifold can be regarded for all practical purposes as a continuous homogeneous system, equivalent to a main channel having a longitudinal slot or porous strip of constant width. Although the substitution of a continuous for a discrete system may be questionable when the number of side outlets is small the step is justified by the fact that with this simplification the fluid mechanical principles lead to a differential, rather than to a difference equation. Results of computations based on the differential equation can be represented more simply and compactly than is the case for calculations using the nonlinear difference equations. However, both types of solutions will be investigated and it will be shown intuitively, as well as mathematically, that the continuous manifolds are but limiting cases of the more interesting, discrete manifolds.

Difference Equations for Discrete, Blowing Manifolds

A sketch of a discrete manifold is shown in Fig. 5. The manifold consists of a number of straight-tube sections i, $i+1$, $i+2$, etc., which are separated by an equal number of discharge ports through which fluid leaves the main section of the manifold. The fluid is supposed to flow from left to right and the discharge ports are located at $x = x_i$, where x denotes the distance along the axis of the main tube. Moreover, it will be assumed for simplicity, that the discharge ports are uniformly spaced.

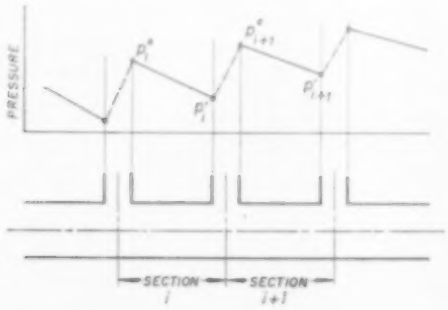

Fig. 5. Nomenclature used for a one-dimensional theory of manifolds.

The Fanning equation is of course applicable to the straight-tube section, so that for section i,

$$p_i' - p_i^* = -\frac{2}{g_c}\rho f_i \frac{u_i^2}{D}\Delta x \tag{1.1}$$

On the other hand, a discontinuity in both the pressure and the velocity occurs at $x = x_i$ because of the presence of a discharge port. These changes in the pressure and the velocity can be obtained from a material balance and a momentum balance. Thus if the arithmetic average of pressures just upstream and just downstream from a side port is used to compute the side flow.

$$u_{i+1} - u_i = -\frac{4\alpha C}{D}\Delta x \sqrt{\frac{2g_c}{\rho}\left(\frac{p_i' + p_{i+1}^*}{2} - p_0\right)} \tag{1.2}$$

from the orifice equation and a material balance. Also, from a momentum balance, as indicated above,

$$p_{i+1}^* - p_i' = \frac{k\rho}{g_c}(u_i^2 - u_{i+1}^2) \tag{1.3}$$

The above three relations are the basic equations for the discrete blowing manifold. They have to be solved, subject to the conditions that at the entrance of the manifold

$$u = u_0$$

and

$$p = p_0' \tag{1.4}$$

These equations can, however, be considerably simplified if a change is made in both the independent and the dependent variables. Thus, letting

$$y \equiv \left(\frac{4\alpha C}{D}\sqrt{2k}\right)x \tag{1.5}$$

$$P_i^* \equiv \frac{g_c}{2k\rho u_0^2}(p_i^* - p_0) \tag{1.6}$$

$$U_i \equiv \frac{u_i}{u_0} \tag{1.7}$$

the basic equations become

$$P_i' - P_i^* = -F_i U_i^2 \Delta y \tag{1.8}$$

where $F_i \equiv \frac{f_i}{2^{3/2} k^{3/2} \alpha C}$ (1.8a)

$$U_{i+1} - U_i = -\Delta y \sqrt{P_i' + P_{i+1}^*} \tag{1.9}$$

VOL. 10 1959

and

$$P'_{i+1} - P'_i = \tfrac{1}{2}\,(U_i^2 - U_{i+1}^2) \qquad (1.10)$$

Next, by combining equation (1.9) and (1.10) one finds that

$$U_{i+1} = \frac{1}{1 + \dfrac{(\Delta y)^2}{2}} \times$$

$$\left\{U_i - \sqrt{\frac{(\Delta y)^4}{4}\,U_i^2 + 2\,(\Delta y)^2 \cdot \left[1 + \frac{(\Delta y)^2}{2}\right] P'_i}\right\} \qquad (1.11)$$

while, at the entrance of the manifold.

$$U_0 = 1$$

and $$P'_1 = \frac{M_0^2}{2} = \frac{g_c\,(p'_0 - p_0)}{2k\,\rho u_0^2} \qquad (1.12)$$

Finally,* equations (1.8), (1.10) and (1.11), subject to the conditions given by equation (1.12), can be solved by a stepwise numerical iteration. This can vary easily be programmed for a digital computer like the Bendix G-15-D machine for example. The closed end of the manifold is at the point where $U = 0$.

It is seen, then, that the change of variables effected by equations (1.5), (1.6) and (1.7) enables one to formulate the problem mathematically in terms of only three dimensionless parameters, namely M_0, F_0 and Δy, where M_0 is related to the pressure and fluid momentum at the open end of the manifold, F_0 is related to the friction in the straight-tube section, and Δy is related to the distance between adjacent discharge ports. Numerical results for this problem, in terms of the above three parameters, are given below.

Differential Equations for Continuous, Blowing Manifolds

So far, the discussion has been confined to discrete manifolds only. However, the special, continuous case merits attention, because of its relative simplicity. These manifolds, as was mentioned above contain a very large number of discharge ports along the main tube. The mathematical equations for this special case can readily be obtained from the basic equations for the discrete manifold by letting $\Delta x \to 0$ while keeping α, the fractional discharge area, constant.

Thus, as $\Delta y \to 0$, equations (1.8), (1.10) and (1.13) can be combined formally* to give

$$\frac{dP}{dy} + U\,\frac{dU}{dy} + F_0\,U^{7/4} = 0 \qquad (1.14)$$

while, equation (1.9) becomes formally

$$\frac{dU}{dy} = -\sqrt{2P} \qquad (1.15)$$

These last two relations can finally be combined to give the basic differential equation for the continuous, blowing manifold.

$$\left(\frac{d^2U}{dy^2}\right)\left(\frac{dU}{dy}\right) + U\left(\frac{dU}{dy}\right) + F_0 U^{7/4} = 0 \qquad (1.16)$$

with the conditions that, at $y = 0$

$$U = 1 \qquad (1.17)$$

and $$\frac{dU}{dy} = -M_0$$

Equation (1.16) is now a non-linear, second-order, ordinary differential equation which, can easily be integrated numerically. Again, a digital computer, like the Bendix, can readily be employed with advantage in carrying out the numerical computations. The solution to this problem is expressible in terms of only two dimensionless parameters, namely M_0 and F_0, Δy having been eliminated in the limiting process. Therefore, as one would have expected intuitively the basic equation for the continuous manifold can be obtained as a limiting form from equations (1.8), (1.9) and (1.10), by formally letting $\Delta y \to 0$. Equation (1.16) can, however, also be derived directly, that is independently of the relations for the discrete manifold, by making a momentum balance on a differential element of volume in the main channel.

*If we assume that the friction factor varies with fluid velocity according to the generally accepted relationship for smooth tubes we should write

$$F_i = F_0\,U_i^{-1/4}. \qquad (1.13)$$

*The purely formal limiting process outlined below can be justified rigorously, although the details will be omitted here.

Sucking Manifolds

In this section the basic equations for both the discrete and the continuous sucking manifolds will be briefly derived. The details of the derivation are essentially identical with those of the equations for the blowing manifolds.

The mathematical equations for the sucking manifolds differ from the corresponding relations for the blowing manifolds for two reasons: first, fluid flows *into* the main tube from the ports; second, the distance along the manifold is measured again from the open end so that the direction of increasing x will be opposite to that of the fluid flow.

If distances are measured from the open end of the manifold, one easily finds that

$$\mathring{P}'_i - \mathring{P}^{\circ}_i = -F_0 U_1^{7/4} \Delta y \tag{1.18}$$

$$\mathring{P}^{\circ}_{i+1} - \mathring{P}'_i = -\tfrac{1}{2}(U_i^2 - U_{i+1}^2) \tag{1.19}$$

$$U_{i+1} - U_i = -\Delta y \sqrt{\mathring{P}'_i + \mathring{P}^{\circ}_{i+1}} \tag{1.20}$$

where

$$\mathring{P}^{\circ}_i = \frac{g_c}{2k\rho u_0^2}(p_0 - p^{\circ}_i) \tag{1.21}$$

Otherwise, the nomenclature is the same as before. Also, if equations (1.19) and (1.20) are combined, one obtains

$$U_{i+1} = \frac{1}{1 - \dfrac{(\Delta y)^2}{2}} \times \left\{ U_i - \sqrt{\frac{(\Delta y)^4}{4} U_0^2 + 2(\Delta y)^2 \left[1 - \frac{(\Delta y)^2}{2}\right] \mathring{P}'_i} \right\} \tag{1.21}$$

Equations (1.18), (1.19) and (1.21), together with the conditions that at the open end of the manifold,

$$U_0 = 1$$

and

$$\mathring{P}^{\circ}_i = \frac{M_0^2}{2} \tag{1.22}$$

can then be solved by a simple iteration. The solution is again expressible in terms of the three dimensionless parameters M_0, F_0 and Δy.

Finally, the basic equation for the continuous sucking manifold can be derived from the above relations by letting $\Delta y \to 0$ formally, as was done earlier in conjunction with the blowing manifold. Thus, it is found that

$$\left(\frac{d^2U}{dy_2}\right)\left(\frac{dU}{dy}\right) - U\left(\frac{dU}{dy}\right) + F_0 U^{7/4} = 0 \tag{1.23}$$

with the conditions that at $y = 0$

$$U = 1 \tag{1.24}$$

and

$$\frac{dU}{dy} = -M_0$$

The basic equations for the manifolds, when solved numerically with a digital computer or otherwise, enable one to predict the rate of discharge through the ports as a function of the distance along the main tube. Any proper design of the manifold demands that this rate of discharge be as uniform as possible. This, as will be shown by the numerical calculations, can be realized when M_0, which is related to the pressure at the open end of the manifold, is made large.

Calculated Manifold Flow Distributions

Owing to the fact that the one-dimensional flow pattern for continuous manifolds depend on only two parameters, M_0 and F_0, whereas a third parameter, Δy, is needed for manifolds with finite numbers of ports, calculated flow distributions for the former type will be presented more completely than those for the latter. Figure 6 shows a typical set of curves resulting from computer calculations for a family of blowing manifolds characterized by $M_0 = 1{\cdot}0$ and by various values of F_0. From its definition, M_0 can be seen to represent the ratio of fluid pressure to specific kinetic energy (or momentum flow) at the entrance. The pressure rise is therefore expected to be smaller the greater M_0 is. On the other hand, F_0 is proportional to the wall friction factor; the greater its magnitude the greater will be the tendency for pressure to fall in the direction of flow. For each value of M_0 there should be a value of F_0 that will cause the momentum and friction effects to be about equal on the average. The calculations show, however, that no pair of values of M_0 and F_0 gives a perfectly uniform

VOL. 10 1959

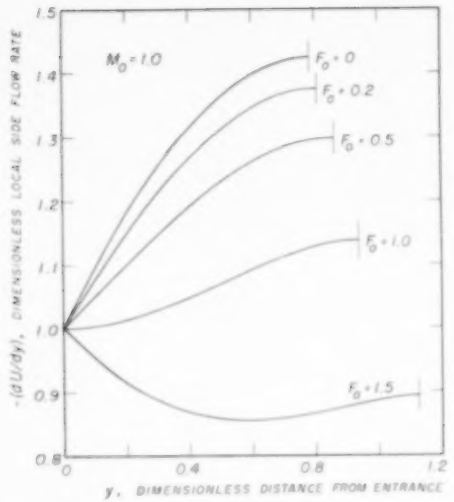

FIG. 6. Calculated side-flow distributions for a group of continuous "blowing manifolds" with closed ends.

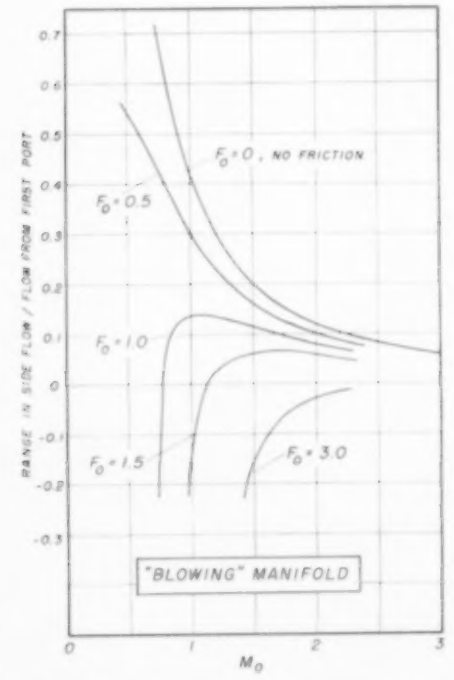

FIG. 7. Results of calculations for continuous "blowing" manifolds showing difference of extreme values of side flow. When ordinate is negative maximum flow occurs at entrance; when ordinate is positive maximum flow is at closed end and minimum may be at entrance or at an intermediate position.

sideways flow. If the side flow is the same at the entrance and the closed end, as will the case for $M_0 = 1{\cdot}0$ and $F_0 \sim 1{\cdot}3$, for example, according to Fig. 6, the side-ways flow rate will have a minimum value near the middle of the manifold.

Fig. 7 shows the condensed results of calculations similar to those just described by plotting the difference in the extreme values of the side flow rate against M_0, with F_0 as a parameter. The figure shows that, although the flow distribution may be approximately uniform at any value of M_0 provided the value of F_0 is properly chosen, the distribution is best in all cases when the value of M_0 is large. M_0 can be varied by a designer most readily by varying the entrance velocity through a change in the cross-section. Large cross-sections lead to low velocities and, thus, to large values of M_0. F_0 contains factors that are not subject to independent variation in a design, except for α, the ratio of port area per manifold unit to the inside surface area. Often this can be made as small as desired by spacing

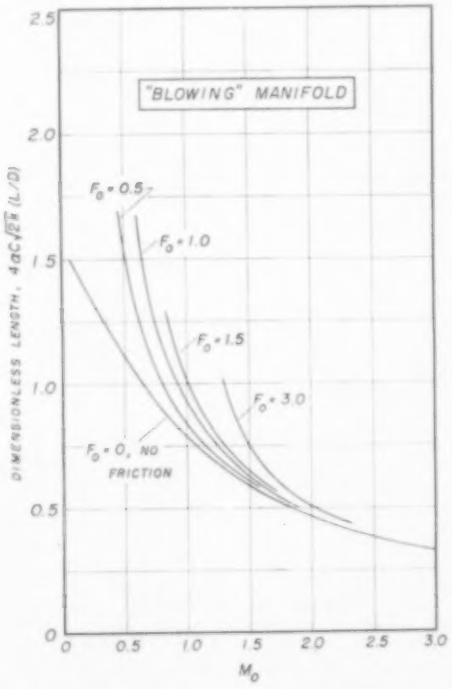

FIG. 8. Results of calculations for continuous "blowing" manifolds showing dimensionless length required to discharge total input stream.

the side outlets far apart. Presumably, also, extra friction devices could be installed between the ports, if necessary.

Fig. 8 shows another result of the same set of calculations that led to Fig. 7. The dimensionless length of the manifold is plotted against the same two parameters. The length required to discharge all the input stream from a manifold with a closed end is seen to depend strongly on M_0. The effect of F_0 is strong if M_0 is small, the required length being greater when friction is present because generally the flow is most non-uniform when friction is absent and the greater side flow rates near the closed end cause the fluid to be discharged more quickly. If the side flow were perfectly uniform, a simple material balance shows that

$$4\pi C\,(2k)^{1/2}\,(L/D) = M_0^{-1} \equiv \left(\frac{k\rho u_0^2}{g_c\,\Delta p_0}\right)^{1/2} \qquad (1.25)$$

Most of the dimensionless lengths read from Fig. 7 are larger than this, owing to the imperfect distribution. Equation (1.25) shows that when the flow is nearly uniform k has little effect on L, since it appears on both sides of the equation. On the other hand, since it influences the pressure rise, k has a large effect on the flow distribution.

The dimensionless length shown on Fig. 7 is a direct indication of one of the main features of a manifold. If $C\,(2k)^{1/2} \sim 1{\cdot}0$,

$$4\pi C(2k)^{1/2}(L/D \sim \frac{\text{total port area}}{\text{cross-sectional area of main tube}}$$

Keller [5] concluded that this ratio should not exceed unity and that the ratio of length to

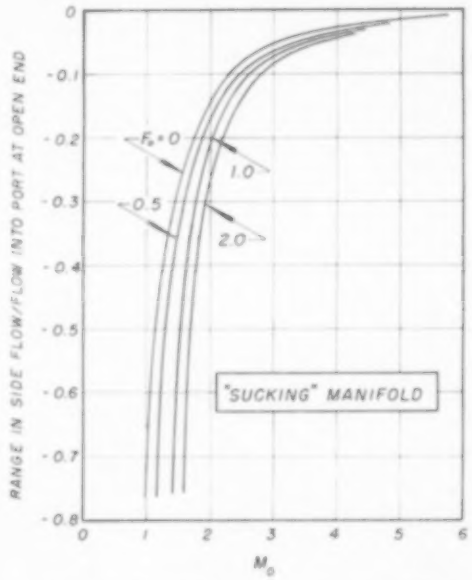

Fig. 9. Results of calculations for continuous " sucking " manifolds showing difference in extreme values of side flow. Maximum flow into manifold always occurs at port nearest open end.

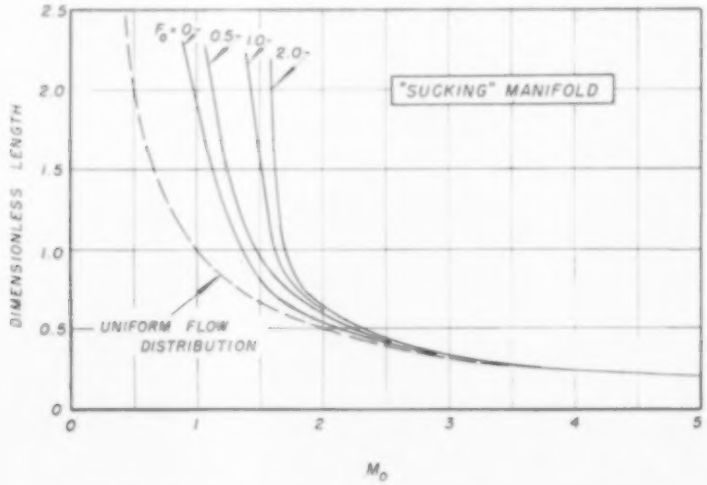

Fig. 10. Results of calculations for continuous " sucking " manifolds showing dimensionless length required to receive total output stream.

diameter should not be greater than 70 for substantially uniform distribution to be obtained. Using $4\alpha C\,(2k)^{1/2}\,(L/D) = 1{\cdot}0$ and $L/D = 70$, $\alpha C = 1/280$. Assuming $f_0 = 0{\cdot}006$, $F_0 = 0{\cdot}84$. This represents one point on Fig. 8 for which $M_0 = 0{\cdot}90$. From Fig. 7 the range in side flow under these extreme conditions permitted by KELLER's rule is found to be 18 per cent of the flow from the first port. When *smaller* length : diameter ratios are used, however, F_0 and M_0 are reduced and the flow variation is *increased*. The specification of a single pair of maximum allowable values of area ratio and of L/D thus appears to be insufficient to insure good flow control; however, values of M_0 larger than 0·90 usually are needed and ordinarily these will correspond to area ratios less than unity.

Figs. 9 and 10 are similar to the two just discussed, but they apply to sucking manifolds into which fluid flows from an outside, constant-pressure source. Here the friction effect and the momentum effect act in the same direction, causing the pressure inside the manifold to grow smaller in the direction of flow, i.e., toward the open end of the manifold where the fluid leaves. There are no minima in the side flow distribution curves and at a given pair of values of M_0 and F_0 the flow distribution is less uniform than it is for the blowing case. To handle the same quantity of fluid, therefore, a sucking manifold will have a larger cross-section than a blowing manifold if both are to produce similar flow distributions. Moreover the influence of fluid pressure on density has been neglected in the calculations described in this paper and it appears likely that when this additional influence of fluid expansion is allowed for the required area for such manifolds will be even greater than that indicated by Figs. 9 and 10.

EFFECT OF FINITE NUMBER OF SIDE PORTS

The basic equations were derived above in terms of three parameters, M_0, F_0 and Δy. It was only by going to the limit $\Delta y \to 0$ that the differential equations (1.16) or (1.23) were obtained. The results obtained by integrating these equations have been regarded as useful idealizations of flow distributions for actual distributors, although they apply in fact only to flow from a continuous slot of constant width. In this section we return to the non-linear difference equations (1.8), (1.10) and (1.11) for the blowing manifold with a finite number of side ports. By solving the system for various values of Δy but constant values of M_0 and F_0 we determine how many side connections are needed to make the distribution essentially like that for a slot opening.

Fig. 11 shows the results of such calculations, plotted with the same co-ordinates as Fig. 6. The upper curve on Fig. 11 is the same curve as that

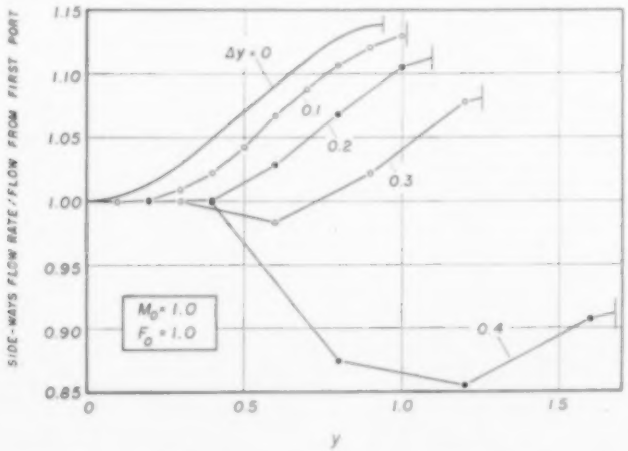

FIG. 11. Effects of finite distance between ports on flow distribution.

shown on Fig. 6 for $M_0 = 1$ and $F_0 = 1$; it evidently applies to the case $\Delta y = 0$. The other curves show the distributions calculated from the difference equations for $\Delta y = 0{\cdot}1$, 0·2, 0·3, and 0·4, corresponding to approximately 10·1, 5·5, 4·2 and 4·1 side ports, respectively. (Since the computation started at the open end of the manifold, where the main fluid stream entered, it did not lead to a precisely zero value of U_i following one port, so that the numbers of ports did not turn out to be integers. This does not destroy the value of the comparison with the solution of the differential equation, however.) Fig. 11 shows that reducing the number of side ports makes the distribution more uniform initially, until the distance between adjacent ports becomes so great that the friction in these sections produces a deep minimum in the sideways flow in the middle of the manifold. Ten side ports produce a distribution that is very nearly like that calculated for a continuous slot.

Fig. 11 also shows that the length of tubing required for the manifold increases as the distance between side ports increases, the ratio of port cross-section to total inside surface of the manifold tube being held constant all the while. Evidently the increasing influence of friction in the manifold tube causes such a reduction in pressure that the distant ports are " starved " for fluid.

Sample Calculation

Suppose that 50 gal/min of water are to be split into ten nearly equal parts by means of a manifold composed of a straight pipe D′ in. in internal diameter to which ten, one-inch, schedule-40 pipes are to be welded at right angles. The manifold will be 10 ft long, the interval between adjacent 1 in. pipes being 1 ft. Calculate the percentage variation in the flow rate through the ten small pipes and the pressure inside the manifold at the entrance for D' equal to 3, 4 and 5 in.

From the stated dimensions and using 1·049 in. for the inside diameter of the branch lines,

$$\alpha = \frac{10 \times 1{\cdot}049^2 \times \pi}{4 \times \pi \times D' \times 10 \times 12} = 0{\cdot}0229/D'$$

$$4\alpha C\,(2k)^{1/2}\,(L/D) = 4(0{\cdot}0229/D')\,(0{\cdot}6)\,(2 \times 0{\cdot}6)^{1/2}$$

$$(10 \times 12/D') = 7{\cdot}22/(D')^2$$

$$u_0 = \frac{50 \times 231 \times 4 \times 144}{1728 \times 60 \times \pi\,(D')^2} = 20{\cdot}4/(D'^2),\ \text{ft/sec.}$$

$$N_{Re} = \frac{(D')\,(20{\cdot}4)\,(62{\cdot}3)}{(12)\,(D')^2\,(0{\cdot}000673)} = 157{,}200/D'$$

$$F_0 = \frac{(f_0)\,(D')}{(2)^{5/2}\,(k)^{3/2}\,(C)\,(0{\cdot}0229)} = 27{\cdot}7\,f_0\,D',$$

based on $k = C = 0{\cdot}6$. Similarly,

$$M_0^2 = \frac{(32{\cdot}17)\,(\Delta p')\,(144)\,(D')^4}{(0{\cdot}6)\,(20{\cdot}4)^2\,(6{\cdot}23)} = 0{\cdot}298\,(\Delta p')\,(D')^4$$

where $\Delta p'$ is in lb/in² gauge.

Using $D' = 4$ in. to illustrate the calculations, $N_{Re} = 39{\cdot}200$ and $f_0 = 0{\cdot}0063$ for commercial pipes. Furthermore, $F_0 = 0{\cdot}70$ and $4\alpha C\,(2k)^{1/2}\,(L/D) = 0{\cdot}452$. From Fig. 8 the required value of M_0 is 1·86 and from Fig. 7 the fractional variation in the distributed flow is 0·115. Trial of the other two diameters leads to the numerical results shown in the following table:

Manifold diameter, D′ (in.)	F_0	$4\alpha C\,(2k)^{1/2}\,(L/D)$	M_0	*Per cent range in side flow*	$\Delta p'$, (lb/in²)
3	0·50	0·80	1·05	28	0·046
4	0·70	0·45	1·86	11	0·045
5	0·91	0·29	2·52	5	0·034

VOL. 10 1959

Observed Flow Distributions

In order to compare the predicted flow non-uniformity with experimentally observed distributions several tests were carried out using equipment, described in a previous section, that had been employed in the determination of the pressure-rise coefficient, k. For this purpose many of the side tubes were allowed to discharge simultaneously and the rate of flow through each tube was measured by means of a sensitive micromanometer and a Pitot tube made from hypodermic tubing. Pressures at intermediate points on the bottom of the main channel were also observed using the micromanometer.

Typical data for one run are shown by Fig. 12, which represents a run in which all twenty-four of the ports were opened and the valve downstream from the last port was completely closed. As shown by the figure, the fluid pressure decreased in the direction of flow owing to fluid friction as the air approached the first port. Then, within the area in which ports were discharging the pressure fell to a shallow minimum and rose owing to the fluid momentum effect described above. Finally, after the last port the pressure was constant because flow had ceased in the manifold, the last hole having discharged the last portion of the main stream.

The upper plot on Fig. 12 shows the corresponding increase in flow from the manifold. The

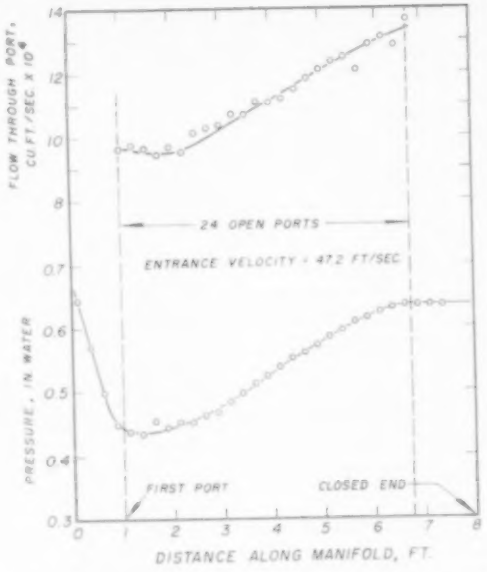

Fig. 12. Typical data from test of "blowing" manifold curves show increase in side flow owing to increased internal manifold pressure near closed end.

fractional variation in sideways flow is seen to be (13·2–9·6)/9·6, or 0·38. This is one of the figures appearing in Table 1, which compares the observed departure from flow uniformity with the value predicted from Fig. 7 at the values of M_0 and F_0 corresponding to the existing entrance

Table 1. Summary of flow distribution data from experimental manifolds.

No. holes open	M_0	F_0	*Max. range of side flow, % of of flow from first port*		*Dimensionless length of manifold* $4\alpha C(2k)^{1/2}(x/D)$	
			Observed	*Predicted*	*Observed*	*Predicted*
8	2·79	2·60	6 ± 1	3 ± 2	0·29	0·28
16	1·38	1·30	12 ± 1	9 ± 1	0·77	0·69
16	1·20	0·65	15 ± 2*	8 ± 1	0·97*	0·74
32	0·77	0·65	33 ± 1	30 ± 5	1·55	1·08
12	1·32	1·03	14*	12	0·95*	0·91
24	0·83	0·50	38	39	0·82	0·92
24	0·80	0·50	30*	40	1·55*	1·00

*Manifold open at downstream end in these runs. Figure tabulated is found by approximate extrapolation of observed flow distribution to point beyond end of manifold where inside stream would have been exhausted.

velocity and excess pressure and to the values of k and C found in the previous single-port experiments.

Table 1 also includes three comparisons of observed and predicted quantities in which the manifolds tested were not completely closed on the end. Since Figs. 7 and 8 apply only to closed-end manifolds it was necessary to extrapolate the observed port flow rates in these cases to hypothetical positions beyond the end of the actual manifold to the point where the flow rate of the main stream would have been expected from a similar extrapolation to have reached zero. Possibly because these extrapolations had to be made in a somewhat arbitrary manner the comparisons in the table are not quite as good as those for the four "normal" runs. In most cases the predicted and observed dimensionless lengths also agreed satisfactorily, though one of the "normal" runs seems to show a large deviation for no apparent reason.

Generally speaking the table shows that expected and observed flow distributions agreed approximately, justifying the expectation that Figs. 7 and 8, and presumably also Figs. 9 and 10 can be used for the design of piping systems.

Acknowledgement—The authors wish to express their appreciation to Messrs. D. Ewing and T. Festin, respectively undergraduate and graduate students at the University of Delaware, who assisted with the experimental work. Computing facilities were made available by the University of California, Berkeley, California, and by the Computing Centre at the University of Delaware.

Notation

The following nomenclature is employed:

p''_i = the pressure at the left end of the straight tube-section i

p_i' = the pressure at the right end of the straight tube-section i

p_0 = the uniform pressure outside the discharge ports

u_i = the velocity in the straight-tube section i

D = the diameter of the main tube

$\Delta x = x_{i+1} - x_i$ = the distance between adjacent discharge ports

α = fraction of internal area of the tube that is occupied by discharge ports, assumed uniformly spaced along the tube

$\alpha\pi D\Delta x$ = the discharge area of a port

f = the Fanning friction factor

ρ = the fluid density

C = the discharge coefficient for the orifice equation, applied to the side outlets

L = the distance between the closed end and the entrance to the manifold

References

[1] Babcock B. D. *B.S. Thesis* University of Delaware, 1952.

[2] Berman A. S. *J. Appl. Phys.* 1953 **24** 1232.

[3] Cadigone C. *Appl Sci. Res.* 1953 **A4** 76 *Hague.*

[4] Dow W. M. *Mech. Engng.* 1950 **72** 748.

[5] Keller J. D. *Trans. Amer. Soc. Mech. Engrs.* 1949 **71** 77.

[6] Rouse H. *Engineering Hydraulics*, p. 437. J. Wiley and Sons, New York 1950.

[7] Soucek E. and Zelnick E. W. *Trans. Amer. Soc. Civil Engrs.* 1945 **110** 1357.

[8] Weissberg H. L. Report No. K-1187, Mar. 29, 1955, Carbide and Carbon Chemicals Co., Union Carbide and Carbon Corporation, K-25 Plant, Oak Ridge, Tenn.

[9] Zijnen B. G. and van der Hegge, *Appl. Sci. Res. Hague* 1952 **A3** 1944.

Book Reviews

SEITH u. RUTHARDT: **Anleitungen für die Chemische Laboratoriumspraxis. Band 1. Chemische Spektralanalyse. Eine Anleitung zur Erlernung und Ausführung von Emissions-Spektralanalysen. Fünfte neu bearbeitete Auflage von Walter Rollwagen.** Springer Verlag, 1958. pp. 162. DM 26·00.

DIE neue Auflage hält an der durch die vorgegebenen Auflagen festgelegten Richtschnur des Buches, "weder ein Lehrbuch noch eine Rezeptsammlung" für die Ausführung von Spektralanalysen zu sein, fest. Dieses Ziel wird im besten Sinne dadurch erreicht, dass im ersten Teil in klarer und leicht verständlicher Form die notwendigen Grundlagen zum Verständnis der zur Spektralanalyse benötigten Apparate gelegt werden. Der zweite analytische Teil befasst sich mit der Ausführung von qualitativen und quantitativen Emissionsspektralanalysen. Es werden an Beispielen aus der Praxis die verschiedenen bewährten Analysenverfahren erläutert. Auch hierbei ist es Herrn Rollwagen gelungen, das gesteckte Ziel zu erreichen, nämlich "jene technischen Kleinigkeiten zu vermitteln, für die der Anfänger (und nicht nur dieser) das meiste Lehrgeld zahlen muss."

In einem spektralanalytischen Laboratorium wird dieses Buch ein häufig befragter Ratgeber sein, und es eignet sich sehr für die Einführung von Laboranten in dieses Arbeitsgebiet.

H. KIRCHER.

Talanta Vol. 1, 1958. Numbers 1/2. Pergamon Press Ltd., London. 120s. per volume.

TALANTA is a new journal of analytical chemistry, with Professor C. L. WILSON as its Editor-in-Chief. The first double number contains three review articles (on methods for the analysis of the platinum metals and cobalt and on recent advances in recording polarography), nineteen research papers, two short communications, book reviews and notices. In this number all but three of the papers are in English – although, in accordance with the international character claimed for the journal, papers may be presented in English, French or German and summaries of each paper are given in all three languages.

The present number and the list of articles accepted for publication in the future suggests that Talanta will soon achieve an equal place with the more established journals of analytical chemistry and become a necessary part of any library which claims to provide a reasonable cover of this rapidly expanding field.

J. A. W. DALZIEL.

W. MATZ: **Die Wirbelschicht als Energieübertragungsfläche.** Springer, Berlin 1958. 66 Seiten, DM. 10-50.

DIE Abhandlung setzt sich zum Ziel, dem Leser die Behandlung mechanischer und thermodynamischer Energieübertragungen mit Hilfe vektoranalytischer Methoden nahezubringen. Mit den Begriffen des flächennormalen Feldes einer skalaren Ortsfunktion und dessen Rotor zeigt Matz in überzeugender Weise die Nützlichkeit dieses dem Ingenieur leider zu wenig geläufigen mathematischen Werkzeuges. Die anschauliche physikalische Deutung des Rotors als Wirbelschicht bietet gerade eine der Denkungsart des Ingenieurs angepasste Betrachtungsweise, die sich bisher hauptsächlich in der Strömungslehre als ausserordentlich fruchtbar erwiesen hat (Prandtl'sche Tragflügeltheorie). Die ganz allgemein erforderliche Existenz einer Wirbelschicht in einem flächennormalen Feld als notwendige Bedingung für Energieübertragungsflächen gibt dieser Theorie einen universellen physikalischen Charakter und besitzt darüberhinaus didaktischen Wert.

Die ersten Seiten des Buches stellen zunächst die vektoranalytischen Grundlagen bereit. Der grösste Teil des Buches ist dann anschaulichen Beispielen aus der Mechanik und Thermodynamik gewidmet, wie zum Beispiel der Reibungsleistung fester Körper, der Arbeitsleistung eines Blattrührers, dem Wirkungsgrad thermodynamischer Kreisprozesse und der Wärmeübertragung bei Gegenstromkühlung. Bei den thermodynamischen Anwendungen kommen in der vektoranalytischen Behandlungsweise besonders anschaulich die Begriffe des unvollständigen Differenzials und des integrierenden Nenners sowie der Inhalt des zweiten Hauptsatzes zum Ausdruck.

Abschliessend sei noch darauf hingewiesen, dass der im deutschen Schrifttum teilweise immer noch gebräuchliche Begriff der "Wirbelschicht" in der Bedeutung eines Fliessbettes mit dem hier benutzten, aus dem Rotor eines Vektorfeldes abgeleiteten Begriff der Wirbelschicht (*vortex sheet*) unvereinbar ist. Für den ersteren Begriff ist daher das Wort "Fliessbett" (*fluidized bed*), das auch den physikalischen Sachverhalt besser beschreibt, unbedingt vorzuziehen.

N. SCHOLZ

W. N. LACEY and B. H. SAGE: **Thermodynamics of One-Component Systems.** Academic Press, London, 1957. 376 pp., £3 4*s*. 0*d*.

THIS book is an introduction to engineering thermodynamics though this fact is not indicated in the title. The authors state in the preface that their aim has been to help the student "in his transit from science studies

to engineering, from idealized thermodynamics to the combination of thermodynamics with mechanics needed for dealing with everyday problems of the engineer." Broadly speaking it may be said that the authors have succeeded in their aim. It is clear however that to derive much help from this book the student should already have had the benefit of a first year university course in thermodynamics. The book is divided into two parts entitled "Thermodynamic Principles" and "Flow Processes" respectively. The first part consists of a rapid recapitulation of fundamental thermodynamics and its application to single-phase and two-phase fluid systems of fixed weight, followed by chapters dealing with irreversible processes and systems of variable weight. In the second part Bernoulli's equation is derived in its generalized form and a discussion is given of some special flow processes (such as flow through nozzles) in which kinetic energy is important. A variety of practical pieces of equipment are then considered such as the dynamo (Chapter 11), the reciprocating engine (Chapter 12) and the gas compressor (Chapter 13). Refrigeration and the liquefaction of gases at low temperatures are considered in final chapters. The authors do not discuss methods of refrigeration depending on an absorption process or the internal combustion types of reciprocating engine since these involve systems of more than one component. An interesting feature of the book is the treatment of friction. The frictional effects are considered to be concentrated in the walls of the system and the friction j is defined as being "the discrepancy between the mechanical transfer from the system and the corresponding transfer to the surroundings." The quantity j, which is analogous to the "uncompensated heat" of Clausius is inserted where appropriate into the equations in both sections of the book. The section on the law of corresponding states is disappointing. The statement "owing to the general similarity of the behaviour of all pure substances a relation referred to as the law of corresponding states has been hypothesised as applicable to the members of a homologous series of substances" is almost misleading since it might imply that substances such as *n*-butane or hexadecane would obey the same law of corresponding states as methane whereas the rare gases (which are not members of the same homologous series) would not. A statement in simple language of the work of Pitzer on this subject would be a help to the student since this would give him an insight into the reasons for deviation from the law. This criticism is however very small in relation to the scope of the book. This is an interesting book which can be recommended. There are many worked numerical examples in the text and these should prove helpful to the student.

M. B. King

S. Kiesskalt: **Verfahrenstechnik** (Process Technology) 3rd edition. Carl Hanser Verlag, Munchen, 1958. 202 pp.

Dr. Kiesskalt has undertaken to write a series of monographs for the primary purpose of presenting the advancements in unit operations technology to the practicing process engineer. This is the third edition of his effort. The book is divided into three main sections: one is on "general" techniques, processes, and equipment; the second is a short review of some of the basic laws governing the various unit operations; and the last, which occupies half the book, is on unit operations and associated equipment. A very useful bibliography at the end of each section is, perhaps, the salient feature of the book. Almost five hundred literature references are given, practically all of which are to German books and journals published since 1950. This appears to be, as the author had hoped, a quite handy guide into the last decade of German chemical engineering literature.

In the first main section are contained descriptions and many pictures and diagrams of such industrial equipment as reactors, pressure vessels, mills, packed columns, ovens, screw conveyors, pumps, materials of construction, and instruments for measurement and control. A few pages of the first section are devoted to methods of symbolic representation for drawing flow sheets. The suggested schemes, although precise, appear to be too elaborate to be of much general use. In the second section, Dr. Kiesskalt briefly discusses the present status of fundamental theories underlying the fields of rheology, fine particle behaviour, heat transfer, and mass transfer. The third section includes material on many of the industrially important unit operations: screening and magnetic sorting, crushing and grinding, sedimentation, filtration, flotation, centrifugation, dust removal and electrofiltration, drying, sublimation, freeze drying, crystallization, salting out, fractional solution and extraction, evaporation, distillation and rectification, solvent extraction, absorption, mixing and agitation, pelleting and briquetting, sintering, emulsification, defoaming, melting and freezing processes, vacuum and compression techniques, and ice production. Dr. Kiesskalt has drawn upon several other workers to edit some of these topics.

The author has written a well organized book on a field in which organization is difficult.

J. R. Bartlit

Catalysis in Practice.* Edited by C. H. Collier. Reinhold, New York, Chapman and Hall, London. 1957, V + 153 pages, 22 figures, 11 tables, Price $3·95.

This book contains the papers read before the symposium by ten American experts on the industrial application of catalysis. According to the preface the book purports to "be of maximum utility to the young practising chemical engineer." It comprises the following chapters:

* A collection of papers originally presented in Philadelphia, Pa., in April 1957, under the auspices of the Philadelphia-Wilmington section of the American Institute of Chemical Engineers and the School of Chemical Engineering, University of Pennsylvania.

VOL. 10 1959

1. "What Catalyst and Why," by Martin Kapp.
2. "Commercial preparation of industrial catalysts," by F. C. Ciapetta, C. D. Helm and L. L. Baral.
3. "Fixed Bed Catalyst Systems," by A. B. Stiles.
4. "Moving Bed Processes," by J. M. Bourget and S. J. Wantuck.
5. "Economics of Catalyst Use," by R. E. Reitmeier.
6. Operating Problems in Catalytic Processing," by J. Mc. A. Harris.
7. "Trends and Prospects in Catalysis," by Charles L. Thomas.

The fact that collaborators of companies which have made their mark in the field of catalysis (Houdry, Davison, Dupont, Socony Mobil Oil, Catalysis and Chemicals, Rhom and Haas, Sun Oil) relate from their practical experience, will undoubtedly make students jump at the book.

As it reads easily, it provides a pleasant orientation in this important division of the chemical industry. Experts will hardly find anything new in it, however.

The most valuable part seems to be Chapter 2, because of its systematic treatment of industrial preparation processes. The absence of a chapter on fluid bed catalyst systems is felt by the reviewer as a serious lack, the more so as separate treatment *is* given to fixed and moving beds.

Some, to the reviewer's mind, striking pronouncements are the following:

"It is now apparent that there may never be a single theory which will explain all catalytic reactions. Instead, four or five theories for different types of catalysis may eventually be established. In spite of our ignorance we need not be dismayed. We should remember that the whole chemical industry is founded on reactions which are not so well understood."

"The concept of a catalyst being a chemical reagent is an important one for both the chemist and the chemical engineer."

The book is well produced but, in view of its size, rather expensive.

D. W. van Krevelen

Chemical Engineering Practice, Volume IV. Fluid State. Butterworth's Scientific Publications, London, 1957 vi + 623 + xix pp., 95*s*.

Volume 4 of "Chemical Engineering Practice" falls into three parts which overlap to some extent both with each other and with the contents of previous volumes. "Thermodynamic Properties of Physical Systems" by Strickland-Constable is, so far as the non-specialist can express an opinion, an extremely able and lucid survey of the thermodynamics of physical equilibrium (chemical equilibrium is deferred until Volume 8, which seems to be an unfortunate arrangement). The thermodynamics of heat engines are barely discussed (for instance, Refrigeration, apart from the Joule-Thomson effect, is covered in three-quarters of a page), and one wonders whether they will be dealt with in a later volume.

The first three chapters (75 pages) are devoted to the formal development of the subject and are followed by two on "Properties of Single Substances" and "Properties of Mixtures." I should have liked to see much less space devoted to the formal aspect (which is already available in a multitude of text-books on physical chemistry, and has already been sketchily dealt with in Volume 1), and much more to explaining the way in which the results can be applied in practice, to worked examples, and to a critical survey of methods of estimating thermodynamic properties. To my mind it is unlikely that many people will turn to this book to find out how the formulae of thermodynamics are developed from first principles, however well this topic is expounded; they are much more likely to be seeking a practical guide as to how these formulae can be applied to industrial problems.

The sixth chapter incorporates a good deal of material, under the heading of "Sum and Difference Properties," which has appeared in earlier volumes or will (I suspect) appear in later ones, or both. For instance, the treatment of counter-current processes and of the triangular diagram construction for solvent extraction was anticipated in volume 1, and is pretty certain to crop up again in Volumes 5 and 6.

The last chapter in this first section deals with the thermodynamics of fluid flow, and inevitably overlaps with the succeeding section on fluid mechanics; for instance, the total energy equation is derived twice (pp. 205, 305) with different symbols.

The second section of the volume (which suffers from chaotic chapter titles) is a gallant attempt to deal with the whole of fluid mechanics in 281 pages, and on a fairly sophisticated level; it might be regarded as a condensed version of an undergratuate text-book combined with "Modern developments in Fluid Dynamics." It is a tribute to the expository powers of the authors, Franklin and Cass, that they have achieved such a measure of success. I think it is possible that a first-class mind with no previous knowledge of fluid mechanics could master this section; but it will be principally useful to those already acquainted with the subject, either as an *aide-mémoire* or as an introduction to the more advanced aspects. Personally, I should have liked to see these authors given a complete volume to enable them to expound the whole subject of fluid mechanics in a more leisurely way, and to introduce a lot of material which at present requires reference to the literature or is dealt with piecemeal in other volumes.

The final section, on "Measurement of Process Variables," by Pollard and Carruthers, is an excellent introduction to methods of measuring pressures, temperatures, flow-rates and liqiud levels. Since the whole

subject is covered in 100 pages the treatment is necessarily somewhat diagrammatic, and the section can in no sense be regarded as a practical manual on instrumentation. One wonders whether the subject will be dealt with in greater detail elsewhere in the work. If so, the present section seems to be unnecessary ; if not, it is surely quite inadequate. It is somewhat dispiriting to find the equations of fluid flow derived again in this section (some of them for the third time in this volume).

In a sense, each successive volume in this work may be regarded as another stage in the unfolding of a grand design. The design indeed exists, in the form of the original outline of the twelve projected volumes ; this may be compared to a rough pencil sketch for an elaborate tapestry, indicating its main dimensions and proportions but nothing more. If such a sketch were cut into twelve pieces and distributed to twelve honest weavers, with no further instructions, one would expect the resulting twelve sections of the tapestry to show striking variations in interpretation, colour and texture. Only the personal intervention of the designer at the loom can assure balance and coherence.

There are indications that this work will turn out to be more of a patchwork than a tapestry because too little guidance has been exercised over the individual authors. I cannot help feeling that to be really satisfactory an enterprise of this sort needs a substantial full-time editorial staff, with strong convictions about the way the book should be written, and prepared to wrestle with the authors until they toe the line. It would also be a great advantage to have a much larger bulk of material collated – the whole work, if possible – before starting to publish, instead of issuing volumes piece-meal. However, these are counsels of perfection. Engineers must never let the best be the enemy of the good, and we must be grateful for the valuable things which are emerging as the volumes appear.

It is sad to have to record the untimely death of Mr. Trefor Davis, the Managing Editor of this work, to which he had devoted so much effort.

P. V. Danckwert

SELECTION OF CURRENT PAPERS FROM NON-CHEMICAL ENGINEERING JOURNALS OF INTEREST TO CHEMICAL ENGINEERS

V. G. Jenson : Viscous flow round a sphere at low Reynolds numbers (< 40). *Proc. Roy. Soc.* 1959 **A249** 346-366.

G. K. Batchelor : Small scale variation of convected quantities like temperature in a turbulent fluid. Part I. General discussion and case of small conductivity. *J. Fluid Mech.* 1959 **5** 113-133.

G. K. Batchelor, I. D. Howells, A. A. Townsend. Small scale variation of convected quantities like temperature in a turbulent fluid. Part II. The case of large conductivity. *J. Fluid Mech.* 1959 **5** 134-139.

B. L. McFarland. Comparison between the linear and non-linear steady-state behaviour of a heated tube. *J. Appl. Phys.* 1958 **29** 1682-1684.

S. G. Bankoff, A. J. Hajjar, B. B. McGlothin Jr. On the Nature and location of bubble nuclei in boiling from surfaces. *J. Appl. Phys.* 1958 **29** 1739-1741.

S. Badzioch : Collection of gas-borne dust particles by means of an aspirated sampling nozzle. *Brit. J. Appl. Phys.* 1959 **10** 26-32.

G. F. Eveson, E. W. Hall, S. G. Ward : Interaction between two equal-sized equal-settling spheres moving through a viscous liquid. *Brit. J. Appl. Phys.* 1959 **10** 43-47.

E. Gottesman : Efficiency of evaporative water-cooling towers. *Appl. Sci. Res.* A 1958, **8** 28-44.

H. J. Merk : The macroscopic equations for simultaneous heat and mass transfer in isotropic, continuous and closed systems. A 1958 **8** 73-99.

SELECTION OF CURRENT SOVIET PAPERS OF INTEREST TO CHEMICAL ENGINEERS*

E. N. Eremin, N. I. Kobozev and B. G. Lukovskaya: Conversion of methane to acetylene in high voltage arc. *Zh. fiz. Khim.* 1958 **32** 2315-2323.

R. M. Flid: Kinetics and mechanism of catalytic conversion of acetylene. *Zh. fiz. Khim.* 1958 **32** 2339-2346.

A. V. Storonkin: Some problems concerning the thermodynamics of multicomponent heterogeneous systems. I. Equilibrium conditions of ternary three-phase systems. *Zh. fiz. Khim.* 1958 **32** 2347-2355. Equations are derived describing changes in equilibrium states and conditions established under which a given phase process makes a transition to another one.

E. V. Vagin and A. A. Zhukhovitski: Theory of thermo-adsorption separation. *Zh. fiz. Khim.* 1958 **32** 2362-2373. Theory is based on pressure equality in the adsorbent layer. It is shown that components of a gas mixture with linear or Langmuir isotherms should separate completely. Effect of longitudinal diffusion and finite adsorption rate on boundary spread is represented mathematically.

E. T. Denisov and V. M. Emanuel: Liquid-phase oxidation of benzene to phenol at temperatures near the critical. *Zh. fiz. Khim.* 1958 **32** 2374-2382.

V. A. Malyusov, N. A. Malafeev and N. M. Zhavoronkov: Determination of relative volatilities of a mixture of dibutylphthalate and dibutylazelate. *Zh. fiz. Khim.* 1958 **32** 2403-2409.

M. M. Egorov, K. G. Krasilnikov and V. F. Kiselev: Influence of the nature of silica gel and quartz surfaces on adsorption properties. I. Study of the hydration of silica surface. *Zh. fiz. Khim.* 1958 **32** 2448-2454.

K. M. Nikolaev and M. M. Dubinin: Adsorption properties of carboniferous adsorbents. 3. Study of gas and vapour adsorption isotherms on active carbon within large temperature ranges, including temperatures of critical area. *Izv. Akad. Nauk SSSR, Otd. khim. Nauk* 1958 No. 10, 1165-1174.

G. A. Kurov and Z. G. Pinsker: Investigation of thin films obtained by evaporation of indium antimonide under vacuum. *Zh. tekh. Fiz.* 1958 **28** 2130-2134.

L. S. Palatnik and A. I. Landau: Determination of phase composition of an equilibrium multicomponent system by measuring phase masses. *Zh. tekh. Fiz.* **28** 2340-2343.

A. V. Voronel: On the equation of the melting curve. *Zh. tekh. Fiz.* 1958 **28** 2630-2634. Combination of the empirical equation of Simon and Glatzel with the Clausius Clapeyron equation by assuming a linear relation between the ratio of latent heat to change in volume and pressure.

G. V. Korovina, S. G. Entelis and N. M. Chirkov: Rate of absorption of ethylene and propylene by sulphuric acid of different concentrations. *Dokl. Akad. Nauk. SSSR* 1958 **121** 1038-1040.

I. R. Krichevski and Yu. V. Tsekhanskaya: Convective diffusion in liquid solutions in the turbulent regime. *Dokl. Akad. Nauk SSSR* 1958 **122** 258-259. Discussion of results obtained with rotating discs.

M. G. Kaganer: Isotherm of nitrogen adsorption at low pressures. *Dokl. Akad. Nauk SSSR* 1958 **122** 416-419.

N. A. Kleimenov and A. B. Nadbandian: Study of low temperature oxidation of methane initiated by oxygen atoms formed during thermal decomposition of ozone. *Dokl. Akad. Nauk SSSR* 1958 **122** 420-423.

L. M. Gindin, P. I. Bobikov, E. F. Kouba, I. F. Kopp, A. M. Rozen, N. A. Ter-Oganesov and N. I. Zagarskaya: Separation of metals by ion-exchange extraction method. *Dokl. Akad. Nauk SSSR* 1958 **122** 445-448.

Yu. G. Mamedalyev, M. M. Guseinov and F. A. Mekhtyeva: Production of carbon tetrachloride by chlorination of methane in a fluidized catalyst bed. *Dokl. Akad. Nauk SSSR* 1958 **122** 817-820.

D. A. Epstein, N. M. Tkachenko, M. A. Minyovich and N. V. Dobrovolskaya: A two-stage catalyst for oxidation of ammonia. *Dokl. Akad. Nauk SSSR* 1958 **122** 874-878.

Z. P. Gorbits: Fundamental equations for convectional heat transfer in two-phase flow. *Izv. Akad. Nauk SSSR, Otd. tekh. Nauk* 1958 No. 9, 94-102. Theory of similarity is applied to present fundamental equations in the form of dimensionless groups, and coefficients are determined from experimental data.

E. A. Sidorov: Convective heat transfer in non-steady state. *Izv. Akad. Nauk SSSR, Otd. tekh. Nauk* 1958 No. 9 116-117.

I. I. Mezhirov: On flow of gas through a cylindrical pipe in presence of friction and heat transfer. *Izv. Akad. Nauk SSSR, Otd. tekh. Nauk* 1958 No. 9 118-119.

P. M. Ogibalov: Tests of thick walled tubes under high inside pressures of short duration. *Izv. Akad. Nauk SSSR, Otd. tekh. Nauk* 1958 No. 9, 134-138.

*To assist readers, translations of any article appearing in the above list can be obtained at a reasonable charge. All orders should be addressed to the Administrative Secretary of the Pergamon Institute at either 4 Fitzroy Square, London W.1, or 122 East 55th Street, New York 22, whichever is more convenient.

V. P. Isachenko and F. Salomzoda: Heat transfer and hydraulic resistance of pipes at transverse flow of water. *Teploenergetika* 1958 No. 11 69-70.

V. N. Popov and N. V. Tsederberg: Thermal conductivity of liquid fuels. *Teploenergetika* 1958 No. 11 72-75.

S. V. Donskov: Heat transfer from pipe bundles to granular material (sand) in transverse flow. *Teploenergetika* 1958 No. 11 76-80.

M. I. Gerber, V. P. Teodorovich and A. D. Shusharina: Investigation of the rate of absorption of hydrogen sulphide by arsenic–soda solutions. *Zh. prikl. Khim.* 1958 **31** 1624-1627.

S. Bretsznajder: Application of the theory of similarity to some chemical engineering operations. *Zh. prikl. Khim.* 1958 **31** 1636-1647. Application of dimensional analysis to absorption of ammonia by acids, effect of ammonia on light-sensitive paper and scaling-up of processes accompanied by chemical reaction.

I. P. Mukhlenov and E. S. Tumarkina: Kinetics of heat and mass transfer in foam layers. *Zh. prikl. Khim.* 1958 **31** 1647-1655. Determination of coefficients and exponents in equations arranged in the form of dimensionless groups.

A. I. Levin: Laboratory column for microfractionation. *Zh. prikl. Khim.* 1958 **31** 1655-1661.

S. N. Ushakov and E. M. Lavrenteeva: Synthesis of copolymers of vinyl acetate with crotonic acid and its derivatives. *Zh. prikl. Khim.* 1958 **31** 1686-1691.

I. A. Arbuzova, S. N. Ushakov and E. N. Rostovski: On correlation of components in heterogeneous contact synthesis of vinyl acetate. *Zh. prikl. Khim.* 1958 **31** 1704-1708.

M. A. Miniovich, A. L. Shneerson and V. A. Klevke: New cooling medium for condensation of nitrogen oxides from nitrous gases. *Zh. prikl. Khim.* 1958 **31** 1739-1741.

A. F. Alabishev, M. F. Lantratov and L. I. Sokolova: Electrical conductivity in the system $NaOH - Na_2CO_3 - NaCl$. *Zh. prikl. Khim.* 1958 **31** 1749-1752.

P. A. Moshkin, E. A. Preobrazhenskaya and L. D. Peitsov: Hydrogenation of adipic nitrile to hexamethylene diamine on cobalt catalyst. *Khim. Prom.* 1958 399-401.

A. N. Bushin, B. Ya. Soldatov, I. Ya. Tyupaev, T. M. Troitskaya and P. S. Gubina: Dehydrogenation of *n*-butane in semi-industrial plant with moving catalyst. *Khim. Prom.* 1958 406-409.

G. P. Korneychuk, V. A. Royter and Ya. V. Zhigaylo: Methods of increasing efficiency and selectivity of vanadium oxide catalysts in oxidation of naphthalene to phthalic anhydride. *Khim. Prom.* 1958 410-413.

M. A. Lyudkovskaya, S. D. Fridman and L. I. Saveleva: Separation of mixtures of carbon dioxide and ammonia by aqueous solutions of monoethanolamine. *Khim. Prom.* 1958 423-429.

S. Z. Kagan, M. E. Aerov, T. S. Volkova and V. N. Vostrikova: Investigation of extractors with mechanical mixing of phases (rotating disc extractors). *Khim. Prom.* 1958 432-438.

F. A. Rozental: Methods of improvement of the process of drying in the photographic industry. *Khim. Nauk Prom.* 1958 **3** 654-657.

S. D. Gromakov and A. P. Cherkasov: On methods of calculating the properties of ternary and quaternary systems. Viscosity and specific gravity of the system water–ethanol–methanol–glycerol. *Zh. fiz. Khim.* 1958 **32** 2473-2478.

D. P. Timofeev: On the rate of desorption. *Zh. fiz. Khim.* 1958 **32** 2483-2486. Assuming negligible effect of outer diffusion an equation is derived for the rate of adsorption at low flow rates.

N. N. Motorina and A. N. Popov: Effect of temperature on ion-exchange equilibrium. I. Basic factors determining the change in ion-exchange adsorption with temperature. *Zh. fiz. Khim.* 1958 **32** 2557-2560.

M. M. Egorov, T. S. Egorova, K. G. Krasilnikov and V. F. Kiselev: Effect of the nature of silica gel and quartz surface on adsorption properties. II. Adsorption of vapours of water, methanol and nitrogen on silica gel of different degrees of hydration. *Zh. fiz. Khim.* 1958 **32** 2624-2633.

E. A. Sidorov: Effect of non-isothermal conditions on hydraulic resistance in laminar motion of liquids in tubes. *Zh. tekh. Fiz.* 1958 **28** 2711-2712.

N. A. Chernishev: Effect of oil viscosity on control problems. *Teploenergetika* 1958 No. 12 66-71.

L. I. Cherneeva: Experimental determination of specific heat of Freon 142. *Teploenergetika* 1958 No. 12 71-78.

A. F. Begunkova: Effect of thermal contact resistances in a pellet insulation. *Teploenergetika* 1958 No. 12 85-86.

V. D. Miseev, Yu. I. Liadova, V. I. Vedeneev, M. B. Neuman and V. V. Voyevodski: Methods of formation of propylene and ethylene in the cracking of *iso*butylene. *Dokl. Akad. Nauk SSSR* 1958 **123** 292-294.

I. V. Smirnova and K. V. Topchieva: Adsorption of hydrocarbons at elevated temperatures. *Dokl. Akad. Nauk SSSR* 1958 **123** 316-319.

A. P. Prudnikov: Analytical investigation of heat and mass transfer processes in convection drying. *Izv. Akad. Nauk SSSR, Otd. tekh. Nauk* 1958 No. 10 63-67.

O. V. Yakoblevski: On thickness of the zone of turbulent mixing at the boundary of two gas streams of different velocities and densities. *Izv. Akad. Nauk SSSR, Otd. tekh. Nauk* 1958 No. 10 153-154.

S. I. Kosterin and A. D. Magomedov: Investigation of the motion of viscous liquid under conditions of heat transfer in the range of large Prandtl numbers. *Izv. Akad. Nauk SSSR, Otd. tekh. Nauk* 1958 No. 10 155-157.

A. Kh. Mirzadzhanzade and V. V. Mustafaev: On displacement of gas by water in porous media. *Izv. Akad. Nauk SSSR, Otd. tekh. Nauk* 1958 No. 11 95-97.

T. P. Zhuze, T. P. Safronova and G. N. Yushkevich: Extraction of ozokerit from ozokerit deposits by compressed gases. *Izv. Akad. Nauk SSSR, Otd. tekh. Nauk* 1958 1958 No. 11 123-125.

V. V. Kafarov and V. I. Trofimov: On analysis of diffusional processes on the basis of fully developed turbulence. *Zh. prikl. Khim.* 1958 **31** 1809-1816. Study of effects of molecular diffusion on the rate of absorption in the inversion regime. A general correlation is given.

E. K. Styrde and P. G. Romankov: Investigation of the process of distillation by means of steam. *Zh. prikl. Khim.* 1958 **31** 1817-1823. Studies of bubbling and entrainment.

D. S. Tsiklis: Soubility of lubricating oils in liquid ethylene. *Khim. Prom.* 1958 404-406.

Yu. A. Balatnikova, L. O. Apelbaum and M. I. Tenskin: Radiosulphur study of poisoning of ammonia synthesis catalyst by hydrogen sulphide. *Zh. fiz. Khim.* 1958 **32** 2717-2724.

E. N. Ergmin, N. I. Kobozev and B. G. Lyudkovskaya: Conversion of methane to acetylene in high voltage arc. II. Effect of hydrogen. *Zh. fiz. Khim.* **32** 2767-2771.

N. Matorina and A. N. Popov: Influence of temperature on ion-exchange equilibrium. II. Effect of temperature variations in ion-exchange adsorption on sulpho-resins. *Zh. fiz. Khim.* 1958 **32** 2772-2779.

G. M. Panchenkov, T. S. Maksareva and V. V. Erchenkov: Temperature dependence of diffusion coefficients of some organic liquids. *Zh. fiz. Khim.* 1958 **32** 2787-2791.

S. V. Dobrovolski and V. Ya. Palatnyuk: On the kinetics of consecutive reactions in a recirculating flow system. *Zh. fiz. Khim.* 1958 **32** 2792-2796.

S. R. Serguienko, E. V. Lebedev and A. A. Petrov: Selective catalytic dehydrogenation of saturated high molecular hydrocarbons in the liquid phase. *Dokl. Akad. Nauk SSSR* 1958 **123** 704-706.

K. V. Topcheva and B. V. Romanovski: Determination of adsorption coefficients of ether, water and ethylene by the kinetic method. *Dokl. Akad. Nauk SSSR* 1959 **124** 135-138.

P. A. Smirnov: Schemes for gas-separating plants in oil refineries. *Zhim. Tekhnol. Topl. Masel* 1958 No. 9 1-7.

A. N. Planovski and L. A. Vlasenkov: Kinetics of continuous adsorption in a fluidized bed. *Khim. Tekhnol. Topl. Masel* 1958 No. 9 7-13.

B. A. Lipkin: Effect of structure and composition of synthetic sorbents on their activity in percolation purification of lubricating oil. *Khim. Tekhnol. Topl. Masel* 1958 No. 24-29.

S. P. Rogov, M. V. Rysakov and I. Ya. Fersht: Regeneration of hydrogenation catalysis by hydrogen. *Khim. Tekhnol. Topl. Masel* 1958 No. 29-33.

P. G. Eisenstein and A. N. Kurchuk: On some peculiarties of de-emulsifiers soluble in oils. *Khim. Tekhnol. Topl. Masel* 1958 No. 10 34-36.

Yu. L. Khmelnitski and T. A. Tsiguro: Solubility of aluminium chloride in *iso*butane. *Khim. Tekhnol. Topl. Masel* 1958 No. 10 36-40.

A. V. Mazov, Yu. I. Turski and L. E. Danchenko: Extraction of phenols from tar fractions by aqueous solutions of methanol. *Khim. Tekhnol. Topl. Masel* 1958 No. 44-49.

I. M. Razumov and I. G. Fabeev: Transport of catalyst in a continuous stream. *Khim. Tekhnol. Topl Masel* 1958 No. 11 15-20. Pneumatic conveying.

S. N. Aleksandrov and S. L. Skop: Rapid dynamic method for determination of specific surface of catalysts. *Khim. Tekhnol. Topl. Masel* 1958 No. 11 62-66.

I. K. Romankova, N. M. Kamakin and L. I. Oglobina: Simple method of determination of activity of aluminosilicate catalysts. *Khim. Tekhnol. Topl. Masel* 1958 No. 11 66-68.

P. S. Kogan and L. A. Potolovski: Study of influence of water vapour on pyrolysis of technical ethane fraction for the the purpose of production of ethylene. *Khim. Tekhnol. Topl. Masel* No. 12 22-26.

A. V. Kiselev and Yu. S. Nikitin: Influence of thermal and steam treatment on structure and catalytic activity of aluminosilicate catalysts. *Khim. Tekhnol. Topl. Masel* 1958 No. 12 27-32.

G. I. Kichkin: Application of thermal diffusion to separation of hydrocarbons. *Khim. Tekhnol. Topl. Masel* 1958 No. 12 59-63.